University of
South Australia

Optimisation of an impact mill that processes chaff exiting a combine harvester to devitalise annual ryegrass (*Lolium rigidum*) seeds

Nicholas Berry, BEng(Hons)

Barbara Hardy Institute,

School of Engineering,

University of South Australia

21st March 2014

Submitted for the degree of Doctor of Philosophy

Abstract

Herbicide resistant weeds are one of the biggest threats to global grain production and, hence to food security. To address this challenge, a non-chemical weed control method was investigated that uses an impact mill to devitalise weed seeds in the chaff residues exiting a combine harvester's cleaning sieve. A method was developed in this thesis to predict the devitalisation of weed seeds processed with an impact mill based on two functions; a material function which described the probability of devitalisation of a seed exposed impact loads and a machine function which described the impact loads generated in an impact mill based on its geometry and operating conditions.

A material function was developed for the seeds of problematic weed species, annual ryegrass (*Lolium rigidum*) by exposing the seeds to sequences of up to 16 impacts at speeds ranging from 20-90 m/s. Seed devitalisation was measured by counting emergence in soil bins compared to un-impacted seeds. A mastercurve was found that could accurately predict seed devitalisation based the number of impacts and the impact speed.

A machine function was developed for an impact mill using a theoretical vector impact model and a computational fluid dynamics impact model. Both methods predicted the number of impacts and impact speed based on the simplified two dimensional geometry of an impact mill.

The material and machine functions were combined to predict annual ryegrass seed devitalisation for an existing mill to validate the prediction method with experimental results. Upon validation, the method of predicting seed devitalisation was used to develop two new prototype mill designs that can fit within the size, power and weight constraints of a modern combine harvester.

Annual ryegrass seed devitalisation was experimentally determined for the existing mill and both prototype mills at a wheat chaff mass flow of 0.5 kg/s. The experimental results were within 15% of the predicted results. Both prototype mills were also tested

at a higher mass flow of 1.5 kg/s. Both prototype mills were able to achieve greater than 90% seed devitalisation at a chaff throughput of 0.5 kg/s chaff throughputs and greater than 85% seed devitalisation at 1.5 kg/s.

A pair of the first prototype mills were integrated into a large capacity combine harvester and tested in the field in wheat at chaff throughputs of up to 12.4 t/h (tonnes per hour) (≈ 1.7 kg/s per mill) and grain throughputs of up to 41 t/h of wheat. The power to process chaff was evaluated for both the existing mill and both prototype mills; to achieve 90% seed devitalisation at 10.8 t/h required approximately 100 kW.

The methods developed in this thesis showed how to design and improve a mill for seed devitalisation. Furthermore, the work has provided two new prototype mill designs that were able to be integrated into a combine harvester for harvest time weed control that could improve the sustainability of grain production.

Acknowledgements

Foremost, I would like to express my sincere gratitude to my two supervisors, Associate Professor John Fielke and Dr. Chris Saunders for their enthusiasm, hard work, trust and support. They have both continually made my work a priority and I am eternally grateful.

I would also like to acknowledge the tireless work of Senior Research Engineer Mr. Andrew Burge, and Technical Assistant Mr. Dean Thiele who have both been pivotal in design and construction of equipment and instrumentation that was very important to my thesis.

I want to also make mention of Dr. Graeme Quick and Dr. Jack Desbiolles who have provided me with a lot of insight from their extensive research experience.

John, Chris, Andrew, Dean and Graeme were all part of a research team at the University of South Australia funded by the Australian Grains Research and Development Corporation (GRDC) under projects USA00008 and USA 00010 to develop a weed seed devitalisation system for harvest time weed control. The overall output of the research was a team effort and I would like to acknowledge the contributions of each member.

I would like acknowledge the support I have received in the form of Australian Postgraduate Award (APA) scholarship.

I would like to express my deepest gratitude to the Australian Grains Research and Development Corporation (GRDC) for funding this research and providing me with a research scholarship top-up. Their vision and commitment in supporting engineering research in agriculture has and will continue to provide excellent outcomes to the grains industry.

I would like to acknowledge the University of South Australia for providing me a scholarship top-up, for co-funding this research and for providing the excellent research facilities, without which this research would not have been possible.

I would like to thank my family and friends for supporting me through this process. In particular I want to thank my parents Lloyd and Christine Berry for encouraging me and drawing on their wealth of experience as farmers to give me advice and perspective along the way.

Finally, I would like to thank my wife Emma Berry. She has been a source of continual support and has sacrificed a lot for me to complete this degree. I truly could have not done it without her.

Declaration

I declare that:

This thesis presents work carried out by myself and does not incorporate without acknowledgment any material previously submitted for a degree or diploma in any university; to the best of my knowledge it does not contain any materials previously published or written by another person except where due reference is made in the text; and all substantive contributions by others to the work presented, including jointly authored publications, is clearly acknowledged.

Signature: 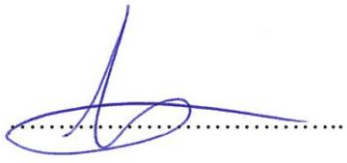

Date: 21/03/2014

Table of Contents

List of figures

List of tables

Glossary of terms

Abbreviation	
RSE	Reduced seedling emergence
HWSC	Harvest weed seed control
CFD	Computational fluid dynamics
HSD	Harrington Seed Destructor
SHS	Square hollow section

Definitions	
Seed devitalisation	The proportion of seeds that are damaged sufficiently to prevent emergence. Expressed as a percentage of control emergence and called reduced seedling emergence (RSE).
Annual ryegrass	Common name for *Lolium rigidum*; a problematic weed species in Australian and global grain crops

Application	Software used
Statistical Analysis	IBM® SPSS® Statistics Version 19.0 (SPSS Inc. 2010, IBM Corp., NY, USA)
Data analysis and programming	MATLAB® R2012a (MathWorks, Inc., Natick, 148 MA, USA).
3D Computer Aided Design (CAD) and Computational Fluid Dynamics (CFD)	SolidWorks® Flow Simulation 2012 (Dassault Systèmes)

Nomenclature

A	total impact face area (m^2)
a	crack length
a	acceleration (m/s^2)
A	area of milling zone (m^2)
a	no load power coefficient
A	no load fitting factor of mill predicted using CFD
A^*_{surf}	normalised surface area based on equivalent sphere
A_{proj}	projected area of the immersed body (m^2)
B	constant representing sum of the squared radial location of impacts (m^2)
b	processing power coefficient
C	overall constant for reduced impact speed due to particle to particle impacts (1/kg):
C^*_D	shape factor normalised coefficient of drag
c_1	constant for the suppression of impact speed due to particle to particle impacts
c_2	constant relating residence time to rotational speed
C_D	coefficient of drag
C_{shape}	Newton shape correction
d	particle diameter (m)
d	diameter of fan (m)
D	depth of seed (m)
d	data density ($points/m^2$)

D	displacement of the motor (m^3/rev)
$d_{\perp}$	normal diameter of an ellipsoid (m)
$d_{\|\|}$	parallel diameter of an ellipsoid (m)
$d_{ryegrass}$	effective diameter of an ellipsoid representing ryegrass seeds (m)
e	coefficient of restitution
E	aspect ratio of an ellipsoid
E_{eff}	effective specific impact energy available for seed damage (kJ/kg)
E_{impact}	specific impact Energy (kJ/kg)
E_{loss}	loss of kinetic energy (J)
E_{min}	threshold specific impact energy for seed fracture that causes seed devitalisation (kJ/kg)
E_{rotor}	energy input of rotor (J)
E_{spec}	specific impact energy (kJ/kg)
E_{spec}	specific input energy of rotor (kJ/kg)
F_D	drag force (N)
f_{Mat}	material and particle property parameter (kg/J/m);
F_{seed}	Resistance of the seed to fracture that results in seed devitalisation (kg/kJ);
f_{shape}	Stokes shape correction
$f_{v,z}$	volume factor to account for volume of mill bars
H	thermal enthalpy
I	moment of inertia ($kg.m^2$)
k	number of impacts
k	number of impacts
KE	kinetic energy (J)
K_{IC}	fracture toughness of the seed

L	length of seed (m)
m	mass of particle
m	rotor mass (kg)
$\dot{m}_{chaff}$	mass throughput of chaff through the mill
m_f	solids loading (kg solids/ kg air)
n	rotational speed (rpm)
N	rotational speed of motors (rev/s)
$\hat{\boldsymbol{n}}$	unit normal vector relative to impact surface
n_p	number of particles
P	power of mill (W)
p	pressure (Pa)
$\mathbf{P}(x,y)$	particle position vector at point of impact
$P_{no\ load}$	no load power consumption of the mill (W)
P_{proc}	processing power consumption of the mill (W)
P_{tot}	total power consumption of mill (W)
p_x	x coordinate of particle position data point (m)
p_y	y coordinate of particle position data point (m)
q	diffusive heat flux
Q	oil flow rate (m^3/s)
$\dot{Q}$	volumetric flow rate (m^3/s)
Q_H	volume specific heat source or sink
r	radial location of the centreline of impact bar (m)
Re^*_p	shape factor normalised Reynolds number
Re_d	Reynolds number based on effective diameter

Re_p	Reynolds number of a particle
RSE	reduced seedling emergence
S	probability of particle breakage
SE	maximum emergence counts of seedlings in soil bins
S_i	external force per unit mass due to a combination of porous media, buoyancy, and coordinate system rotation
$\hat{\boldsymbol{t}}$	unit tangential vector relative to impact surface
t_{res}	residence time of particle (s)
t_{step}	time step (s)
u	fluid velocity (m/s)
v	velocity of particle (m/s)
V	tip speed of impact bar (m/s)
V	velocity of the fluid (m/s)
$\mathbf{V}$	particle velocity vector (m/s)
v_T	tangential speed of impact bar (m/s)
$\bar{V}$	volume of zone (m^3)
$\mathbf{Ve}$	effective velocity vector relative to rotor (m/s)
v_n	normal component of velocity relative to impact surface (m/s)
$\mathbf{V_n}$	normal component of impact velocity (m/s)
$\mathbf{V_R}$	rotor velocity vector at point of impact (m/s)
V_s	circumferential velocity of suspension (m/s)
V_t	terminal velocity of an object in a fluid (m/s)
$\mathbf{V_t}$	tangential component of impact velocity (m/s)
W	width of seed (m)
$W_{m,kin}$	mass specific impact energy (J/kg)

$W_{m,min}$	mass specific threshold energy for particle breakage (J/kg)
x	initial particle size (m)
Δp	pressure drop from the motor inlet to motor outlet (Pa)
ε	air volume as a proportion of total volume
ζ	angle of impact bar forward of radial
η_o	overall efficiency of the hydraulic motor
η_v	volumetric efficiency of the hydmotor
θ	angle made with impact bars before impact
λ	mean free path length of a particle (m)
μ_{RSE}	mean RSE
v	fluid kinematic velocity (s/m^2)
ρ_a	density of fluid (kg/m^3)
ρ_a	density of air (kg/m^3)
ρ_s	density of suspension (kg/m^3)
σ_c	critical stress to cause crack propagation
σ_c	critical stress to cause crack propagation
τ_{ij}	viscous shear stress
τ_{ij}^{R}	Reynolds-stress tensor
φ	angle made with impact bars after impact
χ	angle between particle path and radial vector
ω	rotational speed (rad/s)

1 Introduction

1.1 Background

Nearly two thirds of the world's harvested crop calories are from the grain crops of wheat (*Triticum aestivum* L.), rice (*Oryza sativa* L.), maize (*Zea mays* L.) and soybean (*Glycine max (*L.*) Merr.*) (Ray et al. 2013). Global crop demand in 2050 is expected to be double the 2005 production level because of a 2.3 billion (33%) increase in population and greater per capita income (Tilman et al. 2011). To meet this increased demand, increasing crop yield rather than clearing more land has a lower environmental impact (Tilman et al. 2011). However, the current rates of yield increases in maize, soybean, rice and wheat are insufficient to meet predicted demands without bringing more land into production (Ray et al. 2013). There are many factors that limit crop yield and these factors must be managed as a system if yields are to increase.

One factor that can considerably reduce crop yield is the infestation of crop fields with weeds, which compete with the crop for sunlight, nutrients and water (Rajcan & Swanton 2001). Traditionally, weed seedlings have been removed from crop fields using human, animal and mechanical means (tillage). Increasingly, over the past 40 years herbicides have largely replaced these methods because they efficiently and effectively remove weeds from the crop fields (Powles & Yu 2010). Furthermore, herbicides have helped enable conservation agriculture practices based on minimum soil disturbance and maximum residue retention by removing the need for pre-seeding tillage (Yu, Cairns & Powles 2007). Conservation agricultural techniques have revolutionised the production of cereal crops by reducing soil erosion, compaction, evaporation and fuel used for tillage, while increasing soil organic matter and water holding capacity (Kassam et al. 2009). The area of grain grown under conservation agriculture has reached 125 million ha and is growing at a rate of 7 million hectares per year (Friedrich, Derpsch & Kassam 2012).

The annual use of herbicides to control the weed problem provides selection pressure for weeds to evolve herbicide resistance (Powles & Yu 2010). As a result of an almost ubiquitous reliance on herbicides in many grain growing regions, herbicide resistance has been reported in 66 different crops and in 61 countries, for a total of 218 different weed species (Heap 2013). Thus, herbicide resistance threatens global food security (Powles & Yu 2010). In Australia one particular weed, annual ryegrass (*Lolium rigidum*), has become very difficult to control, developing resistance to both of the main broad spectrum herbicides, glyphosate and paraquat (Yu, Cairns & Powles 2007). Annual ryegrass also has demonstrated an ability to evolve multiple resistance to the three main residual herbicides prosulfocarb, triallate and pyroxasulfone (Busi & Powles 2013) that are applied pre seeding. Annual ryegrass is highly competitive with a crop for nutrients which causes significantly reduced yields (Goggin, Powles & Steadman 2012). The cost of annual ryegrass infestation in Australia is estimated to be in the hundreds of millions of dollars annually (Goggin, Powles & Steadman 2012). Thus, annual ryegrass was chosen as a focus weed for this thesis.

Alternative weed control methods are needed to reduce the selection pressure for herbicide resistance (Walsh & Powles 2007). Some alternative weed control methods include, increasing crop competition, delayed seeding and returning to tillage while losing the gains made through adopting conservation agriculture (Walsh, Newman & Powles 2013). These alternative weed control methods target weed seedlings. Inevitably, some weed seedlings are likely to survive any control measure applied to the seedling, herbicide or otherwise (Walsh, Newman & Powles 2013). The surviving weeds mature with the crop and produce high quantities of seed, which replenish the weed seedbank (Walsh, Newman & Powles 2013). The annual replenishment of the weed seedbank ensures that each year a high number of weeds emerge, perpetuating the weed problem (Walsh, Newman & Powles 2013). There is a need for methods to prevent weed seeds from replenishing the seedbank to compliment any methods used to control weed seedlings (Walsh, Newman & Powles 2013; Walsh & Powles 2007).

A new paradigm in weed control has begun in Australia with a focus on methods that achieve Harvest Weed Seed Control (HWSC) (Walsh, Newman & Powles 2013). The combine harvester residues are known to contain a high proportion of weed seeds that are normally spread back onto the field and, thus replenish the weed seedbank (Petzold 1956; Shirtliffe & Entz 2005; Walsh & Powles 2007). HWSC methods intercept the

dispersal of weed seeds by collection or processing of crop residues. HWSC methods include burning windrows of straw and chaff material, chaff collection with a chaff cart and direct baling of residues (Walsh, Newman & Powles 2013). HWSC methods have provided effective control of a range of weed species that have not shed seeds prior to harvest (Walsh, Newman & Powles 2013). One issue with all three of these methods is that they remove crop residues from the field, which goes against the philosophy of conservation agriculture (Walsh, Harrington & Powles 2012). Furthermore, each method requires a post-harvest operation to either burn or remove the crop residues. The emissions from burning residues have an environmental impact and both burning and removing residues has associated labour costs. An alternative HWSC method that retains all residues and does not require post-harvest operation is to mill the residues sufficiently to devitalise any weed seeds.

The Harrington Seed Destructor (HSD) (Figure 1.1) is a recently commercialised HWSC method which mills the chaff residue fraction with a cage mill as it exits a combine harvester (Walsh, Harrington & Powles 2012; Walsh, Newman & Powles 2013). Over 90% of weed seeds within the chaff fraction are damaged sufficiently during the milling process that they are devitalised (Walsh, Harrington & Powles 2012). The HSD uses a blower fan to collect the chaff material exiting the harvester sieve, as shown in Figure 1.2. The chaff is transferred pneumatically through a duct to a cage mill mounted on a trailer and driven by a 147 kW engine.

The HSD cage mill has two rotors, each with three concentric rows of cylindrical impact bars, as shown in Figure 1.3. The two rotors fit together and counter rotate at 1440 rpm. Chaff material enters at the centre of the inner rotor and is impacted at high speeds on each row of impact bars from alternating rotors. The HSD cage mill was adopted from the mining industry where it is primarily used for particle size reduction of friable materials that are significantly denser than chaff (Rodriguez et al. 2010). The HSD cage mill was modified from other cage mills by using flat rotor blades on the outer cage (Figure 1.3) to generate air flow through the mill (Harrington 2009). The air flow was essential to move the low density chaff material through the mill without blockage. A conveyor belt transfers the straw through to a chopper at the rear of the HSD. The processed chaff and straw are mixed and spread back onto the field with a chopper. The HSD has undergone three generations of development and is now being manufactured under licence.

Figure 1.1: Harrington Seed Destructor (HSD) attached to a CASE IH 2388

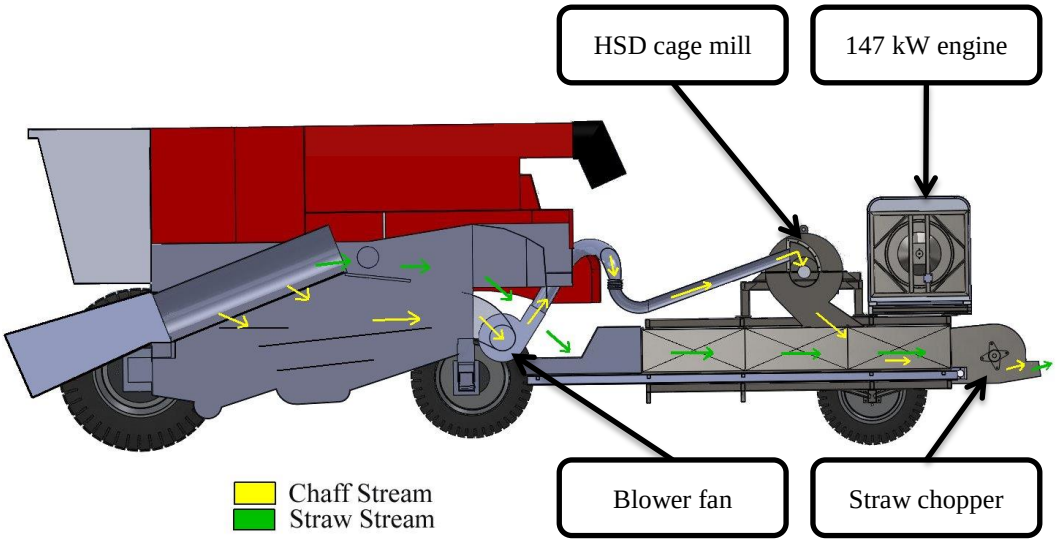

Figure 1.2: HSD material flow

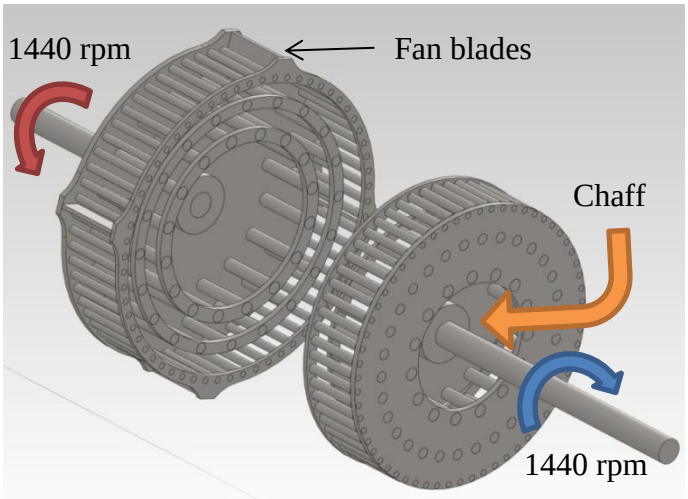

Figure 1.3: HSD cage mill with two rotors separated

The HSD is a complex machine with multiple moving components, a high power requirement and high purchase cost. Additionally the HSD weighs approximately 5 tonnes adding a considerable load to the harvester's drive train. The majority of the HSD's complexity is in the transfer of both chaff and straw residues. If a machine was

developed that could integrated the milling process into a combine harvester, the machine could be much simpler and cheaper than the HSD, and more readily adopted by farmers. The HSD cage mill does not suit being integrated into the harvester because it has a complicated counter rotating drive, weighs over 1 tonne with its support frame, has a high power requirement and has a small feed inlet of 300 mm diameter.

1.2 Project goal

The goal of this project was to simplify the process of mechanically devitalising weed seeds by developing and optimising a prototype mill that could be integrated into and powered by a combine harvester. The prototype mill had to:

- devitalise more than 90% of a key weed species annual ryegrass (*Lolium rigidum*)
- have a low enough power requirement to be driven from the harvester engine (< 100kW);
- move sufficient air as to not affect the harvester sieve performance (> 3 m^3/s);
- not significantly alter the material motion on the sieve area;
- handle high mass flow of chaff material (11 tonnes per hour);
- be of a size that fits within the current harvester framework less than 1500 wide, 800mm long and 400mm deep;
- be of a mass that does not significantly stress the harvester's frame (< 500kg);
- be able to be simply driven from the harvester's drive system.

The approach taken to develop the prototype mill was to use modelling to predict the performance of a mill design prior to construction.

1.3 Thesis statement and contributions

This dissertation contributes to the field of engineering of agricultural machinery. Specifically it introduces a modelling approach to milling harvest residues to devitalise weed seeds by developing a cross disciplinary research approach from weed science and

comminution (particle size reduction) science. The primary objective of this thesis was to test the hypothesis that:

The devitalisation of annual ryegrass (Lolium rigidum) seeds processed with an impact mill along with wheat chaff, can be predicted by developing and combining:

1) *a material function specifying the devitalisation of seeds exposed to impact loads;*

2) *a machine function specifying the impact loads generated within an impact mill based on the mill design and operating conditions.*

This hypothesis is assessed in this thesis by evaluating the current HSD cage mill and two new prototype impact mills that were designed based on the prediction of annual ryegrass seed devitalisation found in this thesis.

1.3.1 Objectives

1) Determine a mastercurve that predicts the devitalisation of annual ryegrass seeds based on the number of impacts and impact speeds; entitled the material function.

2) Develop a method to predict the number of impacts, impact speed and power consumption based on the design and rotational speed of an impact mill; entitled the machine function.

3) Combine the material and machine function to predict the devitalisation of annual ryegrass seeds processed with an impact mill.

4) Use the prediction to design two new mill designs that are able to fit within the constraints of a combine harvester and efficiently devitalise annual ryegrass seeds.

5) Validate predictions of seed devitalisation by experimentally evaluating the existing HSD cage mill technology and the two new mill technologies.

6) Determine the mass flow rate of wheat chaff to be processed with a weed seed devitalisation mill.

7) Determine the power consumption of the existing HSD cage mill technology and the two new mill technologies.

8) Compare the two prototype mill designs based on the devitalisation achieved and the power consumed.

1.3.2 Research approach

1.3.2.1 *Initial experimental testing*

The research commenced with a review of relevant literature. The review showed the importance of harvest time weed control (HWSC) and the need for new milling technology suitable for devitalising weed seeds in chaff and attaching to a combine harvester. The most important performance criteria was the ability of an impact mill to devitalise weed seeds. Seed devitalisation of the existing HSD cage mill was first determined by processing wheat chaff laced with annual ryegrass seeds. Seed devitalisation was measured by comparing the emergence counts of the processed samples to unprocessed control samples in indoor controlled environment soil bins. The evaluation method was validated by comparing results to published data.

The literature review showed that the power and weight of combine harvesters are finely tuned and harvest timeliness is crucial. Therefore, the power requirement of an attached weed seed devitalisation mill was a critical performance parameter that would determine how an integrated mill would affect harvester performance. The literature review also identified that there was a need to determine the wheat chaff mass flow required to be processed by a mill on a modern combine harvester. Field trials of the HSD were performed to determine the power used to process the chaff material and the mass flow of chaff that the HSD cage mill must process.

1.3.2.2 *Modelling seed devitalisation*

Modelling was used to firstly understand the mechanisms that enable the HSD cage mill to devitalise seeds, and then to develop two new prototype mills for attaching to a combine harvester. The literature review showed that particle size reduction using an impact mill has been modelled by separating the process into a material function and a machine function. The devitalisation of weed seeds using an impact mill was similarly split into a material and machine function in this thesis, as per Figure 1.4. The material function specifies the probability a seed is devitalised based on the number of impacts

and impact speeds it is exposed to. The machine function specifies the number of impacts and impact speeds imparted on a particle in a particular design of impact mill. Seed devitalisation can be predicted for a particular mill design and operating conditions and a particular seed species by combining the material and machine function.

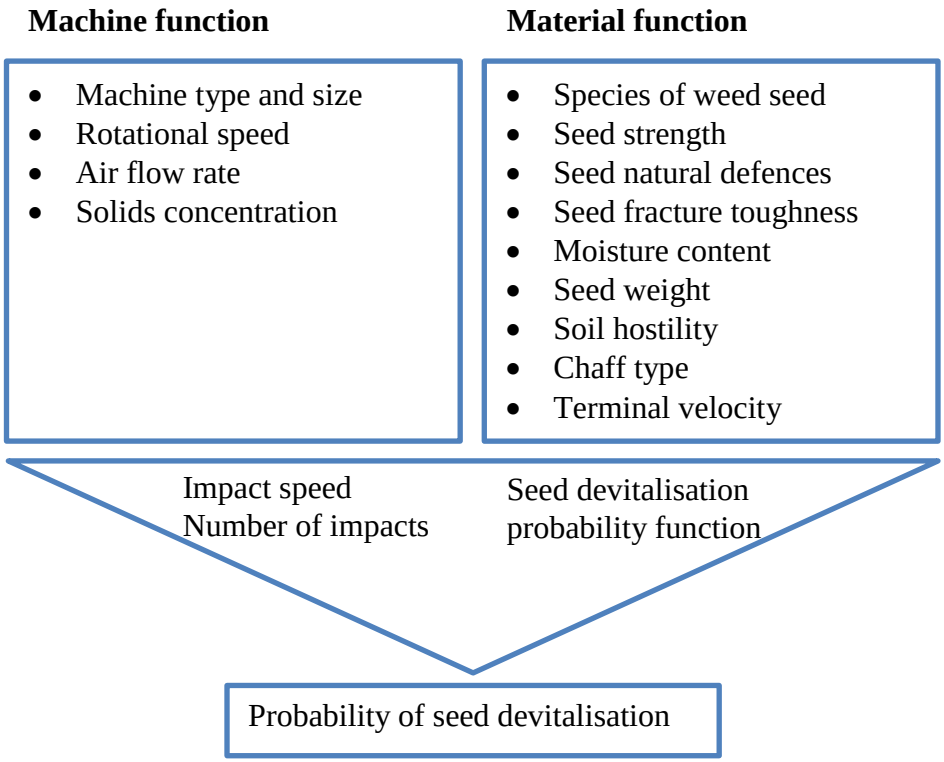

Figure 1.4 Isolation of machine and material functions for the process of reducing seed germination in a chaff stream, modified from Vogel and Peukert (2003a)

The literature review identified that the material function can be found by using single particle impact testers. In this thesis, the material function for weed seed devitalisation was determined by using a rotational impact tester that applies a single sided impact to individual seeds. Annual ryegrass seed devitalisation was evaluated by comparing the emergence of processed samples to unprocessed samples in indoor, controlled environment soil bins. A mastercurve was created that accurately described the probability of seed devitalisation based on number of impacts and impact speed.

The literature review identified that the machine function can be found using mechanistic modelling techniques that estimate the number of impacts and impact speeds based on the design of an impact mill. In this thesis, two different mechanistic approaches were developed to find a machine function for the HSD cage mill: a theoretical vector impact model; and a computational fluid dynamics (CFD) impact model.

The theoretical vector model was based on the two-dimensional geometry of the HSD cage mill. Impact trajectories were calculated using the angle of impact bars, rotational speed, and the coefficient of restitution.

A computational fluid dynamics (CFD) impact model was developed using the two-dimensional CAD geometry HSD cage mill. Initially the continuous fluid phase (air) was solved to determine the motion of air through the mill and the air pumping effect of the mill. Discrete particles were then entered into CFD model used the aerodynamic properties of the annual ryegrass seeds, and the non-spherical particle drag modelling found in literature. The aerodynamic properties of annual ryegrass seeds was determined using the terminal velocity testing of seeds as part of using the CFD method.

The material and machine function were combined to predict seed devitalisation using the HSD cage mill. The prediction of seed devitalisation using both the vector impact model and CFD impact model was very similar to the experimental measurements. Furthermore, the vector impact model was able to accurately predict the specific power consumption of the HSD cage mill. Thus, the modelling method was validated for further use to develop prototype mills.

1.3.2.3 *Concept design*

A concept design of an impact mill integrated into a combine harvester was the basis for the development of two new prototype mill designs described in this thesis. The focus combine harvester was a CASE IH 9120 Axial Flow, which is marketed as a Class 9 harvester; it has a rated engine power of 360 kW and a maximum engine power of 390kW (CASE IH Agriculture 2011). The prototype mill needed to process the chaff fraction that exits the combine harvester. The prototype had to be able to be retrofitted onto the harvester without major modification of the harvester. The space available on the CASE IH 9120 where the chaff and straw exits the harvester was limited to the area between the harvester sieve and straw spreaders, as shown in Figure 1.5. The chaff pan was to be removed and the prototype mill was to fit in that space. The space available was approximately 800 mm between the spreaders and the harvester chassis and 1500 mm across the width of the harvester.

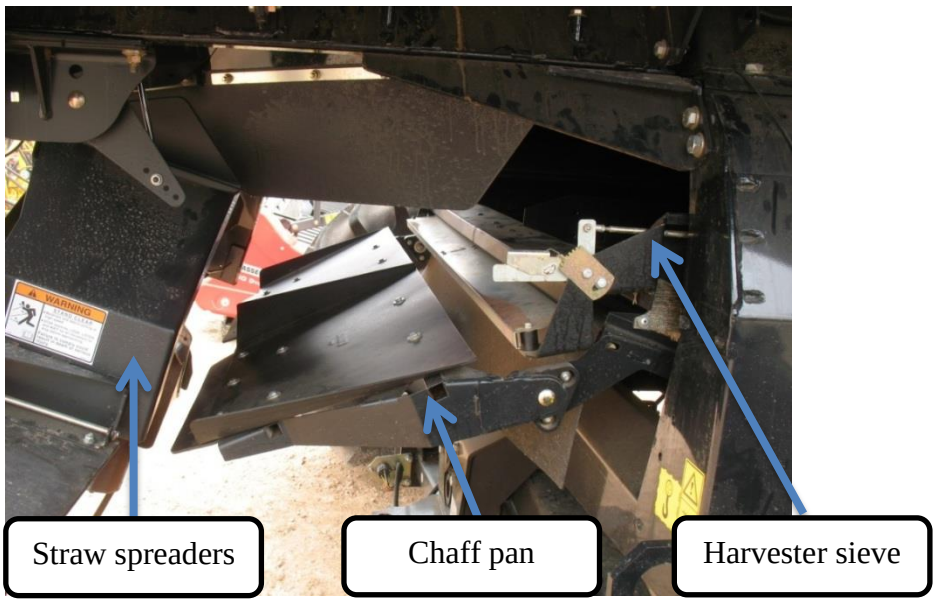

Figure 1.5: Unmodified CASE IH 9120 chaff pan and straw spreaders

A solution was to sit two mills side by side behind the chaff sieves, as shown in Figure 1.6. Simple inlet chutes into each mill split the material from the sieve without significantly altering its motion (a project goal). To prevent restricting the harvester sieve air flow, it was important for the two mills to generate significant air flow; upwards of 3 m^3/s was desired as a project goal. The mill air flow was also important in ensuring it could handle high mass flow of chaff without blockages, as was found with the HSD cage mill.

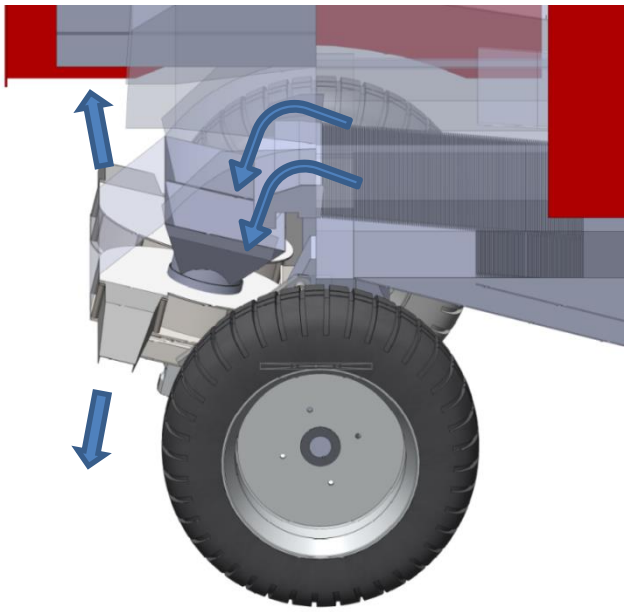

Figure 1.6: Concept design showing the location for an integrated prototype mill

Once the modelling technique had been validated with the HSD cage mill, new mill designs were modelled. The theoretical impact vector model was used for the preliminary design of the first prototype mill (Prototype 1). The preliminary design included the number of rows of rotating and stationary bars and spacing between bars. The spacing was set sufficiently small that particles were unlikely to pass through a row of rotating or static bars without impacting a bar. The CFD impact model approach was then implemented to develop the finer design details through design iteration. The continuous phase solution was first investigated to develop a design that had at least 1.5 m^3/s per mill to not restrict the harvester sieve and to maximise chaff mass flow capacity. CFD impact model particle trajectories were used to estimate seed devitalisation with the project goal to achieve at least 90%. A trial and error procedure was used to evaluate numerous different bar shapes, sizes, angles, and radial positions before settling on a final design for construction and testing Prototype 1.

1.3.2.4 *Prototype 1 design*

The Prototype 1 design was based on concentric rows of rotating and stationary bars, as shown in Figure 1.7. The rotor consisted of three inlet paddles and two rows of square hollow section (SHS) bars with rounded edges mounted on a large disk. The centreline of the outer rotor bars was on a 600 mm diameter. The stator consisted of two rows of flat bars angled 15^o against the rotation of the rotor to increase the normal component of impact making impacts with the stator more direct. Material is fed into the centre of the mill and is distributed by three paddles. The material was exposed to multiple impacts on the rotating and static rows before exiting the mill.

Prototype 1 was constructed and evaluated at the same equivalent chaff mass flow as the HSD cage mill 3.6 t/h and at a higher mass flow of 10.8 t/h (total for two mills). The higher chaff mass flow was much more representative of the throughputs expected on a modern combine harvester based on the data collected from field testing of the HSD. A pair of Prototype 1 mills were attached to a CASE IH 9120 combine harvester and field tested in wheat (Figure 1.8) at grain throughputs up to 40 t/h and chaff throughputs up to 12.4 t/h. The power to drive the Prototype 1 mills was evaluated along with the mass flow of chaff.

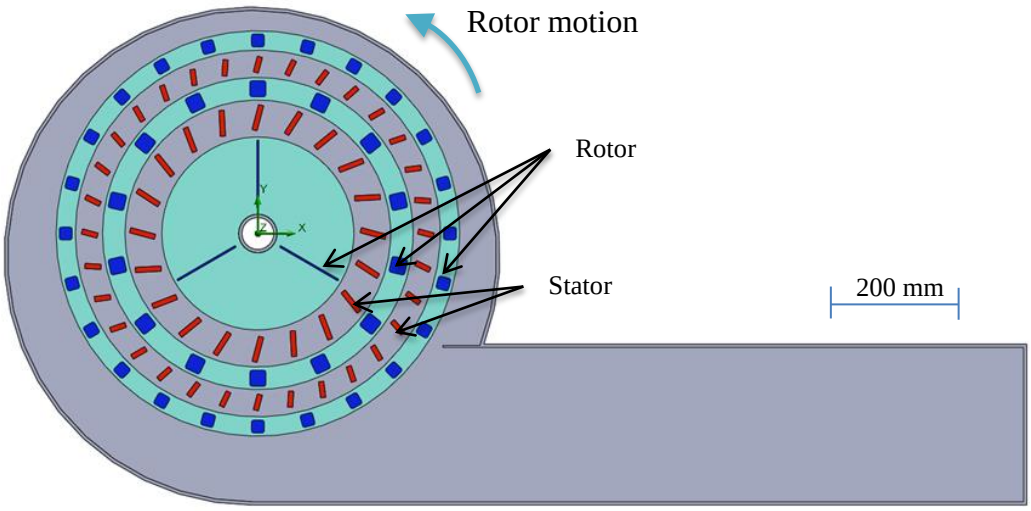

Figure 1.7 Cross section of Prototype 1: two rows of rotor bars, two rows of stator bars

Figure 1.8: a) CASE IH 9120 with two Prototype 1 mills attached (left) b) harvesting wheat at approximately 40 t/h grain throughput (right)

From testing the Prototype 1, a few issues were discovered:

1) Seed devitalisation reduced at the higher chaff mass flow.

2) Wear was likely to limit the life of the mill because the rotor bar wall thickness was thin (1.6-2 mm).

3) Material exited the mill at very high speed and, thus there was likely some remaining kinetic energy that was not used for seed devitalisation. Furthermore, material exiting at high velocity was hazardous. If a foreign object passed through the mill it could become a dangerous projectile and the chaff material impacted the ground at such speed that it generated a lot of dust.

1.3.2.5 *Prototype 2 design*

To mitigate some of these issues with the Prototype 1 design, a Prototype 2 design was developed. The same vector and CFD modelling techniques were used to develop the Prototype 2 design. The CFD modelling technique identified that it was the rounded edges and large side wall area of the Prototype l that were causing some of the material to stagnate in the mill. This meant that there could be more inefficient particle to particle impacts in these zones. To reduce the amount of particle to particle impacts the material had to pass through the mill more quickly. A design was sought that provided as close to one impact on each row of impact bars as possible. To achieve this, the rotor bars were replaced with 6 mm flat bar, which gave the rotor a sharp edge and far less side wall area than the Prototype 1. Using the 6 mm flat bar also gave higher potential wear life than using the (SHS) of the Prototype 1 because it was three times as thick. To reduce the velocity of material exiting the mill and, thus to reduce the amount of wasted energy, an extra stator row was used. In this way, the kinetic energy that material gained on the last rotating row is effectively used for seed devitalisation by impacting the outer static row.

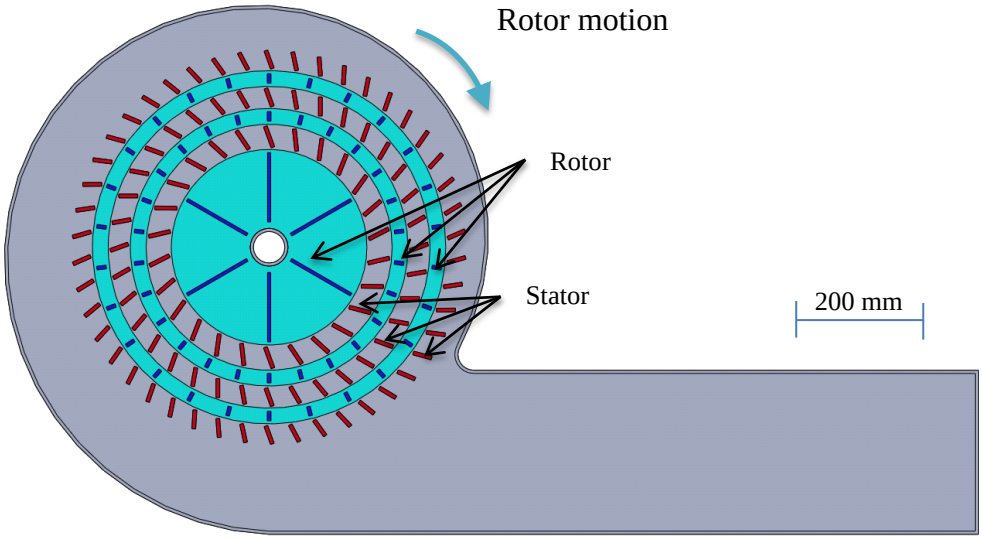

Figure 1.9 Cross section of Prototype 2: two rows of rotor bars, three rows of stator bars

The Prototype 2 was also based on concentric rows of rotating and static bars, as shown in Figure 1.9. The rotor consisted of 6 inlet paddles and two rows of flat impact bars. The stator consisted of three rows of flat bars angled 20^{o} against the rotation of the rotor to maximise direct impact. The same size housing was used for Prototype 2 as was used for Prototype 1. Thus, to fit the extra stator row, both the rotor and stator was reduced in

diameter compared to Prototype 1. The centreline of the outer rotor bars was on a 535 mm diameter. The Prototype 2 seed devitalisation was evaluated using the same method as Prototype 1. To date, the power consumption of Prototype 2 has only been evaluated in the lab and is awaiting field evaluation.

1.3.2.6 *Summary*

This study showed that the devitalisation of annual ryegrass seeds can be predicted through combining a material and machine function. The predictive methods developed provide a backdrop for future development of seed destruction systems for targeting different weed species or attaching to different harvesters. The two prototype mills that resulted from this study are significant advancements over previous technology. The new designed for purpose mills, have resulted in a provisional patent being filed for the protection and commercialisation of this novel technology.

1.3.3 Thesis structure

In this thesis, the multitude of vector and CFD impact models used to finalise the two prototype designs have been omitted; only the impact models of the existing HSD cage mill and the two prototypes are described along with experimental validation. The thesis is structure has 5 chapters. After a literature review (Chapter 2), the experimental and modelling methods are described (Chapter 3), the results are shown (Chapter 4) and concluded on (Chapter 5). The methods and results chapters are both structured based on the levels of testing performed and are split into:

1) Impact testing to find the material function for annual ryegrass seeds;
2) Vector and CFD impact modelling to find the machine function for the HSD cage mill, Prototype 1 and Prototype 2;
3) Seed devitalisation testing for the HSD cage mill, Prototype 1 and Prototype 2;
4) Field testing of the HSD cage mill and Prototype 1 for power and chaff throughput and lab testing of the Prototype 2 for power.

2 Literature review

2.1 Overview

The literature review begins with the workings of a combine harvester and where weed seeds travel within the harvester. The proportion of weed seeds exiting the harvester in the residues was identified. The review covers currently adopted Harvest Weed Seed Control (HWSC) technologies and the need for new harvest weed seed control strategy based on milling technology. The previous research on using milling to devitalise weed seeds was reviewed. The milling process was looked at in terms of a more widely researched area of particle size reduction (comminution). The review identified theory of milling and the important factors that determine the milling outcome. Finally, research on modelling impact mills using a material and machine function was reviewed.

2.2 Combine harvester

2.2.1 Operation

The modern combine harvester is a sophisticated machine that collects crop material and separates grain from material other than grain (MOG). The functional components of a combine harvester are shown in Figure 2.1.

The operation of the combine harvesters was detailed by Srivastava et al. (2006) and is summarised as:

- The header either cuts and collects the crop or picks up a wind-row of cut crop.
- The feeder house conveys the cut crop to the thresher.
- The crop material is forced between the threshing cylinder and concave where impact, compression and shear forces detach the grain from the heads. Small material which includes 70-90% of the threshed grain falls through the concave grate onto the cleaning shoe.

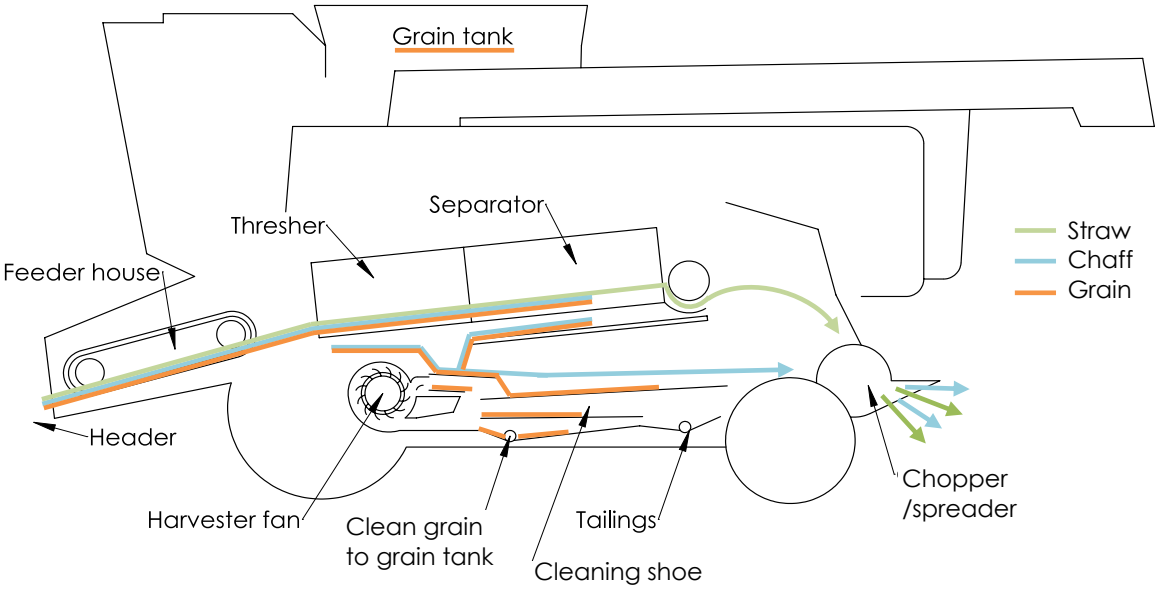

Figure 2.1: Diagram of a combine harvester showing the three main material streams

- The remaining larger material, including mostly straw moves to the separator. The separator removes the remaining grain from the straw material and transfers the grain to the cleaning shoe.

- The cleaning shoe performs the last separation of grain from material other than grain (MOG) using a combination of aerodynamic separation and mechanical sieving. The cleaning shoe uses a set of oscillating sieves with air passing through to mechanically separate large material and pneumatically separate low terminal velocity material from the grain. Clean grain passes through the whole sieve set. Material that has sufficiently high terminal velocity to travel through the first set of sieves but is too large to travel through second set of sieves (ie. un-threshed heads) is referred to as tailings and is sent back for repeat threshing. The harvester sieve is setup with the vertical component of air velocity that is lower than the terminal velocity of the grain and higher than the terminal velocity of the chaff. The grain falls through the sieve against the air flow, and the chaff is pneumatically conveyed out of the harvester. For wheat, the terminal velocity varies considerably from the different conditions, as shown in Table 2.1. Therefore, harvesters need to be setup specifically for the variety, moisture content and other harvester variables.

Table 2.1: Wheat grain terminal velocity of different researchers

Reference	Terminal velocity (m/s)
(Bilanski & Lal 1965)	8.8-9.2
(Uhl & Lamp 1966)	5.7-9
(Shellard & MacMillan 1978)	7.5-8.5
(Gorial & O'Callaghan 1990)	6.5-10
(Khoshtaghaza & Mehdizadeh 2006)	6.8-8.6
(Rajabipour, Tabatabaeefar & Farahani 2006)	6-7.3

- Clean grain is sent to the grain tank via a clean grain elevator and auger. The grain tank stores clean grain while harvesting and then when it is full, grain is unloaded through an auger.

- The straw residue that exits the separator is often cut smaller and spread evenly onto the field with a straw chopper. Reducing the size of straw residues is important to prevent blockages when seeding with a no-tillage implement. The chaff material that exits the cleaning shoe is either spread onto the field with chaff spinners or a straw chopper.

The combine harvester's grain throughput capacity has been characterised by manufacturers using a class system. The harvester class system in the past has been based on harvester power, cleaning area and threshing area (White 2010). However, manufacturers market their harvester's class based on engine power alone, as shown in Table 2.2. The grain throughput capacity of combine harvesters has grown substantially over recent years, which aligns with demand for larger capacity harvesters. In Australia, the largest growing sector of combine harvester sales is harvesters with more than 280 kW (Saunders 2012). In 2011, more than half of harvesters sold had more than 280 kW (Saunders 2012).

Table 2.2: Harvester class specification, from White (2010)

Harvester class	Engine power (hp)	Engine power (kW)
7	350-400	261-289
8	400-450	298-336
9	450-500	336-373
10	500-550	373-410

2.2.2 Combine harvester and weed seeds

The combine harvester is known to cause significant dispersal of weed seeds (Shirtliffe & Entz 2005). The combine harvester collects weed plants and seeds that are higher than the cutting height of the header. The retention of weed seeds at harvest time at a

height that allows collection by a combine harvester was greater than 50% in many studies (Walsh, Newman & Powles 2013), as shown in Table 2.3.

Table 2.3: Proportion of total weed seed retained at harvest. Data collated by Walsh, Newman and Powles (2013)

Species	Seed retention (%)	Crop, Location	Reference
Ivy leaf morning glory (*Ipomea hederacea* L. Jacq. IPOHE)	75	Maize, US	(Davis 2008)
	85	Soybean, US	(Davis 2008)
Giant foxtail (*Seteria faberi Herrm.* SEFTA)	55	Soybean, US	(Davis 2008)
	65	Maize , US	(Davis 2008)
Prickly sida (*Sida spinosa* L. SIDSP)	60	Soybean, US	(Davis 2008)
	80	Maize, US	(Davis 2008)
Velvetleaf (*Abutilon threophasti* Medik. ABUTH)	35	Maize, US	(Davis 2008)
	50	Soybean, US	(Davis 2008)
Wild oats (*Avena fatua*)	20	Wheat, Canada	(Shirtliffe, Entz & Van Acker 2000)
	50	Wheat, Canada	(Feldman & Reed 1974)
Annual ryegrass (*Lolium rigidum*)	96	Wheat, Spain	(Blanco-Moreno et al. 2004)
Chinese thomapple (*Datura ferox* L.)	90	Soybean, Argentina	(Ballaré et al. 1987)
Common lambsquarters (*Chenopodium album* L. CHEAL)	34 - 46	Maize, US	(Forcella, Peterson & Barbour 1996)
Leersiea orzoides (L), *Echinochloa* spp. *and Scirpus* spp.	95[a]	Rice, Italy	(Balsari, Airoldi & Finassi 1994)
Echinochloa spp. *Raphanus raphanistrum, Polygonum persicaria, Vicia sativa,Setaria glauca* and *Chenopodium* spp.	56[a]	Wheat, Italy	(Balsari, Airoldi & Finassi 1994)

[a] proportion of weed seeds combined for all species

The weeds that are above the cutting height are transported to the combine harvester's thresher. If the weed seeds are threshed or separated from the straw, the weed seeds end up on the cleaning shoe with the grain and chaff material. Weed seeds with a terminal velocity higher than the vertical component of air velocity through the sieve most likely end up in the grain tank. Weed seeds with a terminal velocity lower than the vertical component of air velocity through the sieve most likely exit with the chaff residues. Many species of weed seed have a terminal velocity lower than the grain being harvested such as wheat, as shown in Table 2.4. Therefore, many species of weed seeds are likely to be aerodynamically separated from the grain on the harvester sieve and, hence are returned to the soil along with chaff residues.

Table 2.4: Terminal velocity of wheat, chaff and a selection of weed species. Data from Kahrs (1994)

	Mass (mg)	Required velocity to separate (m/s)		Terminal velocity (mean) (m/s)	Standard deviation (m/s)	Coefficient of variation (%)
		1%	99%			
Triticum aestivum (wheat)						
> 2.8 mm	51.1	6.1	9.8	8.8	0.79	9.0
2.2 - 2.5 mm	28.2	5.7	8.7	7.7	0.68	8.9
< 2mm	11.6	4.5	7.5	6.4	0.7	11.0
Chaff	-	0.8	2.3	1.6	0.35	22.3
Weed species						
Matricaria recuita	0.06	1.1	2	1.6	0.24	14.4
Sonchus asper	0.25	1	2.7	1.8	0.39	20.0
Apera spica-venti	0.11	1.3	2.7	2	0.31	15.6
Capsella bursa-pastoris	0.1	1.4	2.8	2.4	0.27	11.4
Alopecurus myosursoides	1.82	1.5	4.1	2.9	0.48	16.8
Myostis arvensis	0.29	1.9	3.8	3.2	0.41	13.1
Cirsium arvense	0.7	1.3	4.7	3.3	0.85	25.9
Laminum purpureum	0.73	2.2	4.3	3.6	0.46	12.7
Setellaria media	0.5	2.4	4.6	3.7	0.52	14.1
Viola arvense	0.29	2.5	4.6	4	0.41	10.2
Chenopodium album	0.64	2	4.8	4	0.52	13.1
Atriplex patulum	1.07	2.8	4.8	4	0.47	11.8
Thlaspi arvense	1.27	2.7	5.2	4.2	0.48	11.5
Rumex crispus	1.35	3.6	4.9	4.4	0.29	6.5
Galeopsis tetrahit	4.57	2.7	5.8	4.9	0.58	11.7
Polygonum convolvulus	4.89	2.5	6.2	4.9	0.75	15.2
Avena fatua	22.54	3	6.2	5	0.52	10.5
Sinapis arvensis	1.9	4.4	6.9	6	0.41	6.8
Galium aparine	8.77	5.3	7.7	6.7	0.55	8.1
Convolvulus arvensis	22.36	3.8	9	7.8	1.1	13.6

The proportions that end up in the chaff fraction compared to the grain tank have been shown to vary greatly and depend on the weed species (Petzold 1956). The chaff stream has been found to contain 74% of wild oat (Avena fatua) seeds that dispersed by the combine harvester (Shirtliffe & Entz 2005), and up to 85% of annual ryegrass seeds were found in the chaff fraction (Walsh & Powles 2007). There is an opportunity to prevent much of the dispersal of weed seeds by the combine harvester by intercepting these residues, thus reducing the weed seedbank without using herbicides (Walsh & Powles 2007).

2.3 Harvest time weed control

The opportunity to capture weed seeds at harvest time has been long known (e.g. Roy & Bailey 1969). Harvest weed seed control (HWSC) is a term used to describe methods of non-chemically destroying or removing weed seeds contained in harvest residues (Walsh, Harrington & Powles 2012; Walsh, Newman & Powles 2013). HWSC methods prevent viable seeds from returning to the soil and, hence prevent replenishing the weed seedbank. Current HWSC methods include windrow burn, chaff cart, baling of residues and milling. The use of HWSC strategies in 17 fields over a 10 year period, has been found to deplete and stabilise the annual ryegrass density to less than 0.5 plants/m^2 (Walsh, Newman & Powles 2013). Whereas, using a herbicide focused weed strategy was found to deplete and stabilise the annual ryegrass density to 5-10 plants/m^2 (Walsh, Newman & Powles 2013). Achieving low weed density through depleting the weed seedbank reduces the weed's effect on crop yield and allows for management flexibility in seeding time, crop choice and herbicide usage (Walsh, Newman & Powles 2013). Furthermore, maintaining low weed densities helps prevent the evolution of herbicide resistant weeds (Walsh, Newman & Powles 2013). Thus, HWSC methods are able to help sustain the current herbicide resources and to reduce the impact of weeds on a farming system.

2.3.1 Windrow burn

Windrow burning is the most widely implemented HWSC method adopted in Australia with an estimated 70% of grain growers using this method in Western Australia (Walsh, Newman & Powles 2013). Windrow burning is widely adopted because it very cheap and simple to setup on a harvester (Walsh, Newman & Powles 2013). A narrow chute is attached to the rear of the harvester to drop straw and chaff material into a narrow windrow, as shown in Figure 2.2. The windrows are later burnt when the conditions permit. To devitalise 99% of seeds within the windrows requires the temperature in the windrows to reach 400^{o}C for 10 seconds for annual ryegrass or 500^{o}C for 10 seconds for wild radish (*Raphanus raphanistrum*) (Walsh & Newman 2007). Factors such as wind, windrow width, summer rain and stock disturbing windrows all have the potential to affect the temperature and, hence efficacy of windrow burning (Walsh & Newman 2007). In ideal conditions, seed devitalisation of up to 99% of ryegrass seeds and 96% of wild radish seeds has been achieved (Walsh & Newman 2007).

Figure 2.2: Creating windrows using narrow chute. (Photo courtesy of A & R Messina)

2.3.2 Chaff cart

Chaff carts are towed behind the combine harvester and are used to collect the material that exits the harvester sieve (chaff), as shown in Figure 2.3. Chaff carts were initially used in Canada over 30 years ago to collect chaff for livestock feed (Olfert et al. 1991). Chaff carts are now a common method of HWSC used in Australia (Walsh, Newman & Powles 2013).

Figure 2.3: Riteway Farming Australia chaff cart attached to a New Holland TX 66 combine harvester

The chaff cart attachment consists of a separator baffle, one or two blower fans and a tow-behind cart. A schematic of the separator baffle and blower fan attachments are shown in Figure 2.4. The separator baffle splits the chaff stream from the straw stream. The blower fans propel the chaff material into a tow-behind cart. When the cart is full, the chaff is dumped in piles in the field, as shown in Figure 2.5. In a subsequent

operation, the chaff piles are either burnt or fed to livestock prior to the next crop being planted (Walsh, Newman & Powles 2013).

The chaff material collected is made up of threshed material that: falls through the concave and separator; is larger than the sieve opening or has a lower terminal velocity than the sieve's vertical component of velocity. The wheat chaff material includes broken straw material and material surrounding the seed such as the rachillas (stem holding florets), lemmas and paleas (surrounding seed). The relative mass flows of the chaff, straw and grain streams when harvesting wheat were estimated using data from Newman (2012), as shown in Figure 2.4. The relative mass flows are expected to vary considerably with crop variety, harvest moisture content, harvester model and harvester setup. The total mass flow of material depends largely on the capacity of the harvester. For example, a modern combine harvester cutting 65 t/h of crop material (typical for Class 7-8), there would be approximately 38 t/h of grain, 11 t/h of chaff and 16 t/h of straw material.

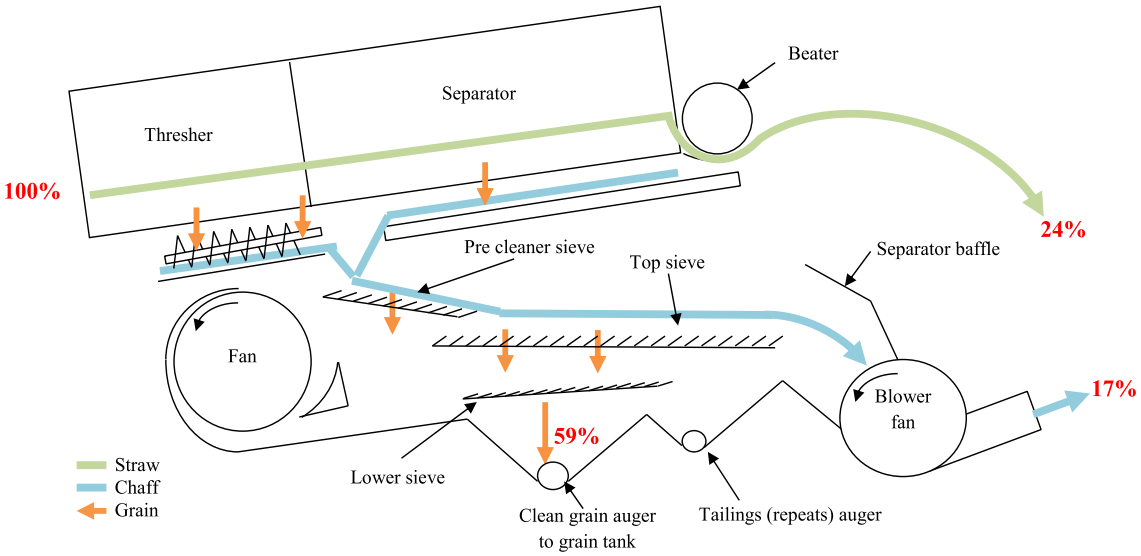

Figure 2.4: Cross section of harvester threshing, cleaning and separating units with chaff cart attachment. Relative mass flows of grain, chaff and straw when harvesting wheat are shown based on data from Newman (2012).

Figure 2.5: Wheat chaff piles left by a chaff cart to be burnt in autumn

2.3.3 Baling of residues

The third HWSC method is baling of crop residues at or after harvest. The simplest way to implement baling of harvest residues is to drop the straw and chaff into a narrow windrow and later use a baler to pick up the windrows. This method provides an opportunity for weed seeds to reach the ground before baling and remain in the field after baling. To prevent seeds from reaching the ground, the Glenvar Bale Direct System™ (Figure 2.6), directly attaches a large square baler to a combine harvester (Walsh, Newman & Powles 2013). The Glenvar Bale Direct System™ directs both the chaff and straw residues that exit the harvester into an inlet chute and a conveyor belt moves the residues to a tow-behind baler. The baler is driven hydraulically from the harvester's engine. The bales are generated while the harvester is running and automatically drop when they are finished. The bales are later collected. The bales contain the weed seeds that were in the chaff and straw residues. The bale direct system collects around 95% of annual ryegrass seeds (Walsh & Powles 2007). This system can be highly profitable if there is a market for the bales. However, it is often the case for many farmers that it is not economical to sell the straw due to lack of market or distance to market (Walsh, Newman & Powles 2013).

Figure 2.6: Glenvar Bale Direct System™

2.3.4 Disadvantages of current systems

The windrow burn, chaff cart or baling HWSC systems all require post-harvest operations and, hence a labour expense to remove or burn the residues. Importantly, removing or burning residues is contrary to conservation agriculture practices as crop residues provide protection against soil erosion, retain soil moisture and return nutrients to the soil (Kassam et al. 2009). There are a number of intangible benefits that are lost when removing residues but the value of removed nutrients has been estimated. Chaff carting and windrow burning remove nutrients such as nitrogen and potassium from the field; a loss which has been valued at $13.20/ha for chaff carts and $43.00/ha for windrow burning in wheat crops yielding 3-4.5 t/ha (Newman 2012). Windrow burning and similarly baling residues have a higher value of lost nutrients because more residue material is removed (chaff and straw) compared to the chaff cart (chaff).

The burning of wheat straw material also releases air pollutants such as particulates and greenhouse gasses (Li et al. 2007). If conditions permit smoke to reach residential areas, burning residues can cause serious health effects for people with respiratory problems (Smil 1999). Furthermore, the smoke can reduce visibility on roads making them highly dangerous (Smil 1999). As a result crop residue burning has been banned in some regions around the world and will not remain a viable weed control option (Smil 1999).

2.3.5 Alternative methods

There are some potential alternatives to burning or baling harvest residues to control weed seeds while keeping the residues in the field. The waste heat of the harvesters exhaust gas can devitalise annual ryegrass seeds (Matthews, J.M et al. 2004). However, given that to devitalise annual ryegrass takes 10 seconds at 400^{o}C (Walsh & Newman 2007), such a method is unlikely to be able to handle the throughput of harvest residue material of a modern combine harvester. Furthermore, harvesters are already a significant fire risk and heating harvest residues to high temperatures would likely increase this fire risk. Another alternative method would be to use microwaves to devitalise seeds (Barker & Craker 1991). However, using microwaves to devitalise seeds also requires long residence times and would be unsuitable on a large harvester; for example, 30 s at above 80^{o}C is needed to devitalise for oats (Avena sativa L.) using microwaves (Barker & Craker 1991). Herbicides can also be directly applied to seeds to provide control of weed seeds (Stone, Peeper & Solie 2001) but this provides selection pressure for herbicide resistance of the applied chemical. Mechanically damaging seeds to prevent germination is currently the most feasible method of controlling weed seeds in harvest residues while keeping the harvest residues and is described in the next section.

2.4 Devitalising seeds using mechanical damage

An alternative HWSC method is to process crop residues as they exit a combine harvester with a mill to damage and devitalise weed seeds within the residues. The milled residues can be spread onto the field providing weed control without removal of valuable crop residues making it fit with conservation agriculture practices (Walsh, Harrington & Powles 2012). Moreover, the milling of residues does not require any post-harvest operation.

The potential for mechanical control of weed seeds at harvest time by milling harvest residues has been identified by a number of individuals. This has resulted in a small number of patents and publications. However, only recently has mechanical control of weed seeds become a commercial reality with the Harrington Seed Destructor (HSD) (Walsh, Newman & Powles 2013).

2.4.1 Effect of mechanical damage to seeds

It has been long known that seeds are susceptible to mechanical damage. Seeds that have undergone physical damage due to impact or attrition can be devitalised because of two factors: disruption of seed tissue, which reduces the seed's ability to maintain metabolic activity, permit germination and allow establishment (Slagell Gossen et al. 1998); and reduction of the seed's natural barriers, which makes the seed susceptible to fungi and phytonematodes (Davis et al. 2008; Slagell Gossen et al. 1998).

Disrupting the seed's tissues sufficiently to prevent metabolic activity and germination may require considerable damage (Hauhouot et al. 1998). Whereas, the seed's persistence in the seed bank can be reduced with only slight damage sufficient to reduce the seed's natural protective barriers (Davis et al. 2008). Therefore, the weed seed bank can be controlled without needing to grind seeds into fine particles (Davis et al. 2008). In practice, it has been found that damaging seeds has a more profound reduction in germination of seeds planted in field soils where seeds are vulnerable to attack than seeds planted in germination trays (Hauhouot et al. 1998). Damaged seeds planted in greenhouse pots where the seed is subject to some soil hostility but less than field hostility had a germination response that was lower than the germination trays and higher than the field soils (Hauhouot et al. 1998). The level of mechanical damage to prevent germination in germination trays may be more than is needed to provide both reduced germination in the field and reduced persistence of seeds in the seedbank.

2.4.2 Seed targeting locations

Different locations within the harvester have been used by researchers to target weed seeds for mechanical control. Processing all the residues (chaff and straw) exiting a combine harvester with a mill would require an inordinate amount of power. Therefore, sieving separation has been used to reduce the amount of material that must be processed with the weed seeds.

One approach was to separate weed seeds from the grain. A patent was filed in 1969 on a weed seed grinder that was to be attached to the outlet of a weed seed separator was the Hart Scour Kleen (Roy & Bailey 1969). Weed seed separators have been used on older harvesters at the top of the clean grain elevator to separate weed seeds and small grains from the clean grain. Some research on mechanical seed devitalisation has suggested that cheat (*Bromus secalinus L.*) could be separated from wheat because of its

lower mean terminal velocity of 3.14 m/s (range: 1.8 - 4.5 m/s), compared to 7.84 m/s (range: 5.79 - 9.81m/s) for wheat (Hauhouot-O'Hara et al. 2000). However, the combine harvester cleaning sieve is usually setup to aerodynamically remove chaff material with terminal velocity lower than wheat. Therefore, the cheat seed is likely to leave the harvester in the chaff fraction and be spread onto the field. Weed seeds in the grain tank are removed from the field with the grain. The weed seeds in the grain are not returned to the field so long as the seed is properly cleaned before planting the following crop. Consequently, targeting weed seeds in the grain tank does not prevent any more seed dispersal than an unmodified modern combine harvester.

Another approach was to use extra sieves to separate weed seeds from the grain and chaff material as used by Reyenga (1991), Balsari, Airoldi and Finassi (1994) and by Zani (2001). One method was to attach two sieves into a conventional harvester; one placed between the grain pan and the concave and one placed beneath the walker return (Balsari, Airoldi & Finassi 1994). The sieves were flat with 3 mm round holes and were used to collect weed seeds falling through the sieve and allowed grain to continue above the sieve (Balsari, Airoldi & Finassi 1994). Therefore, only weed seeds that were significantly smaller than the grain would be collected by the sieve (Balsari, Airoldi & Finassi 1994). The total collection (Table 2.5) was more effective in rice and soybeans than in wheat because of the larger size difference between the grain and weed seeds (Balsari, Airoldi & Finassi 1994).

Another method was developed by Harvestaire Pty Ltd. called the Rotomill (Zani 2001), which used a Ryetec sieve (Jaeschke 1994) to reduce the amount of material processed by the mill. The Ryetec system used a sieve at the rear of the cleaning shoe to separate weed seeds from chaff material. The Ryetec sieve reduced the stream of material that contained the weed seeds down to approximately 20% of the total chaff stream (Holding, Stewart & Sutherland 2006). The annual ryegrass seed collection of the Ryetec seed catching system is shown in (Table 2.6). In legumes, more annual ryegrass passed through the harvester un-threshed because the harvester is setup with lower threshing speed (Matthews, J.M. et al. 1996). Reduced annual ryegrass collection (Table 2.6) was found for peas because un-threshed ryegrass does not easily fall through the Ryetec sieve. The results in Table 2.5 and in Table 2.6 show that sieving to collect weed seeds is possible. However, it does provide another means for the weed seeds to escape as not all the seeds are collected through the sieve.

Table 2.5: Weed seed collection using a sieve collection system in a conventional combine harvester. Data from Balsari, Airoldi and Finassi (1994)

Crop	Weeds present	Collection under concave	Collection under walkers	Collection in grain tank	Total collection
Wheat	135 kg/ha of: Echinochloa spp. Raphanus raphanistrum Polygonum persicaria Vicia sativa Setaria glauca Chenopodium spp.	34 kg/ha (25%)	22 kg/ha (16%)	20 kg/ha (15%)	76 kg/ha (56%)
Rice	120 kg/ha of: Leersia oryzoides (L) Echinochloa spp. Scirpus spp.	84 kg/ha (70%)	6 kg/ha (5%)	24 kg/ha (20%)	114 kg/ha (95%)
Soybeans	220 kg/ha of: Poligonum persicaria Chenopodium album	196 kg/ha (89%)	0.9 kg/ha (0.4%)	20.9 kg/ha (9.5%)	217.8 (99%)

Table 2.6: Ryetec seed catching system: percentage of total annual ryegrass in field. Data from Matthews, J.M. et al. (1996)

Crop	Entering harvester	Caught in Ryetec	Exiting harvester	In grain
Barley	89%	56%	26%	7%
Wheat	93%	63%	22%	8%
Peas	65%	20%	45%	0%

Modern harvesters now have considerably more capacity than the harvesters used at the time of Balsari, Airoldi and Finassi (1994) and (Zani 2001). Power and capacity of the largest combine harvesters has steadily increased from 50 kW in the year 1960 to 300 kW in the year 2000 (Kutzbach 2000). Since then, the harvester power has continued to rise with some manufacturers in 2013 now selling harvesters with over 400 kW of engine power. Correspondingly, sieving systems used to collect weed seeds would require considerably more mass flow capacity to operate on a modern harvester. Designing a Ryetech sieve capable of handling the high mass flow of residue material of large modern harvesters proved difficult (Holding, Stewart & Sutherland 2006) and, consequently, the concept has been put on hold (Zani 2012). The weed seeds that exit in the chaff fraction have a terminal velocity lower than grain or are too large to fall through the sieve. This condition is the same for chaff material and, hence the terminal velocity or the size of the weed seeds would be similar to the chaff material. Consequently, separating weed seeds from the chaff material can only rely on small

differences in size or terminal velocity. When there is a small difference in properties, separation takes more time and a larger sieving area; both time and space are limited in a modern combine harvester.

To minimise the risk of dispersing weed seeds by sieve losses, the entire chaff fraction can be intercepted and processed. The HSD is one machine that processes the entire chaff material flow (Walsh, Harrington & Powles 2012). Processing the entire chaff residue fraction rather than the reduced proportion as attempted by others required processing of a huge amount of material (≈ 11 tonnes per hour). Therefore, processing the entire chaff fraction requires a large amount of power.

There is an opportunity to reduce the amount of material processed by a mechanical destruction system compared to processing the whole chaff sample using sieving. However, significant engineering is needed to create a sieve that matches the capacity of a modern combine harvester and can fit within the harvester. At this time it was considered that to integrate mechanical weed seed control into a modern combine harvester, processing the entire chaff fraction is the most feasible approach.

2.4.3 Mill types tested

Different types of mills have been used to mechanically control weed seeds. A close tolerance, low speed cutting mechanism was used in the mill by Roy and Bailey (1969). Their mill processed relatively pure weed seeds separated from the grain (Roy & Bailey 1969). A rollermill has been proposed by Reyenga (1991), and evaluated by (Lyon & Rush 1993), (Hauhouot et al. 1998) and (Hauhouot-O'Hara et al. 1999). Rollermills use two counter rotating rollers that have a close tolerance to crush the material (Pfost 1976). If there is a speed differential between the rollers, there is a compressing and shearing action (Pfost 1976). Rollermilling has been found to reduce the germination of both jointed goats grass (*Aegilops cylindrical Host.*) seed (Lyon & Rush 1993) and cheat (*Bromus secalinus L.*) seed (Hauhouot-O'Hara et al. 1999; Hauhouot et al. 1998). Germination of seeds reduced with smaller roll gaps (Hauhouot-O'Hara et al. 1999; Hauhouot et al. 1998; Lyon & Rush 1993), with higher tooth density (Hauhouot et al. 1998) and with a higher speed differential (Hauhouot-O'Hara et al. 1999). The lowest growth chamber germination percentage achieved for roller milled pure cheat seed for a roll gap of 0.1 mm and 8-teeth/cm was 25% (Hauhouot et al. 1998). However, when speed differential of 1:1.27 and, thus a shearing action was introduced the germination

percentage was reduced down to 5% (Hauhouot-O'Hara et al. 1999). The rollermill may be an appropriate technology if the processed material could be pure weed seeds. However, as argued previously, separating pure seed is not likely on a modern combine harvester with large mass flow of chaff material. The close tolerances needed to crush weed seeds (0.1mm) are likely to limit the capacity of the rollermills processing the large mass flows of chaff material.

Impact mills cause breakage through kinetic energy developed from a rotor (Nied 2007). A hammermill (Figure 2.7) has been found to devitalise a variety of weed species by more than 90% (Balsari, Airoldi & Finassi 1994; Cash, Zamora & Lenssen 1998; Hauhouot-O'Hara et al. 1999; Hauhouot et al. 1998; Lyon & Rush 1993; Zamora & Olivarez 1994). The devitalisation of weed seeds with a hammermill increases with higher rotational speed (Balsari, Airoldi & Finassi 1994; Hauhouot-O'Hara et al. 1999), smaller screen size (Hauhouot-O'Hara et al. 1999; Lyon & Rush 1993; Zamora & Olivarez 1994) and lower moisture contents (Balsari, Airoldi & Finassi 1994). The devitalisation percentage of seeds processed with a hammermill depends on the weed species (Cash, Zamora & Lenssen 1998; Zamora & Olivarez 1994). Two most likely causes for the difference are because of variations between species of the toughness of a seed and seed mass. The toughness of seed is related to the fibre to starch ratio (Pfost 1976). High fibre content seeds are more difficult to grind than high starch content seeds (Pfost 1976). The energy of the impact is proportional to seed mass. For impact grinding seed mass has been found to be positively correlated with seed mortality (Davis et al. 2008). Despite some research showing the effectiveness of hammer mills for reducing seed germination, no reports were found of a hammer mill being mounted on a harvester and tested for harvest time seed control.

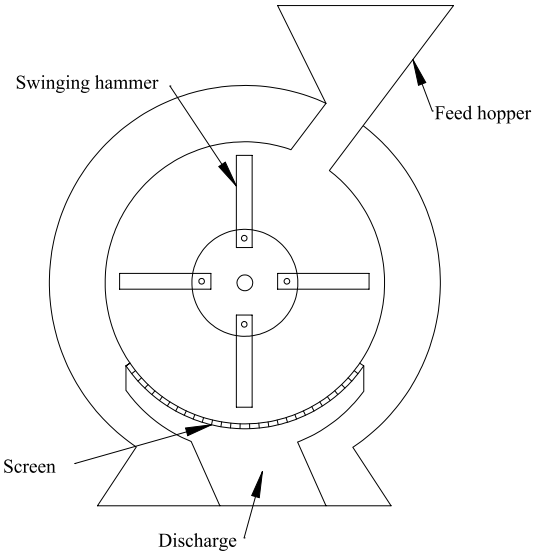

Figure 2.7: Schematic of a typical hammer mill

The Rotomill was a type of pin mill or disintegrator and has a rotating and stationary set of concentric pins which applies high speed impacts to the refined chaff sample created by a Ryetech sieve (Zani 2001). Pin mills are used for fine grinding such as pharmaceutical powders (Nakach et al. 2004). A number of design iterations of the rotor mill were made during the design and testing phase through the 1990's and early 2000's (Zani 2012). Three mill sizes were tried; 300, 400 and 600 mm (Zani 2012). The final mill size selected was 400 mm operating at 3500 rpm with a tip speed of 73 m/s (Zani 2012). No published data exists on the effectiveness of the Rotomill. However, it was communicated by the inventor that it was able devitalise over 90% of annual ryegrass seeds (Zani 2012). The Rotomill was able to work on combine harvesters from the 1990's (Zani 2012). However, harvesters have had a significant increase in capacity in the early 2000's and the Ryetec sieving system could not collect a high enough proportion of weed seeds at high chaff throughputs and the mill could not handle the entire chaff fraction (Holding, Stewart & Sutherland 2006; Zani 2012). Therefore, the Rotomill was not developed any further (Zani 2012).

The HSD uses a cage mill with two counter rotating cages and 3 rows of cylindrical bars on each cage (Walsh, Harrington & Powles 2012). When the two cages are fitted together the cage mill has six concentric rows of impact bars, as shown in Figure 2.8. The cage mill is similar to the rotor mill pin mill in its impact operation; the difference is that there are two rotors on the cage mill rather than a rotor and stator, and the cage mill has the pins held with a support ring at the end. Cage mills are used primarily for reducing the size of brittle materials such as coal and salts (Rodriguez et al. 2010). The

principal grinding mechanism is through impact (Rodriguez et al. 2010). Material enters at the centre of the mill cage and is impacted in each direction by the counter rotating rows of impact bars, as shown in Figure 2.8. Annual ryegrass seed devitalisation increased slightly with speed from 85% at 700 rpm to 94% at 1300 rpm (Walsh, Harrington & Powles 2012). The efficacy of the HSD cage mill was unaffected by chaff type ($p > 0.05$) (Walsh, Harrington & Powles 2012). The HSD cage mill was also measured to devitalise wild radish (Raphanus raphanistrum L.), wild oats (Avena spp.) and brome grass (Bromus spp.) seeds by at least 90% when processed with wheat chaff (Walsh, Harrington & Powles 2012).

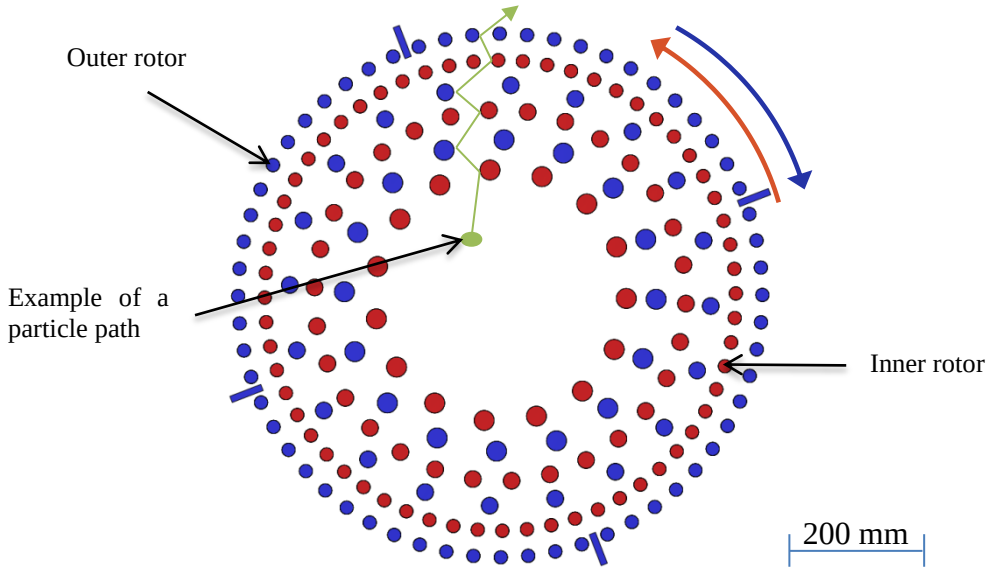

Figure 2.8: Cross section of the HSD cage mill showing a particle impact path

The previous research has shown that both roller mills and impact mills can effectively reduce the germination of weed seeds. It is apparent that impact mills are more suited than roller mills for processing the large volumes of chaff material. Some analyses of the important factors that influence the outcome of the milling operation were identified. However, there has been little insight provided into why particular designs or operating conditions are effective. Hence, there is a need to understand and predict the workings of an impact mill for the application of devitalising weed seeds.

2.4.4 Processing power and chaff throughput requirement

The wheat chaff mass flow was estimated in Section 2.3.2 to be approximately 11 t/h for a Class 7-8 combine harvester. This value was an inferred estimate. An aim of this thesis was to improve on this estimate by measuring mass flow rates of chaff.

The compromise between throughput capacity, power and weight on modern combine harvesters are finely balanced (Baruah & Panesar 2005). Taking power from the combine harvester's engine to run a seed devitalisation mill disrupts this balance. The power available for other operations and, hence the harvester's throughput capacity are reduced. Reducing the throughput capacity of a harvester reduces the harvest timeliness and, hence has a cost associated through reduced yield and grain quality (ASABE-Standards 1998). In addition, the power requirement influences the manufacturing and operating costs of a seed devitalisation mill system. Therefore, the power needed to process chaff and weed seeds is an important performance parameter that must be minimised to reduce the impact on harvester performance.

The specific power to process refined chaff material and kill weed seeds with a hammermill was found to be 67.2 kW.h/tonne and the throughput capacity was 0.83 t/h (Balsari, Airoldi & Finassi 1994). For comparison, hammermilling wheat straw with 3.2 mm screen was found to use 35-50 kW.h/tonne for speeds ranging from 2000-3600 rpm, respectively (Bitra et al. 2009). As identified in Section 2.3.2, the mass flow of wheat chaff material is expected to be in the order of 11 t/h (3 kg/s) at a harvest throughput rate of 38 t/h of wheat. For processing the total 11 t/h of chaff at a specific power requirement of 67.2 kW.h/t gives an approximate hammer mill power consumption of 740 kW. This is an impractical amount of power to be drawn from a combine harvester's engine. Furthermore, the chaff throughput capacity of the hammermill used by Balsari, Airoldi and Finassi (1994) would need to be increased by around 13 times. At the commencement of this work, the power requirement for the HSD cage mill, had not been determined. It was an aim of this research to determine the power requirement of the HSD cage mill and any developed technology.

2.4.5 Evaluation methods

2.4.5.1 Chaff mass flow

To process the entire chaff fraction of a modern high capacity (Class 8/9) combine harvester, the seed devitalisation mill must be able to handle an estimated 11 t/h of chaff

mass flow without blockage. The mill must also be able to devitalise weed seeds within this material. Higher mass flows of material causes less particle size reduction in an impact mill (Drögemeier & Leschonski 1996; Vogel & Peukert 2005). It is also expected that increasing mass flow of chaff through a mill would reduce weed seed devitalisation.

The literature cited in Section 2.4.3 may not be applicable to processing the entire chaff fraction. The mass flow of material tested in each case was considerably lower than the 11 t/h expected. The maximum chaff mass flow tested by Balsari, Airoldi and Finassi (1994) was only 0.83 t/h because it was assumed that sieving could be used to separate weed seeds. Pure cheat seeds were processed by (Hauhouot-O'Hara et al. 1999; Hauhouot 1998) because it was assumed that weed seeds could be completely separated from crop material. The work on processing weed seeds for the application devitalising weed seeds in feed pellets did not specify the mass flow and the material processed was not chaff (Cash, Zamora & Lenssen 1998; Lyon & Rush 1993; Zamora & Olivarez 1994).

The HSD cage mill has been evaluated by processing the entire chaff fraction out of a Class 6 combine harvester (CASE IH 2388) (Walsh, Harrington & Powles 2012). The HSD cage mill was tested in the field at a range of mass flows at up to 2.32 t/h of wheat chaff (Walsh & Harrington 2011; Walsh, Harrington & Powles 2012). This mass flow was far less than the 11 t/h (3 kg/s) that would be expected in a modern high capacity (Class 8/9) combine harvester. The seed devitalisation under higher chaff throughputs may be lower than that published. The effect of processing high chaff mass flows of up to 11 t/h on seed devitalisation has not been reported for any milling technology. Therefore, there is a need to evaluate milling technology at much higher chaff mass flows than previously done.

2.4.5.2 *Germination method*

The germination method to evaluate seed viability has varied between researchers. Where pure seeds have been processed evaluating weed seed viability is easier as there is no other material to deal with. When determining the viability of damaged cheat seeds, Hauhouot et al. (1998) compared laboratory growth chamber, greenhouse pots and field germination of seed only.

The HSD cage mill has been evaluated by processing chaff, laced with dyed seeds (Walsh, Harrington & Powles 2012). The processed material was sieved multiple times and the dyed seeds were hand recovered and germinated in agar (Walsh, Harrington & Powles 2012). The method of recovering dyed seeds was problematic because it was not easy to find all seeds and fragments in a large chaff sample and the method was also highly laborious.

An alternate approach was used by Cash, Zamora and Lenssen (1998) when testing weed seed viability in alfalfa hay when processed with a hammermill. The processed alfalfa meal was split into subsamples. Emergence of the weed seeds was tested in a greenhouse by mixing 10% by weight alfalfa meal and potting mix. This approach requires significantly less labour than finding and assessing each individual seed. Furthermore, there is less likelihood of losing seeds. One issue with this method is that there is a phytotoxicity effect of crop residues breaking down that suppresses germination (Kimber 1973b, 1973a). Therefore, the amount of chaff material mixed with soil must be minimised as much as possible. This method appears to be the most appropriate for rapidly testing impact mill technology at high chaff throughputs.

When germinating annual ryegrass (*Lolium rigidum*) seeds in soil, seeding depth has been found to be critical (Chauhan, Gill & Preston 2006). Annual ryegrass seeds must be covered with soil; seeds that remain on the soil surface only had 16% emergence (Chauhan, Gill & Preston 2006). However, the depth of soil cover cannot be too deep; a seeding depth of 1 cm had the highest field seedling emergence of 49%, followed by 2 cm with 44% (Chauhan, Gill & Preston 2006), 5 cm with 10% and 10 cm had no seedling emergence (Chauhan, Gill & Preston 2006). To maximise *Lolium rigidum* seedling emergence, the seeds must be buried but only shallow (<2 cm).

2.5 Theory on impact milling

2.5.1 Impact energy

A weed seed becomes devitalised if it is broken or damaged sufficiently to prevent its normal function or reduce its natural defences. Therefore, the mechanisms that cause particle breakage are likely to be the same as those that cause seed devitalisation. During an impact in an impact mill, the kinetic energy of a particle is converted into strain energy (Austin 2002). When the strain energy is high enough to cause particle

breakage, some of the strain energy is converted to generating new fracture surfaces (Austin 2002). The remainder is converted to heat and residual kinetic energy of the fragments (Austin 2002). The energy available to cause particle breakage is derived from the kinetic energy lost during impact (Pfost 1976; Rumpf, Hans 1973). To determine the change in velocity of two colliding objects and, hence the kinetic energy lost during impact, the impulse-momentum law is used. For a two dimensional impact between two circular particles, as shown in Figure 2.9, the momentum is conserved before and after impact.

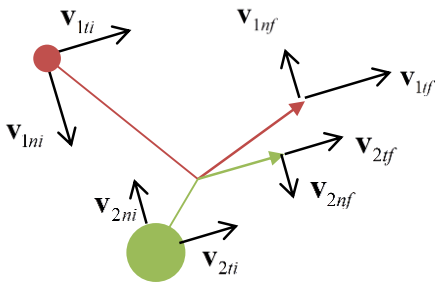

Figure 2.9 Normal (n) and tangential (t) velocity components of two spheres before (i) and after (f) an oblique central impact

Conservation of linear momentum in the normal direction of impact is given by the mass (m) and velocity (v) of the two particles, before (i) and after impact (f) (Goldsmith 2001):

$$m_1 v_{1ni} + m_2 v_{2ni} = m_1 v_{1nf} + m_2 v_{2nf} \tag{2.1}$$

Where: m_1 & m_2 = mass of object 1 and 2, respectively
$v_{1,ni}$ & $v_{2,ni}$ = normal component of velocity of object 1 and 2, respectively before impact
$v_{1,nf}$ & $v_{2,nf}$ = normal component of velocity of object 1 and 2, respectively after impact

Each particle's velocity in the normal direction is related using the coefficient of restitution (e) (Goldsmith 2001):

$$v_{2nf} - v_{1nf} = e\left(v_{1ni} - v_{2ni}\right) \tag{2.2}$$

Where: e = coefficient of restitution

Equations (2.1) and (2.2) shown as two simultaneous equations:

$$\begin{vmatrix} 1 & -1 \\ m_2 & m_1 \end{vmatrix} \begin{vmatrix} v_{2nf} \\ v_{1nf} \end{vmatrix} = \begin{vmatrix} e(v_{1ni} - v_{2ni}) \\ m_1 v_{1nf} + m_2 v_{2nf} \end{vmatrix} \tag{2.3}$$

Solving using row reduction, gives:

$$v_{2nf} = \frac{1}{m_1 + m_2}\left[m_2 v_{2ni} + m_1 v_{1ni} + m_1 e(v_1 - v_2)\right] \tag{2.4}$$

$$v_{1nf} = \frac{1}{m_1 + m_2}\left[m_2 v_{2ni} + m_1 v_{1ni} - m_2 e(v_1 - v_2)\right] \tag{2.5}$$

The loss of kinetic energy of the two particle system is given by (Goldsmith 2001):

$$E_{loss} = \frac{1}{2} m_1 \left(v_{1nf}^2 - v_{1ni}^2\right) + \frac{1}{2} m_2 \left(v_{2nf}^2 - v_{2ni}^2\right) \tag{2.6}$$

Substituting Equation (2.4) and (2.5) into (2.6) gives (Goldsmith 2001):

$$E_{loss} = \frac{1}{2}\left(\frac{m_1 m_2}{m_1 + m_2}\right)\left(1 - e^2\right)\left(v_{1ni} - v_{2ni}\right)^2 \tag{2.7}$$

The loss of kinetic energy (E_{loss}) of an impact is the energy that is available for particle deformation, heat and breakage (Pfost 1976). From Equation (2.7), the energy lost in an impact depends on the mass of the two colliding particles, the coefficient of restitution of the impact, and the square of the relative normal velocity. For an impact between two identical particles ($m_1 = m_2 = m$) the energy lost simplifies to:

$$E_{loss} = \frac{1}{4} m\left(1 - e^2\right)\left(v_{1ni} - v_{2ni}\right)^2 \tag{2.8}$$

For an impact of a small particle on a large plate ($m_1 \ll m_2$), Equation (2.7) simplifies to:

$$E_{loss} = \frac{1}{2} m_1 \left(1 - e^2\right)\left(v_{1ni} - v_{2ni}\right)^2 \tag{2.9}$$

2.5.2 Factors affecting milling outcome

From the impact energy Equation (2.7), it is clear the importance of a number of factors in the likelihood of particle breakage, as follows:

2.5.2.1 *Material properties*

The material properties of the feed material have a significant influence on the milling outcome (Peukert 2004; Pfost 1976). The energy needed to cause particle breakage determines the level of energy loss needed in Equation (2.7). Furthermore, the coefficient of restitution, which depends on material properties, has a significant influence on the kinetic energy loss of an impact. A fully elastic impact ($e = 1$) has no energy loss and a fully plastic impact ($e = 0$) has the maximum energy loss. However, a lower coefficient of restitution is not equivalent to a higher likelihood of particle breakage because the lost kinetic energy can also be used for plastic deformation and heat without breakage (Rumpf, Hans 1973).

2.5.2.2 *impact speed*

The lost kinetic energy is significantly dependent on the impact speed as shown in Equation (2.7). The impact speed is largely governed by the tip speed of the rotor in an impact mill given by the rotational speed of the rotor and the rotor radius ($V_{tip} = \omega r$).

2.5.2.3 *Residence time*

The number of impacts influences the total impact energy of a mill. The residence time of a mill is related to the number of impacts (Vogel & Peukert 2005). Residence time can be increased for a hammer mill with a screen classifier by using a smaller screen size (Vogel & Peukert 2005).

2.5.2.4 *Solids loading*

A particle-particle impact has approximately half the impact energy of a particle-wall impact (compare Equation (2.8) and (2.9)). Therefore, the probability that a particle will impact another particle rather than impact a wall influences the energy exerted on particles within a mill and, hence the breakage. The probability of particle to particle impacts can be characterised by the mean free path length; the average distance a particle will travel before impacting another particle (Rumpf, H. 1959). The mean free path length is related to the volume occupied by particles and air and is given by (Rumpf, H. 1959):

$$\lambda \approx \frac{d}{10(1-\varepsilon)} \tag{2.10}$$

Where: λ = free path length (m)
d = particle diameter (m)
ε = air volume as a proportion of total volume (air + solids)

The volume of solids in a mill is the mass of material in the mill divided by the actual density of the material. Therefore, for constant density material, the solids loading or mass ratio of feed material to air is also a measure of particle to particle impacts in a mill (Drögemeier & Leschonski 1996). Consequently as solids loading increases, less particle size reduction occurs (Drögemeier & Leschonski 1996; Vogel & Peukert 2005).

2.5.2.5 *Impact bar geometry*

The impact bar geometry can determine the relative normal and tangential components of impact velocity. The normal component of impact velocity is the major contributor to particle breakage due to impact (Akiyama, Kozawa & Yoshida 2004; Moreno, Ghadiri & Antony 2003; Samimi, Moreno & Ghadiri 2004). The normal component of impact velocity of particles in an air classifier mill using cylindrical and prismatic rotor bars were compared by Toneva, Wirth and Peukert (2011). The most frequently occurring impact velocity with both cylindrical and prismatic rotor bars occurred at approximately 90% of the tip speed of the rotor. The prismatic bars had a narrow Gaussian density distribution for normal impact speed, with a mean of 80% of the rotor tip speed, which indicated that mostly direct impacts were occurring. However, for the cylindrical pins there was a much larger spread of impact speeds with a mean of 68% of the rotor tip speed, which indicated significant glancing impacts. The higher mean impact speed for prismatic bars corresponded to higher milling efficiency compared to cylindrical bars (Toneva, Wirth & Peukert 2011). Sharp edges also increased the likelihood of particle breakage by maximising the stress in the particle at the point of impact (Pfost 1976).

2.6 Modelling of impact mills

Particle size reduction or comminution through impact milling is an expensive and energy intensive process. Modelling to optimise milling process can provide significant cost and energy savings (Toneva & Peukert 2007). Population balances have been used extensively for comminution modelling since the 1970's (Powell & Morrison 2007). A variety of approaches have been used to find the parameters of population balance

models to model milling operations. Most often, the parameters have often been combined into a breakage rate function based on the output size distribution of the mill giving a machine and ore specific model that can only be extended to similar ore types and machine types (Powell & Morrison 2007).

One approach to improve the applicability of results over a wider range of conditions has been to separate the milling operation into a material function and a machine function (Peukert 2004; Vogel & Peukert 2003a), as shown in Figure 2.10.

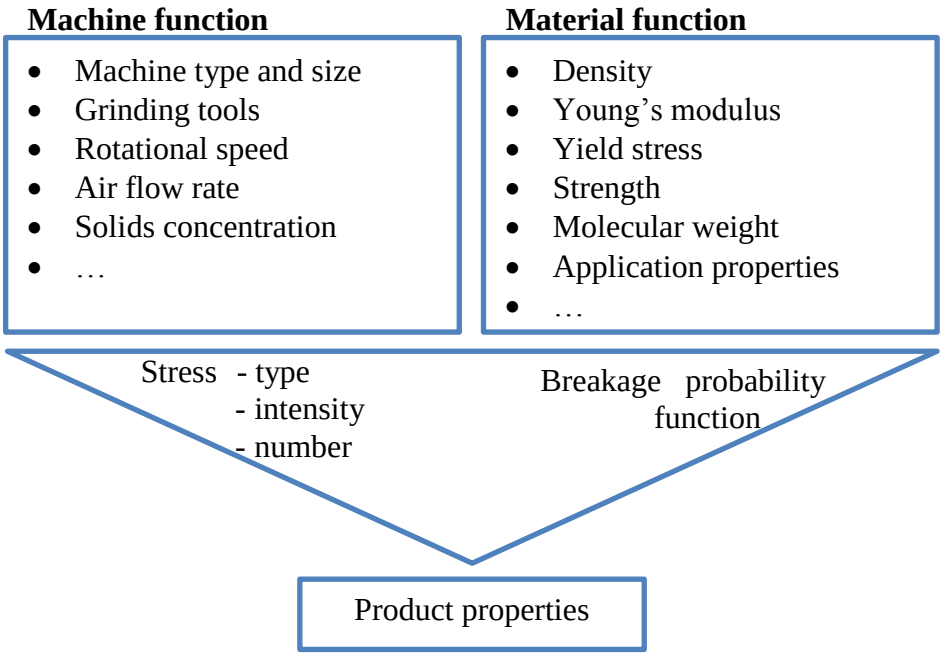

Figure 2.10: Creation of machine and material functions for the grinding process, adapted from Vogel and Peukert (2003a)

This approach enables the effect of the mill to be isolated from the effect of the feed material. The machine function would provide the stress intensity, number of stress events and distribution of both. The material function would provide a breakage probability function related to stress events. Combining the two would provide a prediction of the output size distribution. Separation into the two function enables insight into the workings of the impact mill and reduces the laborious job of trying different mill types and operational parameters to achieve the desired output size distribution.

2.6.1 Material function

2.6.1.1 *Impact testing*

The effect of the properties of the material feed on the output size distribution has been determined using single particle breakage testing. Particle breakage tests can be characterised into single impact tests, double impact tests and slow compression tests (Narayanan 1986). For rotor impact mills, the main mechanism of breakage is through single-sided impact.

Single-sided impact testers

Single impact testers include ejecting rotor, rotational and air gun type impact test machines. Single impact testing is when a particle is impacted from one side and the resultant motion of the particle is unconstrained.

Ejecting rotor impact testers eject particles outwards onto a stationary cylindrical wall using centrifugal force such as one used by Cooke and Dickens (1971). The ejecting rotor impacts particles most similar to a stator in an impact mill. An ejecting rotor impact tester designed by Schönert and Marktscheffel (1986) has been used in a number of studies (Vogel & Peukert 2003b, 2004, 2005). The impact tester also operated in a vacuum (Schönert & Marktscheffel 1986). The velocity of impact using these devices was calculated by assuming that both the radial and tangential velocity were equal. However, friction (rolling and sliding) in the acceleration tube reduces the radial acceleration and, hence the particles may eject at lower radial velocity than calculated (Petukhov, Yevgeny & Kalman 2003). To calculate impact velocity, the particle trajectories have been determined using a high speed video camera in an ejecting breakage tester developed by Shi et al. (2009). The impact velocity was calculated to be 85 to 95% and impact energy between 72.3% and 90.3% of that predicted from theory (Shi et al. 2009).

Air-gun impact testers accelerate particles in an air stream through a pipe and collide the particle with a stationary target at the exit of the pipe. The air-gun impact tester impacts particles most similar to a stator in an impact mill. To determine the impact velocity, a photodiode switch at the tube exit and a vibration transducer on the target have been used by Salman, Gorham and Verba (1995). Non-spherical particles are likely to move into an orientation that maximizes drag force and, hence impacts will occur in preferred orientations rather than randomly (Petukhov, Yevgeny & Kalman 2003). Furthermore,

small particles may be carried around the impact target with the air stream rather than hitting the impact plate (Petukhov, Yevgeny & Kalman 2003).

Rotational impact testers impact particles that are dropped into the path of a rotating impact blade (Petukhov, Yevgeny & Kalman 2003; Petukhov, Y & Kalman 2004). The rotational impact tester impacts particles most like a rotor in an impact mill. Rotational impact testers have some issues with induced air flow; particles where seen in high speed camera footage to miss the target and be carried out by the air stream (Petukhov, Yevgeny & Kalman 2003). The induced air flow causes uncertainty in the impact velocity and, hence impact energy when using a rotational impact tester above a critical speed without a vacuum. However, using a vacuum was found to increase the material loss by material being sucked out of the chamber (Petukhov, Yevgeny & Kalman 2003).

The three single-sided impact testers mentioned have both advantages and disadvantages. For this thesis, the rotational impact tester was selected because it best represents impacts with a rotor in an impact mill such as a HSD cage mill (2 rotors) and pin mill (1 rotor, 1 stator).

2.6.1.2 *Impact testing of seeds*

Impact testing has been used as the basis for determining the maximum safe impact speeds for harvest and post harvest operations. Seed damage has been shown to increase with impact speed (Bartsch et al. 1986; Bilanski 1966; Khazaei et al. 2008; Kirk & McLeod 1967; Leonhardt, Zoerb & Hamann 1961; Turner, Suggs & Dickens 1967). Likewise, seed germination has been shown to reduce with impact speed (Bartsch et al. 1986; Khazaei et al. 2008; Leonhardt, Zoerb & Hamann 1961). Increases in the number of successive impacts have also been shown to increase damage to seeds (Khazaei et al. 2008) and reduce germination (Frączek & Ślipek 1998; Khazaei et al. 2008). Impact testing to find non-detrimental impact speeds does not, in general, involve testing up to speeds needed to damage or reduce germination of all or most of the seeds, as would be required for weed seed control. Therefore, little previous impact testing has been reported at number of impacts or impact speeds high enough that devitalise high proportions of seeds (e.g. >90%).

Moisture content has been found to affect the seed response to impact damage. Increasing moisture content has been shown to reduce dynamic hardness of corn (Jindal & Mohsenin 1978). This reduction in hardness is likely to have a corresponding

increase in fracture toughness. Higher moisture content seeds are less likely to crack under impact loads but may be more easily compressed. Under an impact load, seed damage has been shown to reduce (Bartsch et al. 1986; Bilanski 1966) and germination to increase (Bartsch et al. 1986) with moisture content. Above a critical moisture content, seed damage begins to increase with moisture content (Szwed & Lukaszuk 2007; Turner, Suggs & Dickens 1967). In another study at high moisture contents, seeds were not found to be visibly damaged under impact but germination was reduced significantly (Mitchell & Rounthwaite 1964). Successive low speed impacts have been found to reduce wheat sprouting capacity and sprouting energy more significantly at higher moisture contents (Frączek & Ślipek 1998).

2.6.1.3 *Breakage probability function*

To determine the particle size distribution after a feed material is exposed to a set of impact loads it is important to know (Shi & Kojovic 2007):

- the probability of particle breakage (breakage probability function);
- the particle progeny size distribution (breakage distribution function).

In the context of this thesis, the viability of a seed exposed to impact loads is of interest; the seed is either viable or unviable based on some criteria. The probability that a seed will be devitalised under a set of impact loads depends on the probability that the seed breaks under the impact loads. Therefore, to develop a probability function for seed devitalisation, breakage probability functions were considered.

Perfectly uniform particles exposed to perfectly uniform loading would have a step function for a breakage probability function (Vervoorn & Austin 1990). Below a critical impact energy, no particles would break, above a critical impact energy all particles would break. In reality, the breakage probability function is a distribution determined by four factors (Vervoorn & Austin 1990):

- distribution of strengths of individual particles;
- distribution of applied forces resulting from an impact;
- distribution of strength of particles due to different orientations;
- reduction in strength with repeated impacts.

To generate a material function for the breakage probability of particles and account for these distributions, a mastercurve for breakage probability was derived (Vogel & Peukert 2003a, 2003b, 2004, 2005). The mastercurve was derived from dimensional reasoning by Rumpf, Hans (1973) and a fracture mechanics model based on a statistical distribution by Weibull (1951), as:

$$S = 1 - \exp\left(- f_{Mat} x k \left(W_{m,kin} - W_{m,\min}\right)\right) \tag{2.11}$$

Where: S = probability of particle breakage;
f_{Mat} = material and particle property parameter (kg/J/m);
x = initial particle size (m);
k = number of impacts;
$W_{m,kin}$ = mass specific impact energy (J/kg);
$W_{m,min}$ = mass specific threshold energy for particle breakage (J/kg).

The probability of particle breakage could be expressed in measurable material properties f_{Mat} and $W_{m,min}$. A limitation of the mastercurve model was that it did not account for any damage accumulation below the threshold impact energy ($W_{m,min}$). The impact energy may be less than the minimum needed to cause fracture but may be able to make the particle more susceptible to fracture in the next impact (Tavares 2009; Tavares & King 2002). Damage accumulation can occur in milling operations that have high numbers of low energy impacts. More complex empirical relationships have been found when attempting to properly account for fatigue phenomena, such as those shown in Petukhov, Y and Kalman (2004). However the mastercurve (Equation (2.11)) has a distinct advantage over more complex empirical models: the breakage probability of any combination of impact loads can be easily predicted. Thereby, it was chosen to be adapted for a seed devitalisation probability function in this thesis.

2.6.2 Machine function

An aim of comminution science has been to develop a model of milling that is independent of the feedstock (Toneva et al. 2011), namely the machine function. Two general approaches have been applied to find the material function; an empirical approach based on population balances and a mechanistic model approach based on physical mill geometry.

The empirical approach has been adopted by using both a known material function and results from milling tests and then calibrating a simple population balance model for the

milling operation (Vogel & Peukert 2005). This method assumed an impact velocity based on the tip speed of the mill and then calibrated the number of impacts so that the machine output was what was expected from the material function (Vogel & Peukert 2005). This approach provided a clear separation of the influence of material properties from the machine properties (Vogel & Peukert 2005). This method could be used for predicting the output of the particular mill using different materials when the material properties are known (e.g. f_{mat} and $W_{m,min}$), or under different operating conditions. However, this method is not able to make predictions for a differently designed mill and, hence this method is not very useful in developing new mill designs.

An approach that can make output predictions of differently designed mills is the mechanistic modelling or modelling based on the physical phenomena occurring within the mill (Powell & Morrison 2007). The mechanistic model models the process rather than the outcome of specific equipment with specific material feed (Powell & Morrison 2007). A mechanistic modelling approach enables predictions of output distribution based on mill geometry and operational parameters. Therefore, the mechanistic modelling approach enables design optimisation of mill geometry and the development of new novel mill designs such as a specifically designed weed seed devitalisation mill.

2.6.2.1 *Theoretical impact model*

The mill geometry combined with net milling power has been used with a theoretical model of a hammer mill to predict particle size reduction (Austin 2004). This approach assumed that particles exist in a gas suspension at some velocity less than the hammer velocity. The gas suspension was assumed to stagnate on the rotor blades and therefore the power to drive the suspension was given by (Austin 2004):

$$P = \frac{1}{2}\rho_s A(V - V_s)^3 \tag{2.12}$$

Where: ρ_s = density of suspension (kg/m^3);
A = total impact face area (m^2);
V = tip speed of hammer (m/s);
V_s = circumferential velocity of suspension (m/s).

The breakage applied to particles was based upon specific energy of impact (E_{impact} (kJ/kg)):

$$E_{impact} = \frac{1}{2}(V - V_s)^2 \tag{2.13}$$

Theoretical modelling approaches based on mill geometry are useful for predictions of power and particle size distribution but make significant simplifications of the physical phenomena occurring within the mill. Using theoretical models for design optimisation of mill geometry is limited because they simplify the geometric features. Some geometry that has been simplified for the theoretical model may be important to the mills performance.

2.6.2.2 *CFD modelling*

The air flow in an impact mill is very important to its operation. Air flow can govern the transport of particles into and out of an impact mill as well as the motion of particles through a mill (Toneva, Wirth & Peukert 2011). The air flow field within an impact mill can influence both the number of impacts and the impact velocity that a particle is exposed to (Toneva, Wirth & Peukert 2011). Therefore, knowing the air flow field through an impact mill is important to the mill's operation.

To determine the air flow field Computational Fluid Dynamics (CFD) can be used. CFD is a method of solving the Navier-Stokes equations for a fluid motion (continuous phase) over a discrete mesh (Takeuchi et al. 2012). The motion of solid particles (discrete phase) immersed in the fluid can be solved in some CFD codes. CFD has been used to model different types of impact mills by solving the continuous phase (air) and an immersed discrete phase (feed material) to determine the impacts occurring to the feed material (Akiyama, Kozawa & Yoshida 2004; Anagnostopoulos & Bergeles 1997; Chatzilamprou et al. 2006; Takeuchi et al. 2012; Toneva, Wirth & Peukert 2011). No CFD impact modelling of pin mills or cage mills or modelling the impact of seeds was found in the literature.

Impact mills often have a rotor that generates much of the air flow through the mill. To account for the rotating machinery in a CFD model, multiple-frames-of-reference (MFR) models are implemented (Liu & Hill 2000). The rotating components are modelled within a region with a rotating frame of reference and the stationary

components are modelled with a stationary frame of reference (Liu & Hill 2000). Three interface methods to implement MFR models are sliding mesh, frozen rotor and the circumferential averaging methods (Liu & Hill 2000). Rotating machinery with strong rotor-stator interaction tends to produce unsteady flow fields (Liu & Hill 2000). The sliding mesh method is the only transient method and, hence the only one capable of accurately capturing the unsteady flow fields (Liu & Hill 2000). However, the sliding mesh method is hugely computationally intensive and usually only a segment of the rotor and stator are modelled (Liu & Hill 2000). Therefore, until computational power available is sufficient to model the entire impact mill with the sliding mesh method, it is not appropriate for modelling impacts through the mills. The frozen rotor and circumferential averaging methods are both steady state solutions and are far less computationally intensive than the sliding mesh method. A frozen rotor model was implemented for modelling the operation of a classifier mill by Toneva et al. (2011). However, the frozen rotor model has been shown to over-predict the non-uniformity of the flow field in a centrifugal compressor because of the set position between the rotor and stator (Liu & Hill 2000). A circumferential averaging technique was found to more closely correlated the full sliding mesh method than the frozen rotor model (Liu & Hill 2000). The circumferential averaging technique was the most appropriate to modelling impact mills that have close proximity between rotating and stationary components and, thus was used in this thesis.

To validate the continuous phase solution of an impact mill, static pressure and temperature calculated in the CFD model has been used to compared to static pressure measurements (Chatzilamprou et al. 2006; Takeuchi et al. 2012) and temperature measurements (Chatzilamprou et al. 2006). The pressure and temperature calculated in the CFD code by Chatzilamprou et al. (2006) was different to experimental measurements. The error was taken as a percentage of the total pressure (107 000 – 114000 Pa) and absolute temperature (318-332 K), which was up to 6% and 4%, respectively (Chatzilamprou et al. 2006). The actual error is more significant than the percentage reported suggests. At one point the difference in pressure was 7000 Pa (6.08%) temperature was 14 K (4.24%). The pressure measurements by Takeuchi et al. (2012) also differed from experiments but an error was not specified. Validation of CFD continuous phase using pressure and temperature is likely to be inconclusive in an impact mill and will not be used in this thesis.

Modelling of particles impacting the stator and rotor walls of an impact mill can provide the important machine function parameters. An immersed discrete phase can be solved in some CFD codes to model the motion of particles as influenced by the continuous phase solution and impacts with walls; impacts between particles are not considered. The interaction between the discrete phase and the continuous phase can be solved with either: one-way coupling where the effect of the fluid phase on the solid phase is solved and the effect of the solid phase on the fluid phase is ignored; or two-way coupling where interactions between fluid and solid phase are solved in both directions (Teng et al. 2011). Using one-way coupling can be used for solids loading up to 0.2, above which two-way coupling is needed (Chatzilamprou et al. 2006). The two-way coupling methods can be broken into: Lagrangian coupling where momentum exchange is solved between solid and liquid phase but the effect of the solid volume fraction is not taken into account; and Eulerian coupling where both momentum exchange and the effect of solid volume fraction are taken into account (Teng et al. 2011). Lagrangian coupling is valid for low solid volume fractions up to 10% (Chatzilamprou et al. 2006). Other complex effects are turbulence dispersion which is the effect of turbulence on the particles and turbulent modulation is the effect of particles on the carrier phase (Mandø et al. 2007). The choice of coupling method depends on the solids loading of the impact mill. In this thesis, the solids loading is not known and, hence the simplest coupling method, one-way coupling was chosen.

Some researchers have modelled impact mills using CFD with a two-way Lagrangian coupled discrete particle phase (Akiyama, Kozawa & Yoshida 2004; Anagnostopoulos & Bergeles 1997; Chatzilamprou et al. 2006; Takeuchi et al. 2012; Toneva, Wirth & Peukert 2011). In each case, particles were treated as spheres; particle to particle interaction and particle rotation were neglected. The particle impacts with the mill surfaces were treated using classical impact theory using the coefficient of restitution in the normal and tangential direction. Normal coefficient of restitution has been assumed to be 1 (perfectly elastic) by Akiyama, Kozawa and Yoshida (2004) and Toneva, Wirth and Peukert (2011), 0.3 by Takeuchi et al. (2012) and a function of incidence angle by Chatzilamprou et al. (2006). Tangential coefficient of restitution has been assumed to be 1 (frictionless) by Akiyama, Kozawa and Yoshida (2004), Toneva, Wirth and Peukert (2011) and Takeuchi et al. (2012) and a function of incidence angle by Anagnostopoulos and Bergeles (1997) and Chatzilamprou et al. (2006). The methods

used to model particle motion and impacts require simplifying assumptions which must be carefully selected then validated.

A more complex impact model with applicability in modelling rotor impact mills is the Discrete Element Method (DEM) combined with CFD. DEM is a numerical modelling technique used to model motion and collisions of discrete particles (Weerasekara et al. 2013). Therefore, DEM is able to take into account the particle to particle impacts. DEM combined with CFD has been used by a number of researches to model particle breakage (Brosh, Kalman & Levy 2011; Jayasundara et al. 2011; Kalman, Rodnianski & Haim 2009; Teng et al. 2011). CFD-DEM is likely to be important in the future of impact mill modelling. However, the software is very computationally intensive and requires a large number of input parameters and is beyond the scope of this thesis.

To validate the solid phase solution, a high speed camera was implemented by Chatzilamprou et al. (2006) and Takeuchi et al. (2012) and Particle Image Velocimetry (PIV) was used by Toneva, Wirth and Peukert (2011). Only qualitative agreement was found between the solid phase solution and the high speed camera results implemented by Chatzilamprou et al. (2006) and Takeuchi et al. (2012). The PIV approach was able to provide more quantitative agreement but was limited to one plane of motion (Toneva, Wirth & Peukert 2011). Both methods to validate the solid phase solution required access to the milling gap which is not possible for some styles of mills such as the HSD cage mill. Therefore, the direct approaches of validating solid phase solution will not be used in this thesis.

The motion of fluid and particles in different types of impact mills have been successfully modelled to find: the number of impacts and normal and tangential components of impact velocity relative to impact surface (Akiyama, Kozawa & Yoshida 2004); the distribution of normal impact velocity (Takeuchi et al. 2012; Toneva, Wirth & Peukert 2011); and the total specific energy and number of impacts in each zone (Chatzilamprou et al. 2006). However, very little has been reported on the prediction of the output particle size distribution based on a CFD impact model. The CFD model generated by Takeuchi et al. (2012) was adapted to generate an estimate of particle breakage (Takeuchi, Nakamura & Watano 2013). A reasonable prediction of particle size distribution was found (Takeuchi, Nakamura & Watano 2013). Calibration of the impact model was made using particle breakage data by Anagnostopoulos and Bergeles

(1997). The ultimate validation of a CFD impact model is to be able to predict the particle size distribution. Being able to predict seed devitalisation would enable the aims of this thesis to be met. Therefore, a comparison predicted of seed devitalisation with experimental seed devitalisation was the method selected to validate the modelling methods.

2.6.2.3 *Particle aerodynamic characteristics*

Aerodynamic drag of spherical particles

Particles in an air stream are accelerated by aerodynamic drag force. The aerodynamic drag force (F_D) is given by (Munson et al. 2006):

$$F_D = \tfrac{1}{2} C_D \rho_a V^2 A_{proj} \tag{2.14}$$

Where: C_D = coefficient of drag of the immersed body;
ρ_a = density of fluid,
for air at 20°C ρ_a = 1.204 kg/m^3 (Munson et al. 2006);
V = velocity of the fluid (m/s);
A_{proj} = projected area of the immersed body (m^2).

The coefficient of drag characterises the drag force on a particle in a fluid stream. The coefficient of drag depends on the Reynolds number of the flow, as given by (Munson et al. 2006):

$$\mathrm{Re}_p = \frac{Vd}{\nu} \tag{2.15}$$

Where: V = fluid velocity (m/s);
d = particle diameter (m);
ν = fluid kinematic velocity,
for air at 20°C, $\nu = 1.51\times10^{-5}$ s/m^2 (Munson et al. 2006).

Coefficient of drag has been determined over a wide range of Reynolds number for spherical particles. The drag on a smooth sphere can be characterised into four regions (Loth 2008):

1) attached laminar flow which is characterised by Stokes drag regime:

$$C_D = \frac{24}{\mathrm{Re}_p} \text{ for } \mathrm{Re_p} < 22; \tag{2.16}$$

2) transition to laminar separated flow with laminar wake $22 < \mathrm{Re_p} < 130$ moving to transitional unsteady wake $130 < \mathrm{Re_p} < 1000$, where no analytical solution exists;

3) laminar separation and turbulent wake which is characterised by the Newton drag regime, where coefficient of drag is approximately constant with $\mathrm{Re_p}$ ranging between 0.4 and 0.45 for the range $3000 < \mathrm{Re_p} < 200\,000$;

4) critical Reynolds number ($\mathrm{Re_p} > 300\,000$), turbulent separation and turbulent wake causes a reduction in drag coefficient. (e.g. golf balls)

For sub-critical flows, Loth (2008) recommended using the expression developed by Clift and Gauvin (1970):

$$C_D = \frac{24}{\mathrm{Re}_p}\left(1 + 0.15\,\mathrm{Re}_p^{0.687}\right) + \frac{0.42}{1 + \frac{42500}{\mathrm{Re}_p^{1.16}}} \quad \text{for } \mathrm{Re_p} < 200\,000 \tag{2.17}$$

Aerodynamic drag of non-spherical particles

The discrete phase of a particle is often modelled in a CFD code as a sphere. In many instances a real particle can be approximated as a sphere with acceptable accuracy. However, often particles are non-spherical such as annual ryegrass seeds. The motion of non-spherical particles in an air stream is complex; for certain shapes and flow conditions, secondary oscillatory motion occurs that is significantly different to the motion of a sphere (Mandø et al. 2007). For non-spherical particles, when $\mathrm{Re_p} > 100$, secondary oscillatory motion occurs as the wake becomes unstable and vortex shedding occurs (Mandø et al. 2007).

To model the drag coefficient of non-spherical particles, Ganser (1993) and Loth (2008) used a combination of shape correction for Stokes drag regime and shape correction for Newton drag regime to normalise Reynolds number and drag coefficient as:

$$\mathrm{Re}_p^* = \frac{C_{shape}\,\mathrm{Re}_p}{f_{shape}} \tag{2.18}$$

$$C_D^* = \frac{C_D}{C_{shape}} \tag{2.19}$$

Where: Re_p^* = Normalised Reynolds number
C_D^* = Normalised coefficient of drag
C_{shape} = Newton shape correction
f_{shape} = Stokes shape correction

The spherical drag equation from Clift and Gauvin (1970) was modified by Loth (2008) with normalised Reynolds number and drag coefficient as:

$$C_D^* = \frac{24}{\mathrm{Re}_p^*}\left(1 + 0.15\left(\mathrm{Re}_p^*\right)^{0.687}\right) + \frac{0.42}{1 + \frac{42500}{\left(\mathrm{Re}_p^*\right)^{1.16}}} \qquad \text{for } \mathrm{Re}_p^* < 200\,000 \tag{2.20}$$

This method showed that the normalised Reynolds number and drag coefficient of a variety of circular cross sections shared a common curve with this equation (Ganser 1993; Loth 2008).

Terminal velocity

The terminal velocity of a particle is often measured to determine the aerodynamic properties such as coefficient of drag of a particle. Terminal velocity testing has been the basis for determining the potential for aerodynamic separation of wheat from chaff materials (Gorial & O'Callaghan 1990; Khoshtaghaza & Mehdizadeh 2006; Shellard & MacMillan 1978). The terminal velocity of a range of weed seeds has also found (Kahrs 1994). However, annual ryegrass seed terminal velocity has not been reported.

A common method of determining the terminal velocity of seed grains is to use a vertical wind tunnel. Air is forced vertically through a duct into a test section. The particle is placed into the test section and the air velocity is adjusted until the particle floats. The floatation velocity (≈ terminal velocity) of a particle in an air stream occurs when the drag force (F_D) and gravitational forces (mg) are equal and opposite, as shown in Figure 2.11.

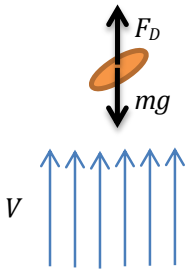

Figure 2.11: Free body diagram of a seed in a vertical air stream

At suspension or terminal velocity (V_t) the drag force (F_D) equals the gravitational force (weight) mg and the coefficient of drag can be solved as (Gorial & O'Callaghan 1990):

$$C_D = \frac{2mg}{\rho_a V_t^2 A_{proj}} \tag{2.21}$$

The calculated drag coefficient using the terminal velocity is at one Reynolds number. To model the acceleration of particles through an impact mill requires the coefficient of drag over a range of Reynolds numbers.

2.7 Summary

In the literature review the application of harvest weed seed control (HWSC) has been explored showing the need for new methods to devitalise seeds such as impact milling. The previous research on milling to devitalise seeds were reviewed but no theory or modelling of this application was found. The theory of impact milling for particle size reduction (comminution) was reviewed to show the most important factors that determine the output of a mill. The modelling techniques that have been used from particle size reduction (comminution) science were identified for modelling of seed devitalisation and have helped when developing the methods used in this thesis.

In light of the literature review, this thesis contributes to the understanding and modelling of impact milling for weed seed devitalisation and has developed new technology as validation. The thesis hypothesis is original as no model or theory on impact mills for the devitalisation of seeds in an impact mill has been published.

3 Research equipment and methodology

3.1 Material function

3.1.1 Rotational impact tester

A rotational impact tester was constructed to impact annual ryegrass seeds (Figure 3.1); it had a two bladed rotor which impacted individual seeds that were dropped into the path of the rotating blade. Impacted seeds travelled through an exit chute and were collected in a semi-permeable bag. The rotational speed of the rotor was set by a frequency controller and measured using a digital tachometer. The maximum test speed using the rotational impact tester to consistently impact annual ryegrass seeds was found to be 90 m/s. This was likely due to aerodynamic acceleration of seeds out of the path of the rotor blade at higher rotational speeds, as seen by (Petukhov, Yevgeny & Kalman 2003).

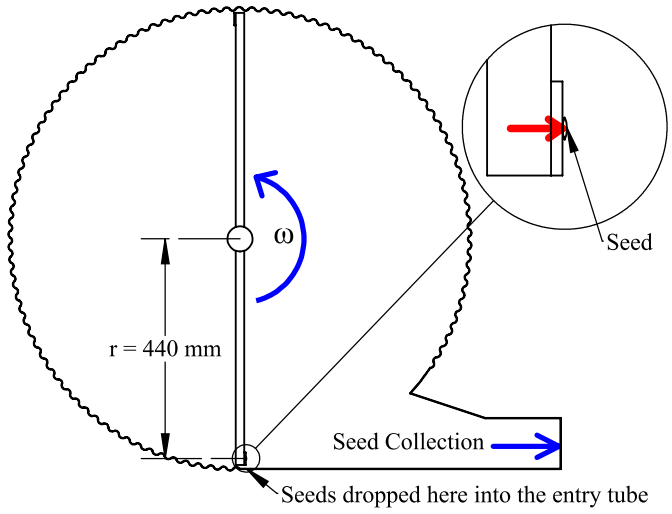

Figure 3.1: Top view of rotational impact tester for single-sided impact of seeds

3.1.2 Seeds used for testing

Annual ryegrass (*Lolium rigidum*) seed used in this thesis was sourced as one batch of seeds from Langseeds, South Australia. A limitation of this study is that the seeds used

were from a dedicated seed crop. Seeds harvested as a weed may be more variable as they may have been affected due to herbicide application and crop competition.

The moisture content of the seed batch was measured using the oven dry technique described by ASAE S352.2 (ASABE-Standards 2006) with three, 5 g samples of ryegrass seeds oven dried at 130^{o}C for 3 hours. The average moisture content was found to be 11.3% w.t. This moisture content would equate to 50% relative humidity at 20^{o}C using moisture isotherm Fig 1 of Steadman, Crawford and Gallagher (2003), which is typical conditions in much of the Australian grain growing regions prior to harvest. The 1000 seed mass was found by counting five, 200 seed samples and then weighing each sample with milligram scales. The standard error of the five measurements was used to calculate a 95% confidence interval of the 1000 seed mass based on the t-distribution, as shown in Table 3.1. The 1000 seed mass was 2.178 ± 0.029 g (95% C.I) and, thus the mean seed mass was 2.178×10^{-3} g. Using the 1000 seed mass, the estimated number of seeds in a given sample size was calculated, as shown in Table 3.2.

Table 3.1: Mass of five, 200g samples of annual ryegrass seeds including confidence interval of 1000 grain weight

Sample no.	Mass (g)	
1	0.440	
2	0.428	
3	0.435	
4	0.436	
5	0.439	
	mean	total
Mass (g)	0.436	2.178
Standard error (SE)	0.0021	0.0106
95% C.I (t-dist)	0.0059	0.0293

Table 3.2: Confidence interval of mean number of seeds in a weighed sample

Sample size (g)	Mean number of seeds	± Confidence interval (seeds)
1.25	574	7.7
2.5	1148	15.5
5	2296	30.9

3.1.3 Soil bin germination method

A constraint to testing weed seeds processed with chaff material was to be able to deal with the large quantities of chaff material. In this thesis, the chaff material was mixed with soil to evaluate milling technology (see later Section 3.3). Tests performed with the impact tester (without chaff) were evaluated in soil bins so the devitalisation measurement was similar to the devitalisation measurement of milling technology (with chaff).

Soil bin emergence tests were used to determine the devitalisation of annual ryegrass seeds processed with the rotational impact tester. Batches of 1.250 g (≈ 574 ± 8 seeds) were processed and the whole batch was germinated in a 700×1500 mm soil bin. The soil bins had a permanent 40 mm layer of sandy loam covered by a weed barrier cloth that prevented roots from penetrating into the permanent layer. A 30 mm layer of fresh 80:20 sand:loam mix was spread on top of the weed barrier cloth. Processed seeds were spread evenly onto the fresh soil layer. The seeds were then covered with a further 15 mm of the same soil. The depth of soil cover was based on the emergence response of annual ryegrass in field conditions as seeds on the surface have low emergence and seeds below 5 cm have low emergence.

The soil bins were placed in an indoor controlled environment room which was cycled between 15^{o}C for 8 hours without light and 25^{o}C for 12 hours under lighting with 2 hours linear ramping between each temperature. Relative humidity of the room was held at a constant 50%. The soil bins were monitored and watered when required to maintain a moist soil. Total seedling emergence was counted at 14 and 28 days.

Six control germinations were performed by planting 1.250 g of unprocessed annual ryegrass samples in soil bins at the same time the processed samples were germinating. Control seedling emergence was consistent between each trial, as shown in Table 3.3. In some tests the seedling count increased and in some tests the seedling count reduced between 14 and 28 days. The maximum count was used to ensure that results were not biased by any deaths due to environmental conditions between the first and second counts. The mean of the maximum control germination count was 448 seedlings out of 574 seeds or 78% of the total seeds added. The maximum emergence count also had the lowest coefficient of variation of 2.35%, confirming that it was the most consistent count.

Table 3.3: Control seedling emergence counts

Replication	Total seeds	Seedlings emerged (SE)			Max proportion emerged
		Day 14	Day 28	Max	
1	574	430	450	450	78%
2	574	438	454	454	79%
3	574	433	430	433	75%
4	574	444	441	444	77%
5	574	434	444	444	77%
6	574	464	464	464	81%
	Mean	441	447	448	78%
	C.V (%)	2.83%	2.61%	2.35%	2.35%

The devitalisation of annual ryegrass seeds was measured using the reduced seedling emergence (RSE). RSE was calculated using the control seedling emergence count and the seedling emergence count of each treatment:

$$RSE = 1 - \frac{SE}{SE_{control}} \tag{3.1}$$

Where: SE is the maximum seedling emergence count of the 14 and 28 days of a treatment
SE_{control} is the average of the control seedling emergence counts

3.1.4 Tests performed

The rotational impact tester was used to impact test annual ryegrass seeds multiple times to determine seed devitalisation under a range of impact speeds and number of impacts. Tests were performed in three series: multiple impacts at constant speed; three impacts at increasing or decreasing speed; and, combinations of impacts at elevated moisture content.

3.1.4.1 *Multiple impacts at constant speed*

In the first set of tests, seeds were subjected to set tip speeds and different numbers of impacts; 1, 2, 4, 8, and 16 impacts. The speeds used were at 10 m/s increments from 20 to 90 m/s. The tests performed are shown in Table 3.4.

Table 3.4: Multiple impact tests at one speed

Number of impacts	Impact speed (m/s) 20	30	40	50	60	70	80	90
1		●	●	●	●	●	●	●
2		●	●	●	●	●	●	●
4		●	●	●	●	●		
8	●	●	●	●				
16		●						

3.1.4.2 *Three impacts in increasing and decreasing speed order*

In the second set of tests, the effect of speed order was investigated for a series of impacts at different speeds. It was hypothesised that impacting seeds in a decreasing speed order would have higher seed devitalisation compared to an increasing speed order based on a basic fracture mechanics argument: A seed with an initial small crack would have a critical magnitude stress event (impact velocity) to cause crack propagation. The critical magnitude of the stress event depends on the crack size and the fracture toughness of the seed. For an edge crack, the critical stress is given by as given by (Gdoutos 2005):

$$\sigma_c = \frac{K_{IC}}{1.12\sqrt{\pi a}} \tag{3.2}$$

Where: K_{IC} = fracture toughness of the seed
σ_c = critical stress to cause crack propagation
a = crack length

If the first impact generated sufficient stress in the seed then this crack could grow. Upon crack growth after the first impact the critical magnitude stress event (impact velocity) is now reduced for the second impact. Therefore, an impact series with the largest stress event first (decreasing order) would be most likely to cause crack propagation upon the first and subsequent impacts and, hence cause maximum seed devitalisation.

To evaluate this hypothesis, seeds were subjected to three impacts at three different speeds in either increasing or decreasing speed order at 10 m/s increments to determine the effect of impact order. The impact speeds used, ranged from 30 to 80 m/s and two repetitions were performed for each test. The sets performed are shown in Table 3.5.

Table 3.5: Sets of three impacts in increasing and decreasing speed order

Impact set	Impact speed (m/s)		
Increasing order	1st pass	2nd pass	3rd pass
Decreasing order	3rd pass	2nd pass	1st pass
1	30	40	50
2	40	50	60
3	50	60	70
4	60	70	80

3.1.4.3 *Combinations of impacts at elevated moisture content*

In the third set of tests, the effect of seed moisture content on seed devitalisation was investigated. From the literature review it was found previous research shows that increasing moisture content reduces the effect of impact on seed damage and seed viability. Therefore, the hypothesis was that increasing moisture content of annual ryegrass seeds would reduced the devitalisation of seeds for a set of impacts. Moisture content was set at 11.3, 13.4, 16.8, and 23.8% by adding measured quantities of water to a 20 g sample of seed and allowing the seed moisture to equalise in a sealed bag at 5^{o}C for 5 days prior to testing. Seed moisture content was verified using the ASABE standard oven drying technique (ASABE-Standards 2006). Four different impact speed sequences were used; 1 impact at 50 m/s, 4 impacts at 50 m/s, 1 impact at 70 m/s and 4 impacts at 70 m/s.

3.1.5 Analysis of results

The energy needed to devitalise annual ryegrass seedling emergence can be expressed as a specific impact energy value. Specific impact energy was calculated using the specific kinetic energy formula and assuming that the coefficient of restitution of each impact was zero (perfectly plastic), as:

$$E_{impact}(kJ/kg) = \frac{1}{1000} \times \sum_{j=1}^{k} \tfrac{1}{2} V_j^2 \qquad (3.3)$$

Where: k = number of impacts;
V_j = rotor tip speed for impact j (m/s)

A material function to predict seed devitalisation based on combinations of impact speed and number of impacts was developed. A relationship between seed breakage phenomena and seed devitalisation was expected based on the literature review; thereby,

statistical models used for particle breakage in comminution (particle size reduction) science were applied for seed devitalisation. The breakage probability mastercurve given by Vogel and Peukert (2003a) (see Equation (2.11)) by was modified to model seed devitalisation. The mastercurve of Vogel and Peukert (2003a) accounted for particle size and since annual ryegrass seeds were not selected for their size, the size factor was included in the material constant ($F_{seed} = f_{mat}x$) and not accounted for separately. The modified form of the mastercurve proposed for this investigation was:

$$RSE(\%) = \left[1 - \exp\left(-F_{seed}\left(E_{impact} - k \times E_{\min}\right)\right)\right] \times 100 \tag{3.4}$$

Where: F_{seed} = resistance of the seed to fracture that results in seed devitalisation (kg/kJ);
E_{impact} = specific impact energy (kJ/kg);
k = number of impacts;
E_{min} = threshold specific impact energy for seed fracture that causes seed devitalisation ((kJ/kg).

The mastercurve hypothesises that there is a minimum impact energy for each impact that does not cause any seed devitalisation (as measured by testing). Therefore, the impact energy of any individual impact must be greater than the threshold energy to cause an increase in seed devitalisation. This effective specific impact energy (E_{eff}) which is available for seed devitalisation is given by:

$$E_{eff} = E_{impact} - k \times E_{\min} \tag{3.5}$$

The amount of damage needed to devitalise a seed depends on the hostility of the medium that the seed germinates in. As discussed in the literature review, seed devitalisation increased from germination trays (low hostility) to green house pots (medium hostility) and further increased in field germination (highest hostility), as per Hauhouot et al. (1998). Therefore, seed damage and seed devitalisation are linked through the hostility level of the soil. The parameters F_{seed} and E_{min} not only depend on the resistance of the seed to impact damage but also on the hostility of the soil conditions. The soil bin testing method would be expected to have lower hostility than in most field situations. Therefore, seed devitalisation calculated in this thesis represent a lower limit on what would be expected in the field.

The mastercurve estimates devitalisation of seeds exposed to a number of impacts at different impact speeds. In this way, both the single speed-multiple impact data set and combinations of impacts data set were used in a linear regression to find material parameters E_{min} and F_{seed}. IBM® SPSS® Statistics Version 19.0 (SPSS Inc. 2010, IBM Corp., NY, USA) was used to perform the regression analysis. First the seed devitalisation data was transformed by linearising Equation (3.4) as:

$$\ln(1-RSE) = -F_{seed}E_{impact} + F_{seed}kE_{\min} \tag{3.6}$$

The linear regression was performed to find the slope ($-F_{seed}$) and the intercept (F_{seed} $k \times E_{min}$).

The moisture content tests generated an insufficient dataset to analyse seed devitalisation using Equation (4.4). Instead, to analyse the effect of moisture content on seed devitalisation, multiple linear regression was used in SPSS®. Dummy variables were used for the four different impact series and moisture content was the fifth independent variable.

3.2 Machine function

3.2.1 Vector impact model

A theoretical vector model was developed to predict the number of impacts and the impact speed that a seed would be exposed to in an impact mill. The vector impact model used the simplified, two dimensional geometry of a seed devitalisation mills to trace the theoretical impact path of a particle through the mill. The vector model used a coefficient of restitution in the normal and tangential direction (See Figure 2.9 for definition) along with the angle of the impact bar, the rotational speed (= 0 for stator rows) and the radial location to determine the impact trajectories. The vector model assumed that the particle velocity does not slow between rows of bars (no effect of air flow or particle to particle impact) and that that energy was applied to particles through normal impact alone (no energy is applied through attrition or through shear).

3.2.1.1 *Generalised model*

The vector impact model was developed to be a generalised model for impact mills using concentric rows of rotating or static impact elements. The vector impact model was calculated based on a number of geometry inputs, as shown in Figure 3.2. Based on

the geometry input conditions, a vector diagram was solved for the generalised geometry of the impacts occurring in the mill to find a normal component of impact velocity of each impact. The normal component of impact velocity for each impact was used to calculate the prediction of seed devitalisation.

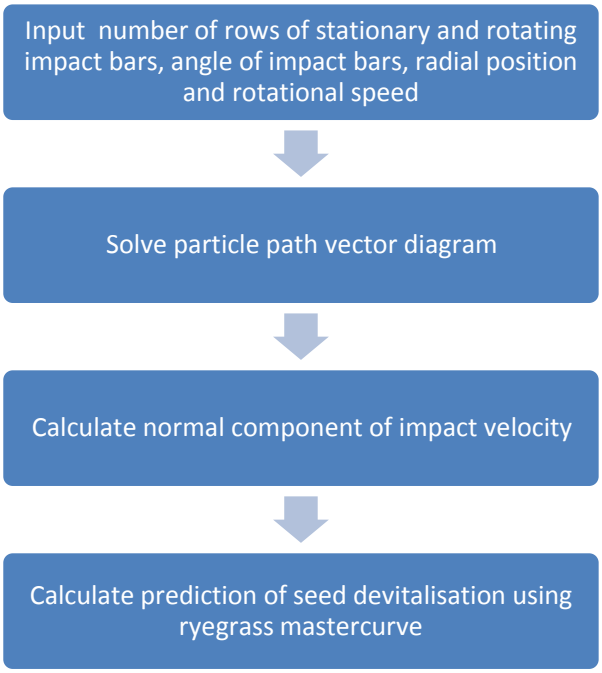

Figure 3.2: Vector model process flow chart

Figure 3.3 shows the generalised geometry of impacts occurring within an impact mill with concentric rows of impact elements. The particle path (orange) shows impact with two concentric rows of impact elements, numbered *j* and *j+1*. The velocity vectors before (red) and after impact (blue) are split into normal and tangential components relative to the impact surface. The tangential speed of the impact bars (purple) was determined using the rotational speed of the row of impact elements and radial location of impact. In this model it was assumed that impact occurred at the centreline of row of impact bars; thus, the number of impacts was equal to the number of rows of impact bars. For each static row of bars the tangential speed was zero.

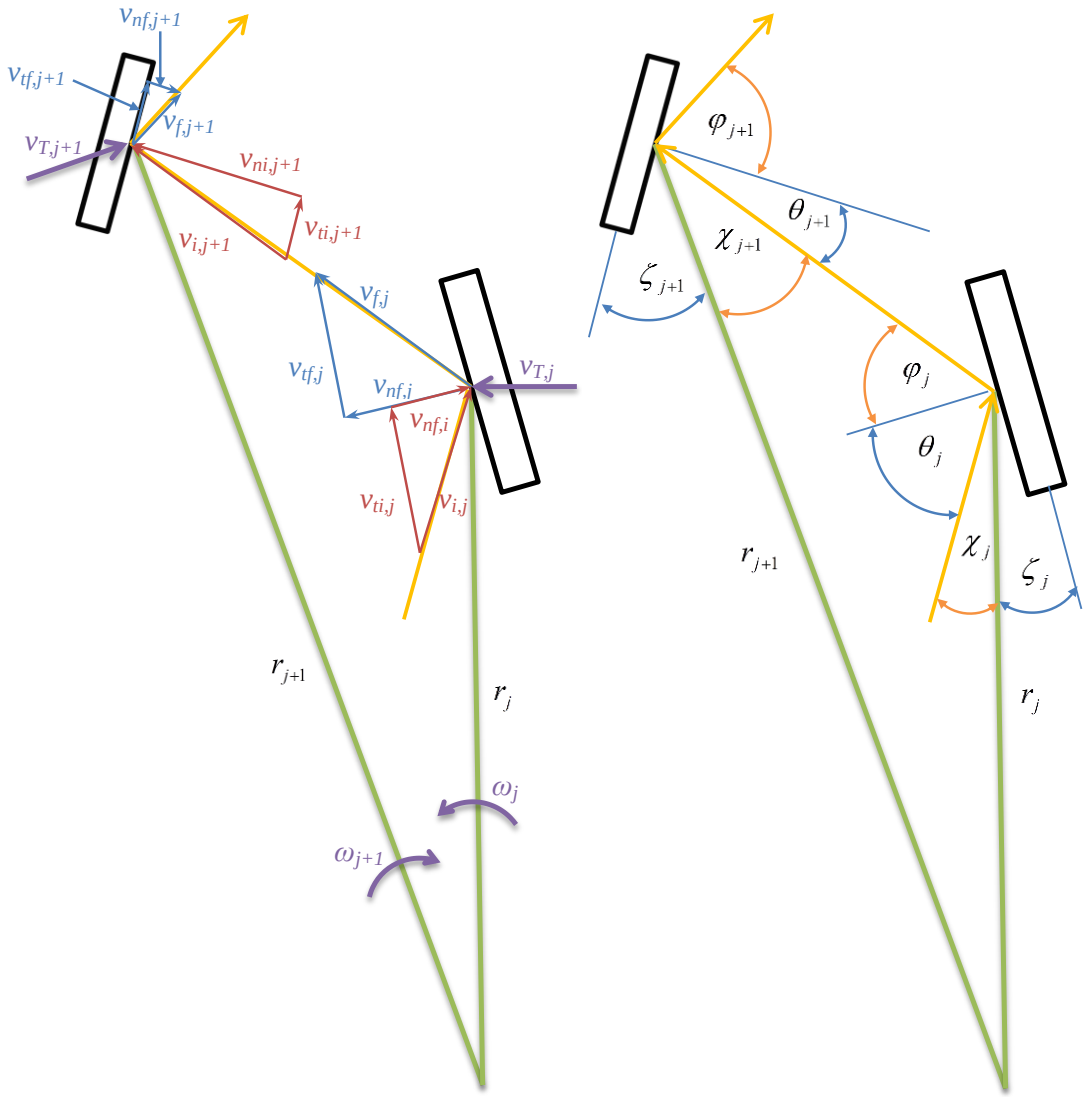

Figure 3.3: Generalised particle path vector diagram: Velocity vectors (left); angular geometry (right)

Where: r_j = radial location of the centreline of impact bar j (m)
θ = angle made with impact bars before impact
φ = angle made with impact bars after impact
ζ = angle of impact bar forward of radial
χ = angle between particle path and radial vector
$v_{T,j} = \omega_j r_j$ = tangential speed at the centreline impact bar j (m/s)
ω_j = rotational speed of impact row j
r_j = radial location of centreline of impact bar j
$v_{ni,j}$ & $v_{nf,j}$ = normal velocity components before ($_i$) and after ($_f$) impact relative to impact bar j (m/s)
$v_{ti,j}$ & $v_{tf,j}$ = normal velocity components before ($_i$) and after ($_f$) impact relative to impact bar j (m/s)
$v_{i,j}$ & $v_{f,j}$ = absolute velocity components before ($_i$) and after ($_f$) impact relative to impact bar j(m/s)

A code was generated using MATLAB® R2012a (MathWorks, Inc., Natick, 148 MA, USA) to solve the geometry in Figure 3.3. For *k* number of concentric rows of impact bars, a *for* loop was used to calculate the particle trajectories for impact bar $j = 2 \rightarrow k$. For $j = 1$, an assumption of the initial velocity of the particle was needed. This was set based on the mill design as will be shown in the next section for the three impact mills. Once this initial assumption was made the velocity after impact $j = 1$ could be calculated in the normal and tangential directions to begin the *for* loop.

The *for* loop began by calculating the magnitude of the particle velocity after impact *j*, given by:

$$v_{f,j} = \left(v_{tf,j}^2 + v_{nf,j}^2\right)^{0.5} \tag{3.7}$$

The angle that the particle trajectory made with impact bar *j* after impact was calculated using the velocity components:

$$\varphi_j = \cos^{-1}\left(\frac{v_{nf,j}}{v_{f,j}}\right) \tag{3.8}$$

It was assumed that there was no particle–particle or particle–air interactions. Thus, the magnitude of particle velocity prior to impact *j+1* was assumed to be the same as the magnitude of the particle velocity impact *j*:

$$v_{i,j+1} = v_{f,j} \tag{3.9}$$

To determine the normal and tangential velocity components of impact *j+1*, the angular geometry in Figure 3.3 is used along with the sign rule:

$$\frac{\sin\left(\chi_{j+1}\right)}{r_j} = \frac{\sin\left(\varphi_j + \theta_j + \chi_j\right)}{r_{j+1}} \tag{3.10}$$

The angle of the impact bars forward of radial (ζ) is known from the geometry of the mill and, hence is substituted in:

$$\frac{\sin\left(\frac{\pi}{2}-\theta_{j+1}-\zeta_{j+1}\right)}{r_j}=\frac{\sin\left(\varphi_j+\frac{\pi}{2}-\zeta_j\right)}{r_{j+1}}$$

$$\therefore \frac{\pi}{2}-\theta_{j+1}-\zeta_{j+1}=\sin^{-1}\left[\frac{r_j}{r_{j+1}}\sin\left(\varphi_j+\frac{\pi}{2}-\zeta_j\right)\right]$$

$$\therefore \theta_{j+1}=\frac{\pi}{2}-\sin^{-1}\left[\frac{r_j}{r_{j+1}}\sin\left(\varphi_j+\frac{\pi}{2}-\zeta_j\right)\right]-\zeta_{j+1} \tag{3.11}$$

Once θ_{j+1} is known, the normal and tangential particle velocity vectors before impact *j+1* can be calculated as:

$$v_{ni,j+1}=v_{i,j+1}\cos\theta_{j+1} \tag{3.12}$$

$$v_{ti,j+1}=v_{i,j+1}\sin\theta_{j+1} \tag{3.13}$$

Using the coefficient of restitution in the normal and tangential direction, the velocity vectors after impact *j+1* are calculated as:

$$v_{nf,j+1}=v_{T,j+1}+e_n\left(v_{T,j+1}+v_{ni,j+1}\right) \tag{3.14}$$

$$v_{tf,j+1}=e_t v_{ti,j+1} \tag{3.15}$$

For static rows of impact bars as used in the prototype mills, $v_{T,j} = 0$. The equations from (3.7) through to (3.15) were continued in the *for* loop until total number of impact rows was reached ($j = k$). Once the *for* loop was complete, the normal impact velocity was known and could be used for estimating seed devitalisation and specific processing power.

3.2.1.2 *HSD cage mill*

As mentioned previously, the calculation of impact velocity required an initial assumption about the initial velocity to begin calculation. For the HSD cage mill the particles were assumed to initially travel radially at 5 m/s. The initial radial velocity was small compared to the tip speeds of the bars and was used simply to initiate the solution. The radial velocity was equivalent to the initial tangential velocity relative to the first row of impact bars ($v_{ti,1}$ = 5 m/s). The initial velocity was purely radial, hence there was

no initial normal velocity relative to the first row of impact bars ($v_{ni,1}$ = 0 m/s). The normal velocity after impact with row 1 ($v_{nf,1}$), and tangential velocity after impact with row 1 ($v_{tf,1}$) was calculated using:

$$v_{nf,1} = v_{T,1} + e_n\left(v_{T,1}\right) \tag{3.16}$$

$$v_{tf,2} = e_t v_{ti,2} \tag{3.17}$$

The HSD cage mill has two cages that counter rotate that have 3 rows of cylindrical impact bars each. An example of the vector impact model idealised path for the HSD cage mill is shown in shown in Figure 3.4. For the HSD cage mill it was assumed that the particles have one direct impact (ζ =0) on the centre line of each row of impact bars. This simplified the calculation of impact path which is expected to be more random given the circular cross section of the HSD cage mill impact bars.

3.2.1.3 *Prototype mills*

The inlet paddles of the two prototype mills was assumed to operate in a slinging action similar to a forage blower as described by Chancellor (1960). The final normal component of velocity (v_{nf}) in the slinging action was the tangential speed of the paddle tip (Chancellor 1960):

$$v_{nf,1} = v_{t,1} \tag{3.18}$$

The final tangential component of velocity (v_{tf}) under slinging action was given by (Chancellor 1960):

$$v_{tf,1} = v_{nf,1}\left(1 - 0.7 f\right) \tag{3.19}$$

Where: f = friction coefficient assumed to be 0.8 for chaff

A quarter section view of the Prototype 1 and Prototype 2 mills, with examples of the vector impact model are shown in Figure 3.5 and Figure 3.6, respectively. Particles enter at the centre of both prototype mills and are distributed by the rotor paddles. The particles are impacted by successive impacts with concentric rows of rotor and stator bars.

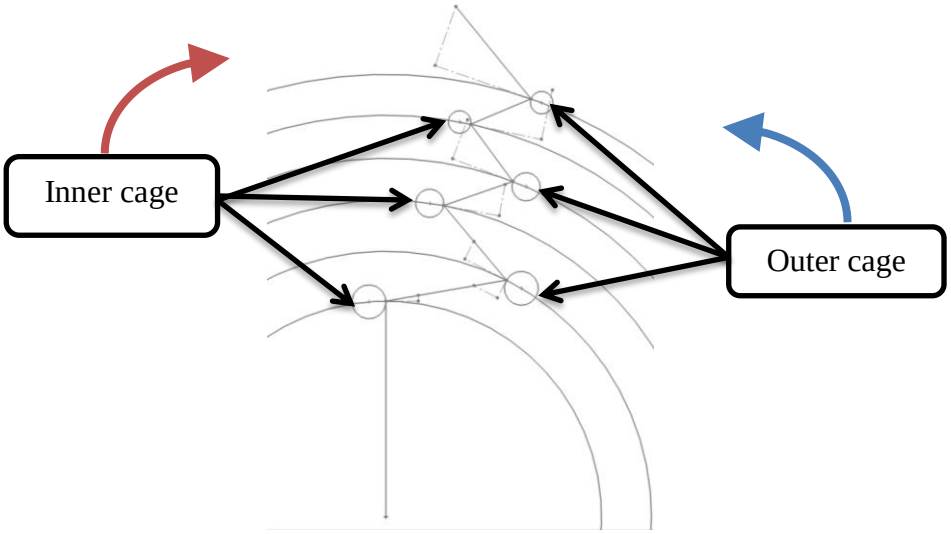

Figure 3.4: The geometry of the HSD cage mill rotor with theoretical velocity vectors

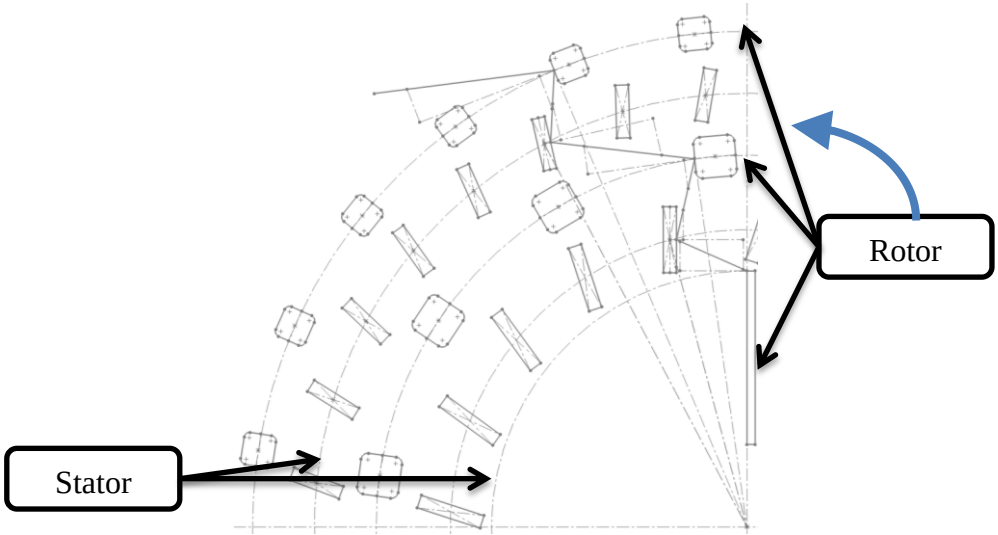

Figure 3.5: The theoretical impact vectors of the Prototype 1

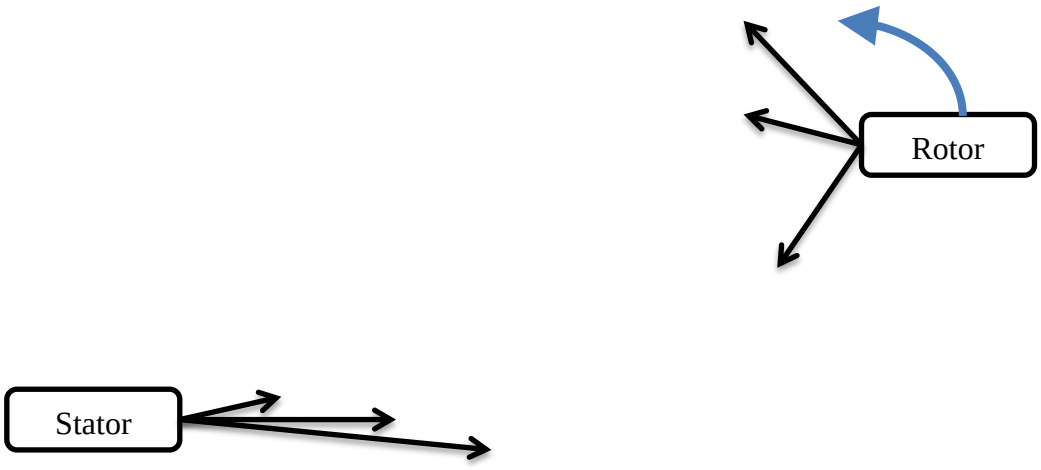

Figure 3.6: The theoretical impact vectors of the Prototype 2

3.2.1.4 *Vector model implementation*

The input variables to the vector impact model included the mill geometry (number of rows, angle of impact bars and radial position), rotational speed and coefficient of restitution in the normal and tangential direction. The coefficient of restitution of annual ryegrass was not known. Rebound height has been used by researchers to calculate coefficient of restitution for some seeds (Sharma & Bilanski 1971). However, annual ryegrass seeds are elongated and rebound height depends on impact orientation. Furthermore, the coefficient of restitution was likely to reduce with impact speed and moisture content, as shown for rape seed by (Wojtkowski et al. 2010). The measured values of coefficient of restitution of annual ryegrass seeds from rebound height experiments would be different to the coefficient of restitution in the high speed impacts (up to 120 m/s) that occur in an impact mill. Thus, the coefficient of restitution was assumed.

In the vector model it was found that having a normal component of coefficient of restitution that was greater than zero resulted in an increase in particle velocity after each impact through the mill. The particle velocity increase after each impact resulted in a build-up of velocity through the mill and unrealistically high impact velocities on the outer rows. Both particle to particle impacts and aerodynamic drag would in reality reduce the particle velocity prior to each impact and prevent this build-up of velocity due to particle restitution but were ignored in the vector model. Therefore, to prevent the build-up of velocity in the vector model it was assumed that impacts were perfectly plastic ($e_n = 0$). The impacts in the vector model were also assumed to be frictionless ($e_t = 1$).

3.2.2 Computational Fluid Dynamics (CFD) modelling

Computational Fluid Dynamics (CFD) impact model using particle tracing was used extend on the vector impact model prediction of number of impacts and impact speed; it included both aerodynamic forces on the particles and accounted for the random particle motion. The CFD impact model was used to model the number of impacts and impact speeds of particles through the HSD cage mill. Then the CFD impact model was used to model different concept designs for that could be integrated, prior to the construction and testing of the two final prototype designs. The CFD simulations were performed using SolidWorks® Flow Simulation 2012 (Dassault Systèmes) to model the air

movement through the three different mills. The trajectories of particles with the equivalent aerodynamic properties of annual ryegrass seeds was modelled using Flow Simulation particle study. The trajectories were exported to MATLAB® R2012a (MathWorks, Inc., Natick, 148 MA, USA) to calculate the number of impacts and impact speeds that a seed would be exposed to in an impact mill. A prediction of seed devitalisation based on the impact history was generated. The solution process is shown in Figure 3.7.

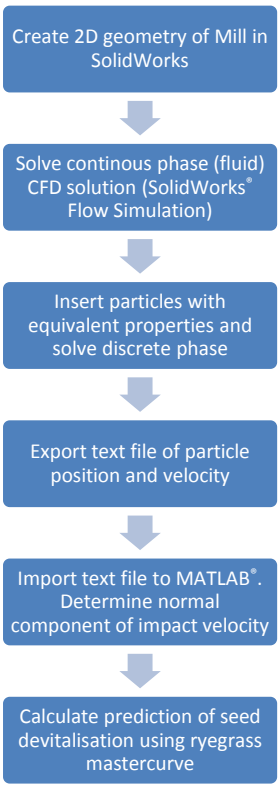

Figure 3.7: CFD particle simulation process flow chart

The SolidWorks® CAD models are meshed using Flow Simulation automatic meshing. Boundary conditions are applied to the model and result goals were set for pressure, velocity and temperature. SolidWorks® Flow Simulation iteratively solves the Navier-Stokes equations that define the conservation of mass, momentum and energy laws for fluid flows (Dassault Systèmes SolidWorks Corp. 2011b). SolidWorks® Flow Simulation uses the Farve-Averaged Navier-Stokes solver with a **k-ε** turbulence model and the Modified Wall Functions approach (Dassault Systèmes SolidWorks Corp. 2011b). The conservation laws for mass, angular momentum and energy in Cartesian coordinates are given by (Dassault Systèmes SolidWorks Corp. 2011b):

$$\frac{\partial \rho}{\partial t} + \frac{\partial}{\partial x_i}\left(\rho u_i\right) = 0 \tag{3.20}$$

$$\frac{\partial \rho u_i}{\partial t} + \frac{\partial}{\partial x_j}\left(\rho u_i u_j\right) + \frac{\partial p}{\partial x_i} = \frac{\partial}{\partial x_j}\left(\tau_{ij} + \tau_{ij}^R\right) + S_i \qquad i = 1,2,3, \tag{3.21}$$

$$\frac{\partial \rho H}{\partial t} + \frac{\partial \rho u_i H}{\partial x_i} = \frac{\partial}{\partial x_i}\left(u_j\left(\tau_{ij} + \tau_{ij}^R\right) + q_i\right) + \frac{\partial p}{\partial t} - \tau_{ij}^R \frac{\partial u_i}{\partial x_j} + \rho\varepsilon + S_i u_i + Q_H \tag{3.22}$$

$$H = h + \frac{u^2}{2} \tag{3.23}$$

Where: ρ = fluid density;
u = fluid velocity;
p = pressure ;
τ_{ij}= viscous shear stress;
τ_{ij}^R = Reynolds-stress tensor;
S_i = external force per unit mass due to a combination of porous media, buoyancy, and coordinate system rotation;
H = thermal enthalpy;
q_i = diffusive heat flux;
Q_H = volume specific heat source or sink;
q_i = diffusive heat flux;
subscripts i and j denote summation over three coordinate directions.

Two-dimensional (2-D) CFD analysis was used to model the air flow through each of the mills, as shown in Figure 3.8, Figure 3.9, and Figure 3.10. Using 2-D analysis significantly reduced the computational requirement. By using 2-D analysis, it was assumed that the motion of air and material through mill were constant across the depth of each mills.

Air without humidity effects was selected as the fluid as humidity was not relevant to this study. The walls were assumed smooth (roughness height = 0 μm) as near wall turbulence was not relevant to this study. The walls were adiabatic (no transfer of heat) as heat transfer was not relevant to this study.

A rotating region around the rotating components in each mill was modelled as a rotating reference frame in SolidWorks® Flow Simulation. The HSD cage mill had two rotating reference frames; one for each of the two cages that counter rotates. Each cage had three rows of impact bars; consequently, each rotating reference frame had three

regions surrounding the rows of bars, as depicted in Figure 3.8. Both the Prototype 1 (Figure 3.9) and Prototype 2 (Figure 3.10) mills were modelled using a single rotating reference frame that encompassed the inner paddles and two rows of rotor bars. The rotating reference frame was treated using the circumferential averaging technique as described in the literature review. Circumferential averaging is a steady state technique that is not sensitive to the relative position of the rotor (unlike the frozen rotor technique). Therefore, the transient flow was not solved for but averaged over time.

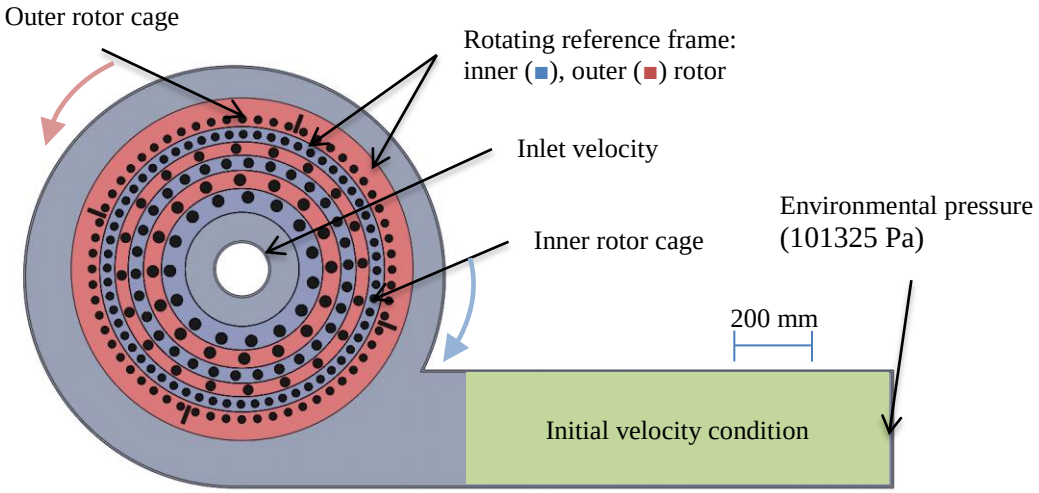

Figure 3.8 CFD model of HSD cage mill

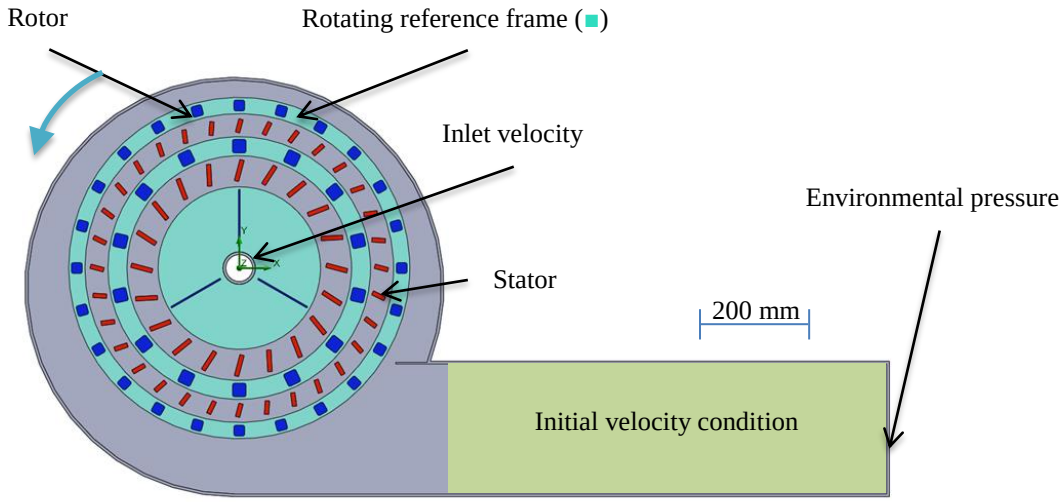

Figure 3.9 CFD model of Prototype 1: two rows of rotor bars, two rows of stator bars

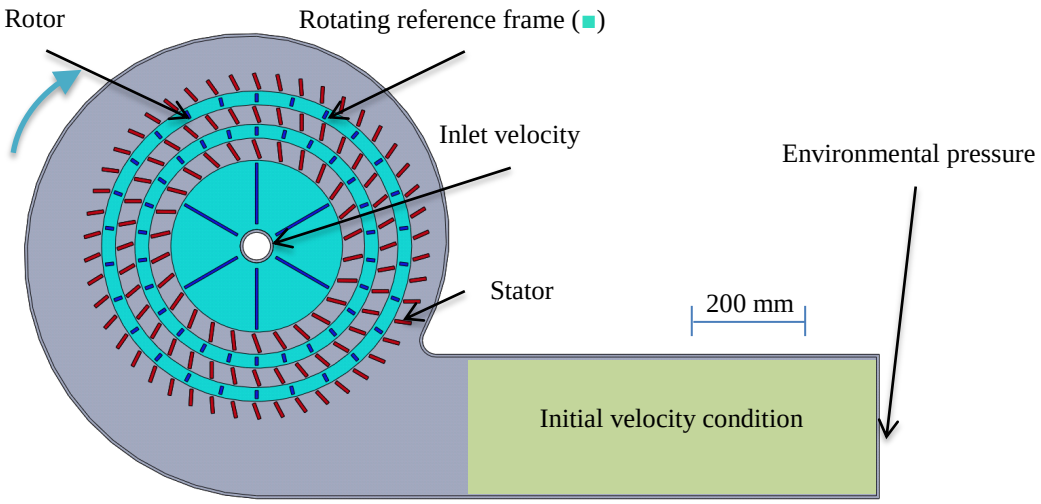

Figure 3.10 CFD model of Prototype 2: two rows of rotor bars, three rows of stator bars

3.2.2.1 *Boundary conditions*

The CFD model required an inlet and outlet boundary condition that specified the velocity or pressure. Using a pressure inlet and pressure outlet boundary condition was found to cause issues with solution convergence. It was found that the Flow Simulation CFD solution converged most stably and quickly with an inlet air velocity and an environmental pressure outlet, as shown in Figure 3.8, Figure 3.9, and Figure 3.10. The volume flow of air through the HSD cage mill was able to be measured. Thus, an inlet velocity boundary condition for the HSD cage mill model could be specified by dividing the volume flow by cross sectional area of the inlet.

At the commencement of the modelling performed in this study, there was no prototype mill to measure the air volumetric flow rate of air. One of the project goals was to achieve at least 1.5 m^3/s of air flow through each mill to maximise chaff mass flow capacity and minimise harvester sieve restriction. The target rotational speed was set at 2500 rpm. Therefore, during the design iterations for Prototype 1 the inlet velocity boundary condition was set so that the volumetric flow was 1.5 m^3/s at 2500 rpm and was scaled linearly with rotational speed. After the continuous phase solution had converged, the inlet pressure of the mill was investigated. If the inlet pressure was higher than atmospheric then the mill was under pressure and the actual air flow through the mill would be less than 1.5 m^3/s. The bar shapes and housing design were adjusted to achieve an inlet pressure of atmospheric or less. Once the Prototype 1 was built, the volumetric air flow was measured and was found to be slightly lower than predicted with the CFD model. The CFD code was run again using the experimental

volumetric flow rates as boundary conditions. A similar procedure was used to develop Prototype 2. The impact study results were found to change very little with the adjusted volumetric air flow for both mills. The results presented in this thesis are based on the updated volume flow rates that were experimentally determined.

Volumetric flow rate measurements

The volumetric flow rate of air of the three mills was determined for the condition of no material throughput by measuring the air velocity across a transect of an exit duct using a pitot tube and electric manometer (TSI® DP-Calc™ Micromanometer 5825). For the two prototype mills, three pitot tubes were mounted equally spaced in the vertical dimension on the rectangular exit duct. Each pitot tube was used to make 5 measurements equally spaced horizontally across the cross section of the exit duct. The five measurements of three pitot tubes created a grid of 15 measurements over the cross section of the exit duct.

The results shown of the 15 air velocity measurements were averaged and multiplied by the cross sectional area to determine the volumetric air flow. The process was performed at the four test speeds of the Prototype 1 and 2 (1500, 2000, 2500, and 3000 rpm). The volumetric flow Prototype 1 was quite high, almost achieving the project goal of 1.5 m^3/s at 2500 rpm. The Prototype 2 had slightly lower air flow because of a smaller rotor and the extra restriction of an extra static row.

The HSD cage mill inlet duct air velocity was measured in a 5 positions across a transect of the circular inlet duct. The average air velocity was multiplied by the cross sectional area to find volumetric flow of the HSD cage mill at the commercial operation speed of 1440 rpm. The volume flow of the Prototype 1 and 2 increased linearly with rotational speed as would be expected under the fan affinity law (Jorgensen 1983):

$$\dot{Q}_a = \dot{Q}_b \left(\frac{d_a}{d_b} \right)^3 \left(\frac{n_a}{n_b} \right) \tag{3.24}$$

Where: $\dot{Q}$ = volumetric flow rate;
d = diameter of fan;
n = rotational speed of fan;
Fan a and b are geometrically similar fans.

The volume flow of the HSD cage mill under slower rotational speeds was approximated by using the fan affinity law. For the rotational speeds in between the test speeds of the Prototype 1 and 2, the volumetric flow rate was linearly interpolated. The volumetric air flow measurements of the three mills is shown in Figure 3.11 along with a linear estimate of the HSD cage mill air flow at lower rotational speeds. The inlet velocity boundary condition of the three CFD models was set to the measured or predicted volume flow divided by the inlet cross sectional area. The inlet temperature was set at 20^{o}C and the inlet turbulence intensity was set at 5%.

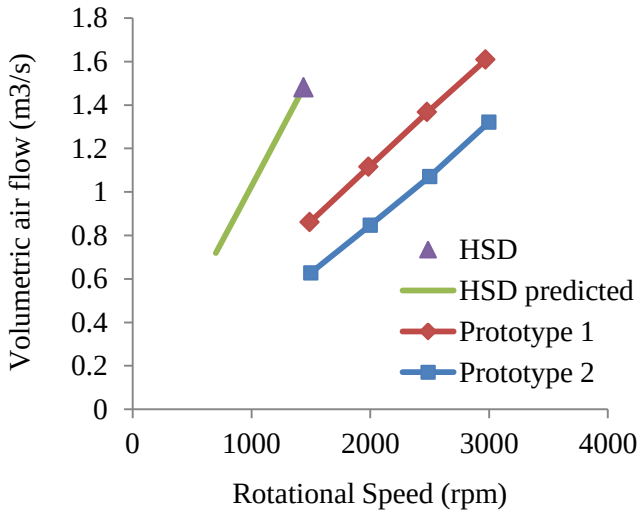

Figure 3.11: Volumetric air flow rate of weed seed devitalisation mills

A volumetric flow rate test of Prototype 1 was also performed at 2500 rpm with the addition of a chaff collection bag as used during seed devitalisation tests (see Section 3.3) and during chaff throughput measurements (see Section 3.4). The chaff collection bag was a minor restriction; it increased the static air pressure in the exit duct by an average of 26 Pa across the cross section and reduced the volumetric air flow from 1.37 m^3/s to 1.31 m^3/s.

3.2.2.2 *Initial conditions*

The global initial conditions were left as the default settings when modelling each mill: turbulence intensity 2%; turbulence length 0.0013 m; temperature 293.2 K; pressure 101325 Pa.

A local initial condition was specified for each mill to help aid convergence of the CFD solution. An initial zone of air velocity in the mill exit duct (see Figure 3.8, Figure 3.9

and Figure 3.10) was specified to set the initial exit air volume flow to the inlet volume flow.

3.2.2.3 *Solution goals*

Solution goals were used in SolidWorks® Flow Simulation to establish physical parameters of interest and were used for solution convergence. The specified solution goals can be plotted and used to monitor how the values change throughout the solution. For the CFD simulations of the weed seed devitalisation mills, the solution goals specified were:

1) static/total pressure – inlet/outlet bulk averaged;
    - to identify the fan properties of the mills;
2) volume flow – inlet/ outlet bulk averaged;
    - used (along with air density) to ensure conservation of mass of the mill simulation ($\dot{Q}_{in}\rho_{in} = \dot{Q}_{out}\rho_{out}$).
3) temperature – inlet/outlet bulk averaged;
    - to calculate power due to heat rise ($\dot{W} = \dot{Q}_{in}\rho_{in}C_p\,\Delta t$)
4) turbulent length/intensity - inlet/ outlet bulk averaged;
    - used to analyse how much turbulence the mills were generating, as generation of turbulence wastes input energy into heat generation;
5) rotor torque;
    - used to determine a prediction of the no load torque required to run the mills and, hence calculate a prediction of no load power requirement ($\dot{W} = T\omega$)

3.2.2.4 *Mesh*

The mesh was setup as per recommendations in SolidWorks® Flow Simulation literature (Dassault Systèmes SolidWorks Corp. 2011a). Flow Simulation starts with a global initial mesh of rectangular cells orthogonal to the Cartesian coordinate system (Dassault Systèmes SolidWorks Corp. 2011b). The density of the global initial mesh was set using

the number of cell divisions in the direction of the x axis and y axis. To generate the CFD mesh, Flow Simulation splits the global initial mesh at locations of fluid-solid interfaces. The mesh was further refined at fluid-solid interfaces based on the global mesh controls; small solid feature refinement, curvature refinement, tolerance refinement, partial cell refinement, and narrow channel refinement. The level of refinement selected for the global mesh controls for each of the mills is shown in Table 3.6. The refinement level refers to the number of times an initial cell is split into 4 (2 dimensional) refined cells. To increase solution fidelity, the mesh was also refined locally around the rotating and stationary impact elements using the mesh controls shown in Table 3.6. Refinement during the solution was used for each of the mills to increase the mesh density in regions of high gradient pressure and velocity. Increased mesh density in these regions helps increase the accuracy of the results. The only control of solution adaptive refinement available to the user is the refinement level which was set to two for all three mills.

Table 3.6: Initial CFD mesh settings for the three mills

		Refinement level				
Mill	Chosen initial mesh density	Small solid feature	Curvature	Tolerance	Partial cells	Narrow channel
HSD cage mill						
Global	150 × 100	3	2	4	3	2
Inner cage local	-	4	5	2	5	1
Outer cage local	-	4	5	2	5	1
Prototype 1						
Global	200 × 100	4	1	0	1	1
Rotor local	-	4	3	3	2	1
Stator local	-	4	3	3	2	1
Prototype 2						
Global	200 × 100	4	1	0	1	1
Rotor local	-	4	3	3	2	1
Stator local	-	4	3	3	2	1

To establish a mesh size independent solution, a mesh size study was performed. Four levels of initial mesh density were used and the solution goals were used to compare the solutions. The converged goals values for the mesh study for the HSD cage mill and Prototype 1 are shown in Table 3.7 and Table 3.8, respectively. Many of the goals had no significant dependence on the mesh density chosen. The exit volume flow was

slightly higher than the inlet volume flow because of the reduced air density at exit due to a temperature rise. For both the HSD cage mill (Table 3.8) and Prototype 1 (Table 3.8), it was apparent that the two highest mesh densities did not improve the results significantly. Thus, to reduce simulation time, the 150×100 division and 200×100 division initial mesh density were chosen for the HSD cage mill and Prototype 1 respectively. The same initial mesh density was used for the Prototype 2 as was used for Prototype 1. The chosen initial mesh density for each of the mills is shown in Table 3.6. An example of the final mesh density after initial refinement and solution adaptive refinement for the Prototype 1 is shown in Figure 3.12. The mesh is refined around the mill impact bars. The exit duct has been cropped shorter in the image for clarity.

Table 3.7: Results from mesh study HSD cage mill at 1440 rpm

Initial mesh	[X×Y divisions]	100×75	150×100	200×150	300×225
Fluid Cells	[cells]	321132	582826	1210788	2685156
Exit Static Pressure	[Pa]	101325	101325	101325	101325
Inlet Static Pressure	[Pa]	100413.1	100407.1	100411.7	100357.2
Exit Total Pressure	[Pa]	102701.7	102698.9	102691.7	102689.4
Inlet Total Pressure	[Pa]	100696.5	100690.6	100695.2	100640.5
Exit Temperature (Fluid)	[K]	295.2931	295.1696	295.0756	295.0437
Inlet Temperature (Fluid)	[K]	293.2	293.2	293.2	293.2
Exit Mass Flow Rate	[kg/s]	-1.77301	-1.77063	-1.7814	-1.77942
Inlet Mass Flow Rate	[kg/s]	1.775843	1.77583	1.776036	1.774961
Exit Volume Flow Rate	[m^3/s]	-1.48429	-1.48166	-1.49017	-1.48851
Inlet Volume Flow Rate	[m^3/s]	1.488726	1.4888	1.488902	1.488807
Exit Velocity	[m/s]	44.86362	44.77937	44.67462	44.69442
Inlet Velocity	[m/s]	21.79	21.79	21.79	21.79
Exit Turbulent Length	[m]	0.01793	0.01845	0.01911	0.01949
Inlet Turbulent Length	[m]	0.000542	0.000542	0.000542	0.000542
Exit Turbulent Intensity	[%]	18.68593	18.81912	18.84413	19.88338
Inlet Turbulent Intensity	[%]	2	2	2	2

Table 3.8: Results from mesh study Prototype 1 at 2500 rpm

Initial mesh	[X×Y divisions]	150×75	200×100	300×150	400×200
Fluid cells	[cells]	406522	657086	1652102	1783216
Exit static pressure	[Pa]	101325	101325	101325	101325
Inlet static pressure	[Pa]	102432	102944	102913	102566
Exit temp	[K]	298.31	297.28	297.11	297.74
Inlet temp	[K]	293.20	293.20	293.20	293.20
Exit total pressure	[Pa]	104526	104714	104672	104509
Inlet total pressure	[Pa]	104688	105212	105180	104825
Exit turbulence intensity	[%]	10.35	11.51	12.35	12.22
Exit turbulence length	[m]	0.00675	0.00741	0.00803	0.00817

Exit velocity	[m/s]	66.98	68.92	68.92	67.52
Inlet velocity	[m/s]	60.66	60.66	60.66	60.66
Exit volume flow	[m^3/s]	-1.41	-1.41	-1.41	-1.41
Inlet volume flow	[m^3/s]	1.37	1.37	1.37	1.37
Rotor torque	[N*m]	-44.58	-44.48	-44.80	-44.92
Rotor force x1	[N]	-5.80	3.39	3.47	2.56
Rotor force y1	[N]	3.25	-4.53	1.16	-0.40
Heating power	[W]	8493	6774	6489	7544
Pressure power	[W]	-222	-683	-696	-434
Rotor power	[W]	14004	13972	14075	14114
Power diff	[W]	-5289	-6515	-6889	-6136

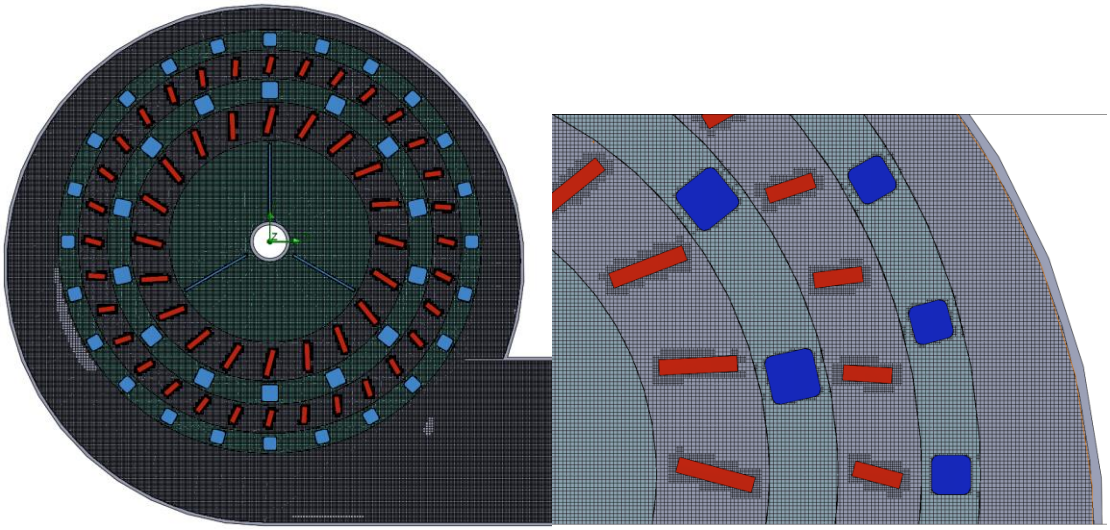

Figure 3.12: Final CFD mesh Prototype 1 overall (left) and close up (right)

3.2.2.5 *Particle tracing*

The converged CFD solution generated in SolidWorks® Flow Simulation was then used to trace particles through the mills using a particle study. The simulation calculated the particle motion based on impacts within the mill and aerodynamic drag forces on the particles. Flow Simulation particle study uses one-way coupling where only the effect of the fluid phase on the solid phase is considered; the effect of the solid phase on the fluid phase is not considered (See Section 2.6.2.2). To model the motion of annual ryegrass seeds through the mill, first the aerodynamic properties of the seeds were needed to input into the CFD model. The seed geometry and the seed terminal velocity were determined. The data was a prerequisite for the machine function; hence both the method and results of seed geometry and terminal velocity are presented in this section. The function for non-spherical drag found in literature was then used to approximate the

change in drag coefficient over a range of Reynolds number. The function for annual ryegrass drag coefficient was then fit onto the equivalent spherical drag function. The diameter and density of the equivalent spheres were entered into the CFD model and the trajectories calculated. The output trajectories were used to calculate the number of impacts and impact speed.

Seed geometry

The first stage to finding an aerodynamically equivalent sphere to represent annual ryegrass seeds was to measure the dimensions of the seed. The length width and thickness of 200 individual annual ryegrass seeds from the same batch of seeds used for impact testing were measured using digital Vernier callipers, as defined in Figure 3.13. To model the seed's shape, a prolate ellipsoid was used, as shown in Figure 3.14.

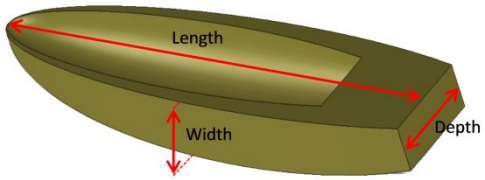

Figure 3.13: Physical Dimensions of annual ryegrass seeds

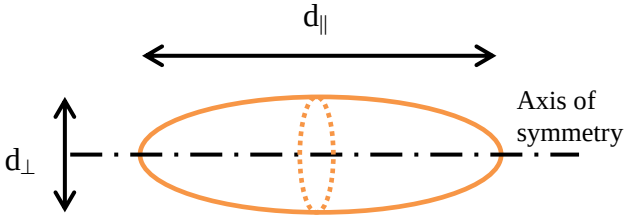

Figure 3.14: Prolate ellipsoid geometry as per (Loth 2008)

The normal diameter ($d_{\perp}$) was modelled as the average of the seed width and depth and the parallel diameter ($d_{\parallel}$) was modelled as the seed length:

$$d_{\perp} = \frac{W + D}{2} \tag{3.25}$$

$$d_{\parallel} = L \tag{3.26}$$

Where: W =seed width
D = seed depth
L = seed length

The aspect ratio (E) is given by (Loth 2008):

$$E = \frac{d_{\parallel}}{d_{\perp}} \tag{3.27}$$

An effective ryegrass diameter ($d_{ryegrass}$) of the prolate spheroid was given by (Loth 2008):

$$d_{ryegrass} = d_{\perp} E^{1/3} = d_{\parallel} E^{-2/3} \tag{3.28}$$

A summary of the results from the measurements are shown in Table 3.9. The annual ryegrass seeds were long and thin and, thus had a high mean aspect ratio of 5.4. Annual ryegrass seeds are also thinner in the width dimension than the depth dimension. The dimensional properties of annual ryegrass seeds varied considerably with the coefficient of variation between 9 and 13%.

Table 3.9: Dimensional properties of annual ryegrass seeds in mm

	Length (l)	Width (W)	Depth (D)	Normal diameter ($d_{\perp}$)	Aspect ratio (E)	Effective diameter ($d_{ryegrass}$)
Mean (mm)	5.82	0.85	1.31	1.08	5.38	1.90
Min (mm)	4.22	0.48	0.99	0.85	3.86	1.51
Max (mm)	8.13	1.17	1.87	1.41	7.35	2.39
Standard deviation	0.74	0.11	0.15	0.10	0.63	0.17
C.V (%)	12.7	12.5	11.1	9.3	11.7	9.0

Terminal velocity measurements

The next stage to finding an aerodynamically equivalent sphere to represent annual ryegrass seeds was to measure the terminal velocity of the seeds. A vertical wind tunnel was built to determine the terminal velocity of seeds, as shown in Figure 3.15. The dimensions of the design were based on Tabak and Wolf (1998). A diaphragm was used to control the volumetric flow rate of air into the fan. After the fan, the air passed through a honey comb, then a contraction section and mesh to straighten the air flow in the test section. Initially the diaphragm was shut. Particles were entered into the test section above the mesh screen. The inlet diaphragm was opened gradually until the particles lifted off the mesh and floated in the test section. The air velocity was measured in the centre of the test section using a hot wire anemometer (TSI^{TM}

VELOCICALC PLUS: multi-parameter ventilation meter 8386) to measure the terminal velocity. The variation in air velocity across the cross section where the seeds floated (not near the wall) was low. Therefore, the single air velocity measurement at the centre of the wind tunnel was considered representative of the terminal velocity of the seed.

Terminal velocity measurements were performed on the same 200 Annual Ryegrass (*Lolium rigidum*) seeds used for testing the dimensional properties. Terminal velocity measurement of each seed was repeated three times and the results of the three replications were averaged.

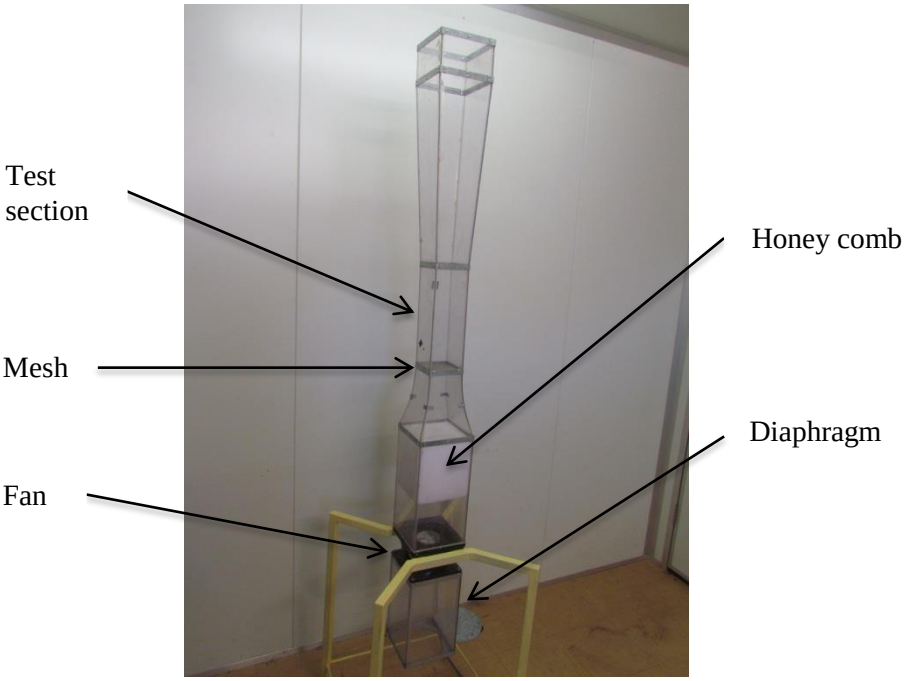

Figure 3.15: Vertical wind tunnel

The annual ryegrass seeds were seen to oscillate in the air stream of the vertical wind tunnel. The seeds spun while orientated at an approximate angle of 45^{o}, with the heaviest part of the seed, the embryo at the base of the oscillation, as shown in Figure 3.16. The seed also moved unstably through the test section of the vertical wind tunnel. The unstable motion of the seed would suggest that flow separation has occurred and a turbulent wake exists that is making the seed oscillate. The terminal velocity of the seed was found when the seed was airborne in the test section in this manner.

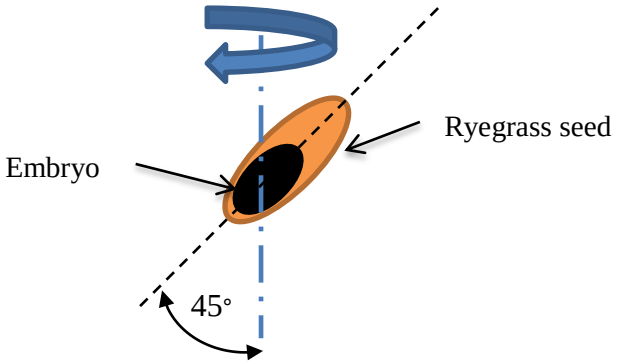

Figure 3.16: Annual ryegrass seed motion in the vertical wind tunnel

The measurement of terminal velocity of individual seeds was repeatable; the mean coefficient of variation between the three replications only 1.95%. The mean terminal velocity for annual ryegrass seeds was found to be 3.1 m/s. The terminal velocity for annual ryegrass was lower than wheat which has been found to range between 6.5-10 m/s (Gorial & O'Callaghan 1990). The annual ryegrass terminal velocity data was approximately normally distributed with a standard deviation of 0.45 m/s (C.V. = 15%), as shown in Figure 3.17.

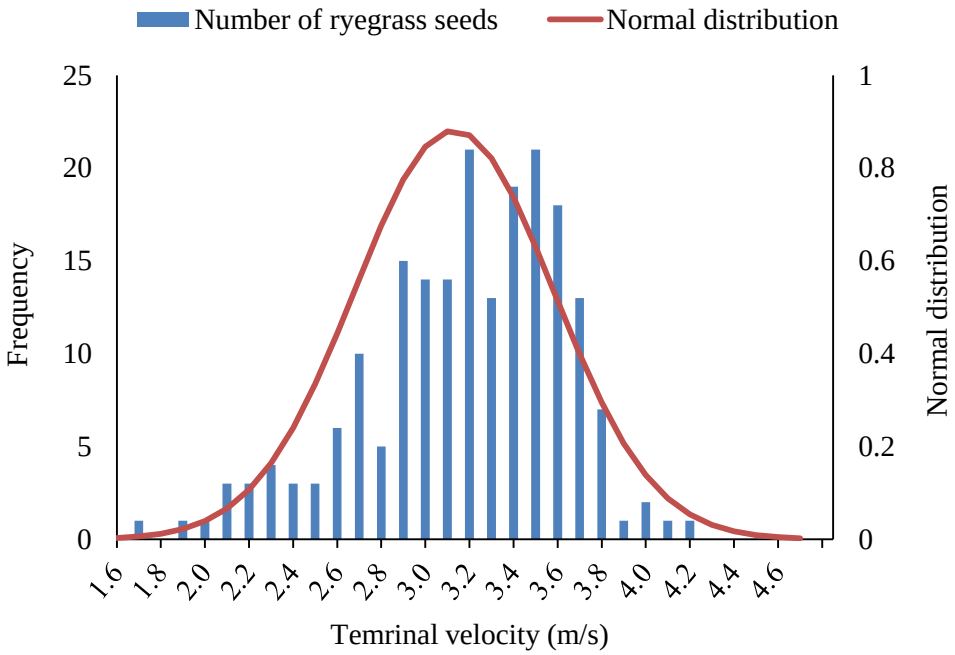

Figure 3.17: Histogram of annual ryegrass seed terminal velocity

Table 3.10: Annual ryegrass seed terminal velocity percentiles

Percentile (%)	2.5	25	50	75	97.5
Terminal velocity (m/s)	2.085	2.880	3.180	3.475	3.840

Calculation of drag coefficient

The next stage to finding an aerodynamically equivalent sphere to represent annual ryegrass seeds was to calculate the drag coefficient of annual ryegrass seeds. The terminal velocity tests and dimensional measurements provided the data needed to calculate the drag coefficient for annual ryegrass seeds.

The drag force on a particle is proportional to the projected area which is normal to the fluid flow (A_{proj}) (see Section 2.6.2.3). For non-spherical particles such as annual ryegrass seeds, the projected area depends on the particle orientation. The projected area of a prolate ellipsoid in Figure 3.14 is the area of a circle if the flow is parallel to the axis of revolution:

$$A_{proj\parallel} = \frac{\pi}{4} d_{\perp}^2 \tag{3.29}$$

If the air flow is perpendicular to the axis of revolution, then the projected area is the area of an ellipse:

$$A_{proj\perp} = \frac{\pi}{4} d_{\perp} d_{\parallel} \tag{3.30}$$

The orientation of the annual ryegrass seeds was at approximately 45° during the terminal velocity testing. As a result, the projected area was taken as the mean of the perpendicular ($A_{proj\,\perp}$) and parallel ($A_{proj\,\parallel}$) projected areas, given by:

$$A_{proj} = \tfrac{1}{2}\left(\frac{\pi}{4} d_{\perp} d_{\parallel} + \frac{\pi}{4} d_{\perp}^2 \right) \tag{3.31}$$

The drag coefficient of ryegrass was given by:

$$C_{D,ryegrass} = \frac{2mg}{\rho_a V_t^2 A_{proj}} \tag{3.32}$$

Reynolds number based on the effective diameter was given by (Loth 2008):

$$\mathrm{Re}_d = \frac{V d_{ryegrass}}{\nu} \tag{3.33}$$

Where: V = fluid velocity (m/s);
$d_{ryegrass}$ = sphere diameter (m);
ν = fluid kinematic velocity, for air at 20°C, $\nu = 1.51\times10^{-5}$ s/m^2 (Munson et al. 2006).

The drag coefficient based on the mean seed dimensions, terminal velocity and projected area is shown in Table 3.11.

Table 3.11: Mean seed dimensions, terminal velocity, projected area and coefficient of drag

$d_{\parallel}$ (mm)	$d_{\perp}$ (mm)	$d_{ryegrass}$ (mm)	E	V_t (m/s)	m (g)	A_{proj} (mm^2)	$C_{D,ryegrass}$	$\mathrm{Re_p}$
5.819	1.084	1.898	5.368	3.131	2.171×10^{-3}	2.926	1.232	393.3

Modelling non-spherical drag with Reynolds number

The drag coefficient calculated using the terminal velocity and geometry of annual ryegrass seeds was at an individual Reynolds number. The drag coefficient over a range of Reynolds number was needed to model the seeds motion in an air stream. In the literature review, a theory was presented by Ganser (1993) and Loth (2008) (see section 2.6.2.3). The theory showed that the $\mathrm{Re_p}$-C_D function of a non-spherical particle could be normalised onto the spherical particle $\mathrm{Re_p}$-C_D function by using shape factors. To model the motion of annual ryegrass seeds in an air stream, annual ryegrass was approximated as a prolate spheroid. The theory used by Ganser (1993) and Loth (2008) (see section 2.6.2.3) was used to approximate the prolate spheroid coefficient of drag over a range of Reynolds number. Using shape correction does not take into account complex secondary motion (e.g. spinning) that was observed. It was assumed that the complex secondary motion can be neglected without significantly affecting predicted trajectories. The shape factors for the Stokes and Newton drag regime normalised the particles $\mathrm{Re_p}$-C_D function with that of a sphere, using (Ganser 1993; Loth 2008):

$$\mathrm{Re}_p^* = \frac{C_{shape}\,\mathrm{Re}_p}{f_{shape}} \tag{3.34}$$

$$C_D^* = \frac{C_{D,ryegrass}}{C_{shape}} \tag{3.35}$$

Where: Re_p^* = Normalised Reynolds number

C_D^* = Normalised coefficient of drag

C_{shape} = Newton shape correction

f_{shape} = Stokes shape correction

The normalised Re_p-C_D function used was (Loth 2008):

$$C_D^* = \frac{24}{\mathrm{Re}_p^*}\left(1 + 0.15\left(\mathrm{Re}_p^*\right)^{0.687}\right) + \frac{0.42}{1 + \frac{42500}{\left(\mathrm{Re}_p^*\right)^{1.16}}} \qquad \text{for } \mathrm{Re}_p^* < 200\,000 \tag{3.36}$$

To estimate shape factor for prolate spheroids in Stokes drag regime, Loth (2008) recommended:

$$f_{shape} = \frac{E^{-1/3}\sqrt{E^2 - 1}}{\ln\left(E + \sqrt{E^2 - 1}\right)} \tag{3.37}$$

To estimate shape factor for prolate spheroids in Newton drag regime, Loth (2008) recommended:

$$C_{shape} = 1 + 0.7\sqrt{A_{surf}^* - 1} + 2.4\left(A_{surf}^* - 1\right) \tag{3.38}$$

Where: A_{surf}^* = the particle surface area normalised by the equivalent sphere, given by:

$$A_{surf}^* = \frac{1}{2E^{2/3}} + \frac{E^{1/3}}{2\sqrt{1 - E^{-2}}}\sin^{-1}\left(\sqrt{1 - E^{-2}}\right) \tag{3.39}$$

The shape correction factors based on the prolate spheroid for the mean seed dimensions are shown in Table 3.12.

Table 3.12: Stokes and Newton drag regime shape factors

f_{shape}	A^*_{surf}	C_{shape}
1.274	1.418	2.455

The Re_p-C_D function of the mean annual ryegrass seed approximated by a prolate spheroid was shifted to a lower Reynolds number and higher drag coefficient than the equivalent, sphere, as shown in Figure 3.18. The Reynolds number shift implies that the flow regimes for the prolate-spheroid at around half the Reynolds number of a sphere. For example, attached laminar flow (Stokes) ends at Re_p = 1000 for a spheroid but would end at Re_p = 520 for the prolate spheroid approximation of annual ryegrass seeds.

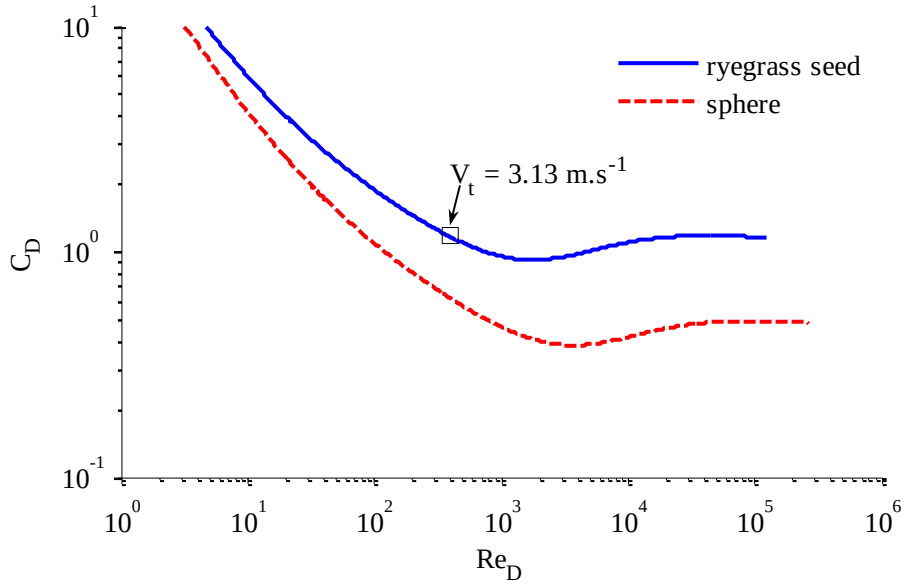

Figure 3.18: Sub-critical coefficient of drag of a sphere and annual ryegrass seed approximated with prolate spheroid using the method presented by (Loth 2008).

Implementing seed aerodynamic characteristics into Flow Simulation

SolidWorks® Flow Simulation uses a spherical Re_p-C_D function to calculate particle trajectories. To model annual ryegrass trajectories in Flow Simulation, an equivalent sphere was used. The equivalent sphere had to transition between different drag regimes (e.g. Stokes, transition and Newton) at the same air velocity as the prolate spheroid approximation of annual ryegrass seeds. The Reynolds number of the equivalent sphere ($Re_{p,sphere}$) was calculated using the annual ryegrass Reynolds number ($Re_{p,ryegrass}$) and the shape correction factors in Table 3.12, using:

$$Re_{p,sphere} = \frac{C_{shape}}{f_{shape}} Re_{p,ryegrass} \qquad (3.40)$$

Substituting in the definition of Reynolds number from Equation (3.33), gives:

$$\frac{Vd_{sphere}}{\nu} = \frac{C_{shape}}{f_{shape}} \frac{Vd_{ryegrass}}{\nu} \tag{3.41}$$

Where: d_{sphere} = diameter of equivalent sphere
$d_{ryegrass}$ = equivalent diameter of mean annual ryegrass seed (1.898 mm)

The air velocity and kinematic viscosity are equal on both sides of the equation. Therefore, the diameter of the equivalent sphere is given by:

$$d_{sphere} = \frac{C_{shape}}{f_{shape}} d_{ryegrass} \tag{3.42}$$

Equation (3.42) effectively shifted the Reynolds number of the equivalent sphere to ensure that transition between drag regimes occurs at the same air velocity that would be expected for the prolate spheroid. However, the coefficient of drag on the prolate spheroid approximation of annual ryegrass seed was also around twice that of a sphere (see Figure 3.18). The drag coefficient cannot be changed in SolidWorks Flow Simulation; consequently, the mass of the equivalent sphere needed to be changed to ensure that the equivalent sphere accelerated at the same rate that the annual ryegrass seed. The aerodynamic acceleration of the sphere was matched to the ryegrass seed at the seed terminal velocity (ignoring gravity):

$$a_{sphere} = a_{ryegrass} \tag{3.43}$$

Where: a_{sphere}= aerodynamic acceleration of the sphere
$a_{ryegrass}$= aerodynamic acceleration of annual ryegrass seed

Applying Newtons Second Law ($F = ma$) and using the drag force from Equation (2.14) gives:

$$\frac{\frac{1}{2} C_{D,sphere} \rho_a V_t^2 A_{proj,sphere}}{m_{sphere}} = \frac{\frac{1}{2} C_{D,ryegrass} \rho_a V_t^2 A_{proj,ryegrass}}{m_{ryegrass}} \tag{3.44}$$

Where: V_t = Seed terminal velocity
m_{sphere} = mass of equivalent sphere (g)

$m_{ryegrass}$ = mean mass of ryegrass seeds (2.171×10^{-3} g)

Therefore, the mass of an equivalent sphere is given by:

$$\therefore m_{sphere} = \frac{C_{D,sphere}A_{proj,sphere}}{C_{D,ryegrass}A_{proj,ryegrass}} m_{ryegrass} \tag{3.45}$$

The coefficient of drag of the sphere was calculated at the Reynolds number of the equivalent sphere using (Loth 2008):

$$C_{D,sphere} = \frac{24}{\mathrm{Re}_{sphere}}\left(1+0.15\,\mathrm{Re}_{sphere}^{0.687}\right)+\frac{0.42}{1+\frac{42500}{\mathrm{Re}_{sphere}^{1.16}}} \tag{3.46}$$

The density entered into SolidWorks® Flow Simulation was calculated by dividing the mass by the volume of the sphere:

$$\rho_{sphere} = \frac{m_{sphere}}{\frac{1}{6}\pi d_{sphere}^{3}} \tag{3.47}$$

Aerodynamically equivalent spheres was calculated based on the annual ryegrass seed terminal velocity (V_t) data, by using the mean and 2.5, 25, 50, 75, and 97 percentiles, as shown in Table 3.13. The sphere properties were calculated in the order of the columns (left through to right). First the diameter of the equivalent sphere was calculated based on the mean seed terminal velocity, using Equation (3.42). As there was no clear relationship found between the equivalent seed diameter and terminal velocity, the same sphere diameter was used for all equivalent spheres.

Table 3.13: Properties of a sphere that is aerodynamically equivalent to annual ryegrass seeds

Reference	V_t (m/s)	d_{sphere} (mm)	m_{sphere} ($g\times10^{-3}$)	$\mathrm{Re}_{p,sphere}$ (V_t)	$C_{D,sphere}$	$A_{proj,sphere}$ (mm^2)	ρ_{sphere} (kg/m^3)
Mean	3.131	3.658	3.187	758.0	0.5041	10.51	124.3
2.50%	2.085	3.658	1.609	504.8	0.5738	10.51	62.77
25%	2.880	3.658	2.766	697.3	0.5170	10.51	107.9
Median	3.180	3.658	3.273	769.9	0.5017	10.51	127.7
75%	3.475	3.658	3.808	841.3	0.4889	10.51	148.6
97.50%	3.840	3.658	4.522	929.7	0.4754	10.51	176.4

Verifying aerodynamic equivalent spheres

A verification model was used to ensure that the equivalent particles that were to be entered into the CFD were behaving with the desired aerodynamic properties. A vertical cylindrical tube with diameter of 500 mm and length of 2000 mm was modelled. An input air velocity boundary condition was set on the base of the tube at the median terminal velocity of the annual ryegrass seeds (3.18 m/s). Atmospheric pressure was set at the top of the tube. The side walls were given a moving wall boundary condition of 3.18 m/s to provide a uniform air velocity across the cross section of the tube. The model was meshed and the CFD simulation solved. Equivalent spherical particles representing the percentiles 2.5, 25, 50, 75 and 97.5% were entered 200 mm from the base of the tube. The particle vertical velocity was measured with time, as shown in Figure 3.19. As expected, the particles that had the equivalent terminal velocity below 3.18 m/s were pneumatically lifted upwards, and the particles with terminal velocity above 3.18 m/s fell against the air flow. The particle with the median terminal velocity of 3.18 m/s was lifted upwards to a velocity of 0.149 m/s. This indicates that the drag equation used by SolidWorks® Flow Simulation was slightly different to the equation used to create the equivalent spheres; an error of 4.7%. This error of equivalent aerodynamic properties was not expected to add significantly to the error to the analysis because terminal velocity of seeds varied considerably anyway (C.V = 15%).

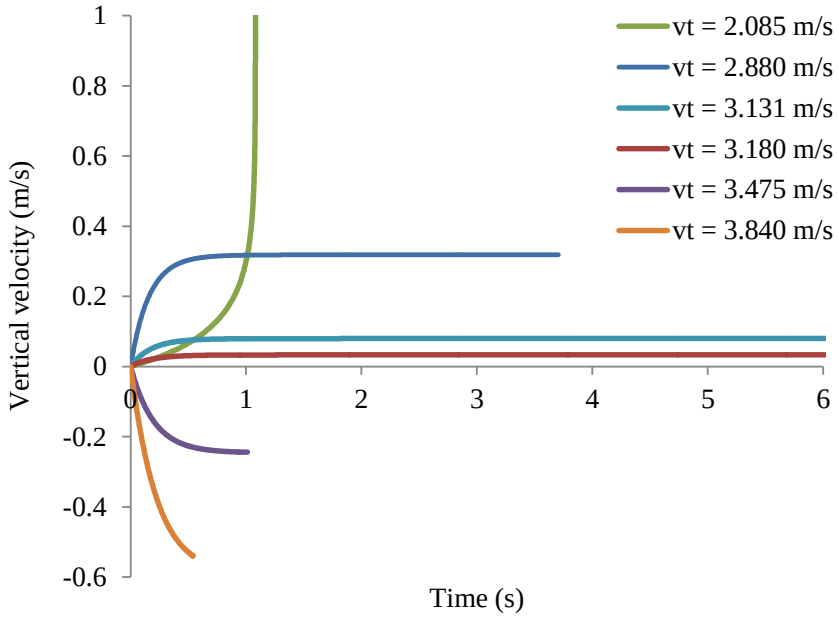

Figure 3.19: Particle vertical velocity in verification model showing different terminal velocities

Particle study

Once the steady state CFD solution had converged, a particle study was performed. Particles with the equivalent properties of annual ryegrass seeds (see Table 3.13) were inserted at the inlet of the mill. The particles were distributed evenly over the inlet of the mill. In all three mills, particles enter in the centre of the mill with some velocity in along the axis of rotation of the mill but with no radial velocity. The initial velocity in direction of axis of rotation was ignored in this 2 dimensional model and the initial velocity of the particles was set to zero.

The impacts in Flow Simulation are treated with the classical theory of impact with a coefficient of restitution in the normal direction and tangential direction. The assumptions of the particle study analysis were:

1) Non-spherical particle behaviour can be modelled as a sphere
2) No particle to particle impacts occur
3) No momentum transfer between particle and fluid phase (one way interaction)
4) Energy available to devitalise seeds is through normal impact alone. No energy is available through tangential impact (attrition) or through shear.
5) Impacts are nearly fully plastic (coefficient of restitution in normal direction; $e_n = 0.1$). Flow Simulation fails to solve at much lower normal coefficient of restitution.
6) Impacts are frictionless (coefficient of restitution in the tangential direction; $e_t = 1$). Flow Simulation was found to fail to solve at lower tangential coefficient of restitution.
7) The particles aerodynamic properties do not change through the mill. For example, under breakage the particle terminal velocity does not change.

The particle trajectories from SolidWorks® Flow Simulation were exported to a text file. In this text file was the time stamp, x and y position, and x and y components of velocity. A MATLAB® code was developed to determine the components of velocity with respect to the impact bar immediately before and immediately after impact. The MATLAB® code identified impacts as a step change (> 2m/s) in the x or y velocity

vectors. The normal component of impact velocity relative to the impact surface was used to estimate seed devitalisation using the annual ryegrass mastercurve (Equation (3.4)). The code converted the Cartesian velocity vectors from the text file into normal and tangential component velocity vectors relative to the impact surface.

Converting the velocity vectors into normal and tangential components involves simply shifting the coordinate system by the angle of the impact surface relative to the Cartesian coordinate system. However, the angle of the impact surface at the location of impact was not known so the normal and tangential components were derived by using the classical theory of impact.

The rotational speed and coefficient of restitution in the normal (e_n) and tangential (e_t) direction from Flow Simulation particle study were input into the MATLAB® code. In this thesis the normal and tangential coefficients of restitution were set at 0.1 and 1, respectively. An example of a vector diagram of an impact calculation is shown in Figure 3.20.

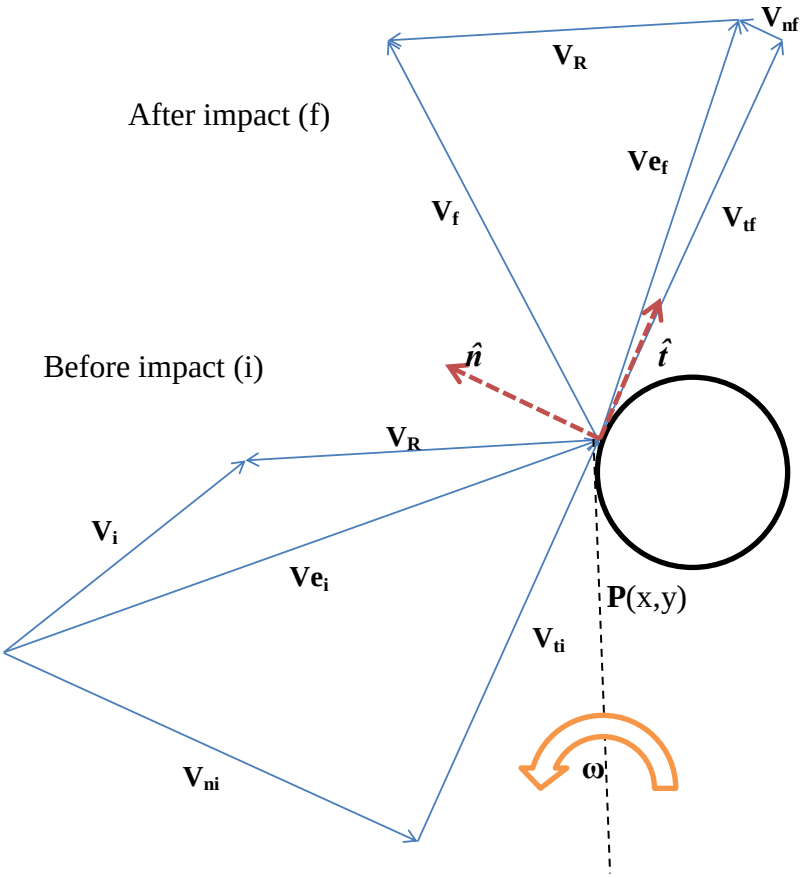

Figure 3.20: Vector diagram of the 2-D impact

Where: $\mathbf{P}(x,y)$ = Particle position vector at point of impact
$\boldsymbol{\omega}$ = Rotational velocity of impacted rotor
$\hat{\boldsymbol{n}}$ & $\hat{\boldsymbol{t}}$ = Unit normal and tangential vectors relative to impact surface
$\mathbf{V_R}$ = Rotor velocity vector at point of impact
$\mathbf{V_i}$ & $\mathbf{V_f}$= Velocity vector before and after impact
$\mathbf{Ve_i}$ & $\mathbf{Ve_f}$ = Effective velocity vector before and after impact
$\mathbf{V_i}$ & $\mathbf{V_f}$= Velocity vector before and after impact
$\mathbf{V_{ni}}$ & $\mathbf{V_{nf}}$= Normal component of impact velocity relative to impact surface.
$\mathbf{V_{ti}}$ & $\mathbf{V_{tf}}$= Tangential component of impact velocity relative to impact surface.

Each of the terms in Figure 3.20 are explained in the steps that the MATLAB® code went through to calculate the normal and tangential velocity components, as follows:

1. Take the particle position, $\mathbf{P}(x, y)$ for each impact and calculate the radial position:

$$r = \sqrt{x^2 + y^2} \tag{3.48}$$

2. Based on radial position, determine either the direction of rotation ($\boldsymbol{\omega}$) of the impact bar (HSD cage mill) or if the impact is with a rotor or a stator (prototype mills).
3. Calculate the velocity vector of the rotor ($\mathbf{V_R}$) at the radial impact location. As the rotor(s) rotate about (0,0), the magnitude of the rotor velocity vector is given by $|\mathbf{V_R}|=\omega r$. The direction of the rotor tip velocity is perpendicular to the particle position ($\mathbf{V_R} \perp \mathbf{P}(x,y)$); hence the rotor tip velocity vector is given by:

$$\mathbf{V_R} = \omega r \frac{[-y, x]}{\sqrt{x^2 + y^2}} \tag{3.49}$$

4. Use the velocity vector of the particle before ($\mathbf{V_i}$) and after ($\mathbf{V_f}$) impact and the velocity vector of the rotor to determine the effective velocity of the particle relative to the motion of the rotor at the impact location:

$$\mathbf{Ve_i} = \mathbf{V_i} - V_R \tag{3.50}$$

$$\mathbf{Ve_f} = \mathbf{V_f} - \mathbf{V_R} \tag{3.51}$$

5. Using the coefficient of restitution, the unknown normal ($\mathbf{V_n}$) and tangential ($\mathbf{V_t}$) components of the effective velocity are related before (i) and after impact (f) by:

$$\mathbf{V_{nf}} = -e_n \mathbf{V_{ni}} \tag{3.52}$$

$$\mathbf{V_{tf}} = e_t \mathbf{V_{ti}} \tag{3.53}$$

6. Let $\hat{\boldsymbol{n}}$ and $\hat{\boldsymbol{t}}$ be the unit vector normal, and tangential to the impact surface of the rotor, respectively. Therefore, $\hat{\boldsymbol{n}} \perp \hat{\boldsymbol{t}}$ and if $\hat{\boldsymbol{n}}$ is of the form [a,b], then $\hat{\boldsymbol{t}}$ is of the form ±[-b,a] (+is $\pi/2$ anticlockwise and – is $\pi/2$ clockwise). From the vector diagram in Figure 3.20:

$$|\mathbf{V_{ni}}|[a,b] + |\mathbf{V_{ti}}|[-b,a]=\mathbf{Ve_i} \quad (3.54)$$

$$|\mathbf{V_{nf}}|[a,b] + |\mathbf{V_{tf}}|[-b,a]=\mathbf{Ve_f} \quad (3.55)$$

Equations (3.50) and (3.51) were substituted into Equation (3.55) to form:

$$-e_n|\mathbf{V_{ni}}|[a,b] + e_t|\mathbf{V_{ti}}|[-b,a]=\mathbf{Ve_f} \quad (3.56)$$

The x and y components of $\mathbf{Ve_i}$, and $\mathbf{Ve_f}$ are $[Ve_{xi},Ve_{yi}]$ and $[Ve_{xf},Ve_{yf}]$ respectively. Equations (3.54) and (3.56) are resolved into x and components to give four equations simultaneous equations with four unknowns:

$$|\mathbf{V_{ni}}|a - |\mathbf{V_{ti}}|b=Ve_{xi} \quad (3.57)$$

$$|\mathbf{V_{ni}}|b + |\mathbf{V_{ti}}|a=Ve_{yi} \quad (3.58)$$

$$-e_n |\mathbf{V_{ni}}|a - e_t |\mathbf{V_{ti}}|b=Ve_{xf} \quad (3.59)$$

$$-e_n |\mathbf{V_{ni}}|b + e_t |\mathbf{V_{ti}}|a=Ve_{yf} \quad (3.60)$$

An inverse matrix was used to solve the four simultaneous equations for $|\mathbf{V_{ni}}|a$, $|\mathbf{V_{ni}}|b$, $|\mathbf{V_{ti}}|a$, and $|\mathbf{V_{ti}}|b$. Thus, the components of impact velocity in the normal and tangential components were known. The process was repeated for each impact that each particle was exposed to. Thus, the MATLAB® code determined the number of impacts and impact speeds that the SolidWorks® particle study predicted.

3.2.2.6 *Solids loading*

The CFD impact models cannot account for particle to particle impacts. The impact energy of particle to particle impacts can be half that of a particle wall impact (see 2.5.1); hence particle to particle impacts are and can significantly affect the milling result. The solids loading is an important milling parameter (see Section 2.5.2.4) that determines the likelihood of particle to particle impacts in the milling gap (Drögemeier & Leschonski 1996). An estimate of solids loading was generated for the three mills using the particle trajectories from the CFD models. The solids loading was estimated using the density of the particle position data points on a constant time stamp.

The output particle trajectories from SolidWorks® Flow Simulation were on an irregular time stamp so the particle trajectories were first interpolated onto a time stamp regular time intervals t_{step} =0.001 s. The trajectories of n =1000 particles were concatenated into one array. For each time point there is an x and y trajectory point for n particles.

The data density (d_i) for each data point i was generated by counting the number of data points within a radius r, from the data point. The number of data points was divided by the area of the circle with radius r. For k data points with Cartesian coordinates (p_x, p_y), the data density was given by:

$$d_i\left(\frac{points}{m^2}\right)=\frac{\sum_{j}^{k}\sqrt{\left(p_{xi}-p_{xj}\right)^2+\left(p_{yi}-p_{yj}\right)^2}<r}{\pi r^2} \tag{3.61}$$

As the time steps were made regular, the data density represented a function of number of particles and time. The data density was divided by the number of particles and multiplied by the time step to give the residence time normalised by area.

$$\frac{t_{res,i}}{A_i}=d_i\frac{t_{step}}{n_p}\left(\frac{s}{m^2}\right) \tag{3.62}$$

Where: t_{res} = residence time in the milling zone i
A_i = the area of milling zone i
t_{step} =0.001 s, time step of interpolated array
n_p =1000 number of particles

The modelled solids loading (mass flow of solids per mass flow of air) of chaff was calculated by dividing the mass of chaff in an impact zone and by the mass of air in the same zone. The air volume displaced by the chaff was neglected because it is small compared to the total volume of air. The solids loading was calculated using:

$$m_{f,i}\left(\frac{kg\,solids}{kg\,air}\right)=f_{v,z}\frac{\dot{m}_{chaff}\times t_{res,i}}{\bar{V}_i\times\rho_a} \tag{3.63}$$

Where: $m_{f,i}$ = solids loading (kg solids/ kg air)
$\dot{m}_{chaff}$ = mass throughput of chaff through the mill
$\bar{V}_i$= volume of milling zone i
ρ_a = density of air (1.204 kg.m^{-3} at 20^{o}C, 101325 Pa)
$f_{v,z}$ = volume factor

The volume factor ($f_{v,z}$) was used to account for the volume taken by the mill bars. Each mill was split in to concentric regions encompassing a single row of mill bars. The volume of the mill bars and the volume of the concentric region were calculated. The volume factor was calculated as:

$$f_{v,z} = \frac{\overline{V}_{region,z}}{\overline{V}_{region,z} - \overline{V}_{bar,z}} \tag{3.64}$$

Where: $\overline{V}_{region,z}$ = volume of the concentric region surrounding row z
$\overline{V}_{bar,z}$ = volume of the mill bars of row z

Using both Equation (3.62) and (3.63), a mass flow rate based specific solids loading equation was developed:

$$\frac{m_{f,i}}{\dot{m}_{chaff}}\left(\frac{kg/kg}{kg/s}\right) = f_{v,z}\frac{d_i A_i t_{step}}{\overline{V}_i \times \rho_a} \tag{3.65}$$

The volume of the milling zone is equal to the area of the milling zone multiplied by the depth of the milling zone, which is the depth of the mill D_i. Therefore, the specific solids loading can be simplified as:

$$\frac{m_{f,i}}{\dot{m}_{chaff}}\left(\frac{s}{kg}\right) = \frac{d_i t_{step}}{D_i \times \rho_a} \tag{3.66}$$

The specific solids loading was evaluated at each data point and then interpolated onto a grid. A contour plot was then able to be produced for each mill showing the specific solids loading across the cross section of the mill. The contour plot can be used to compare the relative likelihood of particle to particle impacts for the three mills.

3.2.3 Combining material and machine functions

3.2.3.1 *Estimation of seed devitalisation*

Combining the machine function with the material function for annual ryegrass seed was used to provide an estimate of seed devitalisation. The machine function generated using both the vector model and the CFD particle tracing both provided an estimate of the number of impacts and their impact speed. The material function provided a prediction of annual ryegrass seed devitalisation based on effective impact energy. To use the mastercurve, the number of impacts and impact speed needed to be converted to effective impact energy for each particle, using:

$$E_{eff,p} = \sum_{j=1}^{k} \left(E_j - E_{\min} \right), \text{ for } E_j > E_{\min} \tag{3.67}$$

Where: $E_j = \frac{1}{2} V_{nj}^2$: specific energy of impact j (kJ/kg)
V_{nj} = the normal impact velocity of impact j(m/s)
E_{min} = minimum energy to cause annual ryegrass seed devitalisation

Using the impact history of each particle in the CFD model a probability of seed devitalisation (in reduced seedling emergence (RSE)) was calculated for each inserted particle, using:

$$RSE_p = 1 - \exp\left(- F_{seed} \left(E_{eff} \right) \right) \tag{3.68}$$

Where: RSE_p = probability of seed devitalisation for particle p
F_{seed} = resistance of the seed to fracture that results in seed devitalisation

The vector model had one particle path and, hence the mastercurve needed only to be calculated once for each speed. The CFD model used 1000 particles and was calculated for each particle. The estimate of seed devitalisation for each mill was the average of the probability for seed devitalisation for each individual particle:

$$RSE = \frac{1}{n} \sum_{p=1}^{n} RSE_p \tag{3.69}$$

Where: n = number of particles

A 95% confidence interval of the predicted seed devitalisation was calculated using the 95% confidence interval of material function parameters, F_{seed} and E_{min}.

3.2.3.2 *Calculation of specific energy consumption*

The specific energy consumption is the energy needed to process a mass unit of chaff material, expressed as either kJ/kg or kW.h/tonne. An estimate of specific energy consumption was made based on the change in normal component of impact velocity of the rotating impact bars. The energy balance for an impact with a rotor bar was given by:

$$KE_{ri} + KE_{pi} = KE_{rf} + KE_{pf} + E_{loss} \tag{3.70}$$

Where: KE_{ri} & KE_{rf} = the kinetic energy of the rotor before and after impact, respectively (J)
KE_{pi} & KE_{pf}= the kinetic energy of the particle before and after impact respectively (J)
E_{loss} = energy lost into heat, deformation and generation of fracture surfaces

Conservation of linear momentum tangential to rotors motion is given by the mass and velocity of the rotor and particle, before and after impact (Beer, Johnston & Clausen 2004):

$$m_r v_{ri} + m_p v_{pi} = m_r v_{rf} + m_p v_{pf} \tag{3.71}$$

Where: m_r & m_p = mass of rotor and particle
v_{ri} & v_{rf} = velocity of rotor before and after impact
v_{pi} & v_{pf} = velocity of rotor and particle after impact

By treating the rotor as rigid, rotor mass can be calculated as a point mass (m) at the radius of the impact location (r), using the rotor's moment of inertia:

$$I = mr^2 \tag{3.72}$$

$$\therefore m = \frac{I}{r^2}$$

The velocity before and after impact are related using the coefficient of restitution (e) (Goldsmith 2001):

$$v_{rf} - v_{pf} = e\left(v_p - v_r\right) \tag{3.73}$$

Equations (3.71) and (3.73) are two simultaneous equations:

$$\begin{vmatrix} 1 & -1 \\ m_r & m_p \end{vmatrix} \begin{vmatrix} v_{rf} \\ v_{pf} \end{vmatrix} = \begin{vmatrix} e\left(v_{pi} - v_{ri}\right) \\ m_r v_r + m_p v_p \end{vmatrix} \tag{3.74}$$

Solving using row reduction, gives:

$$v_{rf} = \frac{1}{m_p + m_r}\left[m_r v_{ri} + m_p v_{pi} + m_p e\left(v_{pi} - v_{ri}\right)\right] \tag{3.75}$$

$$v_{pf} = \frac{1}{m_p + m_r}\left[m_r v_{ri} + m_p v_{pi} - m_r e\left(v_{pi} - v_{ri}\right)\right] \tag{3.76}$$

For a particle with mass much smaller than the rotor mass ($m_p \ll m_r$), the particle final velocity can be simplified to:

$$v_{pf} = v_{ri} - e\left(v_{pi} - v_{ri}\right) \tag{3.77}$$

The final energy of the particle is therefore:

$$KE_{pf} = \frac{1}{2} m_p \left(v_{ri} - e\left(v_{pi} - v_{ri}\right)\right)^2 \tag{3.78}$$

The energy loss term (E_{loss}) can be determined using the coefficient of restitution using (Goldsmith 2001):

$$E_{loss} = \frac{1}{2}\left(\frac{m_p m_r}{m_p + m_r}\right)\left(1 - e^2\right)\left(v_{pi} - v_{ri}\right)^2 \tag{3.79}$$

For a particle with mass much smaller than the rotor mass ($m_p \ll m_r$), the energy loss simplifies to:

$$E_{loss} = \frac{1}{2} m_p \left(1 - e^2\right)\left(v_{pi} - v_{ri}\right)^2 \tag{3.80}$$

The input energy of the rotor (E_{rotor}) to return to its operational speed after impact is given by the change in kinetic energy of the rotor:

$$E_{rotor} = KE_{ri} - KE_{rf} \tag{3.81}$$

Using the energy balance in Equation (3.70), the input energy of the rotor becomes:

$$E_{rotor} = KE_{pf} - KE_{pi} + E_{loss} \tag{3.82}$$

$$\therefore E_{rotor} = \frac{1}{2} m_p \left[\left(v_{ri} - e\left(v_{pi} - v_{ri} \right) \right)^2 - v_{pi}^2 + \left(1 - e^2 \right) \left(v_{pi} - v_{ri} \right)^2 \right] \quad (3.83)$$

For the perfectly plastic case (e = 0), the input energy of the rotor simplifies to:

$$E_{rotor} = m_p \left(v_{ri}^2 - v_{ri} v_{pi} \right) \quad (3.84)$$

The specific input energy of the rotor is the sum of the input energy calculated for each impact j using Equation (3.84) divided by the particle mass:

$$E_{spec} = \sum_{j=1}^{n} v_{ri,j}^2 - v_{ri,j} v_{pi,j} \quad (3.85)$$

The importance of Equation (3.85) is that the input energy of the rotor is not simply equal to the kinetic energy loss (E_{loss}) of the impact. The particle has a final kinetic energy after impact with the rotor and, hence the rotor must input this energy as well. To effectively use the kinetic energy imparted by the rotor onto the particle, a further impact is required to use the final kinetic energy of the particle for breakage.

3.3 Seed devitalisation

3.3.1 Sample generation

3.3.1.1 *Chaff*

The seed devitalisation of annual ryegrass (*Lolium* rigidum) seeds processed with each of the existing HSD cage mill, and the two new prototype mills was evaluated. Annual ryegrass seeds were added to wheat chaff and the mixture was processed by the mills.

The wheat chaff used for seed devitalisation tests was collected from chaff piles left from a CASE IH 8010 AFX harvester with a Riteway chaff cart after the 2009 harvest in Bute, South Australia. The chaff was expected to contain a background population of annual ryegrass seeds. A sampling technique (shown in Figure 3.21) was used to minimise variation in the background population of seeds between chaff samples. The chaff of an individual bag of chaff was placed on a tarp. The chaff was cut into eight approximately equal slices and opposing slices were mixed to make four samples. The process was repeated to make eight slices. Each chaff sample was made by taking a

small amount from of the eight chaff piles until the 2 kg (HSD cage mill) or 1 kg (Prototype 1 and 2) sample was achieved.

Figure 3.21: Chaff sampling technique: to ensure background annual ryegrass seeds are evenly distributed between replicates

3.3.1.2 *Seeds used for testing*

Once the chaff samples had been made, annual ryegrass (*Lolium rigidum*) seeds were added. The annual ryegrass (*Lolium rigidum*) seed used was from the same batch of seed with the same moisture content (11.3% w.t.) used for impact testing (see Section 3.1.2). The 2 kg chaff samples were laced with 5.000 g (weighed using milligram scales) of annual ryegrass seed (2296±31 seeds). The 1 kg chaff samples were laced with 2.500 g of annual ryegrass seed (1148±16 seeds).

3.3.1.3 *Tests performed*

The effect of mill rotational speed was investigated for all three mills. The effect of chaff throughput was determined for the two prototype mills. The tests performed are shown in Table 3.14.

Table 3.14: Seed devitalisation tests performed on each mill typed

Mill type	Speeds (rpm)	Chaff throughput (kg/s)	Chaff sample processed (kg)	Replications	Sub-samples per replication	Sub-samples planted per replication
HSD cage mill	900, 1100, 1300, 1440	≈ 0.5	2 kg	3-4	4	1
Prototype 1	1500, 2000, 2500, 3000	0.5, 1.5	1 kg	2	2	2
Prototype 2	1500, 2000, 2500, 3000	0.5, 1.5	1 kg	2	2	2

3.3.2 Chaff processing and collection

3.3.2.1 *HSD cage mill*

The second generation HSD was tested whilst stationary for seed devitalisation in Minnipa, South Australia on the 14th and 15th of September 2011. The speed of the HSD cage mill was set using the engine speed. The speeds were set based on what was tested by (Walsh, Harrington & Powles 2012), which was 900, 1100, 1300 and 1440 rpm. Due to the centrifugal clutch on the second generation HSD, a lower speed of 700 rpm test was not able to be achieved.

Annual ryegrass seeds (5 g) were thoroughly mixed with the chaff samples (2 kg) and were manually poured into the inlet of the second generation HSD over approximately 4 seconds (≈ 0.5 kg/s). Processed samples were collected on a tarp at the exit of the HSD cage mill, as shown in Figure 3.22. The tarp was setup to allow the air of the HSD cage mill to escape while capturing the processed chaff and seed. The material was swept up and bagged for the germination test. The mass proportion of chaff material collected of that processed reduced with rotational speed, as shown in Figure 3.23. The lowest proportion collected was 75%. The increased loss at higher rotational speeds was attributed to higher generation of fines and more air flow at the higher rotational speeds.

Figure 3.22: Chaff collection for HSD cage mill seed devitalisation testing

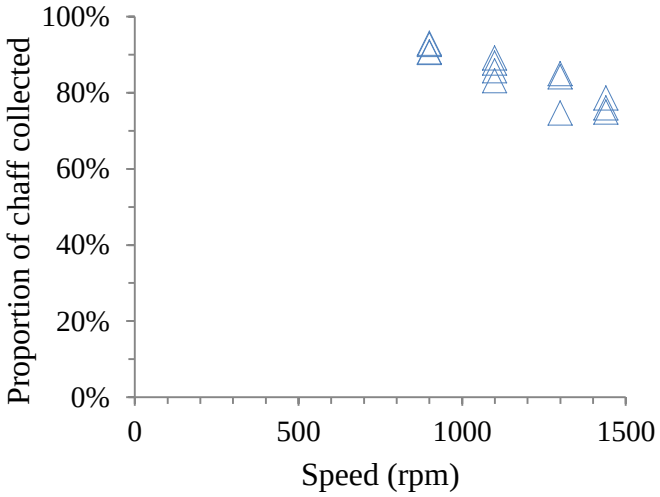

Figure 3.23: Mass proportion of chaff collected seed devitalisation testing Prototype 1

3.3.2.2 *Prototype 1*

The Prototype 1 concept design (developed using the CFD modelling technique) was converted to a 3D CAD design, built and mounted on a test stand, as shown in Figure 3.24. The Prototype 1 test stand was driven with a 30 kW 2 pole electric motor (Rototech Hu200L) through a 55A variable frequency drive (Zener MSC-3R55). The motor speed over the test period was determined by logging an inductive proximity sensor (OMRON TL-X5B1-GE) using LabVIEW (National Instrument Inc., USA, version 7.1) at 10 kHz and then calculating the speed using MATLAB®.

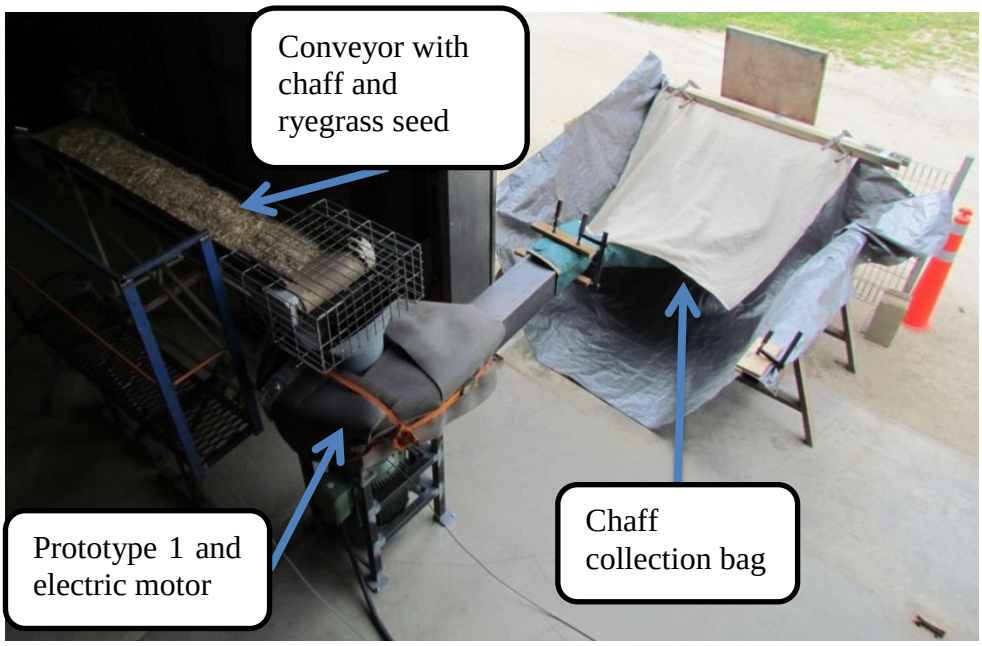

Figure 3.24: Prototype 1 seed devitalisation experimental setup

Testing of the Prototype 1 was performed in the University of South Australia workshop at Mawson Lakes on the 5th of October 2012 (0.5 kg/s) and the 13th of November 2012 (1.5 kg/s). Chaff was spread onto the conveyor belt and annual ryegrass seeds were spread on top of the chaff, along the centreline of the belt. The chaff was shaken by hand to move the seeds through the chaff profile. The conveyor belt speed was set to 1 m/s by setting the frequency controller to 63.5 Hz. The chaff throughput was set at 0.5 kg/s and 1.5 kg/s (3.6 and 10.8 t/h for 2 mills) by spreading the 1 kg chaff sample evenly over a 2 m and 0.667 m length of the belt, respectively.

Only 1 kg of chaff was used for the test because the electric motor drive speed of the rotor dropped too severely at 2500 and 3000 rpm for 2 kg of chaff. The low chaff mass flow of 0.5 kg/s was used because it equated to slightly more than the maximum chaff throughput tested with the HSD cage mill 3.6 t/h for two Prototype 1 mills compared to 3 t/h tested for the HSD cage mill by Walsh, Harrington and Powles (2012);. The 1.5 kg/s test was to replicate the approximate harvester chaff throughput; 10.8 t/h for two Prototype 1 mills. The rotor operational speed was set using the frequency controller but as the material loaded the motor, the speed reduced. The operational speed was calculated as the average operating speed over the test period, as shown in Table 3.15. The chaff was processed by the Prototype 1 rotor and captured in a collection bag. Volumetric air flow of up to 1.6 m^3/s (see Figure 3.11) was generated by the Prototype 1 rotor. The collection system used a bag that had a fine mesh to relieve this air flow

without significant loss off chaff. The amount collected reduced with rotational speed but was more than 85% at all speeds, as shown in Figure 3.25.

Table 3.15: Test rotational speed (rpm) of Prototype 1

Set speed (synchronous)	Operational speed (no load)	Mean operational speed 0.5kgs^{-1}	Mean operational speed 1.5kgs^{-1}
1500	1491	1487	-
2000	1988	1978	1966
2500	2481	2470	2436
3000	2973	2935	2889

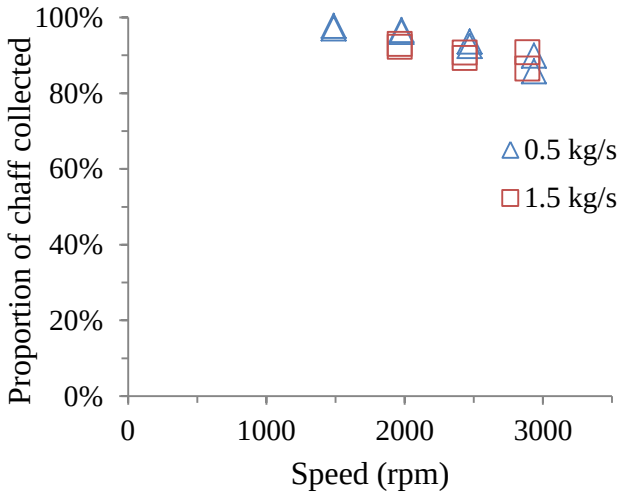

Figure 3.25: Mass proportion of chaff collected seed devitalisation testing Prototype 1

3.3.2.3 *Prototype 2*

To avoid the power limitations of the electric motor, the Prototype 2 was tested attached to the rear of the CASE IH 9120 combine harvester, as shown in Figure 3.26. Tests were performed on the 2nd of May 2013 (1.5kg/s) and the 6th of June 2013 (0.5 kg/s). The Prototype 2 was driven by a 50cc hydraulic motor (Euroline MF 50) which was fed by a 125 cc hydraulic pump (Bosch Rexroth A4VG125cc), driven by the harvester engine. Rotational speed was set using the by the electric controlled pump swash plate. The mill rotational speed was measured using an inductive proximity sensor (OMRON E2A-S08KS02-WP-M1-2M) logged using LabVIEW (National Instrument Inc., USA, version 7.1) at 10 kHz and then calculating the speed using MATLAB®. The same conveyor and collection bag as used for the Prototype 1 testing was used for testing the Prototype 2.

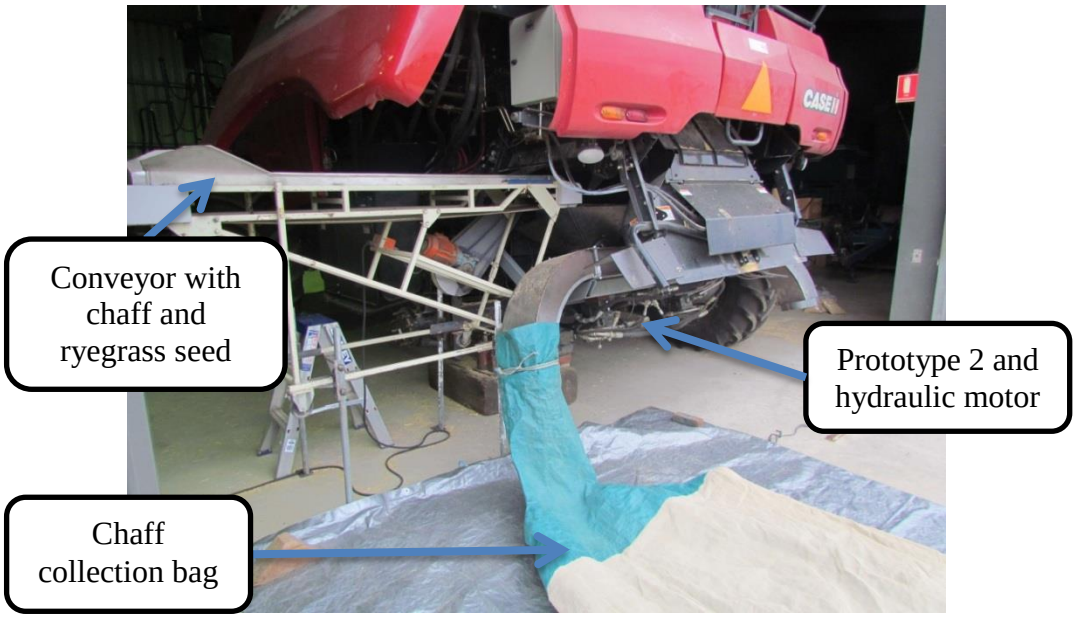

Figure 3.26: Prototype 2 seed devitalisation experimental setup

The rotational speed of the Prototype 2 rotor reduced slightly when the mill was loaded with chaff. The operational speed was calculated as the average operating speed over the test period, as shown in Table 3.16.

Table 3.16: Test rotational speed (rpm) of Prototype 2

Operational speed (no load)	Mean operational speed at 0.5kg/s	Mean operational speed at 1.5kg/s
1500	1488	
2000	1985	1940
2500	2464	2420
3000	2942	2932

The mass proportion of chaff collected reduced with speed but was above 92% at all speeds, as shown in Figure 3.27.

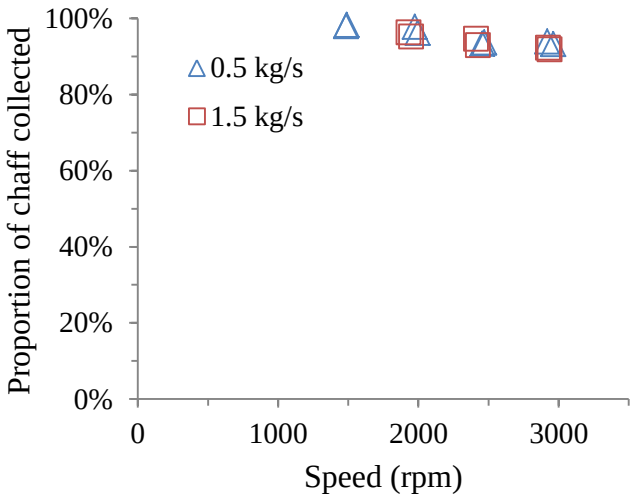

Figure 3.27: Mass proportion of chaff collected seed devitalisation testing Prototype 2

3.3.3 Subsample generation

Wheat residues can suppress germination when they break down in soil (see literature review Section 2.4.5.2). To ensure that the annual ryegrass seeds were not severely affected by the chaff residues breaking down, the concentration of chaff within the soil was maintained as low as practical. To reduce the chaff quantity mixed with soil, the chaff was sieved with an oscillating sieve to remove the larger material from the sample. The sieve width was 750 mm and length was 1700 mm; the oscillating frequency was 7 Hz, with a horizontal amplitude of 9 mm and vertical amplitude of 3.75 mm. The sieve hole diameter was 5mm. The material was spread thin on the rear of the sieve to prevent seeds being carried over the top. The material that did not fall through the sieve was inspected by hand to determine if any annual ryegrass seed was escaping. In no instance was there any annual ryegrass seed found in the material removed.

The HSD cage mill was found to break the chaff material up so much that very little was removed using the sieve. Thus, the sieve was not used for material processed by the HSD cage mill. The proportion of material removed using the sieve reduced with increasing rotational speed of both prototype mills. At higher rotational speeds, the chaff was more broken up and, thus more material fell through the sieve with the ryegrass seeds. For the control (unprocessed chaff) around 30% by weight of chaff was removed. From 1500 to 3000 rpm, the proportion removed reduced from approximately 25% down to 5%.

The chaff material that fell through the sieve was then split into subsamples using a subsampler. Subsamples from the left and right hand side of the subsampler were split

again and cross mixed to reduce the effect of any bias to the left or right. The multiple passes of the subsampler also ensured that the annual ryegrass seed was homogenously distributed through the chaff. The subsampling technique resulted in very low variation in mass between subsamples (Table 3.17) and no measurable bias.

Table 3.17: Coefficient of variation between subsample mass

Test	Coefficient of variation
HSD cage mill	2.0%
Prototype 1	1.6%
Prototype 2	2.4%

3.3.4 Germination method

The chaff subsamples were mixed in a cement mixer with soil and planted in soil bins. To obtain consistent seedling emergence, soil type was important; too much clay and the ryegrass seedlings would struggle to penetrate the hard surface. An 80:20 sand:loam mix was chosen for the soil type to prevent hard layers. 15 litres of soil was mixed with the chaff subsamples (3-6 litres) using a cement mixer. The cement mixer was emptied into a container and cleaned thoroughly using a brush to ensure all seeds were gathered. The soil bins used for the germination were 700×1500 mm in size; they had a permanent 40 mm layer of sandy loam covered with a weed barrier cloth. The soil chaff mixture was spread on top of the weed barrier cloth. A further 7.5 litres (≈ 7mm) of soil was then added to the top of the soil to ensure that there were no seeds remaining on the soil surface. The surface was rolled flat and watered. The quantities of soil used ensured that the seeding depth was a maximum of 40 mm. The soil bin preparation is shown in Figure 3.28.

The soil bins were held in an indoor, controlled environment room. The temperature was held at 25^{o}C for 12 hours during the day (06:00 till 18:00) and 15^{o}C for 8 hours during the night (20:00 till 04:00) with 2 hours linear ramping between day and night temperatures. The temperatures used were based on those specified in the germination tray method outlined in ISTA's international rules for seed testing for *Lolium rigidum* in Table 5A (2009). The humidity of the room was controlled to be at a constant 50% relative humidity. The soil bins were under light during the day period only (12 hours). The large surface area of soil exposed caused significant evaporation to occur which was subsequently condensed by the air conditioner when ramping down to the night

temperature. To prevent the surface of the soil from drying out, frequent watering was required. Seedling counts were performed at 14, 21 and 28 days and the maximum count was taken as the observation.

Figure 3.28: Soil bin preparation: A permanent layer of sand loam (A) was covered with a weed barrier cloth (B); chaff was mixed with sand loam in a cement mixer (C) and the mixture was evenly spread onto soil bin (D); a further layer of soil covered the mixture (E)

For each set of tests performed in the soil bins, a new bag of chaff was used. The background population of annual ryegrass seeds was expected to vary between chaff bags. Therefore, two control samples were created for each set of tests performed: a 1 kg of sample of chaff was collected; the chaff sample was passed over the 5 mm sieve; the remaining material was split into two subsamples; 1.250 g of annual ryegrass seed (574±8 seeds) was added to each subsample; and the control subsamples were mixed with soil and planted in the soil bins.

The control germination of all tests (C.V = 14.2%) varied more than the two controls of the same test (mean C.V = 4.7%), as shown in Table 3.18. The chaff used for each test (two controls and each treatment) were taken from an individual bag of chaff. Therefore, the greater between test variance indicates that the background population of annual ryegrass varied between bags of chaff. From the impact test studies it was found that the average germination of annual ryegrass seeds in the soil bins without chaff was 78%. Tests such as Prototype 1 1.5kg/s test had much higher germination percentage than this indicating that there was a significant background population of annual ryegrass seeds in the bag of chaff used. Whereas, only around 75% of seeds added to the Prototype 1 0.5kg/s test germinated, indicating that the background population was minimal in the bag of chaff used. The small variance between controls of the same test indicates that the chaff splitting method was without significant bias and the germination method was repeatable.

Table 3.18: Control seedling emergence table

		Max emergence count		Emergence (%)		
Test	Seeds added	Control 1	Control 2	Control 1	Control 2	C.V
HSD cage mill	574	447	483	77.9%	84.1%	5.5%
Prototype 1 0.5 kg/s	574	456	423	79.4%	73.7%	5.3%
Prototype 1 1.5 kg/s	574	658	612	114.6%	106.6%	5.1%
Prototype 2 0.5 kg/s	574	559	521	97.4%	90.8%	5.0%
Prototype 2 1.5 kg/s	574	549	529	95.6%	92.2%	2.6%
		C.V total	14.2%		mean	4.7%

To account for the background population of annual ryegrass seeds in the chaff, the seedling emergence of the processed samples were compared to the average control germination of that test. The metric used to describe annual ryegrass devitalisation when testing the three mills was the same as used for impact testing: Reduced Seedling Emergence (RSE) given by:

$$RSE\,(\%) = 1 - \frac{SE}{SE_{control}} \tag{3.86}$$

Where: SE is the maximum seedling emergence count for day 14, 21 and 28
SE_{control} is the average of the control seedling emergence counts

3.3.5 Analysis of statistics

3.3.5.1 Confidence interval

A confidence interval for seed devitalisation was calculated based on the variance of a treatment (not pooled variance). The low variability between subsample mass (Table 3.17) suggests that the proportion of viable seeds in each subsample would not be significantly biased. Thus, to calculate the confidence intervals, each subsample was treated as a trial. The arcsine transform is often used to transform a binomial distribution to a normal distribution (Ahrens, Cox & Budhwar 1990). Arcsine transforms of percentage data are often performed because they are limited to the range 0-100% and therefore are not normal. To generate a confidence interval for the reduced seedling emergence values firstly the values were transformed using the arcsine transform:

$$RSE^* = \arcsin\left(\sqrt{RSE}\right) \tag{3.87}$$

The 95% confidence interval of the true mean of RSE* was then calculated using (Mead, Hasted & Curnow 1993):

$$\mu_{RSE^*} = \bar{x} \pm t_{0.05,n-1} \frac{s}{\sqrt{n}} \tag{3.88}$$

Where: $\bar{x}$ = sample mean, n = number of trials, $t_{0.05,n-1}$ = 5% t score for $n-1$ degrees of freedom, s = standard error of sample mean.

The confidence interval was then transformed back to the original units.

$$\mu_{RSE} = \sin^2\left(\mu_{RSE^*}\right) \tag{3.89}$$

3.3.5.2 Empirical machine function

An empirical machine function was derived from the seed devitalisation results of the three mills. The empirical machine function was a similar approach to that found in literature (Vogel & Peukert 2003b, 2004, 2005); the result of the milling operation and the material function found from single particle impact testing were used to derive the machine function. The annual ryegrass seed devitalisation was assumed to follow the same fundamental mastercurve from impact testing (see Equation (3.4), Section 3.1.5). In Equation (3.4) there was an effective impact energy ($E_{eff} = E_{spec} - k \times E_{\min}$). The

effective energy a seed was exposed to in each of the mills was calculated by rearranging the mastercurve in Equation (3.4) as:

$$\frac{\ln(1-RSE)}{-F_{seed}} = E_{impact} - k \times E_{\min} \tag{3.90}$$

Where: $E_{impact} - k \times E_{min} = E_{eff}$ (effective impact energy);
F_{seed} = resistance of the seed to fracture that causes seed devitalisation (kg/kJ);
E_{impact} = specific impact energy (kJ/kg);
k = number of impacts;
E_{min} = threshold specific impact energy for seed fracture that causes seed devitalisation (kJ/kg).

The specific impact energy can be expressed in terms of velocity of impact j (V_j), given by:

$$E_{eff}(kJ) = \frac{1}{1000} \times \sum_{j=1}^{k} \tfrac{1}{2} V_j^2 - kE_{\min} \tag{3.91}$$

The Prototype 1 and Prototype 2 were tested at four rotational speeds and two mass flows of chaff. Thus, rotational speed and chaff mass flow were included in the empirical machine function. The HSD cage mill was only tested at one chaff mass flow and four rotational speeds and, thus only rotational speed was included. The analysis was performed using multiple regression. The basic form of the equation used for the regression analysis was developed based on some assumptions on how the mills devitalise seeds. The velocity of each impact was assumed to depend on rotational speed and the solids loading of the mill. The impact speed on the rotor and stator reduces with increasing solids loading because of a greater number of particle to particle collisions. The solids loading of chaff at each impact was used as a suppressive function of the impact speed. The suppression of impact speed was assumed to be linearly related to solids loading. The speed of impact j was assumed to be:

$$V_j = V_{th,j}(1 - c_1 m_{f,j}) \tag{3.92}$$

Where: $V_{th,i}$ = theoretical speed of impact j
c_1 = constant for the suppression of impact speed
$m_{f,j}$ = solids loading (kg of material/kg of air) at location of impact j

The theoretical speed of an impact with a rotor bar is calculated using the radial location of the impact and the rotational speed of the mill.

$$V_{th,j} = \omega r_j \tag{3.93}$$

Where: ω = rotational speed of the rotor (rad/s)
r_j = radial location of the impact j

The solids loading of the chaff material in an impact zone can be calculated using the mass flow rate of chaff, the time that the chaff material remains in the impact zone (residence time), and the volume and density of air, using:

$$m_{f,j} = \frac{\dot{m}_{chaff} \times t_{res,j}}{\bar{V}_j \times \rho_a} \tag{3.94}$$

Where: $\dot{m}_{chaff}$ = mass throughput of chaff through the mill
$t_{res,j}$ = residence time in milling zone j
$\bar{V}_j$ = volume of air in the milling zone j
ρ_a = density of air assumed to be 1.2 kg/m^3

The residence time reduces with increasing rotational speed because the particles move faster through the mills when they are impacted at higher velocities. It was assumed that the residence time through a mill is inversely related to the rotational speed of the mill:

$$t_{res,i} = c_2 \frac{1}{\omega} \tag{3.95}$$

Where: ω = rotational speed of the mill (rad/s)
c_2 = constant relating residence time to rotational speed

Therefore, the mass fraction of chaff in milling zone j is given by:

$$m_{f,j} = c_2 \frac{\dot{m}_{chaff}}{\bar{V}_j \times \rho_a \times \omega} \tag{3.96}$$

Combining Equations (3.92), (3.93) and (3.96), the speed of impact j is given by:

$$V_j = r_j \omega \left(1 - c_1 c_2 \frac{\dot{m}_{chaff}}{\bar{V}_j \times \rho_a \times \omega}\right) \tag{3.97}$$

The actual density of wheat chaff is far greater than the density of air. Whereas, the mass flow of chaff and air were of a similar magnitude: the mass flow of air for Prototype 1 was up to 1.9 kg/s based on 1.6 m^3/s air flow (see Figure 3.11); the mass flow of chaff tested was up to 1.5 kg/s. The volume of air passing through the mills was far greater than material passing through the mills. Thus, the volume of air displaced by the presence of chaff was small compared to the volume of air passing through the mill. Therefore, it was assumed that the volume of air in the milling zone remained constant for mass flow of chaff. The constants c_1 and c_2, as well as the volume and density of air were absorbed into one constant C (1/kg):

$$\therefore V_j = r_j\omega - r_j C\dot{m}_{chaff} \tag{3.98}$$

Substitution Equation (3.98) into Equation (3.91) gives:

$$\therefore E_{eff} = \frac{1}{1000}\times\sum_{j=1}^{k}\tfrac{1}{2}\left(r_j\omega - r_j C\dot{m}_{chaff}\right)^2 - kE_{\min} \tag{3.99}$$

As the radial location of each impact was unknown, a second constant B was defined as:

$$B = \sum_{j=1}^{k} r_j^2 \tag{3.100}$$

Therefore, the effective energy of each of the mills is expected to be a function of the form:

$$E_{eff} = \frac{1}{2000}B\left(\omega - C\dot{m}_{chaff}\right)^2 - kE_{\min} \tag{3.101}$$

Non-linear regression was used for each of the prototype mills using SPSS®. The regression found the unknown constants, B, C and k, that fit the dependant variable E_{eff}, based on independent variables; rotational speed ω and mass flow of chaff $\dot{m}_{chaff}$., using:

$$\frac{\ln\left(1-RSE\right)}{-F_{seed}} = \frac{1}{2000}B\left(\omega - C\dot{m}_{chaff}\right)^2 - kE_{\min} \tag{3.102}$$

The estimate of seed devitalisation was then found using by rearranging Equation (3.102), in terms of RSE:

$$RSE = 1 - \exp\left[-F_{seed}\left(\frac{1}{2000}B\left(\omega - C\dot{m}_{chaff}\right)^2 - kE_{\min}\right)\right] \tag{3.103}$$

The HSD cage mill was only tested at one throughput. Therefore, the effect of chaff throughput could not be taken into account. A nonlinear regression was performed using Equation (3.102) with the coefficient *C* removed. The independent variable was ω^2.

3.4 Power and chaff throughput measurement

The power to process chaff and devitalise weed seeds was a key performance criteria. Furthermore the wheat chaff mass flow of a modern combine harvester was an important design parameter for a weed seed destruction mill. The power to process wheat chaff was measured for all three weed seed devitalisation mills. The wheat chaff throughput was measured for the HSD cage mill and Prototype 1, which were both field tested.

3.4.1 HSD cage mill

The chaff mass flow and HSD cage mill power testing was undertaken whilst harvesting wheat during November and December 2011 at three sites across South Australia; Minnipa, Maitland, and Pinnaroo. Testing was performed with the second generation HSD (green) attached to a John Deere 9650 combine harvester. The header front width was 11 m. Three harvester ground speeds at each location were used to vary the throughput of chaff processed by the HSD cage mill. The three speeds were equally spaced and the maximum speed was near the harvester's maximum capacity in wheat (around 27 t/h). The testing parameters for the three sites are shown in Table 3.19.

Table 3.19: HSD cage mill power and chaff throughput test parameters

Site	Minnipa	Maitland	Pinnaroo
Crop variety	Mace	Wyalkatchem	Mace
Crop yield (t/ha)	2.4	7.3	2.7
Run Length (m)	90	30.6	90
Speeds (km/h)	4.5, 7 and 9	1.5, 2.5 and 3.5	3.5, 5.5 and 7.5
Rotor speeds (rpm)	960	960 and 700	700

The harvester was initially setup to the harvester Operator's Manual settings for wheat. Adjustments were made to ensure that the grain sample quality was good and the grain loss monitor was not reading too high. Physical measurements of grain loss were not possible with the HSD fitted because the sieve area was not accessible. The cut height of the crop was set to 150 mm for all trials. The run lengths were based on what could comfortably fit in the chaff collection bag.

To measure the chaff mass throughput, the HSD was modified by attaching a chute to the exit of the mill. Attached to the chute was a semi-permeable bag (Figure 3.29 a)) that was made with a woven cloth top side and a canvas underside. The bag collected the processed chaff material for the test while allowing air to escape. As mentioned in Section 3.2.2.1, the chaff collection bag provided a minor restriction to the air flow and, hence was not expected to significantly affect the power of the mill.

The test was run and the bag was removed and weighed using calibrated tension scales, as shown in Figure 3.29 b). The chaff weight was taken as the difference between the full bag weight and the empty bag weight. Throughput of chaff was calculated using the chaff mass, the plot area and harvester travel speed.

Figure 3.29: a) Chaff collection bag attached to HSD, b) weighing of full chaff bag

The mass throughput of chaff collected was compared to the mass throughput of grain harvested. The grain mass for the test length was measured by using the calibrated yield monitor and logged though the John Deere GreenStar 2 terminal. The harvester was run for approximately one minute after leaving the crop after each test length to ensure all the grain had entered the grain tank. Average grain mass throughput was determined by using the area of the plot, speed of operation and the grain mass for the plot.

The power of the HSD engine was calculated using the Isuzu CAN-BUS torque and speed output, logged with a Datataker DT85. The hydraulic power of the system was estimated using the pressure drop across each of the motors multiplied by the flow rate of the motor and subtracted from the total power to determine the power required to run

the belt driven HSD cage mill. The chopper was disconnected when performing the trials and therefore did not need to be taken into account.

3.4.2 Prototype 1

Harvest trials of the Prototype 1 were performed in a wheat (Scout) crop near Mallala, South Australia on two dates: 24th of December 2012 and 9th of January 2013. The harvester was a CASE IH 9120 Axial Flow modified with a pair of Prototype 1 mills side by side. The chaff was captured by the mills as shown in Figure 3.30.

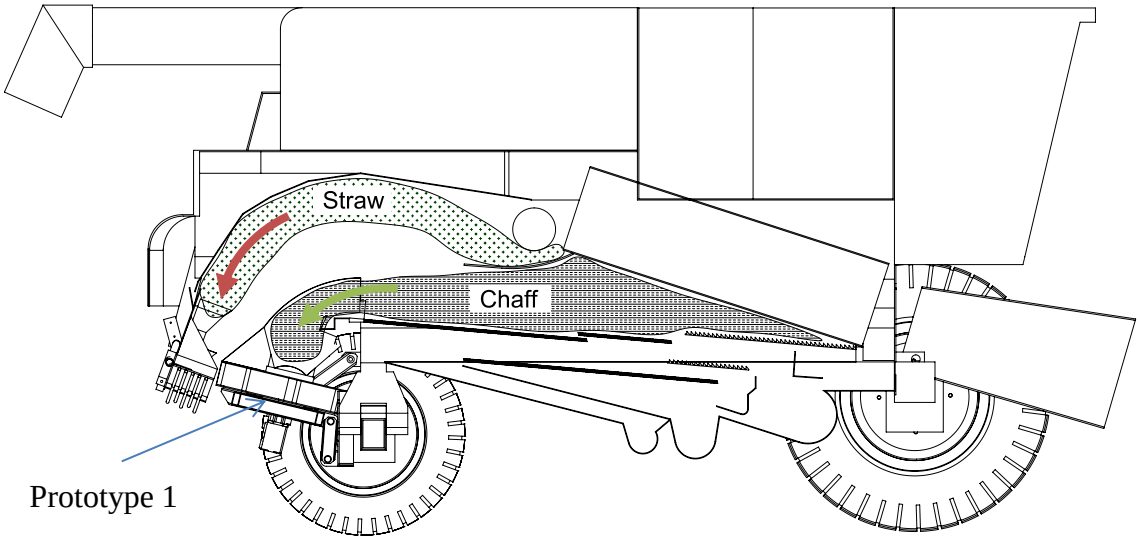

Figure 3.30: Material flow through harvester with two Prototype 1 mills attached

The pair of Prototype 1 mills were driven hydraulically by piggybacking a hydraulic pump (Bosch Rexroth A4VG125cc) off of the harvester drive pump. The flow from the single hydraulic pump was split equally using a flow control valve to supply the two hydraulic motors (Euroline MF50). The harvester was able to achieve harvest capacities up to 40 tonnes per hour in wheat.

The crop yield was approximately 2.5 t/ha. A DataTaker (DT85M) data logger was attached to the harvester and recorded the rotational speed of the left and right rotors (proximity sensor OMRON E2A-S08KS02-WP-M1-2M), the inlet hydraulic pressure (pressure transducer: Pi905-400 bar) of both mill hydraulic motors and the return line hydraulic pressure (pressure transducer: Pi905-200 bar).

The mechanical shaft output power of a hydraulic motor was given by (Doddannavar, Barnard & Ganesh 2005):

$$P_{in}(W) = \eta_o Q_{total} \Delta p \tag{3.104}$$

Where: η_o = overall efficiency of the motor
Q_{total} (m^3/s)= flow rate of the motor
Δp (Pa) = pressure drop from the motor inlet to motor outlet

The total volume flow rate of oil through the motors is given by:

$$Q_{total} = \frac{ND}{\eta_v} \tag{3.105}$$

Where: η_v = volumetric efficiency of the motor
N = rotational speed of the motor (rev/s)
D = displacement of the motor (m^3/rev)

The volumetric and total efficiency of the hydraulic motor depends on the rotational speed, hydraulic pressure and the viscosity of the hydraulic fluid. Viscosity changes dramatically with oil temperature. Therefore, oil temperature has a significant influence on hydraulic motor efficiency. However, typical values for volumetric and overall efficiency for axial piston motors are typically around 95% and 90%, respectively (Doddannavar, Barnard & Ganesh 2005). In the absence of data on the efficiency of the motors used, it was assumed that the power could be approximated using:

$$P_{in}(W) = ND\Delta p \tag{3.106}$$

This equation disregards hydro-mechanical losses in the motor but volumetric efficiency does not affect the results. Therefore, the equation over predicts the shaft power by approximately 5% but this depends on the mentioned factors affecting efficiency.

The average power was calculated by integrating the power data over the test period. The first 5% and last 5% of data from the test was removed to remove the end effects of entering and exiting the crop.

The chaff mass throughput was calculated by collecting and measuring chaff mass over the test length, as shown in Figure 3.31 a) and b), and dividing by the test period. The chaff was collected in bags similar to that used for HSD testing; collection bags had a

permeable top surface and a canvas bottom surface. The harvester settings used for all the trials are shown in Table 3.20.

Table 3.20: CASE IH 9120 harvester settings

Harvester variable	Setting
Rotor speed (rpm)	890
Fan speed (rpm)	940
Upper sieve (mm)	14
Lower sieve (mm)	9
Concave (setting)	1
Cut height (mm)	150
Cut width (m)	12.2

Trials were setup at 50 m lengths on the 24th of December 2012 and 100 m length on the 9th of January 2013. The increased length was tested on the 9th of January 2013 because it was determined that the chaff bags could hold the capacity needed. The variables tested are shown in Table 3.21. The harvester entered the crop at speed and at the last minute the cutter bar was dropped to start the logging in the AFX 600 terminal. At the end of the trial length, the harvester was stopped as quickly as possible and was run until no material was exiting the harvester. Each bag of chaff was removed, weighed and then emptied. The harvester was then reversed to have sufficient run up to achieve the correct speed before starting the next test.

Table 3.21: CASE IH 9120 harvester and Prototype 1 settings

Test variable	Number tested
Test length (m)	50, 100
Mill rotor speed (rpm)	2000, 2500, 3000
Forward speed (km/h)	3.2, 6.5, 9.7, 13.0
Replications	2 or 4

Figure 3.31: a) Prototype 1 chaff collection, b) Chaff mass measurement

3.4.3 Prototype 2

At the time of writing, the Prototype 2 had not been field tested. To measure the power of the Prototype 2, a lab scale procedure was used. A conveyor was used to process chaff at controlled throughput into the Prototype 2. Hydraulic pressure at the inlet and outlet of the hydraulic motor was measured with pressure transducers and logged using LabView at 10 kHz. The pulsed voltage output of the rotor speed sensor was also logged using LabVIEW (National Instrument Inc., USA, version 7.1) at 10 kHz. MATLAB® was used to determine the time stamp of each pulse and used to calculate the rotational speed of the rotor. The displacement of the hydraulic motor was the same as field tested with the Prototype 1. The volumetric flow rate through the hydraulic motor was estimated by multiplying the rotational speed of the rotor by the displacement of the motor. The average power was calculated by integrating the power data over the test period. The first 5% and last 5% of data from the test was removed to remove the end effects of the mill filling up and emptying.

3.4.4 Power and chaff throughput relationship

The power to operate the three devitalisation mills consisted of a no load power component and chaff processing power component:

$$P_{tot} = P_{noload} + P_{proc} \tag{3.107}$$

Where: P_{tot} = total power consumption of the mill (W)
$P_{no\ load}$ = no load power consumption of the mill (W)
P_{proc} = processing power consumption of the mill (W)

The no load power requirement consists of power to pump air and generate turbulence. Therefore, the no load power was assumed to be of the same form as the fan power affinity law (Jorgensen 1983):

$$P_{no\ load} = a\omega^3 \tag{3.108}$$

Where: a = no load coefficient (kg.m^2)
ω = rotational speed of the mill in rad/s

The processing power consumption was based on the sum of impact energy of processing a quantity of chaff:

$$P_{proc} = \sum_{j=1}^{n} \tfrac{1}{2} \dot{m}_{chaff} V_j^2 \tag{3.109}$$

Where: n = number of impacts within the mill
$\dot{m}_{chaff}$ = mass flow rate of chaff through mill (kg/s)
V_j = velocity of impact j

The velocity impacts within a rotor impact mill are driven from the tip speed of the rotor bars which depends on the rotational speed of the mill and radial location of impacts (r_j).

$$\therefore P_{proc} = \tfrac{1}{2} \dot{m}_{chaff} \omega^2 \sum_{j=1}^{n} r_j^{\ 2} \tag{3.110}$$

The sum of the radial location of impact was the fit parameter for processing power (b):

$$\therefore P_{proc} = \tfrac{1}{2} b \dot{m}_{chaff} \omega^2 \tag{3.111}$$

Where: $b = \sum_{j=1}^{n} r_j^{\ 2}$ - processing power coefficient (m^2)

The total power becomes:

$$P_{tot} = a\omega^3 + \tfrac{1}{2} b \dot{m}_{chaff} \omega^2 \tag{3.112}$$

The power and chaff throughput data for the three weed seed destruction mills were used to find the parameters a and b. The rotational speed of the HSD cage mill was

found to not vary significantly during testing. A linear regression was performed using chaff throughput as the independent variable and HSD cage mill power as the dependent variable. The intersection with the y-axis was the no load power to run the mill and the slope, the processing power. However, during testing of the Prototype 1 & 2 rotors, the operational speed of the mills were found to reduce slightly when the mills were loaded. Drops in the harvester engine speed under increasing load caused the rotor speed to drop proportionally. Therefore, linear regression was not a good prediction. To improve on the prediction of the prototype mills rotor power for different speeds and throughputs, a non-linear regression was performed on the power and chaff throughput data using Equation (3.112) in SPSS®.

4 Results and discussion

4.1 Material function

The material function was to specify the number of impacts and impact speeds needed to devitalise annual ryegrass (*Lolium rigidum*) seeds. Individual seeds were passed through a rotational impact tester, which impacted seeds from one side at a controlled speed (See Section 3.1). Seeds were impacted in three series of tests: multiple impacts at constant speed; three impacts at increasing or decreasing speed; and, combinations of impacts at elevated moisture content. Seed devitalisation was measured by planting seeds in indoor controlled environment soil bins, counting emergence and comparing to control germination using reduced seedling emergence (RSE):

$$RSE = 1 - \frac{SE}{SE_{control}} \tag{4.1}$$

Where: SE = the maximum seedling emergence count of the 14 and 28 days of a treatment
$SE_{control}$ = average of the control seedling emergence counts (448)

4.1.1 Effect of number of impacts and impact speed on seed devitalisation

In the first series of tests, annual ryegrass seeds were impacted multiple times at the same impact speed. Seed devitalisation for the annual ryegrass seeds was found to increase with impact speed and number of impacts, as shown in Figure 4.1. There was no measureable seed devitalisation for single impact at 30 and 40 m/s, and up to 71% at 90 m/s. The project goal of above 90% devitalisation was achieved at both 4 impacts at 70 m/s and 8 impacts at 50 m/s. Despite very low devitalisation for 1, 2 and 4 impacts at 30 m/s, up to 48% devitalisation was achieved at 16 impacts at 30 m/s.

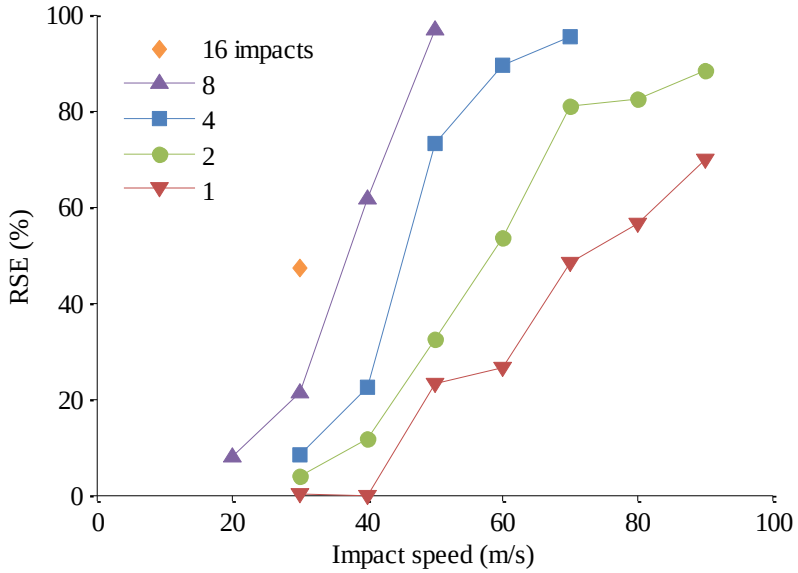

Figure 4.1: Seed devitalisation under successive impacts

Specific impact energy (cumulative) was a better predictor of seed devitalisation than impact speed alone; devitalisation was found to increase with the specific impact energy, as shown Figure 4.2. However, devitalisation for a given specific impact energy tended to reduce with increasing number of impacts. There was a significant range in impact energy needed to cause seed devitalisation in annual ryegrass seeds. At 1 kJ/kg, there was nearly zero seed devitalisation. At around 10 kJ/kg there was nearly 100% seed devitalisation.

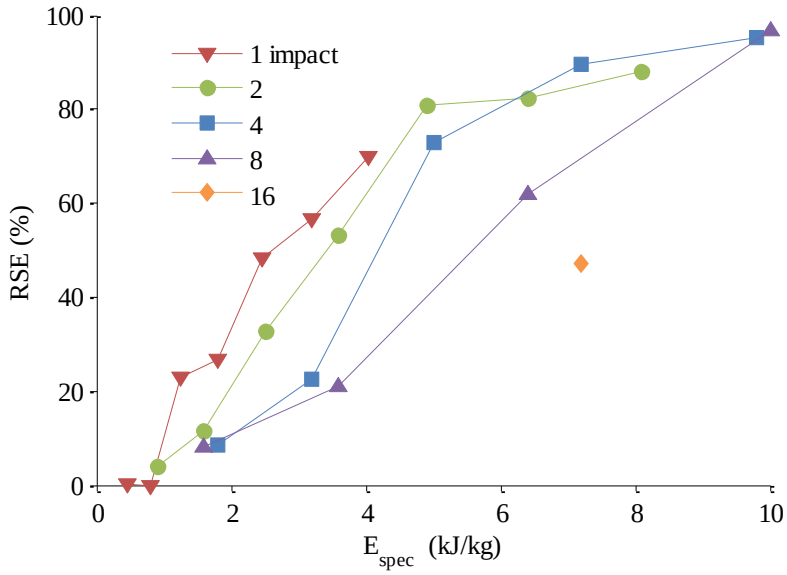

Figure 4.2: Seed devitalisation for specific impact energy calculated from the tip speed

4.1.2 Mastercurve for predicting seed devitalisation

A mastercurve was used to predict seed devitalisation based on the number of impacts and impact speed, as given by:

$$RSE(\%) = \left[1 - \exp\left(-F_{seed}\left(E_{impact} - k \times E_{\min}\right)\right)\right] \times 100 \quad (4.2)$$

Where: F_{seed} = resistance of the seed to fracture that causes seed devitalisation (kg/kJ);
E_{impact} = specific impact energy (kJ/kg);
k = number of impacts;
E_{min} = threshold specific impact energy for seed fracture that causes seed devitalisation (kJ/kg).

The mastercurve was able to accurately model seed devitalisation (r^2 = 0.941), as shown in Figure 4.3. The mastercurve was especially accurate at for higher impact speeds. However, the model was less accurate for multiple impacts at impact speeds close to the threshold specific energy, where the model prediction was most sensitive to the value for E_{min}. This sensitivity to E_{min} is shown by the width of the 16 impact 95% confidence interval in Figure 4.3 at low effective specific impact energy.

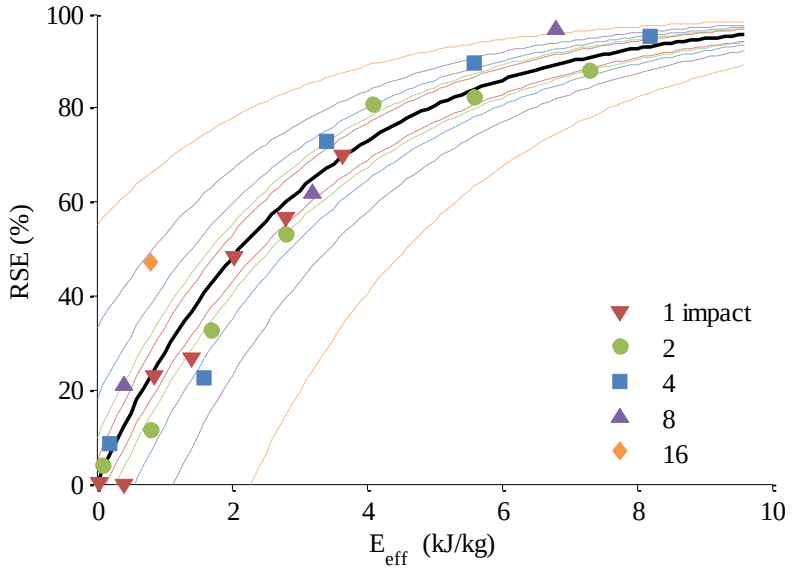

Figure 4.3: Seed devitalisation for effective specific impact energy: Mastercurve prediction of seed devitalisation (-) with 95% confidence interval colour coded for number of impacts (---), F_{seed} = 0.3268 kg/kJ, E_{min} = 0.3991 kJ/kg, r^2 = 0.941

4.1.3 Effect of impact order on seed devitalisation

In the second set of tests, seeds were subjected to three impacts at three different speeds in either increasing speed or decreasing speed order (See Table 3.5). The same set of

impact speeds in increasing and decreasing order had no measureable difference in seed devitalisation, as shown in Figure 4.4. Thus, the data was also used in the mastercurve regression. The mastercurve generated provided a good fit of the speed order data (r^2 = 0.953 in Figure 4.4)

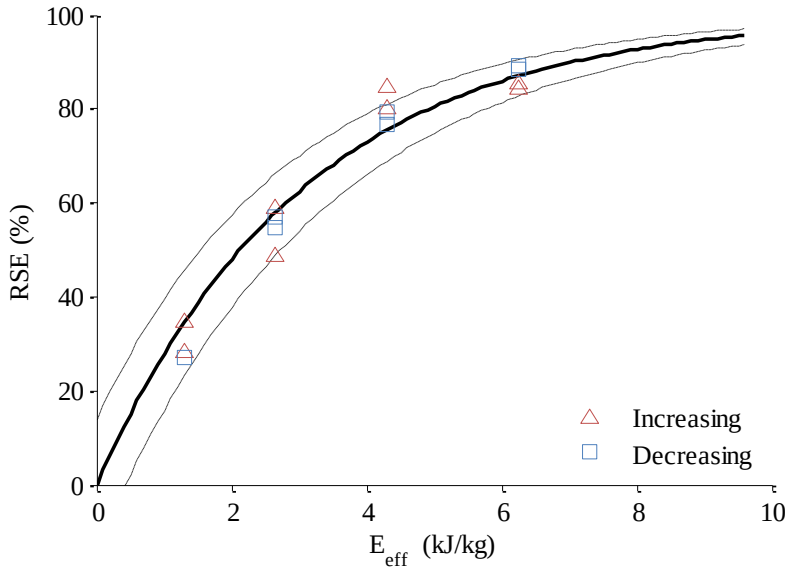

Figure 4.4: Seed devitalisation for a combination of impact speeds for effective impact energy in increasing order and decreasing order. Mastercurve prediction of seed devitalisation with 95% confidence interval (-), F_{seed} = 0.3268 kg/kJ, E_{min} = 0.3991 kJ/kg, r^2 = 0.953

4.1.4 Effect of moisture content on seed devitalisation

In the third set of impact tests, seeds of elevated moisture content were exposed to four different impact series. Increasing the moisture content was found to reduce seed devitalisation for all four of the impact series tested, as shown in Figure 4.5. To quantify the effect of moisture content on seed devitalisation, multiple linear regression was performed. The multiple linear regression showed a statistically significant moisture content effect. The linear regression was a good fit (r^2 = 0.934). The regression parameters can be interpreted here using the regression equation:

$$RSE(\%) = C_{MC} \times (MC - 11.3) + C_{imp} \qquad (4.3)$$

Where: C_{MC} = moisture content regression coefficient
MC = moisture content by weight in %
C_{imp} = regression coefficient from the impact series used

The linear regression parameters are shown in Table 4.1. Each 1% increase in the moisture content above the dry moisture content (11.3%), reduced seed devitalisation by 2.2%.

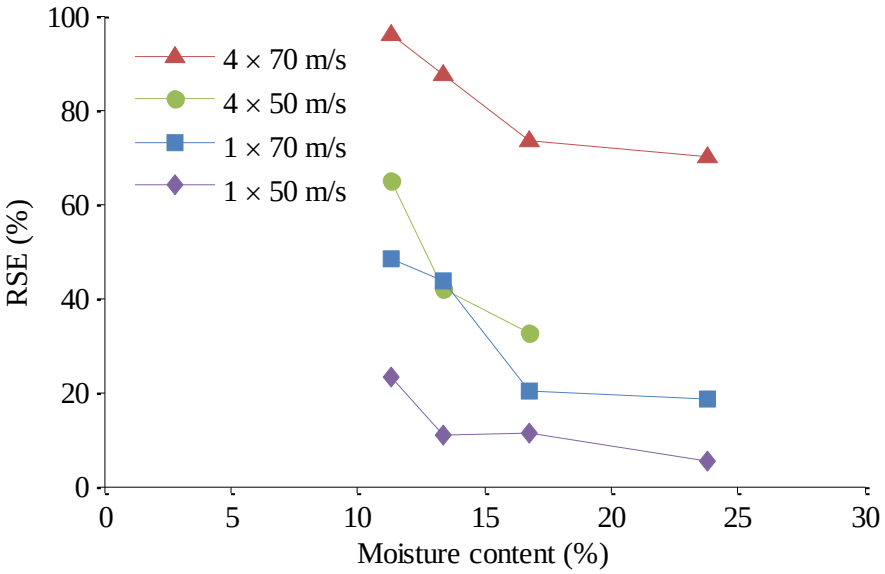

Figure 4.5: Seed devitalisation for different seed moisture contents

Table 4.1: Regression parameters for moisture content with 95% confidence interval

	Coefficient (95% C.I)		
Independent variable	Lower bound	Mean	Upper bound
Moisture content (%)	-3.334	-2.218	-1.102
One impact at 50 m/s	13.540	24.855	36.170
Four impacts at 50 m/s	47.850	57.903	67.957
One impact at 70 m/s	33.364	44.679	55.994
Four impacts at 70 m/s	83.584	93.453	103.321

4.1.5 Discussion

Impact is an effective means to reduce the emergence of annual ryegrass seeds with up to 97% seed devitalisation achieved at 8 impacts at 50 m/s. However, using a single impact achieved a maximum of 71% seed devitalisation at 90 m/s. Multiple impacts were needed at all speeds tested (20-90 m/s) to achieve the project goal of more than 90% seed devitalisation. High impact speeds were needed to achieve the energy required to devitalise annual ryegrass seeds because of the small mass of the seed.

If the population of annual ryegrass seeds had the same strength, and the rotational impact tester applied a uniform load the devitalisation of seeds would be a step function with impact energy. The devitalisation response of annual ryegrass to impact energy

was not a step function but more like a cumulative distribution; at least 1 kJ/kg was needed to cause any seed devitalisation and around 10 kJ/kg was needed to cause 100% seed devitalisation. The distribution in resultant seed devitalisation may be due to variation in seed mass, seed size, seed strength, impact orientation and impact force. For example, a light seed impacted at the same speed as a heavy seed would incur lower impact force and lower impact energy. If the two seeds are similar in strength then the heavy seed may break and not germinate whereas the lighter seed may not.

The probability of annual ryegrass seed devitalisation subjected to multiple impacts in a range of impact speeds and impact orders was able to be approximated using a mastercurve with two seed properties: E_{min} and F_{seed}. The data supports the hypothesis that there is a threshold specific energy for each impact (E_{min}) that does not contribute to seed devitalisation. For annual ryegrass seeds the material parameters F_{seed} and E_{min} were found to be 0.3268 kg/kJ and 0.3991 kJ/kg, respectively. For impacts near the threshold specific impact energy, a considerable proportion of impact energy was wasted through any elastic and plastic deformation that does not cause any seed devitalisation to occur. The threshold specific impact energy equated to an impact speed of 28 m/s. For impact speeds close to the 28 m/s a large number of impacts are needed to achieve significant seed devitalisation and would be energy inefficient. It was more efficient to use a low number of high speed impacts than a high number of low speed impacts.

The speed order of an impact series did not cause any measurable effect on seed devitalisation. Therefore, this data did not support the fracture mechanics derived hypothesis that having the largest stress event first (decreasing speed order) would more likely lead to crack propagation and seed devitalisation than having the smallest stress event first (increasing speed order). The speed order data set (Figure 4.4) confirms the validity of the mastercurve for combinations of impact speed and number of impacts in any order.

The moisture content had a significant effect on the effectiveness of single sided impact to devitalise annual ryegrass seeds. This would result in a modification in one or both material properties E_{min} and F_{seed}. However, a larger data set is needed to quantify these modifications. The effectiveness of seed devitalisation mills under increased moisture contents would be expected to be reduced.

The mastercurve provided a material function to predict annual ryegrass seed devitalisation when a seed is subjected to a set of impact speeds and number of impacts; therefore, it has achieved the first objective of this thesis.

4.2 Machine function

The machine function of three seed devitalisation mill arrangements was evaluated using two methods: a theoretical vector impact model; and a Computational Fluid Dynamics (CFD) impact model. Both methods provided an estimate of the number of impacts and impact speed that an annual ryegrass seed would be exposed to within the three mills discussed in this thesis. The estimate of number of impacts and impact speed was used to evaluate a prediction of annual ryegrass seed devitalisation using the material function mastercurve.

4.2.1 Vector impact model

The theoretical vector impact model assumed that a particle would impact each row of impact bars once at the centreline. The number of impacts was based on the number of rows of impact bars. The normal impact velocity was calculated using the basic two-dimensional geometry of the three mills. The theoretical vector impact model predicted the normal impact velocity of each row of the three mills, as shown in Figure 4.6, Figure 4.7 and Figure 4.8. The impact speed predicted with the vector model increased linearly with rotational speed for all three mills.

4.2.1.1 *HSD cage mill*

Using the vector model, a particle travelling through the HSD cage mill was predicted to have 6 impacts; one for each row of bars. The predicted impact speed of the HSD cage mill of rows 2-6 was 65.9, 70.3, 78.0, 79.7 and 82.4% higher than the tip speed of the impact bars, respectively because of the counter rotation of the cages. At the operational speed of the HSD cage mill (1440 rpm) the rotor bar tip speeds from rows 1-6 were 28.7, 35.3, 42.1, 47.7, 53.4 and 58.8 m/s. Whereas, the predicted impact speeds were 28.7, 58.6, 71.7, 84.8, 95.9 and 107.3 m/s. The residual speed of a particle from impact the previous row of impact bars was important to the generating the impact speeds needed to devitalise seeds in the HSD cage mill.

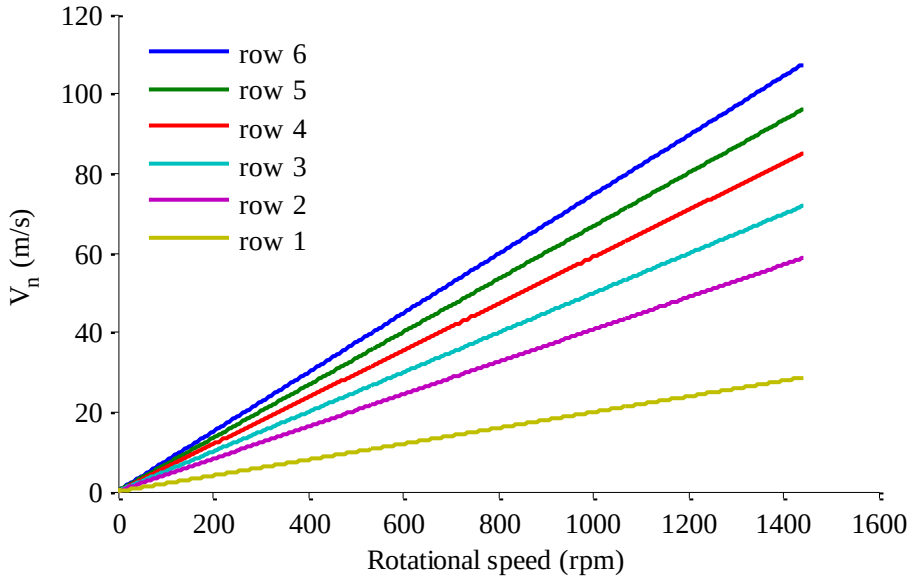

Figure 4.6: Vector model prediction of normal impact speed HSD cage mill

4.2.1.2 *Prototype 1*

A particle traveling through the Prototype 1 was predicted to have 4 impacts using the vector model. The inner distribution paddle was assumed to have a particle slinging action rather than an impact. The paddle accelerates the particle into an impact with the first static row. Most of the particle velocity is lost in the impact with the first stator row because the stator is angled to achieve more direct impact. The particle then impacts the second rotor row and gains kinetic energy. The particle again loses it's kinetic energy with an impact with the second stator row that is also angled to achieve direct impact. The Prototype 1 has a third rotating row that impacts the particle. The particle exits the mill at high velocity. The predicted normal impact speeds of the Prototype 1 rotor rows two and three were 6.7% and 6.2% higher than the tip speeds, respectively. The impacts with the stator rows were predicted to be 3.1% and 1.5% lower than the tip speed of the previous rotor bar row. At 2500 rpm the normal impact speeds were: 0 m/s (rotor 1: slinging action), 36.8 m/s (stator 1), 62.9 m/s (rotor 2), 58 m/s (stator 2) and 83.4 m/s (rotor 3).

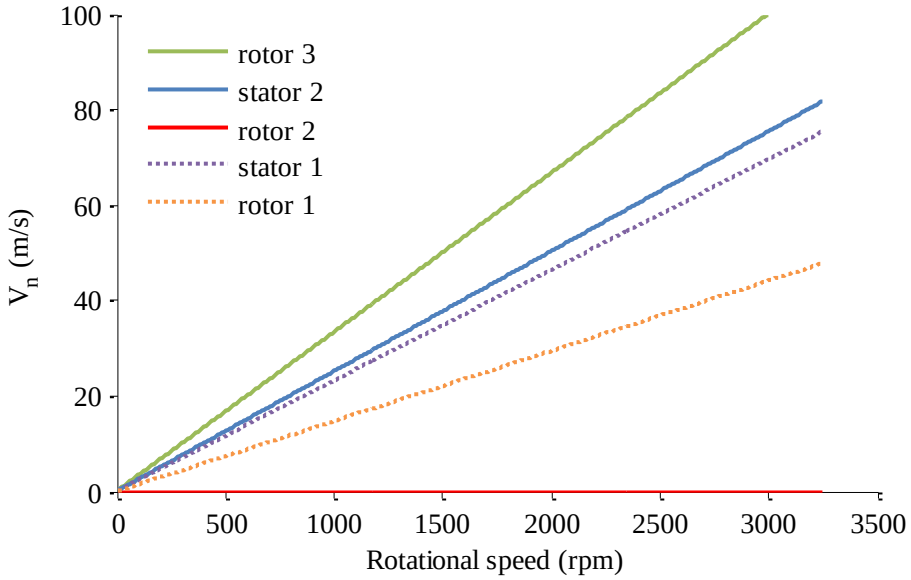

Figure 4.7: Vector model prediction of normal impact speed Prototype 1

4.2.1.3 *Prototype 2*

A particle travelling through the Prototype 2 was predicted to have 5 impacts using the vector impact model. The impacts were similar to the Prototype 1 with the addition of a third stationary row. The normal component of impact velocity of rotors row two and three were predicted to be 13.1% and 9.5% higher than the tip speed. The normal component of impact speed on the first, second and third stator rows 4.5% higher, 0.3% lower, 0.1% lower than the tip speed of the three rotor rows respectively. The Prototype 2 had higher impact velocities on the rotor and stator relative to the rotor tip speeds because the stator angle was $\zeta = 20^{o}$ compared to $\zeta = 15^{o}$ for the Prototype 1. However, the impact speeds were lower than Prototype 1 because of a reduced rotor diameter (600 mm compared to 535 mm); at 2500 rpm the impact speeds were: 0 m/s (rotor 1 slinging action), 42.4 m/s (stator 1), 61.4 m/s (rotor 2), 54.2 m/s (stator 2), 76.7 m/s (rotor 3) and 70.0 m/s (stator 3).

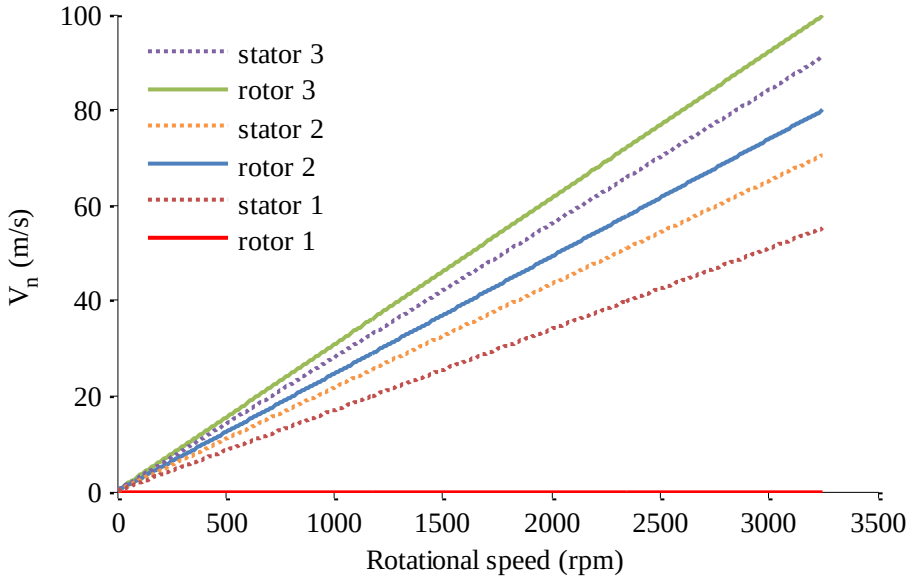

Figure 4.8: Vector model prediction of normal impact speed Prototype 2

4.2.2 Computational Fluid Dynamics (CFD) impact model

Computational Fluid Dynamics (CFD) impact model of each of the three seed devitalisation mills was used to expand on the simple vector impact model. The CFD model was first solved for the continuous fluid phase and then a discrete phase was entered into the fluid phase. The discrete phase used spherical particles that were aerodynamically equivalent to annual ryegrass seeds. The trajectories of the particles were used to calculate the number of impacts and impact speeds.

4.2.2.1 *Continuous phase solution*

The continuous phase solution was solved for each of the three seed devitalisation mills at a range of rotational speeds corresponding to the experimental test speeds of the mills.

HSD cage mill

The pressure and velocity contour plots of the HSD cage mill operating at 1440 rpm are shown in Figure 4.9 and Figure 4.10, respectively. The CFD model shows regions of moderately high pressure (Figure 4.9) in front of the flat blades on the outer row cage. A region of high velocity (Figure 4.10) follows the flat blades. Thus, the flat blades are the main source of the air pumping in the HSD cage mill, as per the design intent described in the introduction.

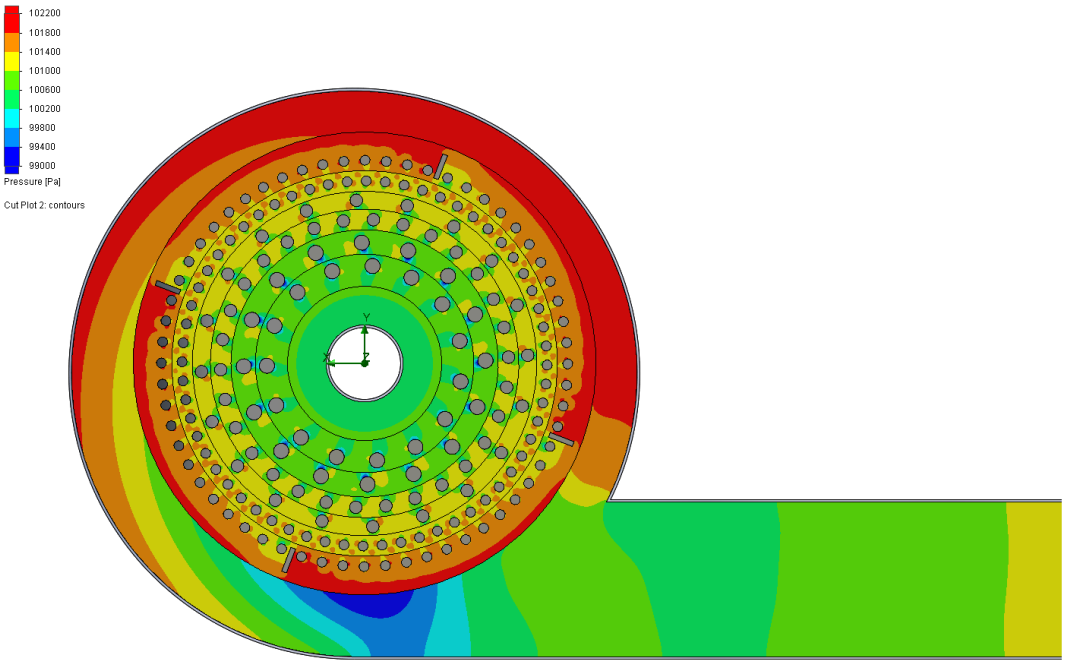

Figure 4.9: CFD pressure contour plot of HSD cage mill at 1440 rpm

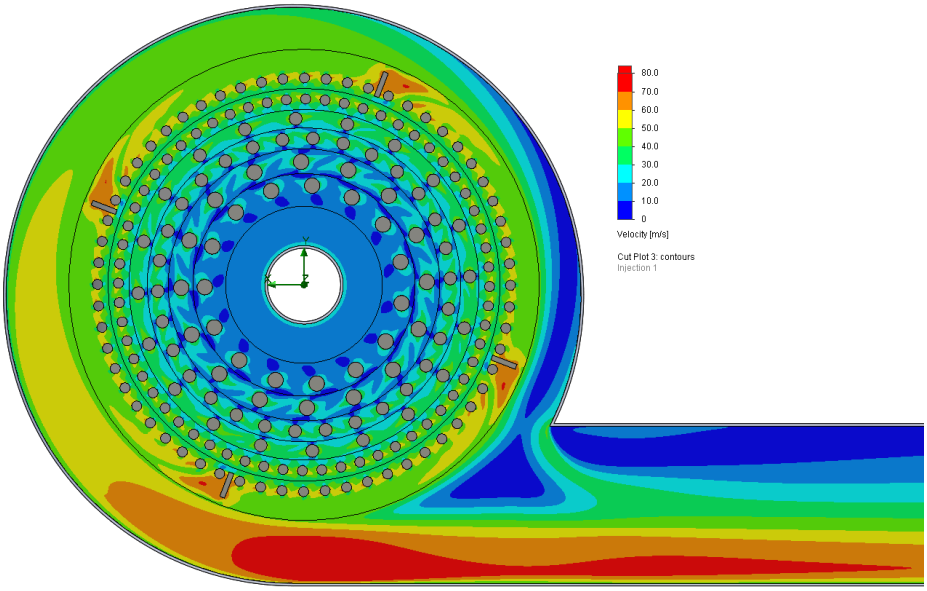

Figure 4.10: CFD velocity contour plot of the HSD cage mill at 1440 rpm

Prototype 1

The pressure and velocity contour plots of the Prototype 1 operating at 2500 rpm are shown in Figure 4.11 and Figure 4.12, respectively. An aim of the design of the mill was to generate sufficient air flow to maximise chaff mass flow capacity and minimise harvester sieve restriction. The inlet paddles and the flat face of the rotor bars were designed to able to add pressure and hence generate an air pumping effect.

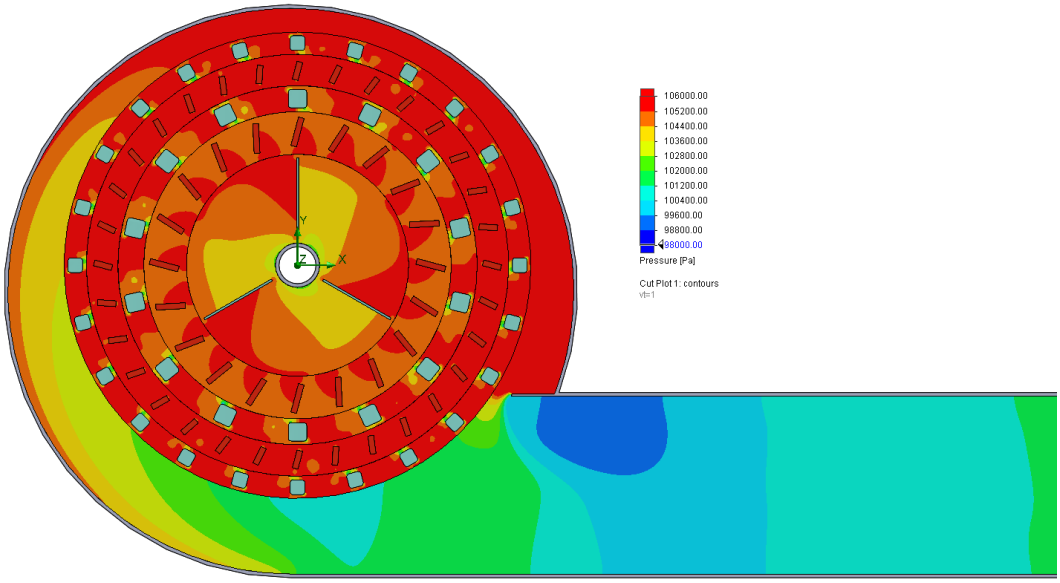

Figure 4.11: CFD pressure contour plot Prototype 1 at 2500 rpm

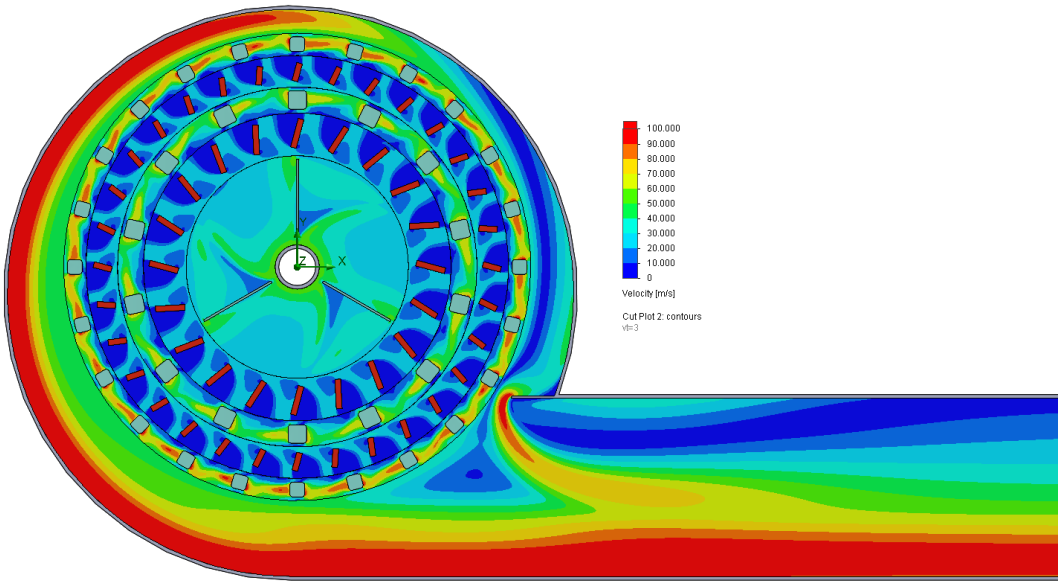

Figure 4.12: CFD velocity contour plot Prototype 1 at 2500 rpm

Prototype 2

The pressure and velocity contour plots of the Prototype 2 operating at 2500 rpm are shown in Figure 4.13 and Figure 4.14, respectively. As with the Prototype 1, the inlet paddles and the flat face of the rotor bars were able to add pressure and hence generate an air pumping effect. The housing of Prototype 2 was designed to be a volute scroll housing which, which resulted in lower pressure (Figure 4.13) than Prototype 1.

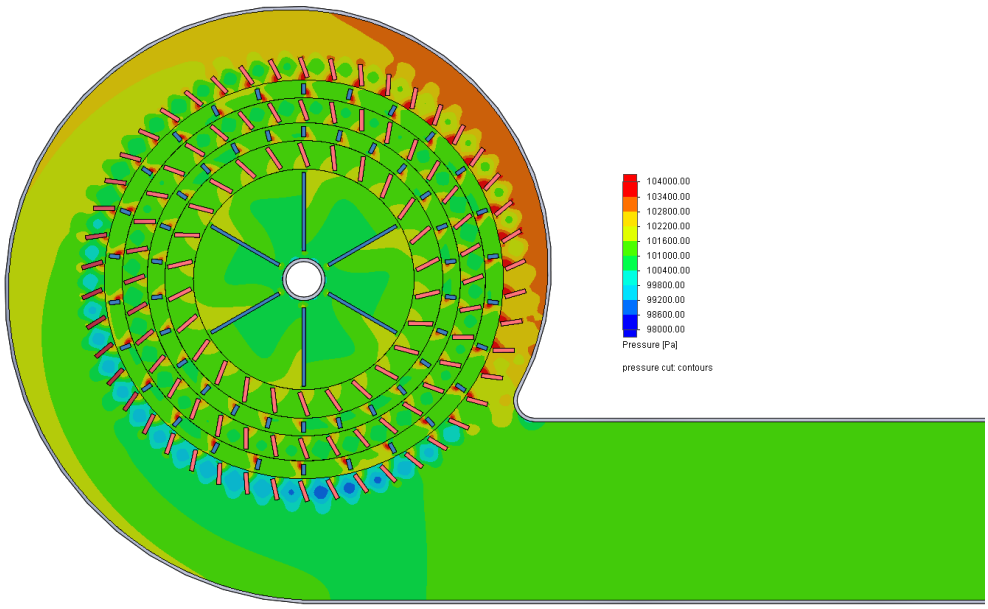

Figure 4.13: CFD pressure contour plot Prototype 2 at 2500 rpm

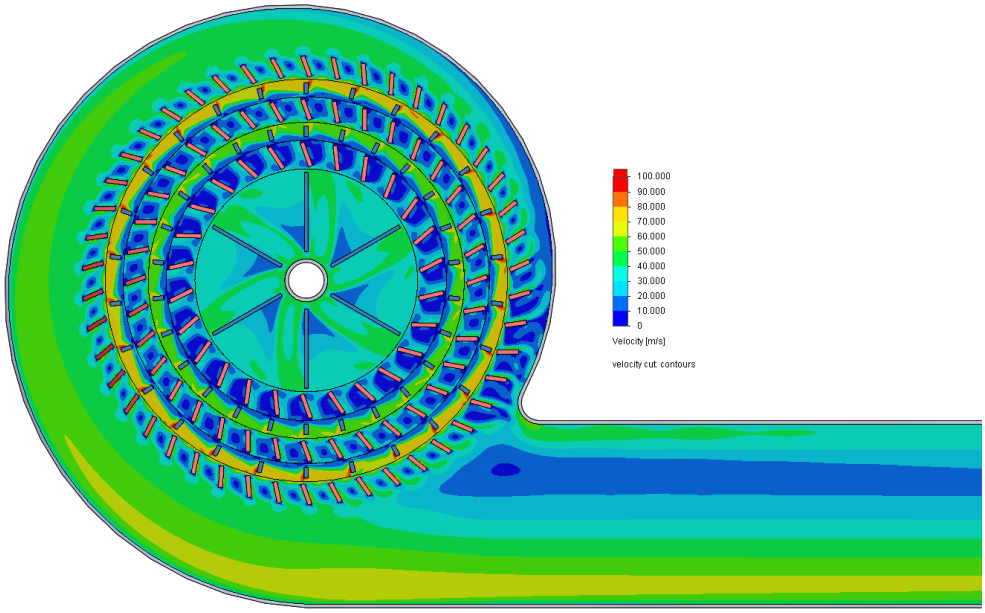

Figure 4.14 CFD velocity contour plot Prototype 2 at 2500 rpm

4.2.2.2 *Particle trajectories:*

Once the continuous phase CFD solution had completed, a particle study was performed by inserting 1000 particles with the equivalent aerodynamic properties as annual ryegrass seeds. To more easily visualise the typical particle trajectories, studies with 50 particles were performed for the three mills as shown in Figure 4.15, Figure 4.16, and Figure 4.17. The particle trajectories have significant change in direction when impacted with a mill bar. The impact does not correspond to the location of the bars in the figures because the location changes with time. The relatively straight lines shows that the particle's trajectories are largely unaffected by the airflow in the milling zone.

The HSD cage mill (Figure 4.15) caused particles to impact randomly throughout the mill due to the circular cross section of the impact bars. Some particles were impacted towards the centre of the often resulting in more impacts than rows of bars.

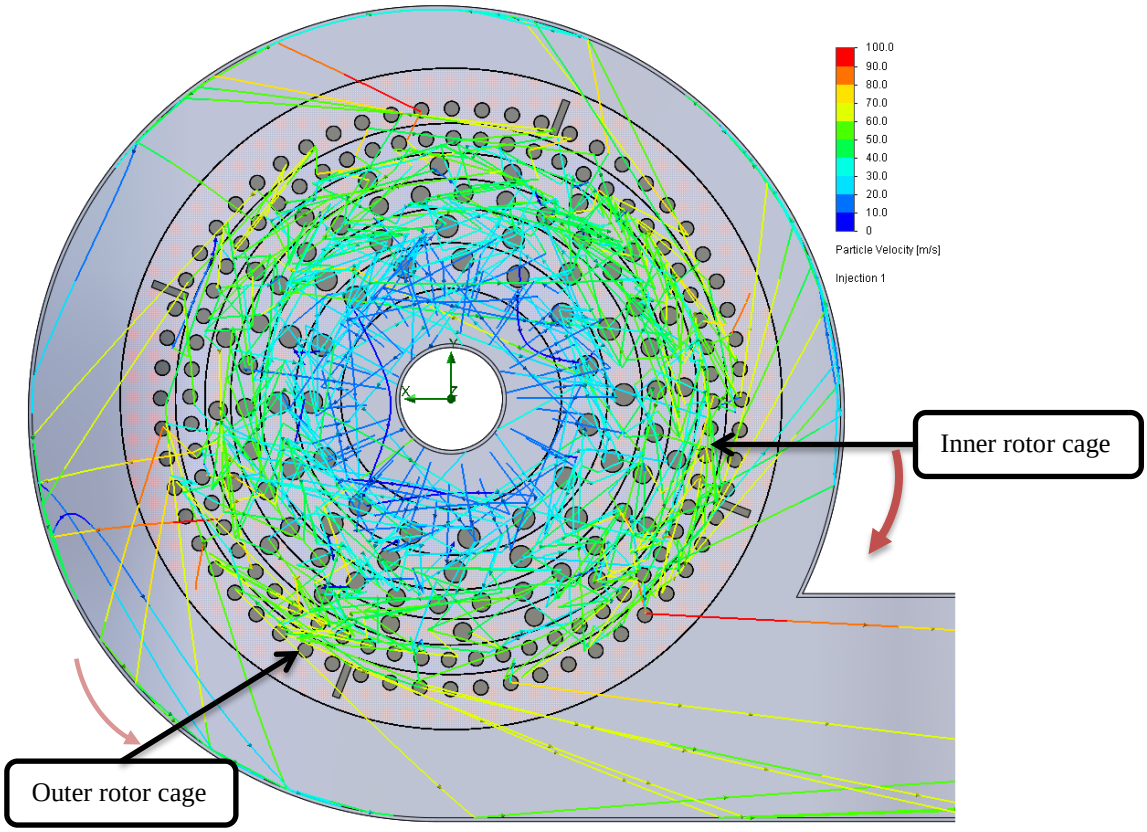

Figure 4.15: HSD cage mill at 1440 rpm, CFD particle trajectories for annual ryegrass

Prototype 1 (Figure 4.16) and Prototype 2 (Figure 4.17) had a much more defined impact set as per the design intent. Most particles impact each row of rotor and stator bars once resulting in a relatively constant number of impacts and impact speeds. There were some impacts on the side walls and the rounded edges of the SHS rotor bars of

Prototype 1, which resulted in some random impacts and stagnant material. Prototype 2 was designed to further reduce the random impacts by using flat rotor bars.

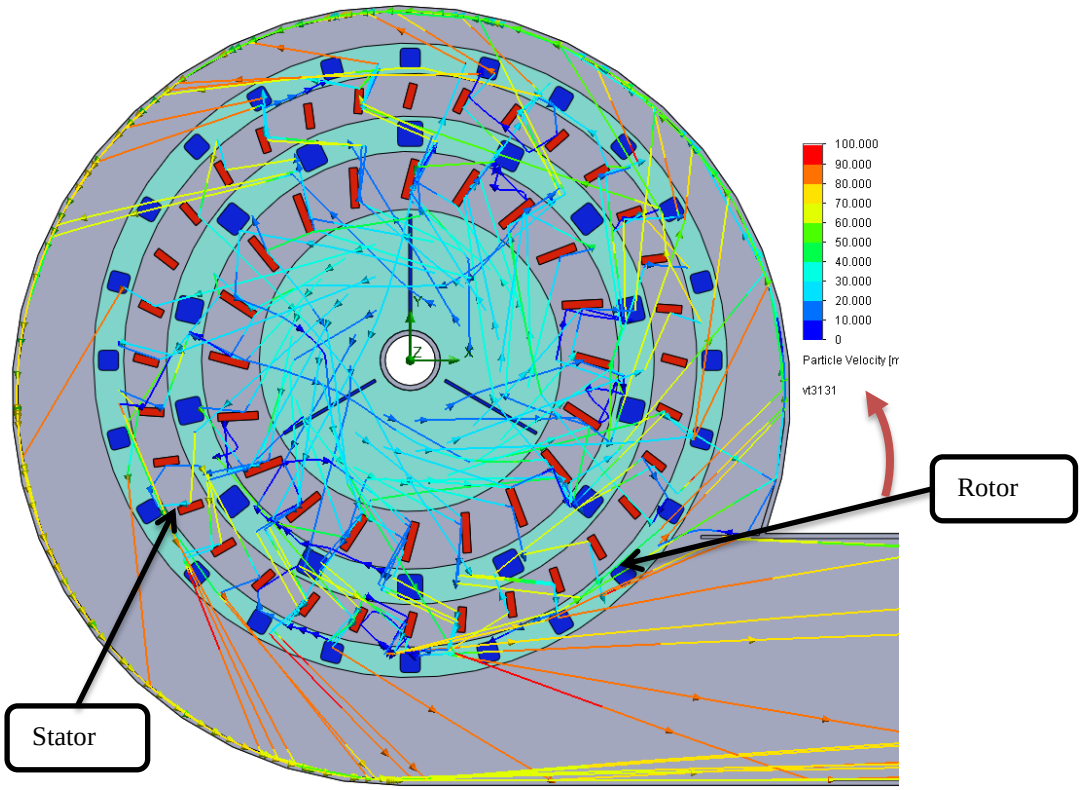

Figure 4.16: Prototype 1 at 2500 rpm CFD particle trajectories for annual ryegrass

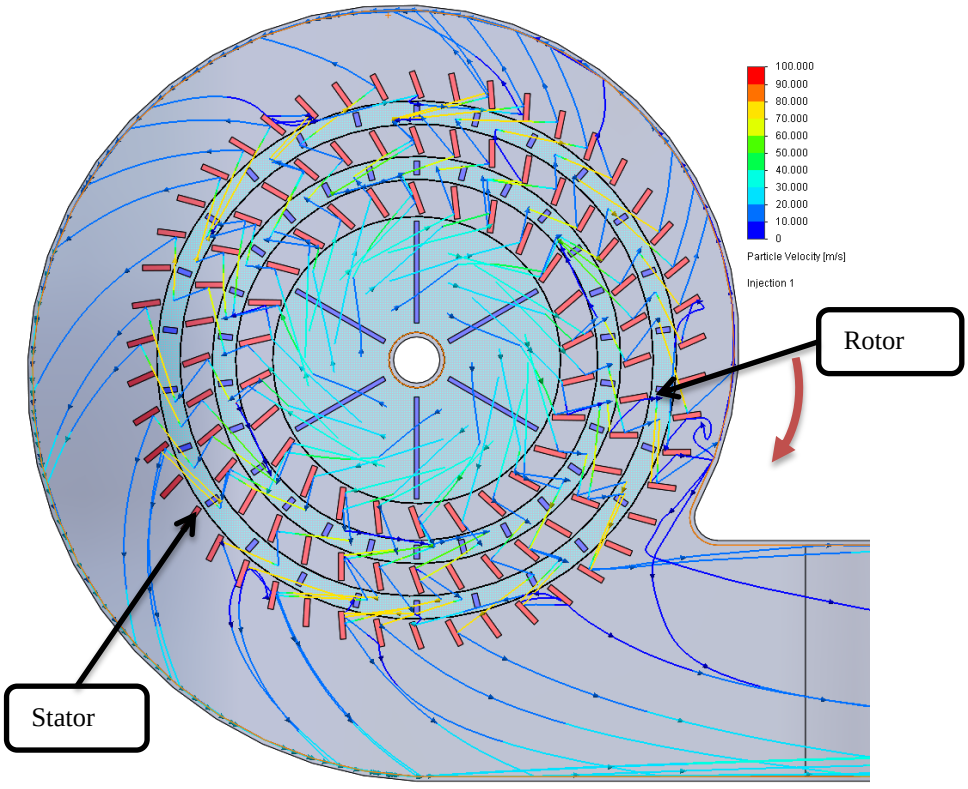

Figure 4.17: Prototype 2 at 2500 rpm CFD particle trajectories for annual ryegrass

4.2.2.3 *Impact velocity and number of impacts*

Once the particle study had been performed in SolidWorks® Flow Simulation, the particle trajectories and velocities were exported to a text file. The text file was imported into Matlab® to calculate the number and distribution of impacts and impact speeds that are likely to occur for a specific mill design at a rotational speed.

The distribution of impact speed and number of impacts is presented as a histogram based on the mean of 1000 particles showing the number of impacts within each speed 5 m/s bins, as shown in Figure 4.18 for the HSD cage mill, Figure 4.19 for the Prototype 1 and Figure 4.20 for the Prototype 2. The total height of each bar in the histograms can be interpreted as the total number of impacts that a seed would be exposed to in the 5 m/s speed range, based on the mean of 1000 particles. The breakdown into the rows of bars (HSD cage mill) and rotor and stator row (prototype mills) is to show the number of impacts in the 5 m/s speed range occur on each row of bars. For example, consider HSD cage mill at 1100 rpm (Figure 4.18), the mean number of impacts per particle between 55 and 60 m/s was 1.7 impacts. There are approximately zero impacts between 55 and 60 m/s from row 1 of the HSD cage mill (inner row); from rows 2-6 the mean number of impacts was 0.06, 0.67, 0.39, 0.40 and 0.18, respectively.

HSD cage mill

The particle motion through the HSD cage mill was random resulting in a wide distribution of number of impacts and impact speeds, as shown in Figure 4.18. The number of impacts on each rotating row and the tip speed of each row of bars are shown in Figure 4.18. Some of the impacts are glancing with its normal component of impact velocity much lower than the bar tip speed. Some impacts have a normal component of impact velocity nearly double the bar tip speed because of the counter rotation of the HSD cage mill rotors; velocity gained from an impact from the previous row of bars increases the normal impact velocity with the subsequent row of bars. It is apparent that more than one impact occurs on average for each row of bars. A large number of glancing impacts occur below the minimum threshold energy E_{min} (≈ 28 m/s).

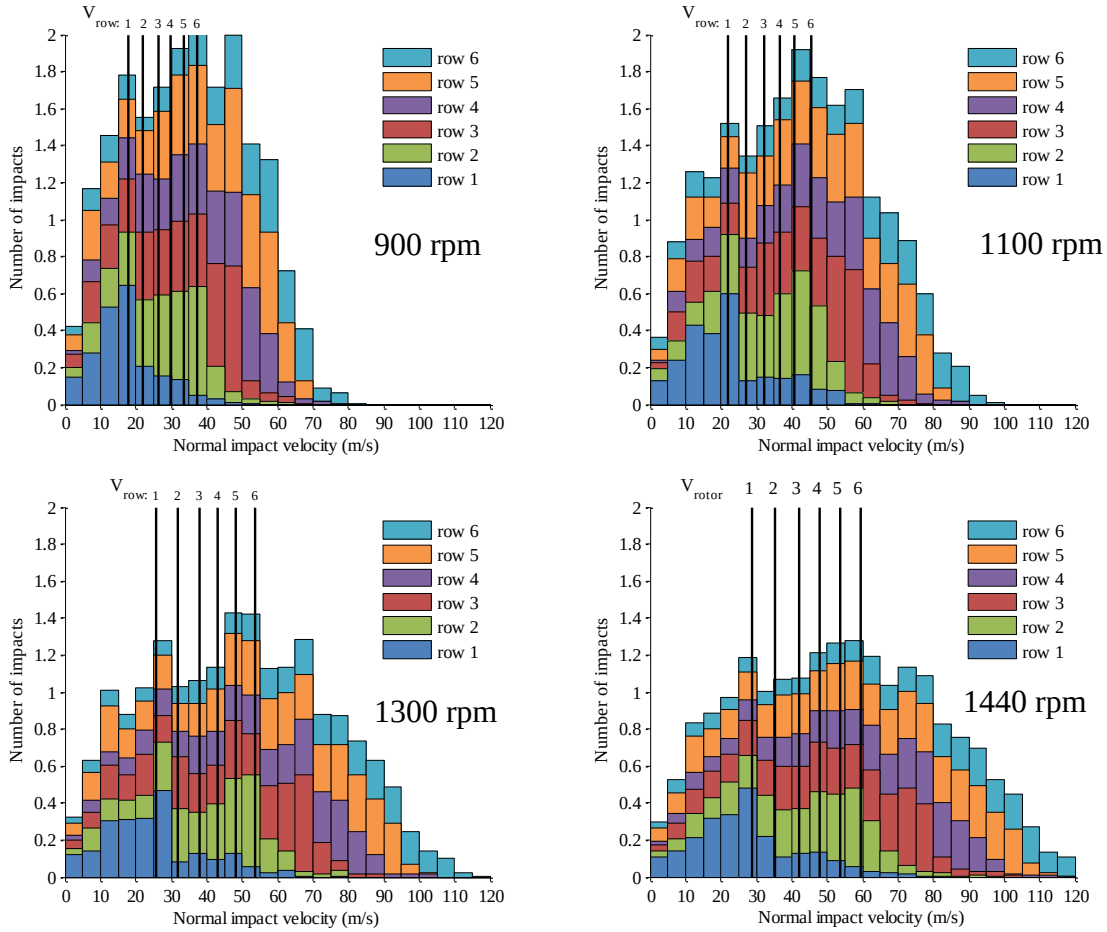

Figure 4.18: Histogram of impacts of particles in the HSD using CFD particle tracing.

Prototype 1

The impacts within the Prototype 1 had a distribution of speed and number of impacts, as shown in Figure 4.19. The rotational speed of the mill determined the range of impact speeds. For each of the four speeds shown in Figure 4.19, there are 3 distinct peaks in the total number of impacts. The speed of these peaks does not correspond perfectly with the tip speeds of the three rotor rows but it does show that there are three distinct impact regions within the mill. The total number of impacts within the Prototype 1 was less than the HSD cage mill.

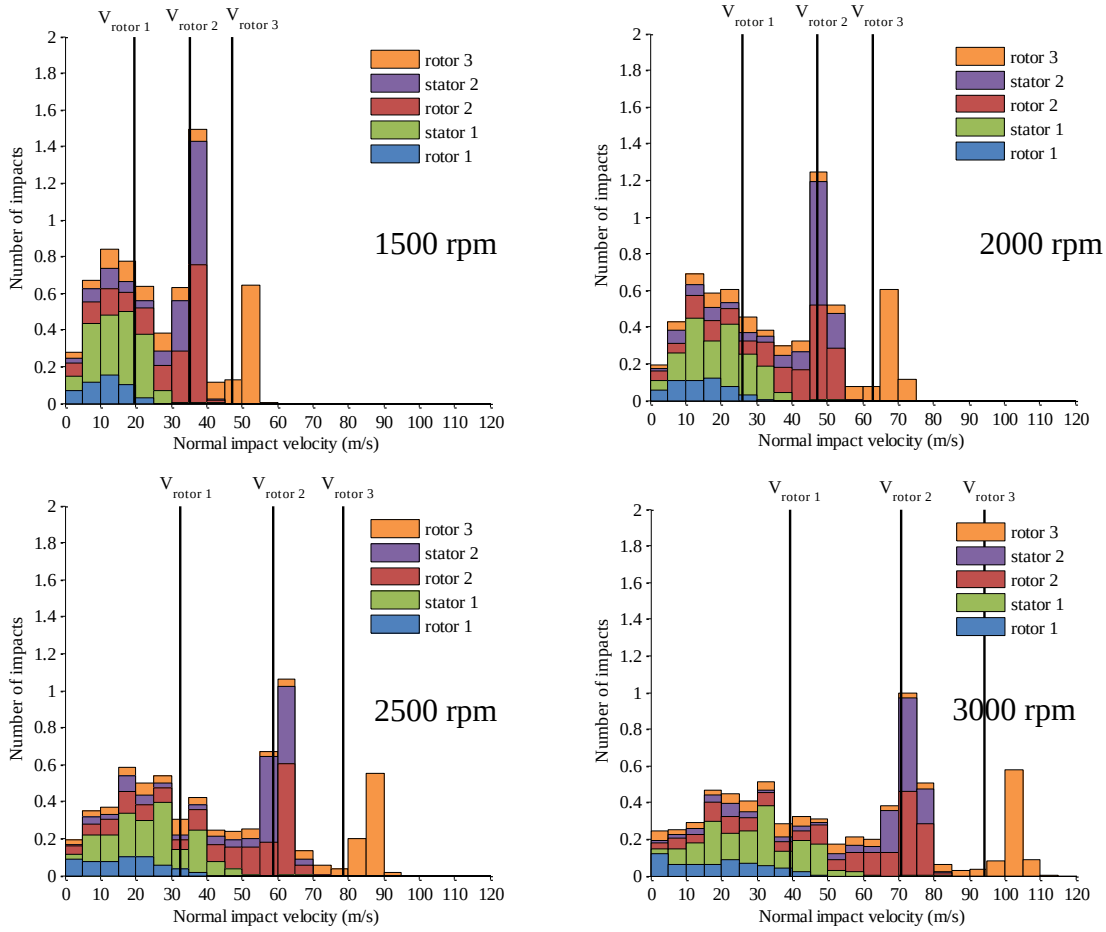

Figure 4.19: Histogram of impacts of particles in the Prototype 1 using CFD particle tracing.

Prototype 2

The Prototype 2 had significantly less spread of the impact speeds compared to both the HSD cage mill and Prototype 1 as shown in Figure 4.20. The Prototype 2 had 6 mm flat rotor blades with sharp edges which was found to produce less glancing impacts than the round edged SHS rotor blades of the Prototype 1. The Prototype 2 had a smaller diameter rotor giving lower tip speeds than the Prototype 1 at the same rotational speeds. However, the Prototype 2 had an extra stator which added an extra high speed impact.

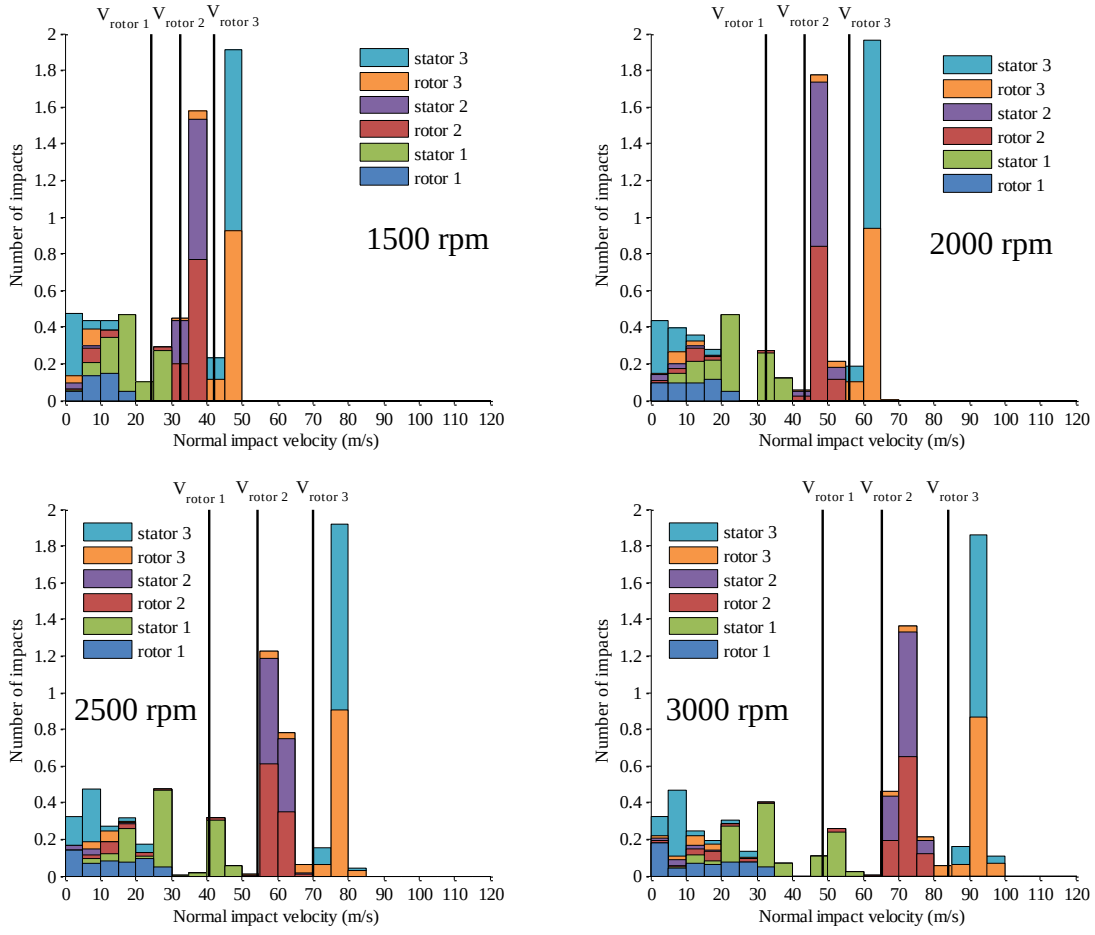

Figure 4.20: Histogram of impacts of particle in the Prototype 2 using CFD particle tracing.

4.2.2.4 *Solids loading*

The solids loading of a mill is the mass ratio of solids to air. A higher solids loading implies that there is more material in the mill. Therefore, in regions of higher solids loading there is a higher likelihood of particle to particle impacts. Particle to particle impacts are far less efficient at breaking particles than particle to wall impacts because of a lower transfer of energy (see Section 2.5). As particle breakage and seed devitalisation are synonymous, in zones of higher specific solids loading, there is likely to be reduced effectiveness on seed devitalisation. Since the CFD particle tracing method neglected particle to particle impacts themselves, an estimate of solids loading was made based on the time particles were in each zone of the mill. The estimate of specific solids loading of chaff in the three mills is shown in Figure 4.21, Figure 4.22 and Figure 4.23.

When comparing the specific solids loading contour plots, note that the HSD cage mill processes the entire chaff fraction and the prototype mills process half of the chaff fraction (2 mills). Therefore, for a commercial harvest rate of 3 kg/s of chaff, to calculate the actual solids loading, the specific solids loading must be multiplied by 3 for the HSD cage mill and 1.5 for the Prototype 1 and 2.

The HSD cage mill showed high specific solids loading of chaff of near 1 s/kg near the inner rows of bars, as shown in Figure 4.21. The specific solids loading reduced outwards from the centre.

The Prototype 1 also had some zones of relatively high specific solids loading near the radial position of the first row of rotating bars, as shown in Figure 4.22.

The Prototype 2 had a lower specific solids loading of chaff throughout the mill compared the HSD and the Prototype 1, as shown in Figure 4.23. The Prototype 2 had mostly direct impacts that caused the material to move outwards upon each impact and, thus particles remained in the milling zone for a minimum amount of time. This indicates reduced recirculating of particles as per the design intent. Therefore, Prototype 2 would be expected to have less inefficient particle to particle impacts than Prototype 1 and the HSD cage mill and hence, would be expected to maintain seed devitalisation at higher chaff throughputs.

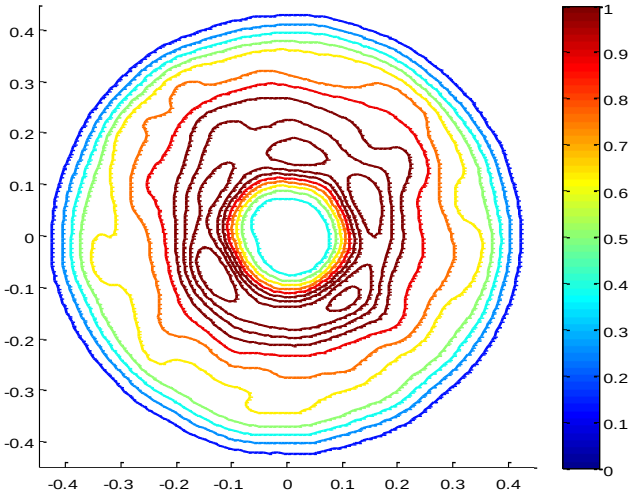

Figure 4.21 Specific solids loading based on density plot, HSD cage mill 1440 rpm

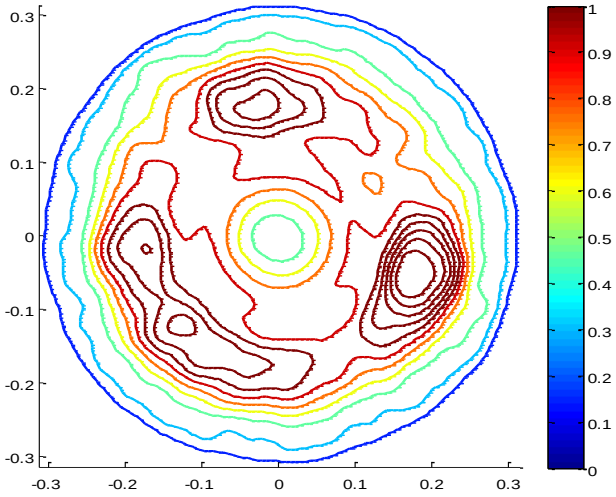

Figure 4.22 Specific solids loading based on density plot, Prototype 1 2500 rpm

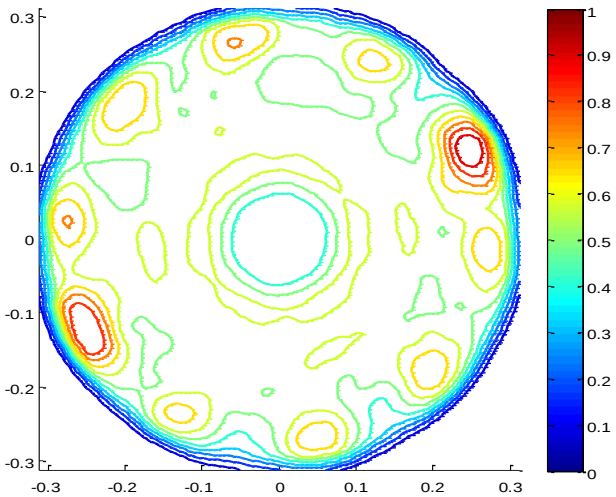

Figure 4.23 Specific solids loading based on density plot, Prototype 2 2500 rpm

4.2.3 Combining material and machine function

4.2.3.1 Seed devitalisation prediction

An estimate of annual ryegrass seed devitalisation using the three mills was developed by combining: the mastercurve for annual ryegrass seed devitalisation from impact testing with the number of impacts and impact speed estimate from both the vector impact model and the CFD impact model. The impact history of each individual particle were converted to an effective impact energy using Equation (3.67), repeated here:

$$E_{eff,p} = \sum_{j=1}^{n} \left(E_j - E_{\min} \right), \text{ for } E_j > E_{\min} \tag{4.4}$$

Where: $E_j = \frac{1}{2} V_{nj}^2$: specific energy of impact j (kJ/kg)
V_{nj} = the normal impact velocity of impact j (m/s)
E_{min} = 0.3991 kJ/kg : minimum energy to cause annual ryegrass seed devitalisation

The effective impact energy is the energy available in each impact to cause seed devitalisation, according the annual ryegrass seed devitalisation mastercurve (Equation (4.2)). Impacts that are not above the minimum energy to cause seed devitalisation do not contribute the effective impact energy. The vector impact model provided a single value for effective impact energy and seed devitalisation for a given rotational speed. The CFD impact model provided a distribution of effective impact energy and seed devitalisation.

The histogram of effective impact energy (*Particle* E_{eff}) applied to particles in the CFD impact model is shown in Figure 4.24 for the HSD cage mill, in Figure 4.25 for the Prototype 1 and in Figure 4.26 for the Prototype 2. The number of particles in each effective energy bin range (x-axis) have been normalised into a percentage of the total number of particles entered into the model (y-axis). An inversed cumulative histogram is also plotted to show the proportion of particles with effective impact energy above the lower value of the bin range. For example, in the bin range of 5-10 kJ/kg: *Particle* E_{eff} shows the percentage of the particles that are exposed to an effective impact energy in the range of 5-10 kJ/kg; the *Cumulative above* E_{eff} shows the percentage of particles that are exposed to an effective impact energy of more than 5 kJ/kg. *RSE* shows the annual ryegrass seed devitalisation mastercurve (Equation (4.2)) prediction using the effective impact energy on a continuous scale.

For the HSD cage mill (Figure 4.24), the mean and spread of effective impact energy increased with rotational speed. The effective energy on each particle varied significantly with some particles receiving less than 5 kJ/kg and other particles receiving more than 40 kJ/kg. From the annual ryegrass material function, effective energy of 14.1 kJ/kg will cause 99% seed devitalisation. Any effective impact energy above 14.1 kJ/kg would largely be wasted into further particle breakage without increase in seed devitalisation. It is shown in Figure 4.24 that 14.6%, 43.8%, 63.3%, and 71.4% of particles receive more than 15 kJ/kg at 900 rpm, 1100 rpm, 1300 rpm and 1440 rpm, respectively. Therefore, the randomness of the impacts in the HSD cage mill is causing some material to be over-processed and more energy is used than is needed to cause seed devitalisation. Furthermore, it is shown in Figure 4.24 that 34.9%, 13.8%, 3.7% and 1.7% of particles are receiving less than 5 kJ/kg at 900 rpm, 1100 rpm, 1300 rpm and 1440 rpm, respectively. Therefore, the randomness of the impacts in the HSD cage mill is causing some material to be under-processed and some particles are not receiving enough energy to cause a high probability of seed devitalisation. This wide distribution of effective impact energy may be a source of inefficiency in the HSD cage mill design.

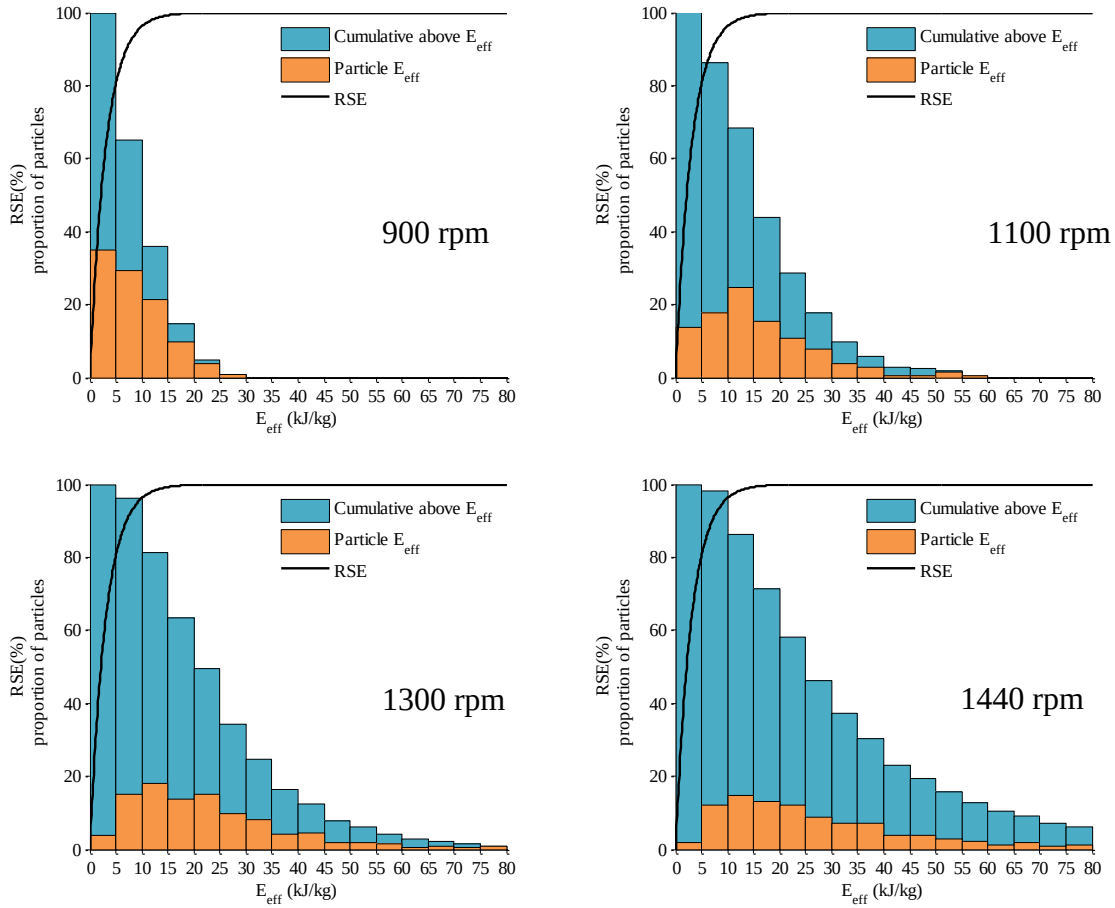

Figure 4.24 Histogram of effective energy available for annual ryegrass seed devitalisation for individual particles in the HSD cage mill using CFD particle tracing and material function for annual ryegrass seed devitalisation.

The particles entered into the Prototype 1 had a distribution of effective impact energy available for devitalisation of annual ryegrass seeds that increased with rotational speed, as shown in Figure 4.25. The effective energy applied to particles was in general, significantly less than for the HSD cage mill. As with the HSD cage mill the distribution of effective impact energy caused some particles to be exposed to significantly more energy than the mean. There was also some particles with significantly less energy than the mean, which are escaping impacts that the majority are receiving. However, the distribution of impact energy was not as wide as the HSD cage mill which is highlighted with a central data peak of particle effective energy.

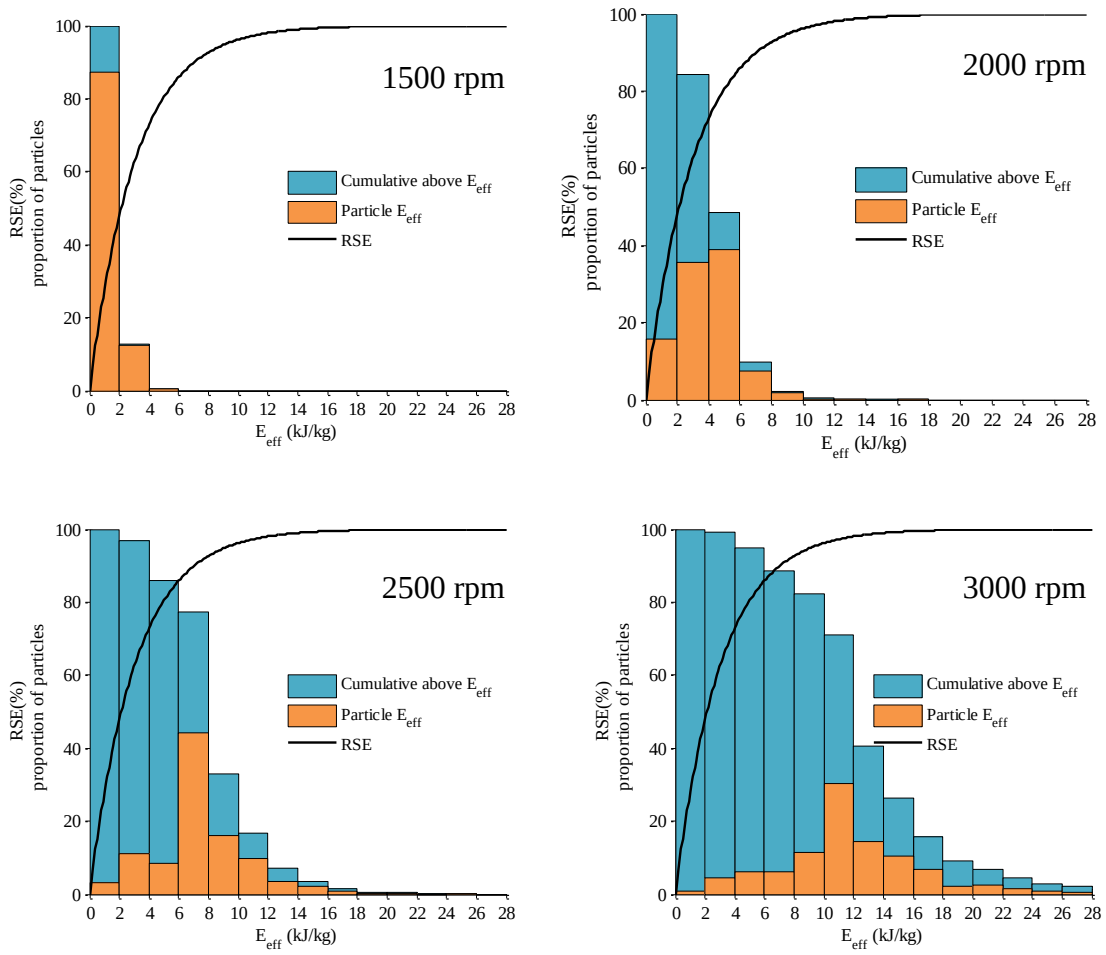

Figure 4.25 Histogram of effective energy available for annual ryegrass seed devitalisation for individual particles in the Prototype 1 using CFD particle tracing and material function for annual ryegrass seed devitalisation.

The Prototype 2 had a lower spread of lower spread of effective impact energy for each particle than both the HSD cage mill and Prototype 1 rotors, as shown in Figure 4.26. This lower spread is due to reduced spread on the number of impacts and impact speed. The majority of particles impact each row of rotor and stator bars once only. Therefore, the amount of over processing and under processing was predicted to be reduced for the Prototype 2.

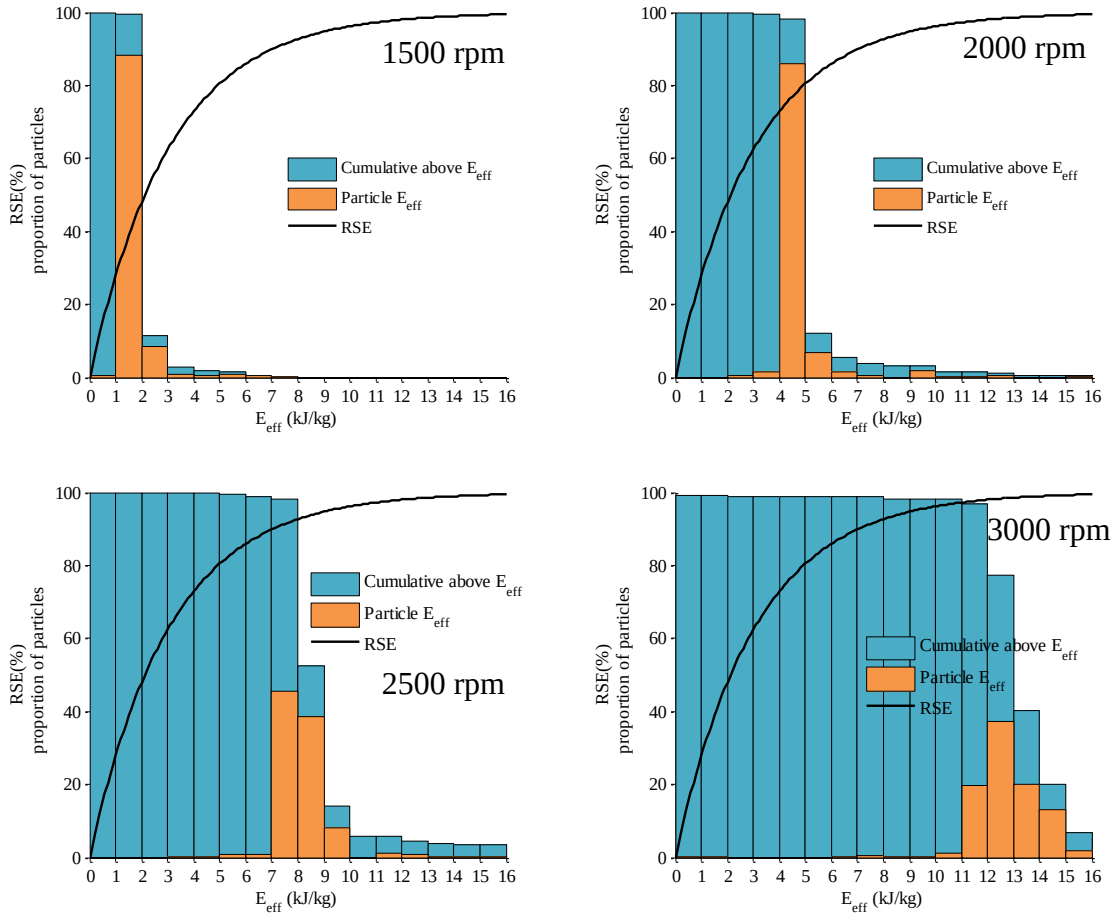

Figure 4.26 Histogram of effective energy available for annual ryegrass seed devitalisation for individual particles in the Prototype 2 using CFD particle tracing and material function for annual ryegrass seed devitalisation.

The mean seed devitalisation for the three mills was determined by averaging the probability of seed devitalisation for each particle in the CFD model. The number of impacts and impact speed from the vector impact model was input into the annual ryegrass seed devitalisation mastercurve (Equation (4.2)) to predict seed devitalisation as a function of rotational speed. The prediction of seed devitalisation of the three mills was nearly identical for the theoretical vector impact model and the CFD impact model, as shown in Figure 4.27. The confidence intervals of both models were calculated based on the confidence intervals for the mastercurve values F_{seed} and E_{min}. Both the vector and CFD impact models predicted slightly higher seed devitalisation for the Prototype 2 than Prototype 1. To achieve the project goal of 90% seed devitalisation, the impact models predicted that the speeds required were approximately 1000 rpm, 2700 rpm and 2400 rpm, for the HSD cage mill, Prototype 1 and Prototype 2, respectively.

The Prototype 2 has a smaller rotor diameter (535 mm) than the Prototype 1 (600 mm) and, hence generates lower tip speeds. The Prototype 2 had one extra impact, which explains the similar predicted seed devitalisation.

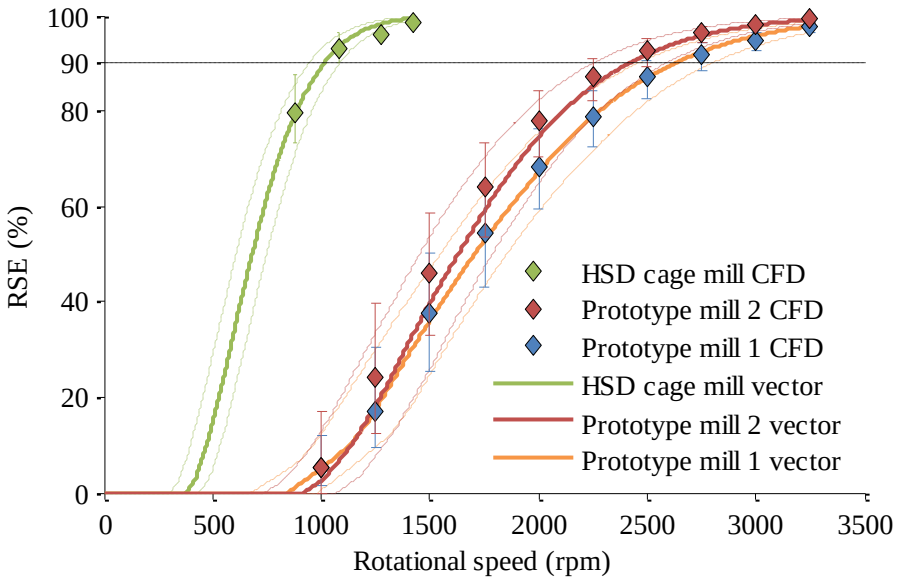

Figure 4.27: CFD and vector impact model prediction of seed devitalisation of the three mills with 95% C.I.

4.2.3.2 *Terminal velocity effect*

The vector impact model and CFD impact model had nearly identical predictions of seed devitalisation despite the CFD model also taking into account the aerodynamic acceleration of particles. To determine the effect of aerodynamic acceleration, the terminal velocity of inserted particles was adjusted. The terminal velocity of annual ryegrass seeds had significant range of values (See Section 3.2.2.5). Seeds with a low terminal velocity are accelerated by the air stream more significantly. Low terminal velocity seeds may be accelerated prior to impact causing reduced impact velocity or may even miss some impact bars. Particles were entered with a terminal velocity equivalent with the annual ryegrass seed percentiles 2.5, 25, 50 (median), 75 and 97.5%, from Table 3.13. The annual ryegrass terminal velocity 25, 50, 75 and 97.5% percentiles had very similar predicted seed devitalisation in the Prototype 1, as shown in Figure 4.28. The 2.5% percentile seeds (2.09 m/s) did show a reduction in seed devitalisation of approximately 9% and 5% at 2000 rpm and 2500 rpm, respectively. In the Prototype 1, the range of annual ryegrass seed terminal velocity has only minor effect on seed devitalisation.

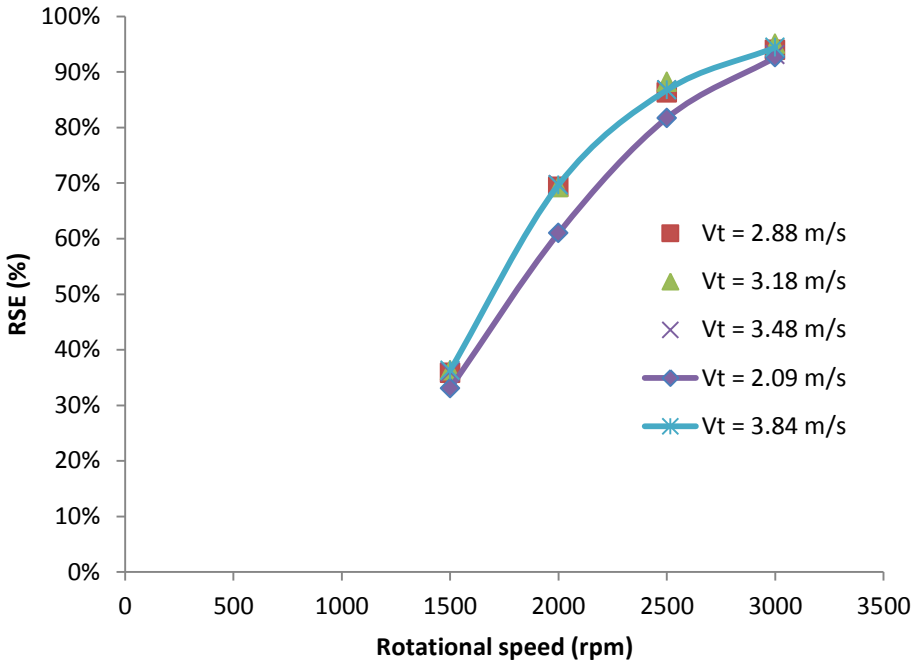

Figure 4.28: The effect of annual ryegrass terminal velocity on mean seed devitalisation for the Prototype 1

4.2.3.3 *Specific processing energy prediction*

The specific processing energy, or the energy needed to process a mass unit (kg) of material was estimated using the vector impact model. Energy is exerted onto particles within an impact mill by the rotor changing the velocity of a particle. The energy exerted by the rotor to a particle is determined by the rotor and particle tangential velocity prior to impact and the normal coefficient of restitution of the impact (See Section 3.2.3.2). The power equation derived in Section 3.2.3.2 was an important development in modelling the specific energy consumption of the milling operation. It showed that the energy required of the mill was not simply calculated using the velocity of the impact bar with the kinetic energy formula (½ ṁ v_T^2) as could be assumed intuitively. The energy needed to impact a particle was governed by the rotor and particle velocity, in the fully plastic case ($e_n = 0$), it was given by Equation (3.85), as repeated here:

$$E_{spec} = \sum_{j=1}^{n} v_{r,j}^2 - v_{r,j} v_{p,j} \qquad (4.5)$$

Where: j = impact number, $1 \rightarrow n$
v_r & v_p = velocity of rotor and particle before impact

The specific processing energy was predicted using the vector impact model, as shown in Figure 4.29. The theoretical vector impact model was not able to predict the power needed to run the mills empty (no load power).

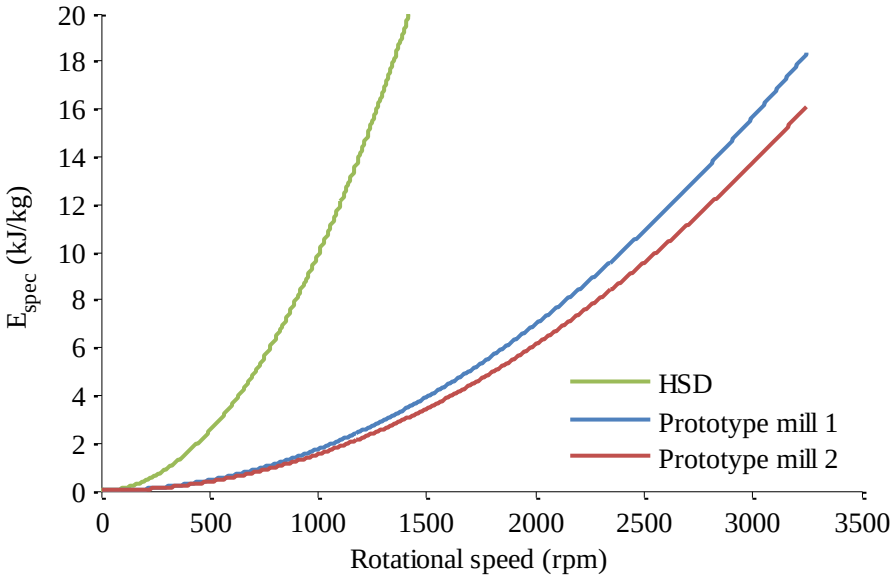

Figure 4.29: Vector model prediction of specific power consumption of the HSD cage mill, Prototype 1 and Prototype 2

The prediction of specific processing energy shown in Figure 4.29 were converted into the fit parameter *b* for chaff processing power as per Equation (3.111). Rearranging Equation (3.111) in terms of specific energy consumption becomes:

$$b(m^2) = \frac{2E_{spec}}{\omega^2} \tag{4.6}$$

The processing power fit parameters for the vector impact model are shown in Table 4.2.

Table 4.2: Vector model specific processing power fit parameter

Mill	Processing power parameter *b* (m^2)
HSD cage mill	1.8436
Prototype 1	0.3169
Prototype 2	0.2781

The predicted seed devitalisation was plotted against predicted specific energy consumption in Figure 4.30. A high efficiency corresponds to a high level of seed devitalisation for the specific processing energy. The Prototype 2 was predicted to be the most efficient, followed by the HSD cage mill and then the Prototype 1. The vector impact model predicted two sources of wasted specific energy: the threshold specific

energy for devitalisation for each impact ($E_{min} \times k$) and the residual specific kinetic energy of particles exiting the mill ($1/2000v^2$). The vector impact model predicted wasted energy at 90% seed devitalisation is shown in Table 4.3. The most significant difference in energy used to achieve seed devitalisation between the three mills was the residual kinetic energy of the particles exiting the mill.

Table 4.3: Vector model prediction of wasted specific energy at 90% seed devitalisation

Mill	Rotational speed (rpm)	Number of impacts	Threshold energy loss (kJ/kg)	Exit velocity of particle (m/s)	Residual kinetic energy loss (kJ/kg)
HSD cage mill	1000	6	2.4	52.0	1.35
Prototype 1	2700	4	1.6	87.5	3.83
Prototype 2	2400	5	2.0	9.6	0.05

The Prototype 1 has the lowest predicted efficiency because the material exits the mill at the highest velocity. The Prototype 2 had the highest predicted efficiency because the last impact is on a static row and, thus the material does not exit the mill with much kinetic energy as the other two mills. This result indicates that it does not matter if the mill is counter rotating cage mill design or a rotor stator design; the energy lost to the system is through particles exiting with some residual kinetic energy. Furthermore, this result highlights the importance of ensuring that the residual kinetic energy of a particle is used for further breakage.

Three limitation of this power analysis are that:

1) It may underestimate the threshold energy loss because the number of impacts may be higher as predicted using the CFD model.

2) Seed breakage could occur with impacts in the mill housing and not all residual energy of particles exiting the Prototype 1 is wasted;

3) The air speed may again accelerate material exiting the Prototype 2 and particles may have a higher residual energy than calculated.

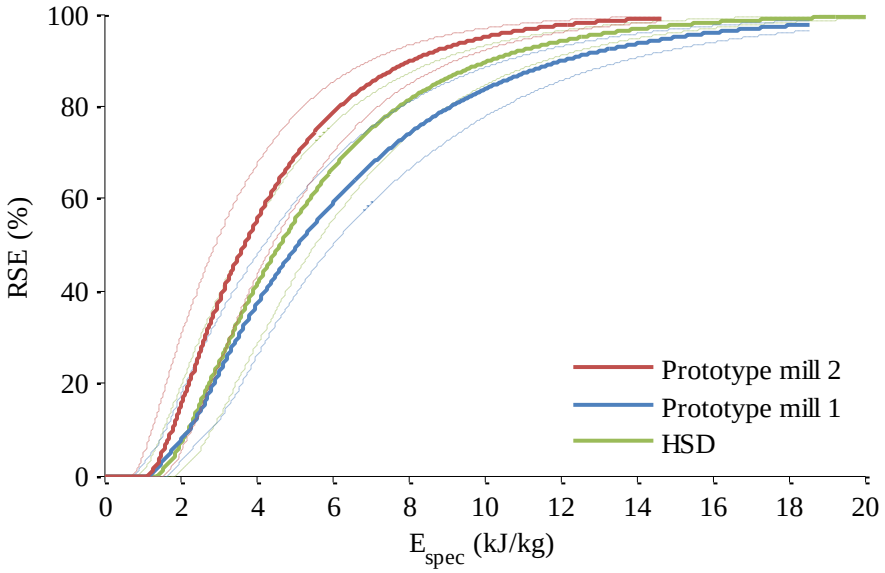

Figure 4.30: Vector model prediction of seed devitalisation against specific processing energy

4.2.3.4 *No load power prediction*

The no load power requirement consists of power to pump air and generate turbulence and was estimated using the CFD continuous (fluid) phase solution. The no load power consumption of the Prototype 1 and 2 were estimated by multiplying the torque goal output of the rotor in the CFD simulation by the rotational speed of the rotor. The torque was not measured in the initial CFD simulations of the HSD cage mill. The no load power consumption prediction of the two prototype mills were very similar, as shown in Figure 4.31. A cubic fit was applied to the data to find the no load fitting parameters for the mill as per Equation (3.108).

$$A = \frac{P_{air}}{\omega^3} \tag{4.7}$$

Where: A– fitting factor of the mill (kg.m^2)
P_{air} = no load power of the mill (W)
ω is the rotational speed of the mill (rad/s)

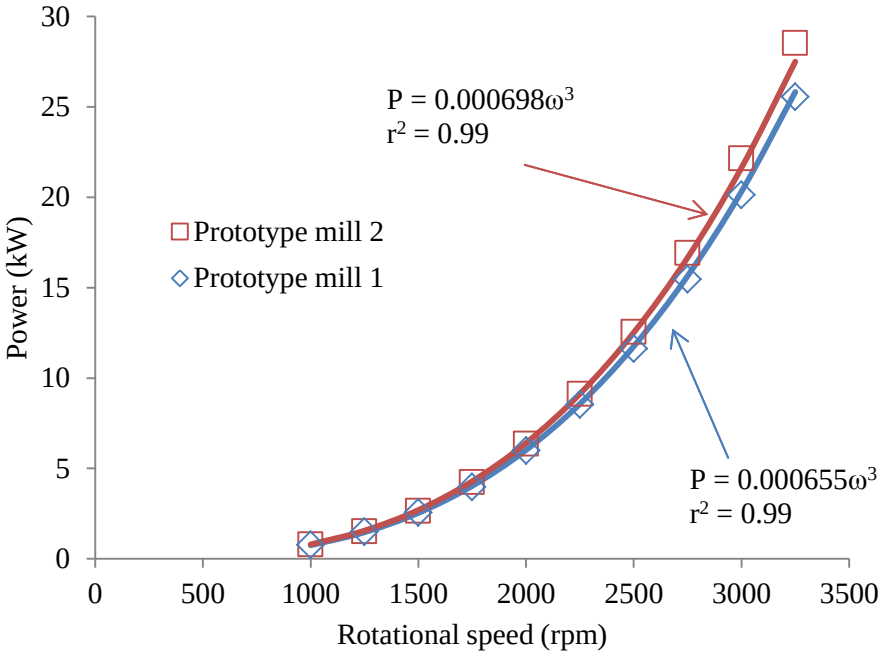

Figure 4.31: No load power prediction of the Prototype 1 and 2

4.2.4 Discussion

The vector impact model and the CFD impact model both provided a prediction of the number of impacts and impact speed based on geometry and operating conditions of three mills. The two modelling techniques used the same classic theory of impact. However, the calculation of number of impacts and impact speed was very different. The vector impact model predicted the normal impact velocity of each row of impact bars based on the mill's two-dimensional geometry and the assumption that one impact occurs on each row of bars. The CFD impact model also took into account the randomness of the particle motion through the mill and included the aerodynamic acceleration of particles. The prediction was a fixed number of impacts and impact speeds from the vector model and a distribution of both from the CFD model.

The CFD model showed that based on the mill geometry there would be significant differences in the particle behaviour through the mill. The round bars of the HSD cage mill caused a large number of low speed glancing impacts; a significant proportion of which were below the threshold minimum energy for seed devitalisation (≈ 28 m/s). Thus, the HSD may be operating inefficiently. In contrast, the Prototype 1 had a much narrower distribution of impacts and impact speed because of the impact bars had flat impact surfaces. The Prototype 2 had an even narrower distribution of impacts and impact speeds.

Seed devitalisation was estimated using the prediction of number of impacts and impact speeds from the vector and CFD impact models and the material function mastercurve. Despite the differences between the vector impact model and CFD impact model, they both provided an almost equivalent prediction of seed devitalisation for the three mills. For the two prototype mills, the impact faces were flat and the design intent to have one impact on each row of bars. Thus, the vector model simulates the physical path very similar to the CFD model as seen in Figure 4.16 and Figure 4.17. The HSD cage mill had cylindrical bars and as found with the CFD modelling, the majority of impacts are glancing (oblique). The vector model of the HSD cage mill had higher impact speeds than modelled using the CFD model. The CFD model showed that some particles are impacted towards the centre of the HSD cage mill, which results in a higher number of impacts than predicted by the vector model. The vector model prediction of seed devitalisation of the HSD cage mill, which uses both speed and number of impacts, was similar to the CFD model.

The effect of aerodynamic acceleration was investigated by comparing the seed devitalisation over a range of particle terminal velocities. Annual ryegrass seeds with a low terminal velocity are accelerated by the air stream more than the seeds with a higher terminal velocity. The CFD model predicted seed devitalisation to be largely unaffected by terminal velocity for the Prototype 1; the 2.5 percentile annual ryegrass terminal velocity (2.09 m/s) showed a maximum of 9% reduction in seed devitalisation at 2000 rpm and minimal differences between the other terminal velocities tested. The effect of aerodynamic acceleration in the Prototype 1 may not be significant for particles in the terminal velocity range of annual ryegrass seeds. This also gives some explanation why the seed devitalisation prediction from the vector model, which did not include aerodynamic acceleration, was so similar to the CFD impact model.

The vector model has an advantage that an estimate of performance can be generated almost instantaneously when the CFD model takes hours or even days to run. The CFD particle study model estimates the distribution of number of impacts and impact speeds that could be expected in a mill. The CFD model provides is an indication that particles may be missing rows of bars and modifications to the mill design can be made. Seed devitalisation achieved is not simply due to the probability of seed devitalisation based on a single energy value but rather a distribution of the applied impact energy.

4.3 Seed devitalisation evaluation

4.3.1 Experimental testing results

4.3.1.1 *Annual ryegrass seed devitalisation*

The three milling technologies were evaluated for annual ryegrass devitalisation using the soil bin testing method. Annual ryegrass (Lolium rigidum) seeds were mixed with wheat chaff and processed at controlled mass flow rate into the HSD cage mill, Prototype 1 and Prototype 2. The rotational speed of the three mills was varied. Seed devitalisation was measured by mixing the chaff-seed mixture with soil and planting in indoor controlled environment soil bins, counting emergence and comparing to control germination using reduced seedling emergence (RSE):

$$RSE = 1 - \frac{SE}{SE_{control}} \tag{4.8}$$

Where: SE is the maximum seedling emergence count of the 14 and 28 days of a treatment
$SE_{control} = 448$ is the average of the control seedling emergence counts

The HSD cage mill was found to have a mean seed devitalisation (RSE) of greater than 90% for the speeds tested in this study, as shown in Figure 4.32. At the three common speeds tested, 900, 1100 and 1300 rpm, there was very little difference between the results presented here and the results generated by Walsh, Harrington and Powles (2012). A linear regression of the seed devitalisation data was found to be non-significant ($p = 0.086$, $r^2 = 0.226$). However, there is insufficient evidence to suggest that speed has no impact on seed devitalisation in the range of speeds tested just that statistical power in this experiment or in the experiment by Walsh, Harrington and Powles (2012) was not high enough to measure very small effects.

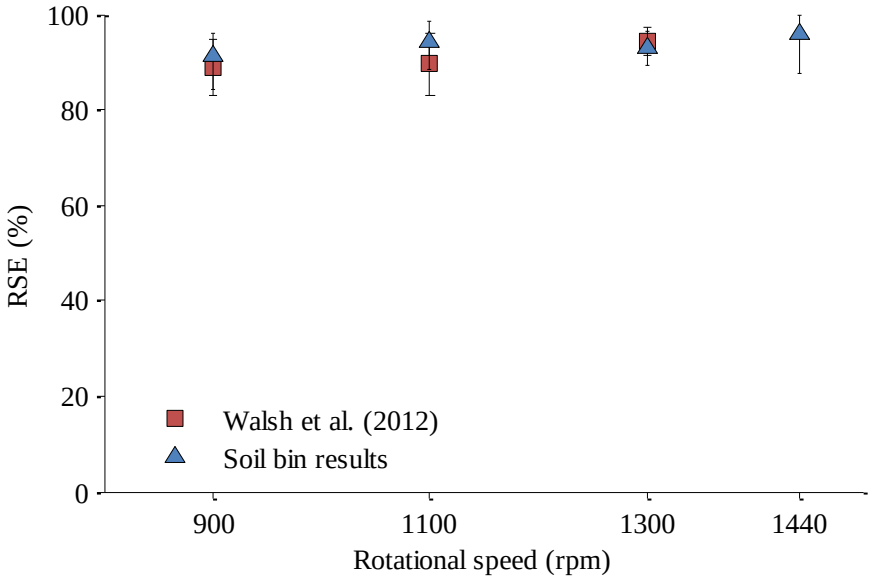

Figure 4.32: Annual ryegrass seed devitalisation processed with wheat chaff in the HSD cage mill with 95% C.I.

The Prototype 1 was found to devitalise up to 97.7% of annual ryegrass seeds at 2970 rpm, as shown in Figure 4.33. Seed devitalisation increased with rotational speed of the mill and reduced with chaff throughput. Significant reduction in seed devitalisation was found with the 1.5 kg/s test compared with the 0.5 kg/s tests. The 1.5 kg/s test is equivalent to the 3 kg/s (10.8 t/h) expected on a high capacity combine harvester because two prototype mills were to be used.

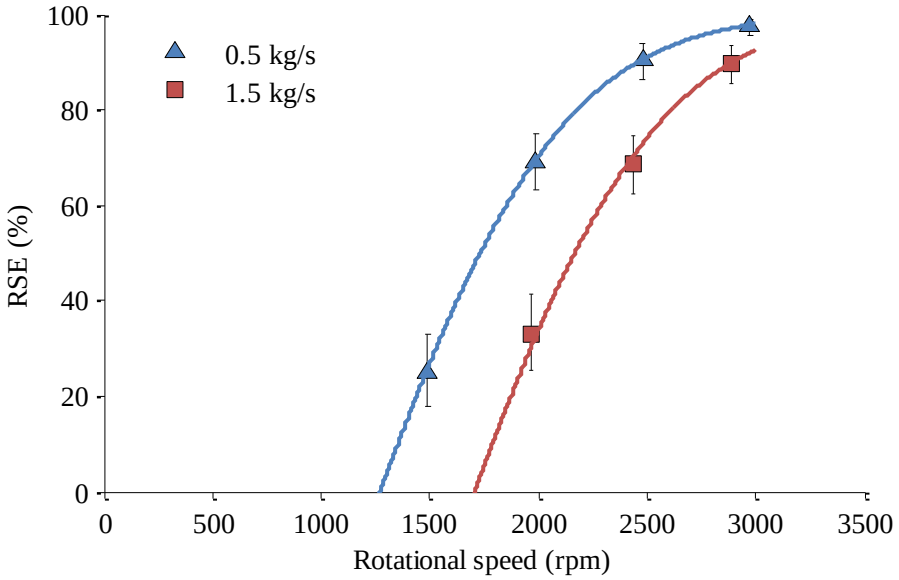

Figure 4.33: Annual ryegrass seed devitalisation processed with wheat chaff in the Prototype 1 with 95% C.I. Non-linear regression curve fit r^2 = 0.982.

Annual ryegrass seed devitalisation increased with rotational speed of the Prototype 2, as shown in Figure 4.34. The Prototype 2 had a lower maximum level of seed devitalisation achieved than the Prototype 1; 91.3% compared to 97.7% at the low throughput of 0.5 kg/s. However, there was minimal difference in seed devitalisation between the two throughputs tested using the Prototype 2

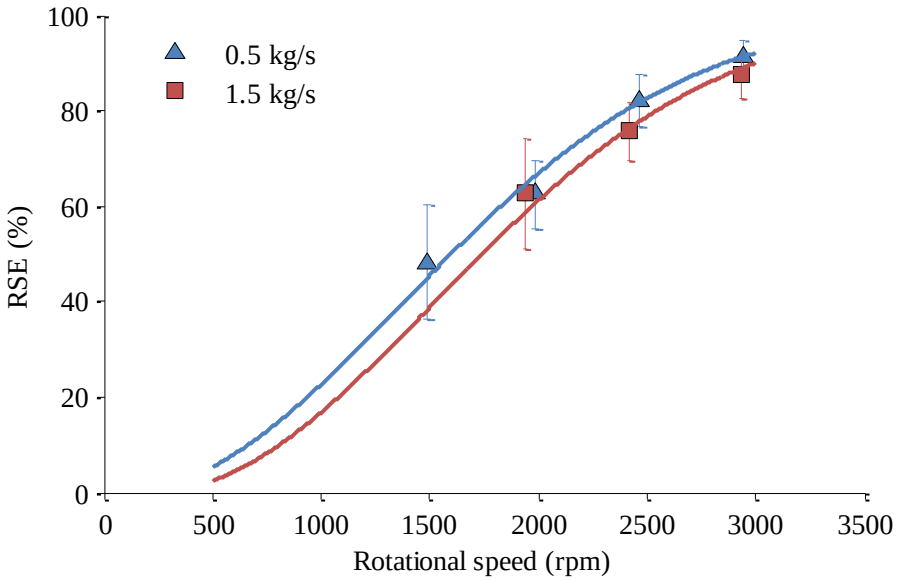

Figure 4.34: Annual ryegrass seed devitalisation processed with wheat chaff in the Prototype 2 with 95% C.I. Non-linear regression curve fit r^2 = 0.912.

4.3.1.2 *Empirical machine function*

The empirical machine function, non-linear regression parameters for the Prototype 1 and 2 mills are shown in Table 4.4, which relate to the coefficients in Equation (4.9). The non-linear regression of E_{eff} was able to fit the data from both the Prototype 1 (r^2 = 0.982) and Prototype 2 (r^2 = 0.912), as shown in Figure 4.33 and Figure 4.34. The value for k for the Prototype 2 was negative in the initial non-linear regression. However, the confidence interval for k also contained zero, which indicated that it was not statistically significant. Therefore, k was removed from the regression for the Prototype 2 (k = 0).

The throughput was found to be a statistically significant (95%) predictor of seed devitalisation for both prototype mills because the 95% confidence interval for C for both mills did not include zero. However, the C value of the Prototype 1 was four times that of the Prototype 2; 45.6 compared to 15.1 (1/kg). Chaff throughput has a larger influence on seed devitalisation for the Prototype 1 compared to the Prototype 2. The chaff throughput effect on seed devitalisation for the Prototype 2 was of little practical significance.

Table 4.4: Prototype 1 and Prototype 2 seed devitalisation, non-linear regression parameters

	Prototype 1 (95% C.I)			Prototype 2 (95% C.I)		
Parameter	L	Mean	U	L	Mean	U
B (m^2)	0.3031	0.3278	0.3525	0.1502	0.1653	0.1804
C (1/kg)	37.16	45.60	54.05	4.15	15.05	25.95
k (impacts)	3.17	4.99	6.81	-	-	-

$$RSE = 1 - \exp\left[- F_{seed} \left(\frac{1}{2000} B\left(\omega - C\dot{m}_{chaff}\right)^2 - kE_{\min} \right) \right] \quad (4.9)$$

There was some correlation between the parameters used in the non-linear regression, as shown in Table 4.5. The correlation between the parameters B and k was the highest for the Prototype 1. The correlation between B and C for Prototype 2 was relatively high. However, the correlation between parameters was sufficiently small that the parameters would be kept.

Table 4.5: Correlations of parameter estimates

mill		B	C	k
Prototype 1	B	1.000	.132	.638
	C	.132	1.000	-.588
	k	.638	-.588	1.000
Prototype 2	B	1.000	.864	
	C	.864	1.000	

4.3.1.3 *Discussion*

For the first time, seed devitalisation has been measured for an impact mill at wheat chaff mass flow rates high enough to represent field conditions of a modern combine harvester (≈ 3 kg/s or 1.5 kg/s per mill). Previous research has reported testing of up to only 0.64 kg/s of wheat chaff (Walsh & Harrington 2011; Walsh, Harrington & Powles 2012). The method to evaluate seed devitalisation presented here also had the advantage of requiring significantly less time to determine seed devitalisation than the method used by other researchers. The method used by Walsh, Harrington and Powles (2012) was to process chaff with dyed annual ryegrass seeds and then recover the seeds out of the processed chaff. This method was very time consuming and there was a possibility of not finding all the seeds.

The both Prototype 1 and Prototype 2 nearly achieved the project goal of 90% annual ryegrass kill at 1.5 kg/s of chaff throughput. The Prototype 1 at 2890 rpm achieved a seed devitalisation of 89.8% and the Prototype 2 achieved 87.6% at 2926 rpm. The

Prototype 1 seed devitalisation was reduced significantly from 0.5 kg/s chaff mass flow to 1.5 kg/s chaff mass flow. The modified design of the Prototype 2 had improved its ability to handle an increased mass flow of chaff without a reduction in seed devitalisation. Chaff throughput does not affect the Prototype 2 as significantly as the Prototype 1 because the material passes through the Prototype 2 in less time. Therefore, the solids loading of chaff in the milling gap is reduced for the Prototype 2, as was predicted in the CFD model of solids loading (Figure 4.22 and Figure 4.23). The likelihood of inefficient, particle to particle impacts in the Prototype 2 was therefore lower than the Prototype 1.

The level of seed devitalisation depends heavily on the hostility of the soil conditions. The tests performed were indoors, with controlled temperature and humidity with a non-hostile sand-loam soil. In the field, the weather and soil conditions can be more unfavourable to emerging seedlings. The prototype mills may also have other effects which would also improve the control of the weed seed bank such as dormancy breakage due to scarification and reduced persistence in the soil (Davis et al. 2008) (Dalling et al. 2011). Therefore, the level of seed devitalisation seen in the field is expected to be equal to or greater than the level achieved in the laboratory.

The non-linear regression model was found to fit the seed devitalisation data well. The physical meaning of the parameters in Equation (3.102) may not have physical meaning. For example, k was supposed to indicate number of impacts that occurred within the mill. The Prototype 1 had an estimated mean of number of impacts of $k = 5$, which was a feasible estimate of number of impacts. Whereas, the Prototype 2 had an estimated mean number of impacts of $k = 0$, which does not represent a real number of impacts. With $k = 0$, the response of seed devitalisation with rotational speed has a shallower slope, which is able to fit the Prototype 2 dataset. It was expected that the 1500 rpm would have lower seed devitalisation than was measured because the tip speeds were closer to the threshold energy (E_{min}). Equation (4.9) assumes that the applied impact energy increases with the square of rotational speed. This implies that the impact speed is the only mechanism for change in impact energy and, hence the same number of impacts occurs at all rotational speeds. However, it is possible that the number of impacts changes with rotational speed. In the Prototype 2, it could be that at 1500 rpm, a higher number of impacts occurred than at other speeds causing increased seed devitalisation.

The regression procedure presented, isolated the machine function of the two prototype mills from the material function for annual ryegrass seed devitalisation found during impact testing in a similar way to Vogel and Peukert (2003a). The prediction of seed devitalisation in Equation (4.9) has variables from both the machine and material function. The machine variables includes: mill specific parameters based on radial location of impact bars (B), effect of chaff (C) and number of impacts (k); and mill operating parameters, rotational speed (ω) and chaff mass flow ($\dot{m}_{chaff}$). The material variables include the seed specific properties found from impact testing: seeds resistance of impact induced seed devitalisation (F_{seed}); and threshold energy for seed devitalisation (E_{min}). The importance of this separation is that a prediction of seed devitalisation in the two prototype mills can be made for different operating conditions and potentially even for different weed species. If a different operating condition was needed, adjustments could be made to the mass flow of chaff or rotational speed in Equation (4.9). If different weed species were of interest, impact testing would find seed specific properties F_{seed} and E_{min}. There would be some error in the estimate, especially if the conditions were extrapolated outside the range of testing. Therefore, validation testing would also be needed to confirm the prediction. However, the prediction provides a method of reducing the amounts of tedious and expensive testing required to find an optimal operating condition.

4.3.2 Comparison to modelling

The prediction of seed devitalisation using the vector impact model and the CFD impact model were compared to the experimental results of the three mills. The comparison was used to determine if the mechanistic modelling techniques were effective at modelling the performance of the existing HSD cage mill technology and if they were an accurate design tool for predicting the effectiveness of two new prototype mill designs.

4.3.2.1 *Comparison of predicted models*

The vector and CFD impact models of the HSD cage mill predicted a slight increase in seed devitalisation with rotational speed over the range of impact speeds tested. Whereas, rotational speed was not significant in the experimental results of the HSD cage mill, as shown in Figure 4.35. Despite the different trend, there was less than 10%

difference in seed devitalisation between the experimental results and the vector and CFD impact models over the range of speeds tested.

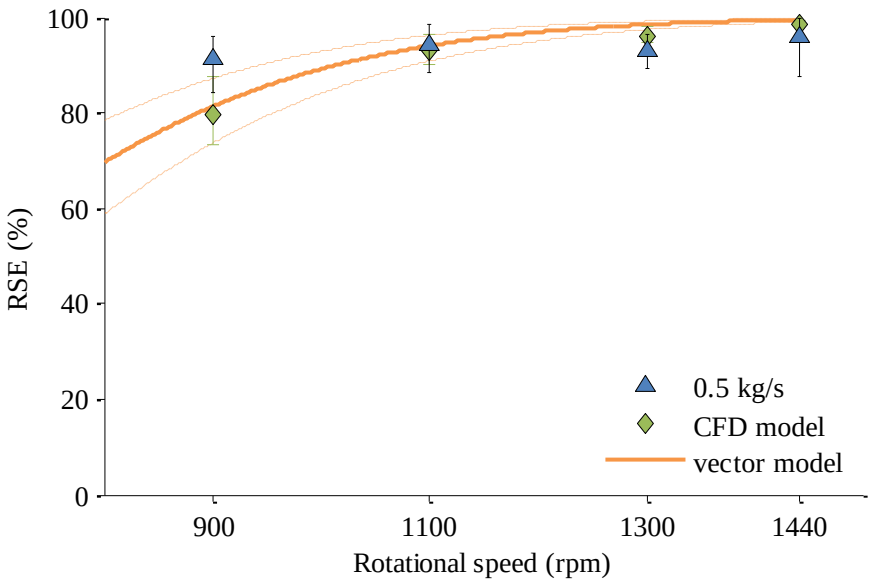

Figure 4.35: Comparison of vector and CFD impact models to HSD cage mill soil bin testing results at 0.5 kg/s. Vector impact model r^2 = 0. CFD impact model r^2 = 0. (0.5 kg/s)

The vector and CFD impact models were able to accurately predict (r^2 = 0.948) the annual ryegrass seed devitalisation when processed with the Prototype 1 at a chaff mass flow of 0.5 kg/s, as shown in Figure 4.36. However, at the higher chaff mass flow, the prediction of seed devitalisation was significantly higher than the experimental results. The vector and CFD impact models did not account for particle to particle impacts, which would be expected to be more significant at the higher chaff mass flow.

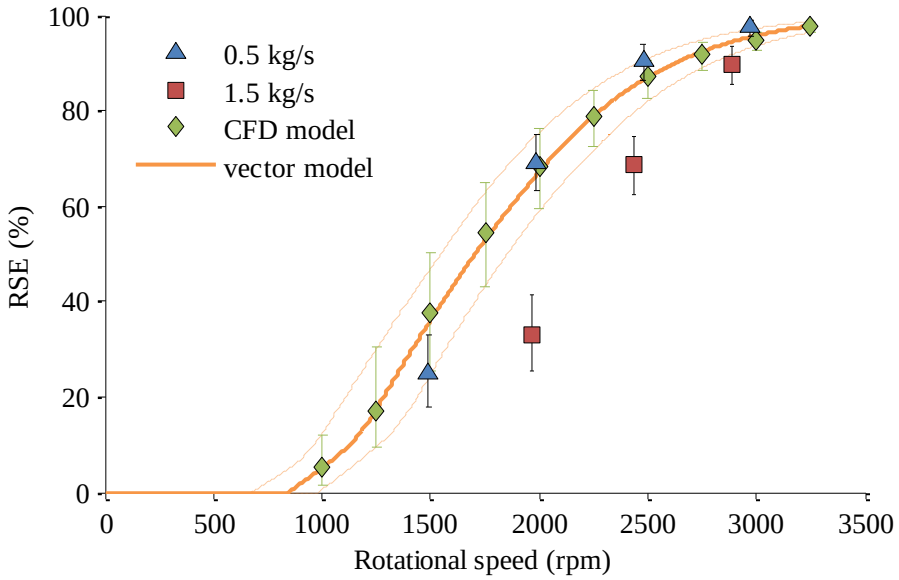

Figure 4.36: Comparison of vector and CFD impact models to Prototype 1 soil bin testing results at two throughputs. Vector impact r^2 = 0.948 (0.5 kg/s) and 0.18 (1.5 kg/s). CFD impact model r^2 = 0.948 (0.5 kg/s) and 0.125 (1.5 kg/s).

The vector and CFD impact models predicted seed devitalisation for annual ryegrass using the Prototype 2 and soil bin results for two throughputs are shown in Figure 4.37. The coefficient of determination was low for both throughputs. However, the prediction was still relatively accurate and within 17% of the mean seed devitalisation of the soil bin results. The seed devitalisation experimental results had a flatter response to rotational speed than what was expected with the vector and CFD impact models.

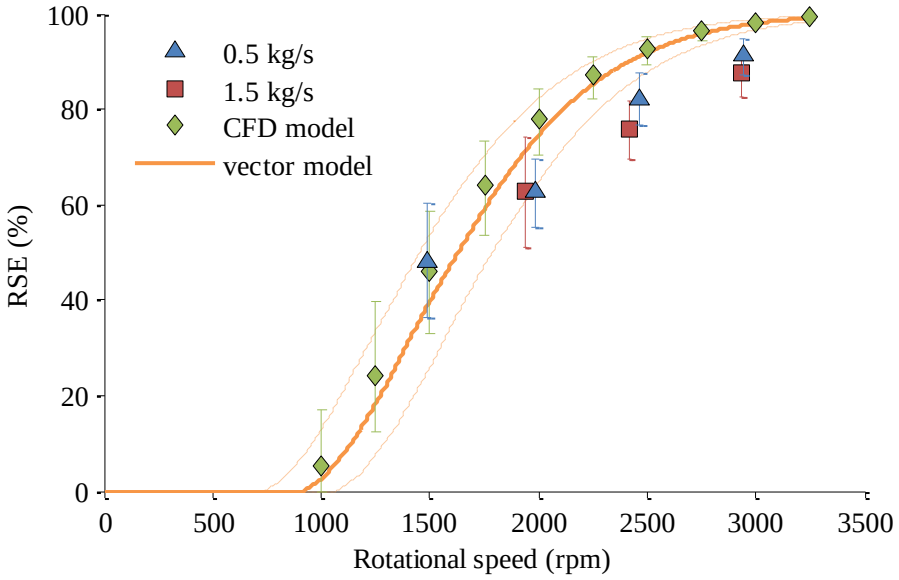

Figure 4.37: Comparison of vector and CFD impact models to Prototype 2 soil bin testing results at two throughputs. Vector impact r^2 = 0.680 (0.5 kg/s) and 0.289 (1.5 kg/s). CFD impact model r^2 = 0.664 (0.5 kg/s) and 0.0 (1.5 kg/s).

4.3.2.2 *Discussion*

The vector impact model and the CFD impact model were both able to predict seed devitalisation of the three impact mills within a reasonable accuracy for most tests.

The vector and CFD impact models of the HSD cage mill both showed a larger increase in seed devitalisation with rotational speed than was found with experimental results. One explanation for this difference could be that the material had a longer residence time and the number of impacts was higher at low rotational speeds than was predicted in the model.

The vector and CFD impact models of the Prototype 1 accurately predicted the seed devitalisation at 0.5 kg/s mass flow of chaff. At the increased chaff mass flow of 1.5 kg/s, the model predictions were significantly higher than the experimental results, especially at the lower rotational speeds of 2000 and 2500 rpm. Both impact models did not include particle to particle impacts of the chaff. Particle to particle interaction are expected to be more significant at higher chaff mass flow and at lower rotational speeds because of a higher solids ratio of chaff in the milling zone. Particle to particle impacts reduce the energy of impact and are likely to reduce the probability of seed devitalisation. Therefore, assuming no particle to particle interaction was not valid at the higher throughput test. However, the CFD impact model showed that the solids loading of Prototype 1 (Figure 4.22) was around twice that of Prototype 2 (Figure 4.23). Therefore, the CFD model was able to predict that Prototype 1 would be more susceptible to particle to particle impacts than Prototype 2.

The experimental seed devitalisation of Prototype 2 had a flatter response to rotational speed than predicted by both the vector impact model and the CFD impact model. This could be due to a combination of experimental variability and the CFD modelling not taking into account some of the physical phenomena occurring within the Prototype 2. This physical phenomena could be causing a higher number of impacts to occur at low rotational speeds. Alternatively, it could be that the sharp impact edges of the Prototype 2 cause a secondary mechanism for seed devitalisation; some seeds could be cut on the sharp edges resulting in higher seed devitalisation at low rotational speeds than would be expected for normal impact alone.

The mechanistic modelling techniques used in this study have provided useful predictions of machine performance prior to prototype construction. The machine

function can be separated from the material function using the regression techniques. However, using regression techniques only allows for predictions of performance under new operating conditions and for different materials. The regression technique does not allow for predictions of newly designed mills. Therefore, mechanistic modelling techniques were valuable for mill design. The importance of the mechanistic modelling techniques was the ability to try a multitude of configurations and predict performance before prototype construction. A combination of both methods is to be employed for future iterations because both methods add value. The vector model can be used for the initial sizing and speeds and then the CFD method can be used to determine the likely number of rotor and stator bars that are needed to ensure seeds are impacting each row of bars.

4.4 Power and chaff throughput

4.4.1 HSD cage mill

Harvest trials using the second generation HSD towed by a John Deere 9650 were performed to determine the wheat chaff processing requirement and power consumption of the HSD cage mill. Chaff was collected in semi-permeable bags and weighed to determine chaff mass flow over set run lengths and set run speeds. Wheat mass flow was determined using the harvesters yield monitor and measured using the Green Star 2 terminal. The HSD cage mill power was measured by logging the engine power through the Isuzu CAN-BUS.

4.4.1.1 *Chaff throughput*

The total chaff mass and grain mass over the run length and the average speed were used to calculate the grain and chaff throughput. The chaff throughput increased with grain throughput for the three locations and two rotor speeds tested up to a maximum of 9.3 t/h at 28.5 t/h of grain, as shown in Figure 4.38. A linear regression was performed for the data for each location with the intercept set at zero to give a proportional relationship. For each location the relationship between chaff throughput and grain throughput was linear in the range of grain throughputs tested. The linear relationship implies that for each site, the mass throughput of chaff for a given mass throughput of grain (chaff to grain ratio) remained relatively constant.

The chaff to grain ratio was calculated for each individual test and was found to range from 0.215 to 0.388 tonnes of chaff per tonne of wheat. The mean chaff to grain ratio for each test condition was compared using Tamhane's T2 post hoc analysis in SPSS®, as shown in Table 4.6. There was a statistically significant difference between three of the four test conditions. Despite using an identical harvester setup, Minnipa had a higher chaff to grain ratio than Maitland, which shows the effect of different crop varieties and conditions at each location. At Maitland, the 960 rpm rotor speed had a higher chaff to grain ratio than 700 rpm. Increasing the rotor speed causes more breakage of material through the concave that ends up in the chaff residue fraction. The tests at Maitland and Pinnaroo with a rotor speed of 700 rpm were not statistically different at the 95% confidence level.

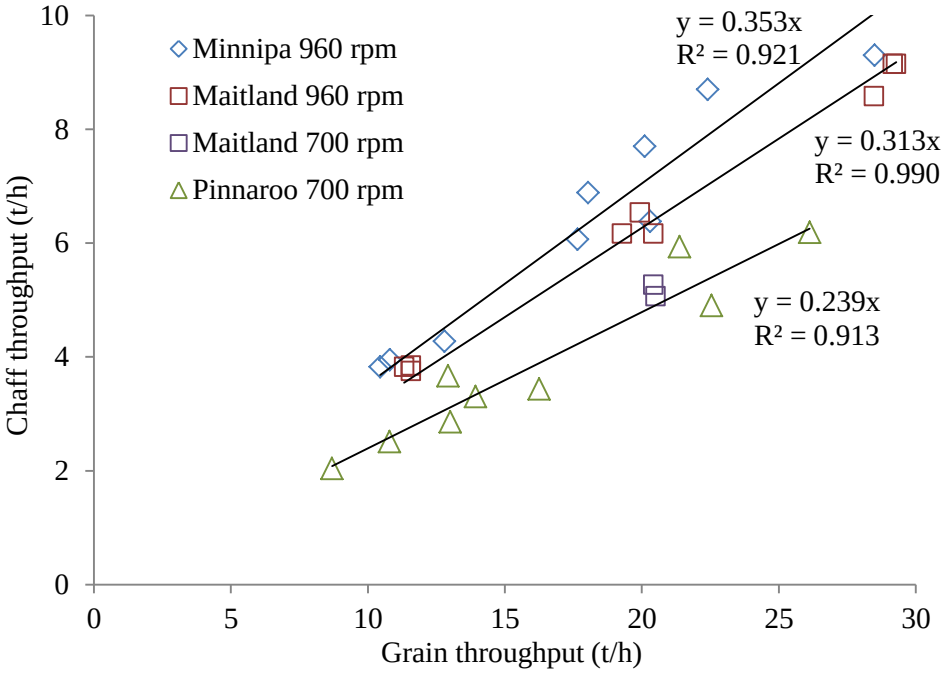

Figure 4.38: Chaff throughput for wheat throughput at three locations

Table 4.6: Mean chaff to grain ratio for each test condition

Site	Rotor speed (rpm)	Chaff to grain ratio*
Minnipa	960	0.356[a]
Maitland	960	0.319[b]
Maitland	700	0.253[c]
Pinnaroo	700	0.239[c]

*means with different letters are statistically different at 95% C.L

4.4.1.2 *Power for chaff throughput*

The HSD cage mill power was determined for each test at each trial location and the results were plotted against chaff throughput, as shown in Fig. 5. A linear regression

was performed using SPSS® for the whole data set. The linear model's intercept, 95% confidence interval was found to be 35.9 ± 4.5 kW. The intercept can be interpreted as the power requirement of the HSD cage mill when not processing any material. Analysis of the mean power consumption when running empty over the whole harvest data set showed a similar result of 36.5 kW. The linear model's slope, with 95% confidence interval was found to be 5.75 ± 0.82 kW.h/t. The slope coefficient can be interpreted as the HSD cage mill's specific energy to process chaff.

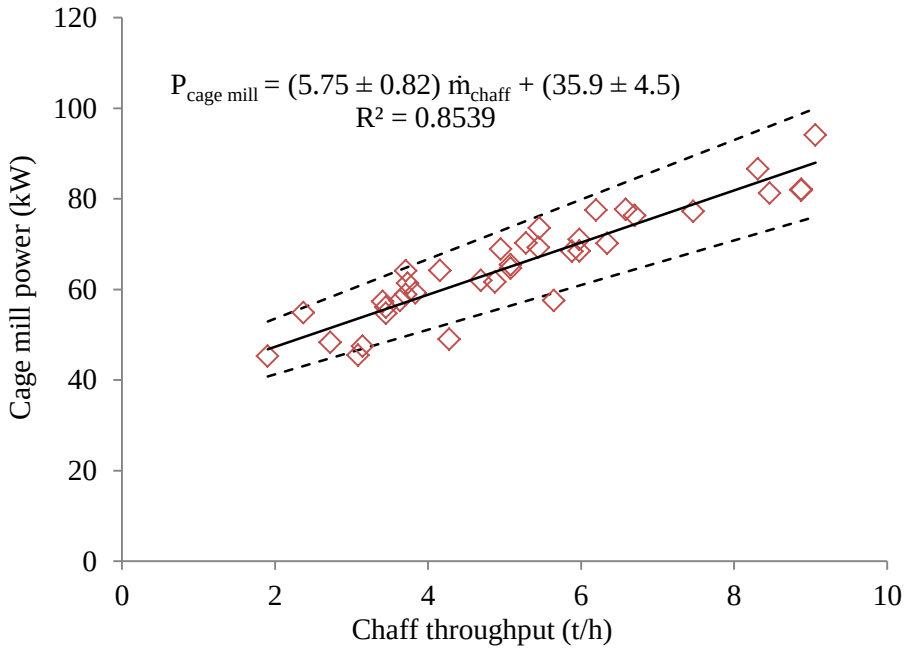

Figure 4.39: HSD cage mill power for chaff throughput at three locations

4.4.2 Prototype 1

Two Prototype 1 mills were attached to a CASE IH 9120 and driven hydraulically from the harvester's engine. Harvest trials were performed in wheat to determine the wheat chaff processing requirement and power consumption of the Prototype 1 over set run lengths and set run speeds. The chaff throughput was measured by collecting chaff in semi-permeable bags attached to the exit of both mills. Wheat mass flow was determined using the harvesters yield monitor and measured using the AFX 600 terminal. The Prototype 2 power was determined by logging the hydraulic pressure drop across each mill motor and the rotational speed.

4.4.2.1 *Chaff throughput*

The two Prototype 1 mills were able to process up to 12.4 t/h of wheat chaff without blockage. The chaff throughput increased linearly with grain throughput for the both

test days and ranged from 2.8 t/h of chaff for 7.6 t/h of grain through to 12.4 t/h of chaff for 41 t/h of grain, as shown in Figure 4.40. Linear regression analysis was performed using SPSS® with the chaff throughput as the dependant variable; grain throughput, date (dummy variable) were the independent variables. Grain throughput, date and a constant were all statistically significant ($p<0.05$). The 9th of January 2013 harvest day had a higher chaff throughput for the grain throughput compared to the 24th of December 2012. There were a number of days above 35°C between the two trail dates and the crop was noticeably more mature and brittle on the later harvest date. The January 9th harvest day had more broken up straw in the chaff because of the brittle material and, thus there was more chaff for the amount of grain harvested. The data was separated into the two harvest dates and the regression analysis was repeated without date as an independent variable. The regression parameters are shown in Table 4.7.

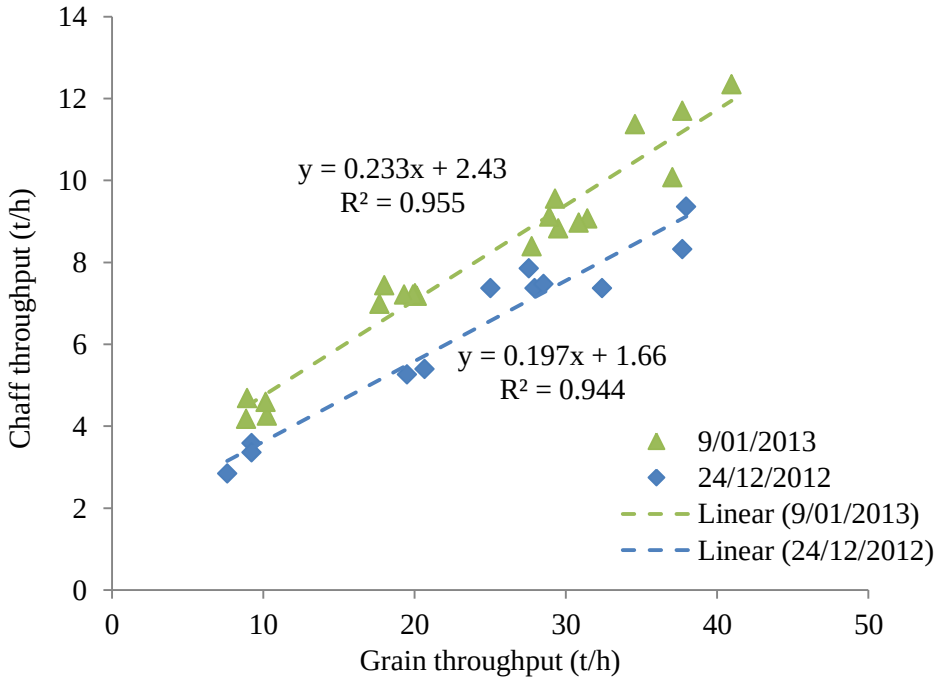

Figure 4.40: Chaff throughput against grain throughput

Table 4.7: Chaff throughput linear regression parameters ($\dot{m}_{chaff} = R\dot{m}_{grain} + O$)

	R (95% C.I)			*O* (95% C.I)		
Date	Lower	Mean	Upper	Lower	Mean	Upper
24/12/2013	0.163	0.197	0.231	0.797	1.665	2.533
9/01/2013	0.208	0.233	0.258	1.779	2.426	3.073

The linear relationship between chaff throughput and grain throughput was different than what was found for the HSD cage mill. It was found that the linear correlation intercepted at (0, 0) and, thus the ratio of chaff to grain remained constant over the

range of throughputs when testing the HSD behind a John Deere 9650. However, in Figure 4.40 the linear regression has a constant term which means that the grain to chaff ratio reduced with grain throughput, as shown in Figure 4.41. The chaff to grain ratio ranged from 0.22 to 0.53, compared to 0.24 to 0.36 found when testing the HSD. It was noticed that at low throughputs, hardly any straw exited the straw spreaders which suggests more of the straw was being processed by the Prototype 1 at low grain throughputs. At normal operational throughputs of 30-40 t/h of grain, the chaff to grain ratio was between 0.22 and 0.33. This chaff to grain ratio was in the range that was found with the HSD (0.215 to 0.388) and what was found by (Newman 2012) (0.223 to 0.375).

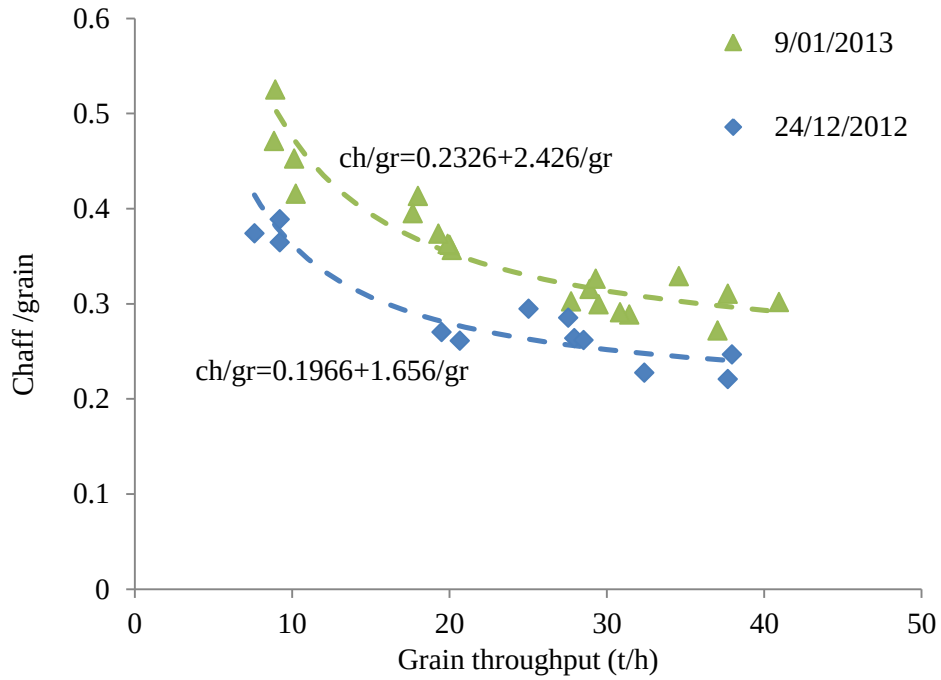

Figure 4.41: Ratio of chaff to grain for grain throughput

4.4.2.2 *Power for chaff throughput*

The power for each mill (left and right) was found to depend on the chaff throughput of material and the rotational speed of the mills, as shown in Figure 4.42. Linear regression was used for each of the speeds tested and showed a reasonable prediction of power from chaff throughput. The slope of the regression is specific power to process chaff and the intercept is the air pumping or no load power requirement. The specific processing requirement and no load power consumption both increased with speed. However, the increase in no load power consumption with speed had more effect on the

overall power consumption of the Prototype 1. Much of the variability in the power results for the Prototype 1 were due to variation in the rotational speed of the mills.

To account for variation in mill speed, non-linear regression was performed on the power and chaff throughput data in SPSS®, using:

$$P_{tot} = a\omega^3 + \tfrac{1}{2} b\dot{m}_{chaff}\omega^2 \qquad (4.10)$$

Where: a = no load power factor which takes into account heat generation and pressure rise (kg.m^2);
ω = rotational speed of the mill (rad/s);
$b = \sum_{j=1}^{k} r_j^2$, which is the factor for processing power, which is the sum of the square radial locations (r) of k impacts (m^2);
$\dot{m}_{ch}$ = mass flow of chaff (kg/s).

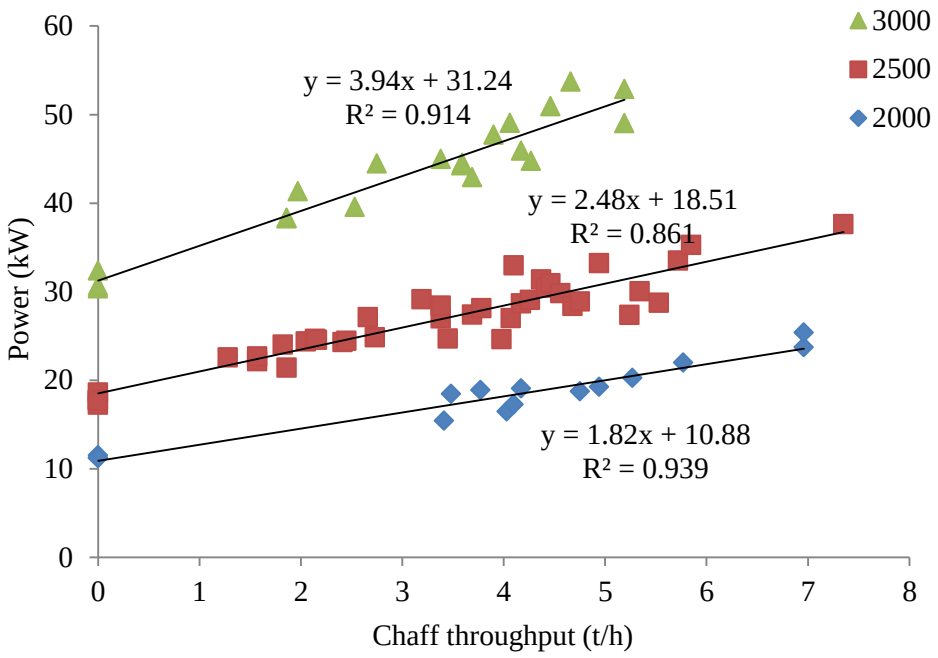

Figure 4.42: Calculated power consumption of the individual Prototype 1 mills for chaff throughput

The best fit parameters are shown in Table 4.8 and the actual power is plotted against predicted power in Figure 4.43. The simple power equation had a high Pearson's R-Squared coefficient of 0.945. Rotational speed and chaff throughput therefore can be used to accurately predict the power consumption of the mills when processing wheat chaff material. Furthermore, the relationship may be used backwards to estimate the chaff throughput based on the power consumption of the mills.

Table 4.8: Prototype 1 power model non-linear fit parameters

			95% confidence interval	
Fit parameter	Estimate	Standard error	Lower	Upper
a ($kg.m^2$)	0.000958	0.000027	0.000905	0.001011
b (m^2)	0.316881	0.015086	0.286814	0.346948

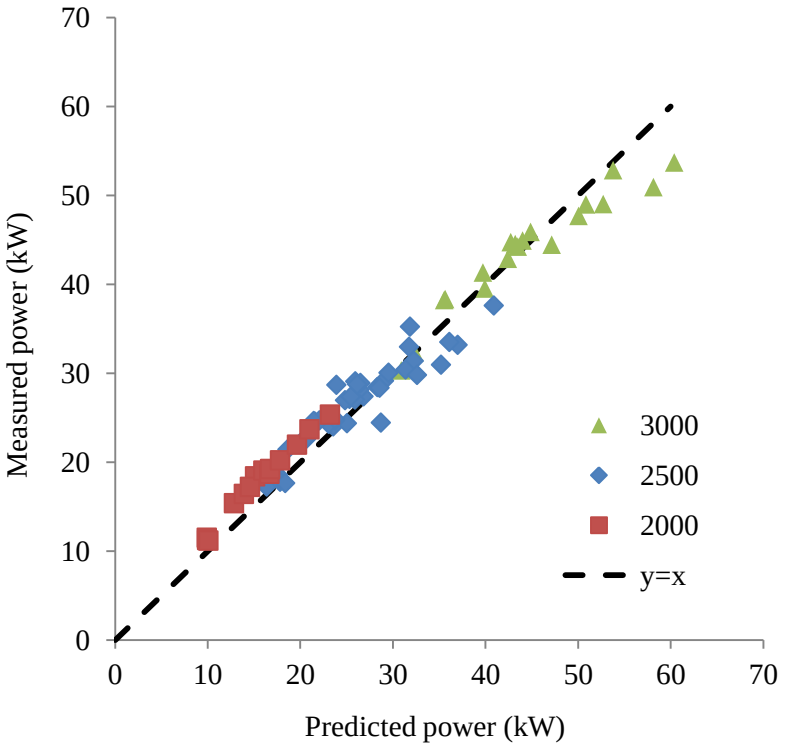

Figure 4.43:Predicted power against measured power for Prototype 1 - r^2 = 0.945

4.4.3 Prototype 2

4.4.3.1 *Power for chaff throughput*

The power of the Prototype 2 was determined by using set flow rates of chaff on a conveyor belt. The power consumption of the Prototype 2 was linear with chaff throughput, as shown in Figure 4.44. The process was more controlled than the field trials and, thus the power showed less variability than the field testing.

The rotational speed of the rotor reduced with increase in throughput and, thus was less than the set speed. To account for fluctuations in mill speed, non-linear regression was performed as was done with the Prototype 1. The model fit parameters were slightly different for the Prototype 2 compared to the Prototype 1 as shown in Table 4.9. The no load power parameter was higher than the Prototype 1 and the processing power was lower than the Prototype 1.

Table 4.9: Prototype 2 power model non-linear fit parameters

			95% confidence interval	
Fit parameter	Estimate	Standard error	Lower	Upper
a ($kg.m^2$)	0.001038	0.000015	0.001008	0.001069
b (m^2)	0.283499	0.009518	0.264340	0.302659

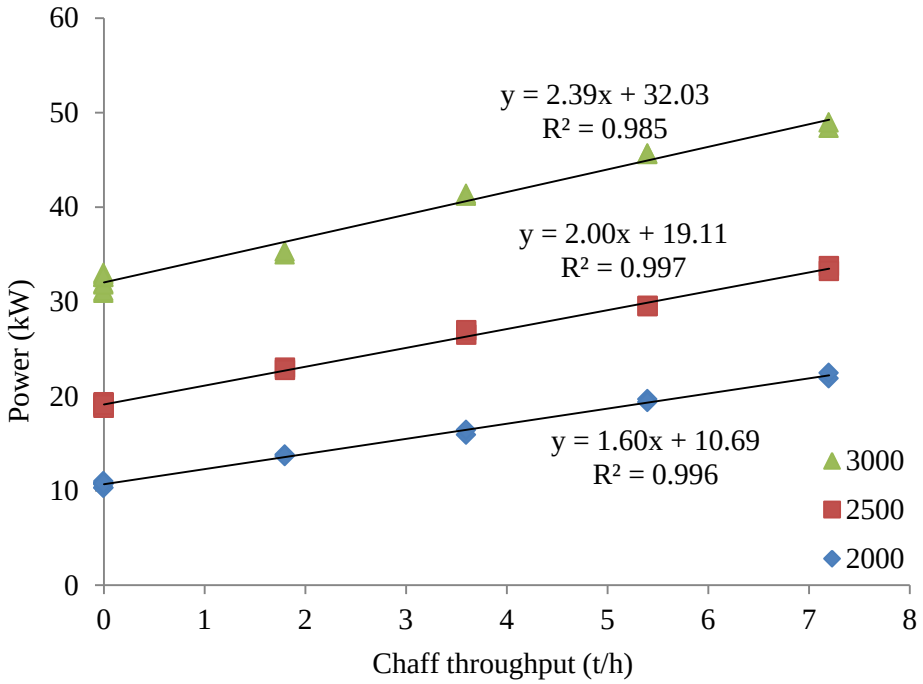

Figure 4.44: Calculated power consumption of the Prototype 2 for three set speeds

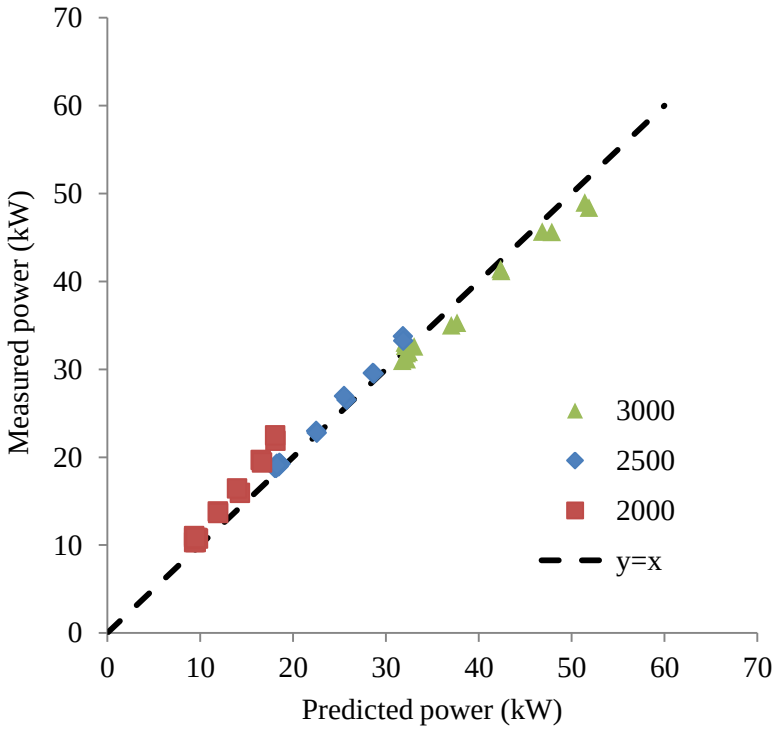

Figure 4.45:Predicted power against measured power for Prototype 2 - r^2 = 0.977

4.4.4 Comparison to modelling

4.4.4.1 *Specific processing energy comparison*

The specific processing power of the experimental results and simulation were compared using the fit parameter *B*, as shown in Table 4.10. The vector impact model was able to predict the specific processing power of the three mills within 2% of the measured values.

Table 4.10: Comparison of specific processing power fit parameter

Mill	b-Experimental	b – Vector impact model
HSD cage mill	1.8206	1.8436
Prototype 1	0.3168	0.3169
Prototype 2	0.2835	0.2781

4.4.4.2 *No load power comparison*

The no load fit parameter *A* from experimental testing and from of the CFD modelling method (Figure 4.31) were compared in Table 4.11. The CFD model under predicts the power consumption of the Prototype 1 by 32% and the Prototype 2 by 33%. The HSD cage mill CFD model did not incorporate an estimate of no load power. The CFD model was only a 2D approximation of the mill geometry. The built mills (3D) have a lot more friction surfaces which would add to the torque load not accounted for in the CFD simulation.

Table 4.11: Comparison of no load fit parameter

Mill	a-Experimental	a – CFD model
HSD cage mill	0.01047	-
Prototype 1	0.00096	0.000655
Prototype 2	0.00104	0.000698

4.4.5 Discussion

Wheat chaff is made up of the lemma and palea that encase the wheat seeds, the stem holding the seed (rachis) and the remainder is any straw that broken up small enough by the thresher or separator to end up on the cleaning shoe. The amount of straw broken up during threshing and separating determines the chaff to grain ratio. The chaff to grain ratio was found to depend on the harvester's rotor speed, location and harvest date. Increasing rotor speed causes a higher chaff to grain ratio because it increases the breakage of straw. The harvest dates for the HSD trials were normal for Pinnaroo and Maitland but was late for Minnipa. This meant that the crop at Minnipa was very mature and friable resulting in more straw breakage and a higher chaff to grain ratio. The harvest dates that the Prototype 1 was tested in were both late for the Mallala region. The crop was very dry and friable, which contributed to an increased of chaff to grain ratio.

The wheat chaff processing requirement was found to vary linearly with grain throughput for both the HSD cage mill and the Prototype 1. The maximum chaff throughput of the HSD cage mill tested was 9.3 t/h for 28.5 t/h of wheat. The Prototype 1 mills were tested up to 12.4 t/h of chaff at 41 t/h of grain. The high throughput testing of 1.5 kg/s per mill (10.8 t/h total) was 13% less than the maximum chaff throughput found in the field. Therefore, the seed devitalisation testing performed in this thesis was near commercial harvest chaff throughputs. The chaff processing of an impact mill would be highly variable. A desirable mill characteristic would be that it's ability to devitalise weed seeds was not significantly altered under varying chaff throughputs. The Prototype 2 is improved in this area over Prototype 1 with a significantly reduced effect of increased chaff throughput on seed devitalisation.

The no load power consumption was a significant proportion of the total power for all three mills. The no load power of the two prototype mills was proportional to the rotational speed cubed. The no load power consumption of the Prototype 2 was approximately 8% higher than the Prototype 1. This difference in no load power can be explained because the flat bar with sharp edges used for the rotor bars in the Prototype 2

have a higher drag coefficient than the SHS with rounded edges used in the Prototype 1. The Prototype 2 would generate more turbulence and, hence more energy loss to heat.

The specific processing energy was proportional to the rotational speed squared. The specific processing energy of the Prototype 2 was 10% less than the Prototype 1. The diameter of the Prototype 2 rotor was smaller (535 mm) than the Prototype 1 rotor (600 mm) and, thus the tip speed and impact energy was lower.

The power equation that was developed would be useful for predicting the power requirement of the mills under different operating conditions. Furthermore, the power equation could be used to backwards calculate the instantaneous chaff throughput of each of the mills if the power of the mills was being monitored. The instantaneous throughput could be a useful predictor of mill loading and may be displayed to prevent blockages. The estimate of chaff throughput could also be used to calculate the instantaneous seed devitalisation using the empirical machine function.

4.5 Power to devitalise seeds

The power to devitalise weed seeds was the most important performance criteria of a seed devitalisation mill. There was a trade-off between the power consumption of the milling systems and seed devitalisation. Increasing the rotational speed of the prototype mills was found to increase the seed devitalisation but significantly increase the power consumption of the mills. From the seed devitalisation testing it was found that the seed devitalisation of the two prototype mills could accurately be predicted using:

$$RSE = 1 - \exp\left[-F_{seed}\left(\frac{1}{2000} B\left(\omega - C\dot{m}_{chaff}\right)^2 - kE_{\min} \right) \right] \tag{4.11}$$

From the power and chaff throughput testing it was found that the power needed to process chaff material could be accurately predicted using:

$$P_{tot} = a\omega^3 + \tfrac{1}{2} b\, \dot{m}_{chaff}\omega^2 \tag{4.12}$$

Using the seed devitalisation and power relations at a throughput of 10.8 t/h, (1.5 kg/s per mill) the power requirement for a pair of Prototype 1 or 2 mills is shown in Figure 4.46. To achieve 90 % seed devitalisation took over 100 kW using either Prototype 1 or 2 mills. The HSD cage mill was not tested at the high mass flow of chaff and, thus

could not be compared for seed devitalisation. However, for comparison, the cage mill power operating at 1440 rpm at 10.8 t/h would be approximately 100 kW based on the linear regression in Figure 4.39.

The power requirement of the Prototype 2 had similar total power but with 8% higher no load power and 10% lower processing power. The Prototype 2 was had higher annual ryegrass seed devitalisation at 2000 rpm. However, at 2500 and 3000 rpm, there was no statistically significant difference in seed devitalisation between Prototype 1 or 2 (see confidence intervals in Section 4.3). Therefore, both mills were approximately equally as efficient operating at 1.5 kg/s of wheat chaff per mill in the speed range between 2500 and 3000 rpm. However, the non-linear regression model suggests that at further increased chaff mass flow the Prototype 2, would be more efficient than Prototype 1. The Prototype 2 also has added benefits of increased potential wear life and is less dangerous due to an outer static row. Therefore, the Prototype 2 is considered a superior mill for integration into a combine harvester.

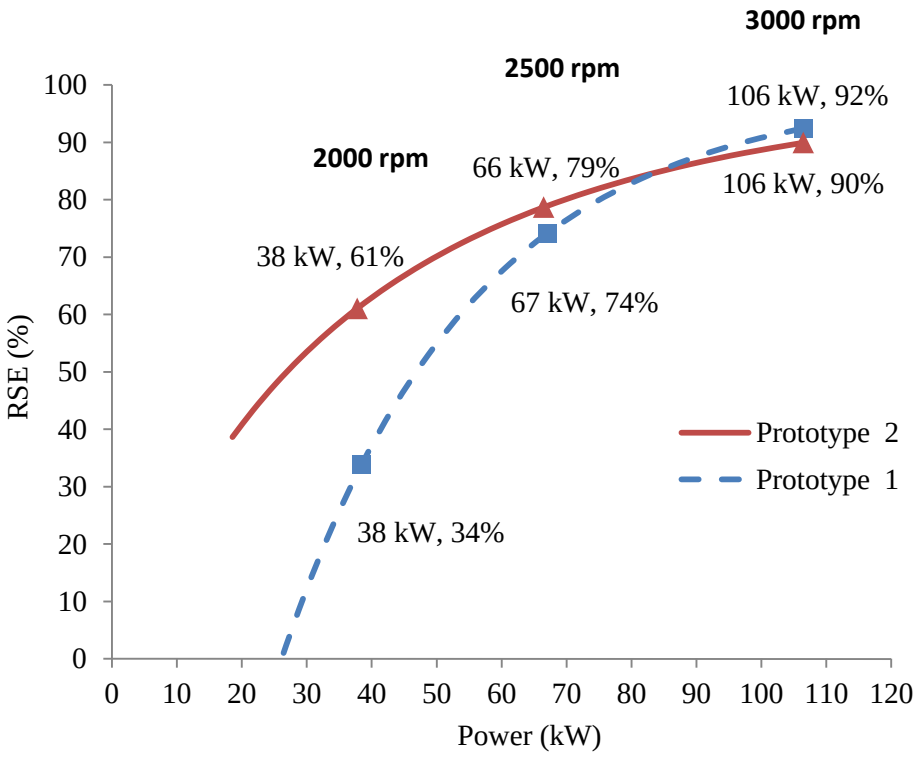

Figure 4.46: Comparison of seed devitalisation and power to process 3 kg/s (10.8 t/h) of chaff using a pair of mills

There is some potential for increased efficiency through further mill optimisation. This could be through reducing the no load power of the mill. However, this no load power is

used to generate the mills air flow, which is critical for maximising chaff mass flow capacity and minimising effect on harvester sieve. Processing the entire chaff fraction exiting a modern combine harvester sieve sufficiently to devitalise a high proportion of annual ryegrass seeds may always take a considerable amount of power. This power consumption will likely reduce the throughput capacity of a combine harvester. Therefore, there is a trade off between the power needed to process chaff material and level of devitalisation achieved. The ability to change the rotational speed of the mills enables operators to select the rotational speed based on their desired level of weed devitalisation. There are a number of factors that would determine an optimal speed setting such as: value of mechanical control on reducing weed seed bank; cost of extra fuel input; cost of machine depreciation due to extra hours harvested; cost of delayed harvest. The more hostile field soil conditions may also mean that a level below 90% seed devitalisation as measured in this thesis provides sufficient weed seed control in the field.

5 Conclusions and future work

5.1 Summary

In this thesis, a new method was developed to predict the devitalisation of weed seeds processed with an impact mill. The method was based on the devitalisation of seeds exposed to impact loads and the geometry and operating conditions of an impact mill; a material and a machine function. The developed method enables impact mills to be designed and setup to devitalise weed seeds based on the seed properties. Furthermore, this method enables impact mills to be designed to fit within the constraints of a chosen combine harvester to control weed seeds exiting a harvester in the chaff. The method was successfully applied to develop two new prototype mills to devitalise annual ryegrass (*Lolium rigidum*) seeds and fit within and be driven by CASE IH 9120 combine harvester. Therefore, the developed techniques and results in this thesis provide evidence in support of the thesis hypothesis.

The main conclusions addressing the objectives of this thesis are:

5.1.1 Material function

Exposing annual ryegrass seeds to single-sided impact from a rotational impact tester caused a proportion of seeds to not emerge when planted in soil bins; i.e. they were devitalised. Annual ryegrass seed devitalisation reduced with increasing moisture content. A linear regression showed that every 1% increase in moisture content reduced seed devitalisation by approximately 2.2%. Using single-sided for mechanical control of weed seeds will require increased impact energy (higher impact speeds and/or number of impacts) at higher moisture contents. Seed devitalisation increased with increasing impact speed and number of impacts. Up to 70% of seeds were devitalised for one impact at an impact speed 90 m/s. Above 90% devitalisation was achieved with 4 impacts at 70 m/s and 8 impacts at 50 m/s. Thus, multiple single-sided impacts was an effective means of devitalising annual ryegrass seeds.

The order in which successive impacts occur was not found to have any significant effect on the seed devitalisation. A seed is equally likely to be devitalised if it is impacted with the same set of differing impact speeds in increasing or decreasing impact speed order.

The devitalisation of annual ryegrass seed (11.3% w.t.) subjected to a range of impact sequences was able to be approximated with a mastercurve involving total specific impact energy (E_{impact}), the number of impacts (k), and two material parameters: threshold specific energy for seed fracture that causes seed devitalisation (E_{min} = 0.3991 kJ/kg) and resistance of the seed to fracture that causes seed devitalisation (F_{seed} = 0.3268 kJ/kg). Seed devitalisation depends primarily on the impact energy imparted on a seed above the threshold specific energy, which equates to an impact speed of 28 m/s. Impact speeds close to the 28 m/s require a large number of impacts to devitalise seeds and are energy inefficient. The mastercurve provided a material function to predict devitalisation of annual ryegrass seeds subjected to a sequence of impacts and, thus achieved the first objective of this thesis.

5.1.2 Machine function

Two methods were developed to determine the number of impacts and impact speeds that a seed would be exposed to in an impact mill based on the mills geometry and operating conditions: a theoretical vector impact model; and a computational fluid dynamics (CFD) impact model.

The theoretical vector impact model assumed that one impact occurred on each concentric row of impact elements. The number of impacts was predicted using the number of concentric rows of impact bars resulting in 6 impacts with the HSD cage mill, 4 impacts with Prototype 1, and 5 impacts with Prototype 2. Impacts trajectories and normal impact velocity were calculated using the angle of the impact bars, the tip speed of the rotating bars and the coefficient of restitution. The normal impact speeds estimated with the vector model were found to increase linearly with rotational speed for the three mills. From the impact velocities, the vector impact model was able to make a prediction of the processing power.

The CFD particle tracing method used a 2-dimensional CFD model of the impact mill to solve the single phase flow field. 1000 spherical particles with the equivalent

aerodynamic properties as annual ryegrass seeds were inserted at the entrance of the CFD model. The CFD model took into account the randomness of the particle motion as well as the aerodynamic acceleration of particles. The CFD model prediction was more realistic than the vector model; it showed that based on the simplified geometry of the mills, the particle impacts are stochastic, there is a distribution of impact speeds and number of impacts. The CFD impact model showed that the HSD cage mill would provide a wide distribution of effective impact energy to particles resulting in over processing and under processing of some particles. To reduce over and under processing, the two prototype mills were designed on the principal of one impact on each row of rotating and static impact bars.

5.1.3 Combining material and machine function

The material function mastercurve was combined with the machine function from the vector and CFD impact model to predict seed devitalisation. Despite the differences between the vector impact model and CFD impact model, they both provided an almost equivalent prediction of seed devitalisation for the three mills. The predicted seed devitalisation was used to develop two new prototype mill designs that were able to fit within the size, power and weight constraints of a modern combine harvester. The prototype mills were based on concentric rotor stator impact bars to make the mills easy to mount and drive on a harvester. Prototype 1 had inner distribution paddles, then two concentric rows of stator bars and two concentric rows of rotor bars. The Prototype 2 had a further set of stator bars.

The machine function techniques developed in this thesis could be similarly used to design seed destruction mills to suit the constraints of other harvesters or to target different weed species.

5.1.4 Model validation and prototype evaluation

The existing HSD cage mill and the two new prototype mills were experimentally evaluated by processing wheat chaff laced with annual ryegrass seeds. The processed material was mixed with soil and the emergence of seedlings was counted.

The HSD cage mill was found devitalise more than 90% of annual ryegrass seeds at the four rotational speeds tested (900, 1100, 1300 and 1440 rpm). Speed was not statistically significant. The soil bin testing technique used to evaluate the HSD cage

mill was able to produce similar results to previous published research. This technique was also far simpler and quicker to implement than the previously published research method. The vector and CFD impact model prediction of seed devitalisation for the HSD cage mill was within 10% of the measured values, which validated its use for development of prototype mills.

Prototype 1 was constructed and evaluated based on the developed concept design in the machine function; it was able to achieve greater than 90% seed devitalisation at a chaff throughput of 0.5 kg/s. The vector and CFD impact model prediction of seed devitalisation very accurately predicted the response of seed devitalisation at this throughput ($r^2 = 0.948$). Seed devitalisation reduced substantially at 1.5 kg/s chaff throughput, especially at lower rotational speeds. The effect of increasing chaff throughput was to increase the solids loading in the mill and thus increase the likelihood of inefficient particle to particle impacts. As the vector and CFD impact models did not take into account particle to particle impacts, the model predictions at 1.5 kg/s was poor.

To alleviate the effect of particle to particle impacts on seed devitalisation and the wasted kinetic energy of particles, the Prototype 2 was designed. The Prototype 2 had an extra stator row to use the kinetic energy of particles. A prediction of solids loading was developed using the CFD impact model to predict the likelihood of inefficient particle to particle impacts. Through iterations CFD impact models, the Prototype 2 was developed to have a predicted solids loading of approximately half of the Prototype 1. The resultant design of the Prototype 2 was able to process both throughputs of 0.5 kg/s and 1.5 kg/s with minimal difference in seed devitalisation and achieve approximately 90% seed devitalisation at 3000 rpm

The experimental mill seed devitalisation testing validated the modelling method as an important predictor of mill performance and as a basis for design optimisation. The modelling enabled an initial design to be developed and then be redesigned based on the limitations found in testing.

5.1.5 Chaff processing requirement

The chaff processing requirement of the HSD cage mill and the Prototype 1 was determined during field testing. The chaff was collected in semi permeable bags and weighed. The HSD cage mill processed up to 9.3 t/h of chaff when harvesting 28.5 t/h

of wheat. The wheat chaff processing requirement of the HSD cage mill was proportional to the grain throughput. The chaff to grain ratio ranged between 0.239 and 0.356. Differences in the harvest conditions at each location were shown to affect the chaff to grain ratio. The chaff to grain ratio was found to increase with rotor speed, which highlighted the importance of the harvester setup on the amount of chaff produced.

A pair of the Prototype 1 mills were integrated into to a large capacity combine harvester and tested in the field in wheat in December 2012. The two mills processed up to 12.4 t/h (≈ 1.7 kg/s per mill) at 41 t/h of wheat. Importantly, the two Prototype 1 mills were able to handle the large mass flow of chaff material without blockage. The chaff to grain ratio reduced with increasing grain throughput when testing the Prototype 1.

The chaff processing requirement of an impact mill for devitalising weed seeds attached to a large capacity combine harvester is very high. The ability of the two prototype mills to handle this material was a significant outcome of the design. The data collected supports testing impact mills for seed devitalisation at throughputs relevant to field throughputs as done in this thesis but that has not been done previously.

5.1.6 Power consumption

The power consumption of the HSD cage mill was experimentally determined in field trials in wheat at the set operational speed of 1440 rpm. The HSD cage mill power consumption varied linearly with the wheat chaff throughput in the range of 2–9 t/h. The HSD cage mill was found to have a significant power requirement when running without chaff of 35.9 ± 4.51 kW (95% C.L). The HSD cage mill was found to have a specific energy consumption of 5.75 ± 0.82 kW.h/t (95% C.L) when processing wheat chaff.

The power consumption of the Prototype 1 was experimentally determined in field trails in wheat and the power consumption of Prototype 2 was determined in the lab using wheat chaff. Three approximate operational speeds were used; 2000, 2500 and 3000 rpm. The power needed to process chaff material and the no load power were found to increase with mill speed. The no load power was found to increase with rotational speed cubed. The processing power was found to increase with the square of the rotational

speed and linearly with chaff throughput. The two mills had significantly different designs and diameter but still had very similar power relationships. The no load power constant (a) was 0.000958 and 0.001038 kg.m^2 for the Prototype 1 and 2, respectively. The chaff processing constant (b) was 0.317 and 0.283 m^2 for the Prototype 1 and 2, respectively. Using this prediction at an operational speed of 3000 rpm, the no load power consumption was 29.7 and 32.1 kW and the specific energy consumption was 4.35 kW.h/t and 3.87 kW.h/t for the Prototype 1 and 2, respectively. There were two Prototype 1 mills used on the harvester and, hence the no load power is double. The no load power of using a pair of Prototype 1 mills was higher at 3000 rpm than the single HSD cage mill. The power draw of the prototype mills on the harvester notably reduced the capacity of the CASE IH 9120.

The no load power estimate from the CFD model was a third less than the measured no load power consumption of the mills. This difference was probably due to the CFD model being only 2D when the 3D mill has a lot more surfaces that cause air movement and friction. However, the vector impact model was able to predict the specific processing energy requirement of the three mills within 2% of that measured.

5.1.7 Power to devitalise seeds

An analysis of the power needed to devitalise seeds was used to assess the performance of the two prototype mills. There was a clear trade off between the power needed to operate the mills and the level of devitalisation achieved. To achieve 90% seed devitalisation at a commercial harvest rate of 10.8 t/h of chaff material would require over 100 kW using either the Prototype 1 or Prototype 2 mills. The HSD cage mill at 1440 rpm also used approximately 100 kW at this throughput but the seed devitalisation was not evaluated. The power requirement of the prototype mills drops substantially if a lower level of seed devitalisation was acceptable and the mills could be run slower.

A significant component of the power consumption was the no load power which may be able to be reduced through further mill optimisation. However, the no load power of the prototype mills is not all wasted energy; some of it is used to move the air through the mills and increases the chaff mass flow capacity of the mills while reducing the restriction of the harvester sieve.

5.2 Original contributions of this thesis

1) A mastercurve was generated to predict the annual ryegrass (*Lolium rigidum*) seed devitalisation for a given impact speed sequences based on two seed properties: The threshold specific impact energy for seed fracture that causes seed devitalisation E_{min}; and resistance of the seed to fracture that results in seed devitalisation F_{seed}.

2) Two techniques were developed to estimate the impact speed sequence occurring within an impact mill based on its geometry and operating speed; a theoretical impact vector technique and a computational fluid dynamics (CFD) particle tracing technique.

3) A method to predict the performance an impact mill for weed seed destruction based on the mastercurve and impact sequence. The method was validated through the development and testing of two new prototype mills and the existing HSD cage mill.

4) For the first time, impact mill technology has been evaluated for seed destruction at chaff throughputs relevant to high capacity combine harvester. This testing quantified chaff throughput and more specifically solids loading as important parameters for predicting devitalisation of seeds processed by an impact mill. Where solids loading was higher in the Prototype 1, the emergence was not as significantly reduced compared to Prototype 2.

5) The wheat chaff processing requirement was established to be between 0.22 and 0.35 tonnes of chaff per tonne of grain processed. Chaff loads of up to 12.4 tonnes per hour were seen in the field.

6) The chaff processing and no load power requirement of the HSD cage mill at 1440 rpm was measured to be 5.75 kW.h/tonne and 36 kW respectively.

7) The chaff processing and no load power requirement of the two new prototype mills was established. A function was developed that could accurately predict the power consumption of the mill based on the rotational speed of the mill and the chaff throughput.

8) The processing power of the three mills was estimated using the vector impact model to within 2% accuracy.

9) A provisional patent has been put in place

5.3 Limitations of study and future work

5.3.1 Material function

This study was limited to annual ryegrass (*Lolium rigidum*) seeds. There are many other problematic weed species in Australia and around the world that may be targeted at harvest time (see Section 2.2). Each species will have a different emergence response when seeds are subject impact loads. This response is related to the seed's strength, fracture toughness, mass, terminal velocity and natural defences. Therefore, each target weed species will require a different amount of impact energy to provide effective control. Impact testing other target weed seeds could provide the seed properties E_{min} and F_{seed}. These seed properties can be used in the empirical machine function to predict the effectiveness of the current mill technology developed and at what speeds. If different mill technology is needed mill designs could be modified and modelled as in this thesis.

Seed moisture content was found to reduce seed devitalisation in this thesis. With a larger experimental set, the effect of moisture content could be more accurately characterised through modifying E_{min} and F_{seed} and thus effect the effectiveness of the prototype mills could be predicted.

5.3.2 Machine function

The vector and CFD impact models developed in this thesis were able to provide estimates of seed devitalisation that were validated with experimental testing. However, this did not validate that the modelling techniques were predicting the physical phenomena occurring within the mill. The physical phenomena occurring within the mill could be significantly more complex than the physics included in the 2D vector and CFD impact modelling techniques used. The CFD modelling technique made some significant simplifications of the process. The CFD model was 2D and as such did not accurately predict the no load power consumption of the mills. There is a need for a 3 dimensional CFD model to more accurately predicting the no load power consumption

of a mill. The CFD model did not have momentum transfer from the particles (discrete phase) to the air (continuous phase) and this could be included for improved accuracy. Furthermore, the particle to particle impacts were not included. At high chaff throughputs, the model prediction of the Prototype 1 was different to the testing results. In the literature review it was found that recently there has been some modelling work that combines discrete element method (DEM) and CFD. A CFD-DEM model could account for both particle to particle interaction and two way momentum exchange between the particle phase and carrier phase. Further modelling work may enable better predictions under high solids loading of a mill.

5.3.3 Prototype performance

This study highlighted that to devitalise a high proportion of annual ryegrass seeds considerable power. However, the germination conditions in the soil bins were more hospitable than field conditions commonly are. There was controlled light, temperature, humidity and the soil type was idealised. In the field, the impacted seeds may be more susceptible and, hence emergence could be further reduced. If the emergence of ryegrass is further reduced in the field, the trade off between power consumption and reducing emergence may make the optimum operating speed lower.

As with any weed control method, there is the potential for weeds to evolve resistance to impact milling the chaff exiting a combine harvester. Weeds could evolve to grow lower or shed their seeds early so that their seeds do not end up in the harvester. Weeds could evolve to become more difficult to thresh so that their seeds exit in the straw rather than in the chaff. Weeds could evolve to have tougher seeds that are resistant to mechanical impact. The probability that weeds could become resistant to impact milling of chaff should be carefully assessed. Impact milling chaff would not be an all in one solution to weed control and sustainable weed control will still require diversity of other control measures, including herbicides.

5.3.4 Power and chaff processing

The power and chaff throughput testing was only performed using wheat chaff in relatively dry conditions. Under different crop types, and moisture contents, it is expected that the power consumption would be different and should be investigated to help improve machine design.

5.4 Project outcomes

The Prototype 1 and 2 mills were developed specifically to fit within the size constraints of a CASE 9120 combine harvester. Thus, integration was simple and required minimal modification of the harvester. Both Prototype 1 and Prototype 2 were able to achieve greater than 90 % annual ryegrass seed devitalisation at 0.5 kg/s of wheat chaff and were able to achieve above 85% at 1.5 kg/s. To achieve this required operating at around 3000 rpm, which required slightly more power than the project goal of 100 kW. Thus, the capacity of the harvester would be reduced when trying to achieve 90% seed devitalisation. There may be an opportunity to reduce this power consumption through further mill optimisation. However, if the concept of mechanical control of weed seeds at harvest time becomes popular, manufacturers of harvesters may provide extra power to allow for their attachment.

The two mills have shown to have high air and chaff material handling capacities suitable for large capacity combine harvesters. The air flow capacity of Prototype 1 was 1.6 m^3/s and was 1.3 m^3/s for Prototype 2 per mill at 3000 rpm. The simple inlet chutes that split the chaff material into a pair of Prototype 1 mills were not found to significantly alter or restrict the motion of chaff material. A pair of the Prototype 1 mills attached to a CASE 9120 combine harvester was able to handle up to 12.4 t/h of chaff. This harvest rate equated to a wheat grain throughput of 40 t/h.

The power and seed devitalisation of the Prototype 1 and Prototype 2 mills was very similar. However, the Prototype 2 is expected to devitalise more seeds at further increased chaff throughputs. Furthermore, the Prototype 2 has higher potential wear life because of its thicker bars; it is also less dangerous because material exits at a lower velocity after impacting the last static row.

The two prototype mills are a significant advancement on the HSD technology. The integration of mechanical seed devitalisation into a combine harvester has a number of potential benefits including: no extra engine to operate and maintain, reduced capital and operating costs, reduced mechanical complexity, reduced load on harvester drive train, improved manoeuvrability and increased operator safety.

5.5 Final remark

This thesis has adopted cross-disciplinary research in comminution (particle size reduction) science for the application of devitalising weed seeds using an impact mill. The models generated in this thesis will be used to help improve impact milling technology for devitalising weed seeds. The milling technology generated in this thesis have commercial potential (patent pending) as a retro-fit to help reduce weed burdens and to alleviate the threat of herbicide resistance in global cropping systems.

6 References

Ahrens, WH, Cox, DJ & Budhwar, G 1990, 'Use of the arcsine and square root transformations for subjectively determined percentage data', *Weed Science,* vol. 38, no. 4, pp. 452-458.

Akiyama, S, Kozawa, K & Yoshida, H 2004, 'Effect of blade angle on crystallinity change in a mechanical impact mill', *Journal of Chemical Engineering of Japan,* vol. 37, no. 10, pp. 1207-1214.

Anagnostopoulos, J & Bergeles, G 1997, 'Numerical investigation of the grinding process in a beater wheel mill with classifier', *Journal of Engineering for Gas Turbines and Power,* vol. 119, no. 3, pp. 723-733.

ASABE-Standards 1998, *ASAE D497.4 JAN98: Agricultural machinery management data*, American Society of Agricultural and Biological Engineers, St. Joseph, MI.

ASABE-Standards 2006, *ASAE S352.2 FEB03: Moisture measurement - unground grain and seeds*, American Society of Agricultural and Biological Engineers, St. Joseph, MI.

Austin, LG 2002, 'A treatment of impact breakage of particles', *Powder technology,* vol. 126, no. 1, pp. 85-90.

Austin, LG 2004, 'A preliminary simulation model for fine grinding in high speed hammer mills', *Powder technology,* vol. 143, pp. 240-252.

Ballaré, C, Scopel, AL, Ghersa, C & Sanchez, R 1987, 'The demography of *Datura ferox* (L.) in soybean crops', *Weed Research,* vol. 27, no. 2, pp. 91-102.

Balsari, P, Airoldi, G & Finassi, A 1994, 'Development of a device able to separate and reduce the degree of germination of weed seeds harvested by a combine', paper presented at the International Confererence on Agricultural Engineering, Milano, Italy, 29 Aug - 1 Sep 1994.

Barker, AV & Craker, LE 1991, 'Inhibition of Weed Seed Germination by Microwaves', *Agron. J.,* vol. 83, no. 2, pp. 302-305.

Bartsch, JA, Haugh, GC, Athow, KL & Peart, RM 1986, 'Impact damage to soybean seed', *Transactions of the American Society of Agricultural Engineers,* vol. 29, no. 2, pp. 582-586.

Baruah, DC & Panesar, BS 2005, 'Energy requirement model for a combine harvester, part I: development of component models', *Biosystems Engineering,* vol. 90, no. 1, pp. 9-25.

Beer, FP, Johnston, ER & Clausen, W 2004, *Vector mechanics for engineers: dynamics,* Seventh edn, McGraw-Hill, Inc, New York.

Bilanski, W & Lal, R 1965, 'Behavior of threshed materials in a vertical wind tunnel', *Transactions of the ASAE,* vol. 8, no. 3, pp. 411-413.

Bilanski, W 1966, 'Damage resistance of seed grains', *Transactions of the ASAE,* vol. 9, no. 3, pp. 360-363.

Bitra, VSP, Womac, AR, Chevanan, N, Miu, PI, Igathinathane, C, Sokhansanj, S & Smith, DR 2009, 'Direct mechanical energy measures of hammer mill comminution of switchgrass, wheat straw, and corn stover and analysis of their particle size distributions', *Powder technology.*

Blanco-Moreno, JM, Chamorro, L, Masalles, RM, Recasens, J & Sans, FX 2004, 'Spatial distribution of *Lolium rigidum* seedlings following seed dispersal by combine harvesters', *Weed Research,* vol. 44, no. 5, pp. 375-387.

Brosh, T, Kalman, H & Levy, A 2011, 'DEM simulation of particle attrition in dilute-phase pneumatic conveying', *Granular Matter,* vol. 13, no. 2, pp. 175-181.

Busi, R & Powles, SB 2013, 'Cross-resistance to prosulfocarb and triallate in pyroxasulfone-resistant Loliumrigidum', *Pest Management Science,* vol. 69, no. 12, pp. 1379-1384.

CASE IH Agriculture 2011, *AXIAL-FLOW,* CNH UK Ltd., Cranes Farm Road, Basildon, Essex SS14 3AD.

Cash, S, Zamora, D & Lenssen, A 1998, 'Viability of weed seeds in feed pellet processing', *Journal of Range Management,* vol. 51, no. 2, pp. 181-185.

Chancellor, W 1960, 'Influence of particle movement on energy losses in an impeller blower', *Agricultural Engineering,* vol. 41, no. 3, pp. 92-94.

Chatzilamprou, IG, Youds, MW, Tierney, MJ & Armstrong, B 2006, 'Numerical investigation of a developmental pneumatically fed impact pulveriser', *Applied Mathematical Modelling*, vol. 30, no. 11, pp. 1180-1195.

Chauhan, BS, Gill, G & Preston, C 2006, 'Influence of environmental factors on seed germination and seedling emergence of rigid ryegrass (*Lolium rigidum*)', *Weed Science*, vol. 54, no. 6, pp. 1004-1012.

Clift, R & Gauvin, WH 1970, 'The motion of particles in turbulent gas streams', *Proc. Chemeca '70*, pp. 14-28.

Cooke, J & Dickens, J 1971, 'A centrifugal gun for impaction testing of seeds', *Trans. ASAE*, vol. 14, no. 1, pp. 147-155.

Dalling, JW, Davis, AS, Schutte, BJ & Elizabeth Arnold, A 2011, 'Seed survival in soil: interacting effects of predation, dormancy and the soil microbial community', *Journal of Ecology*, vol. 99, no. 1, pp. 89-95.

Dassault Systèmes SolidWorks Corp. 2011a, *SolidWorks Flow Simulation 2011 Solving Engineering Tasks*, Dassault Systèmes,

Dassault Systèmes SolidWorks Corp. 2011b, *SolidWorks Flow Simulation 2011 Technical Reference*, Dassault Systèmes,

Davis, AS 2008, 'Weed seed pools concurrent with corn and soybean harvest in Illinois', *Weed Science*, vol. 56, no. 4, pp. 503-508.

Davis, AS, Schutte, BJ, Iannuzzi, J & Renner, KA 2008, 'Chemical and physical defense of weed seeds in relation to soil seedbank persistence', *Weed Science*, vol. 56, no. 5, pp. 676-684.

Doddannavar, R, Barnard, A & Ganesh, J 2005, *Practical hydraulic systems: operation and troubleshooting for engineers and technicians*, Elsevier, Burlington , VT , USA .

Drögemeier, R & Leschonski, K 1996, 'Ultra fine grinding in a two stage rotor impact mill', *International Journal of Mineral Processing*, vol. 44-45, pp. 485-495.

Feldman, M & Reed, W 1974, 'Distribution of wild oat seeds during cereal crop swathing and combining', *Annual meeting of the Canadian Society of Agricultural Engineering*, Ste. Foy, QC,, pp. 1-10.

Forcella, F, Peterson, DH & Barbour, JC 1996, 'Timing and measurement of weed seed shed in corn (Zea mays)', *Weed technology,* vol. 10, pp. 535-543.

Frączek, J & Ślipek, Z 1998, 'Influence of moisture content and number of mechanical impacts, upon the energy and sprouting capacity of wheat grains', *International Agrophysics,* vol. 12, no. 2, pp. 97-101.

Friedrich, T, Derpsch, R & Kassam, A 2012, 'Overview of the global spread of conservation agriculture', *Field Actions Science Reports,* vol. Special Issue 6.

Ganser, GH 1993, 'A rational approach to drag prediction of spherical and nonspherical particles', *Powder technology,* vol. 77, no. 2, pp. 143-152.

Gdoutos, EE 2005, *Solid mechanics and its applications: fracture mechanics: an introduction*, 2nd edn, Springer, Norwell, MA, USA.

Goggin, DE, Powles, SB & Steadman, KJ 2012, 'Understanding *Lolium rigidum* seeds: the key to managing a problem weed?', *Agronomy,* vol. 2, no. 3, pp. 222-239.

Goldsmith, W 2001, *Impact : the theory and physical behaviour of colliding solids*, Dover Publications, Mineola, N.Y.

Gorial, BY & O'Callaghan, JR 1990, 'Aerodynamic properties of grain/straw materials', *Journal of Agricultural Engineering Research,* vol. 46, pp. 275-290.

Harrington, R 2009, *Weed and volunteer crop seed destruction*, US Patent 8152610 B2.

Hauhouot-O'Hara, M, Solie, JB, Whitney, RW, Peeper, TF & Brusewitz, GH 1999, 'Effect of hammer mill and roller mill variables on cheat (Bromus secalinus L.) seed germination', *Applied Engineering in Agriculture,* vol. 15, no. 2, pp. 139-145.

Hauhouot-O'Hara, M, Criner, B, Brusewitz, G & Solie, J 2000, 'Selected Physical Characteristics and Aerodynamic Properties of Cheat Seed for Separation From Wheat', *Agricultural Engineering International: the CIGR Journal of Scientific Research and Development,* vol. 2.

Hauhouot, M 1998, 'Mechanically devitalizing cheat (Bromus secalinus L.) seed to reduce germination', PhD. Thesis, Oklahoma State University.

Hauhouot, M, Solie, JB, Brusewitz, GH & Peeper, TF 1998, 'Roller and hammer milling cheat (Bromus secalinus L.) to reduce germination as an alternative method for weed control', *Transactions of the ASAE,* vol. 41, no. 4, pp. 973-980.

Heap, I 2013, *International survey of herbicide resistant weeds*, viewed August 19, 2013, <weedscience.org>.

Holding, D, Stewart, V & Sutherland, S 2006, 'Tactic 4.1 Weed seed collection at harvest', in McGillion, T & Storrie, A (eds), *Integrated weed management in Australian cropping systems - A training resource for farm advisors*, CRC for Australian Weed Management, Adelaide, South Australia.

ISTA 2009, *International Rules for Seed Testing*, International Seed Testing Association,

Jaeschke, R 1994, 'Development of RYTEC System', paper presented at the National herbicide resistance workshop, Adelaide, 24-25 Feb. 1994.

Jayasundara, CT, Yang, RY, Guo, BY, Yu, AB, Govender, I, Mainza, A, Westhuizen, Avd & Rubenstein, J 2011, 'CFD–DEM modelling of particle flow in IsaMills – Comparison between simulations and PEPT measurements', *Minerals Engineering*, vol. 24, no. 3–4, pp. 181-187.

Jindal, VK & Mohsenin, NN 1978, 'Dynamic hardness determination of corn kernels from impact tests', *Journal of Agricultural Engineering Research*, vol. 23, no. 1, pp. 77-84.

Jorgensen, R 1983, *Fan engineering: an engineer's handbook on fans and their applications*, 8th ed. edn, Buffalo Forge, Buffalo, N.Y.

Kahrs, J 1994, 'Aerodynamic properties of weed seeds', *International Agrophysics*, vol. 8, no. 2, pp. 259-262.

Kalman, H, Rodnianski, V & Haim, M 2009, 'A new method to implement comminution functions into DEM simulation of a size reduction system due to particle-wall collisions', *Granular Matter*, vol. 11, no. 4, pp. 253-266.

Kassam, A, Friedrich, T, Shaxson, F & Pretty, J 2009, 'The spread of conservation agriculture: justification, sustainability and uptake', *International Journal of Agricultural Sustainability*, vol. 7, no. 4, pp. 292-320.

Khazaei, J, Shahbazi, F, Massah, J, Nikravesh, M & Kianmehr, MH 2008, 'Evaluation and modeling of physical and physiological damage to wheat seeds under successive impact loadings: mathematical and neural networks modeling', *Crop Science*, vol. 48, no. 4, pp. 1532-1544.

Khoshtaghaza, M & Mehdizadeh, R 2006, 'Aerodynamic properties of wheat kernel and straw materials', *Agricultural Engineering International: the CIGR Ejournal,* vol. VIII.

Kimber, R 1973a, 'Phytotoxicity from plant residues. III. The relative effect of toxins and nitrogen immobilization on the germination and growth of wheat', *Plant and Soil,* vol. 38, pp. 543-555.

Kimber, R 1973b, 'Phytotoxicity from plant residues. II The effect of time of rotting of straw from some grasses and legumes on growth of wheat seedlings', *Plant and Soil,* vol. 38, pp. 347-361.

Kirk, I & McLeod, H 1967, 'Cotton seed rupture from static energy and impact velocity', *Transaction of the ASAE,* vol. 10, no. 2, pp. 217–219.

Kutzbach, HD 2000, 'Trends in Power and Machinery', *Journal of Agricultural Engineering Research,* vol. 76, no. 3, pp. 237-247.

Leonhardt, J, Zoerb, G & Hamann, D 1961, 'Investigations of factors affecting impact damage to sorghum seeds', *ASAE Paper No 61-125*.

Li, X, Wang, S, Duan, L, Hao, J, Li, C, Chen, Y & Yang, L 2007, 'Particulate and Trace Gas Emissions from Open Burning of Wheat Straw and Corn Stover in China', *Environmental Science & Technology,* vol. 41, no. 17, pp. 6052-6058.

Liu, Z & Hill, DL 2000, 'Issues surrounding multiple frames of reference models for turbo compressor applications', paper presented at the 15th International Compressor Engineering Conference at Purdue University, West Lafayette, IN, 2000.

Loth, E 2008, 'Drag of non-spherical solid particles of regular and irregular shape', *Powder technology,* vol. 182, no. 3, pp. 342-353.

Lyon, D & Rush, I 1993, 'Processing reduces seed germination and emergence of jointed goatgrass', *Journal of production agriculture,* vol. 6, no. 3, pp. 395-398.

Mandø, M, Yin, C, Sørensen, H & Rosendahl, L 2007, 'On the modelling of motion of non-spherical particles in two-phase flow', paper presented at the 6th International Conference on Multiphase Flow, Leipzig, Germany, 9 - 13 July.

Matthews, JM, Llewellyn, R, Jaeschke, R & Powles, SB 1996, 'Catching weed seeds at harvest: a method to reduce annual weed populations', paper presented at the 8th

Australian Agronomy Conference, University of Southern Queensland, Toowoomba, 30 Jan. - 2 Feb.

Matthews, JM, Harris, P, Miegel, D, Cloutier, D, Ascard, J, Netland, J, Cottis, T & Brandsaeter, L 2004, 'A device to kill weed seeds captured during crop harvesting', paper presented at the European weed research society. Proceedings of the 6th EWRS workshop on physical and cultural weed control, Lillehammer, Norway, 8-10 March 2004.

Mead, R, Hasted, AM & Curnow, RN 1993, *Statistical methods in agriculture and experimental biology*, Second edn, Chapman & Hall, New York :.

Mitchell, F & Rounthwaite, T 1964, 'Resistance of two varieties of wheat to mechanical damage by impact', *Journal of Agricultural Engineering Research*, vol. 9, no. 4, pp. 303-306.

Moreno, R, Ghadiri, M & Antony, SJ 2003, 'Effect of the impact angle on the breakage of agglomerates: a numerical study using DEM', *Powder technology*, vol. 130, no. 1-3, pp. 132-137.

Munson, BR, Young, DF, Okiishi, TH & Shao, W 2006, *Fundamentals of fluid mechanics*, John Wiley & Sons, Inc.,

Nakach, M, Authelin, J-R, Chamayou, A & Dodds, J 2004, 'Comparison of various milling technologies for grinding pharmaceutical powders', *International Journal of Mineral Processing*, vol. 74, pp. S173-S181.

Narayanan, S 1986, 'Single particle breakage tests: A review of principles and applications to commination modeling', *Bulletin and Proceedings of the Australasian Institute of Mining and Metallurgy*, vol. 291, no. 4, pp. 49-58.

Newman, P 2012, 'Nutrient removal-the hidden cost of chaff carts and windrow burning', *Liebe Group Crop updates, P*, vol. 10.

Nied, R 2007, 'Rotor Impact Mills', *Handbook of Powder Technology*, vol. 12, Elsevier B.V, pp. 230-249.

Olfert, MR, Stumborg, M, Craig, W & Schoney, RA 1991, 'The economics of collecting chaff', *American Journal of Alternative Agriculture*, vol. 6, no. 4, pp. 154-160.

Petukhov, Y & Kalman, H 2003, 'A new apparatus for particle impact tests', *Particle and Particle Systems Characterization*, vol. 20, pp. 267-275.

Petukhov, Y & Kalman, H 2004, 'Empirical breakage ratio of particles due to impact', *Powder technology*, vol. 143, pp. 160-169.

Petzold, K 1956, 'Combine-harvesting and weeds', *Journal of Agricultural Engineering Research*, vol. 1, pp. 178-181.

Peukert, W 2004, 'Material properties in fine grinding', *International Journal of Mineral Processing*, vol. 74S, pp. S3-S17.

Pfost, HB 1976, 'Grinding and rolling', *Feed manufacturing technology*, Feed Production Council, American Feed Manufacturers Association, Chicago, Ill, pp. 71-84.

Powell, MS & Morrison, RD 2007, 'The future of comminution modelling', *International Journal of Mineral Processing*, vol. 84, no. 1–4, pp. 228-239.

Powles, SB & Yu, Q 2010, 'Evolution in action: plants resistant to herbicides', *Annual review of plant biology*, vol. 61, pp. 317-347.

Rajabipour, A, Tabatabaeefar, A & Farahani, M 2006, 'Effect of moisture on terminal velocity of wheat varieties', *International Journal of Agriculture and Biology*, vol. 8, no. 1, pp. 10–13.

Rajcan, I & Swanton, CJ 2001, 'Understanding maize–weed competition: resource competition, light quality and the whole plant', *Field Crops Research*, vol. 71, no. 2, pp. 139-150.

Ray, DK, Mueller, ND, West, PC & Foley, JA 2013, 'Yield Trends Are Insufficient to Double Global Crop Production by 2050', *PLOS ONE*, vol. 8, no. 6, p. e66428.

Reyenga, J 1991, *Grain cleaner and destructor of foreign matter in harvesting crops*, United States Patent 5,059,154.

Rodriguez, F, Ramirez, M, Ruiz, R & Concha, F 2010, 'Scale-up procedure for industrial cage mills', *International Journal of Mineral Processing*, vol. 97, no. 1-4, pp. 39-43.

Roy, MC & Bailey, RV 1969, *Apparatus for use with a combine to destroy the germination of weed seeds*, United States Patent 771302.

Rumpf, H 1959, 'Beanspruchungstheorie der Prallzerkleinerung', *Chemie Ingenieur Technik*, vol. 31, no. 5, pp. 323-337.

Rumpf, H 1973, 'Physical aspects of comminution and new formulation of a law of comminution', *Powder technology*, vol. 7, no. 3, pp. 145-159.

Salman, AD, Gorham, DA & Verba, A 1995, 'A study of solid particle failure under normal and oblique impact', *Wear*, vol. 186-187, pp. 92-98.

Samimi, A, Moreno, R & Ghadiri, M 2004, 'Analysis of impact damage of agglomerates: effect of impact angle', *Powder technology*, vol. 143-144, pp. 97-109.

Saunders, M 2012, 'Harvesters are suddenly big business', *Kindinin Group: Research Report*, March 2012, vol. 26

Schönert, K & Marktscheffel, M 1986, 'Liberation of composite particles by single particle compression, shear and impact loading', *Preprints of the sixth European symposium comminution*, pp. 29–45.

Sharma, R & Bilanski, W 1971, 'Coefficient of restitution of grains', *Transactions of the ASAE*, vol. 14, no. 1, pp. 216-218.

Shellard, JE & MacMillan, RH 1978, 'Aerodynamic properties of threshed wheat materials', *Journal of Agricultural Engineering Research*, vol. 23, no. 3, pp. 273-281.

Shi, F & Kojovic, T 2007, 'Validation of a model for impact breakage incorporating particle size effect', *International Journal of Mineral Processing*, vol. 82, no. Compendex, pp. 156-163.

Shi, F, Kojovic, T, Larbi-Bram, S & Manlapig, E 2009, 'Development of a rapid particle breakage characterisation device - The JKRBT', *Minerals Engineering*, vol. 22, no. 7-8, pp. 602-612.

Shirtliffe, SJ, Entz, MH & Van Acker, RC 2000, 'Avena fatua development and seed shatter as related to thermal time', *Weed Science*, vol. 48, no. 5, pp. 555-560.

Shirtliffe, SJ & Entz, MH 2005, 'Chaff collection reduces seed dispersal of wild oat (Avena fatua) by a combine harvester', *Weed Science*, vol. 53, no. 4, pp. 465-470.

Slagell Gossen, RR, Tyrl, RJ, Hauhouot, M, Peeper, TF, Claypool, PL & Solie, JB 1998, 'Effects of mechanical damage on cheat (Bromus secalinus) caryopsis anatomy and germination', *Weed Science*, vol. 46, no. 2, pp. 249-257.

Smil, V 1999, 'Crop residues: agriculture's largest harvest', *BioScience,* vol. 49, no. 4, pp. 299-308.

Srivastava, AK, Goering, CE, Rohrbach, RP & Buckmaster, DR 2006, 'Grain harvesting', *Engineering principles of agricultural machines*, Second edn, American Society of Agricultural and Biological Engineers, St. Joseph, Michigan, pp. 403-436.

Steadman, KJ, Crawford, AD & Gallagher, RS 2003, 'Dormancy release in Lolium rigidum seeds is a function of thermal after-ripening time and seed water content', *Functional Plant Biology,* vol. 30, no. 3, pp. 345-352.

Stone, AE, Peeper, TF & Solie, JB 2001, 'Cheat (Bromus secalinus) Control with Herbicides Applied to Mature Seeds', *Weed technology*, vol. 15, no. 2, pp. 382-386.

Szwed, G & Lukaszuk, J 2007, 'Effect of rapeseed and wheat kernel moisture on impact damage', *International Agrophysics*, vol. 21, no. 3, pp. 299-304.

Tabak, S & Wolf, D 1998, 'Aerodynamic Properties of Cottonseeds', *Journal of Agricultural Engineering Research,* vol. 70, no. 3, pp. 257-265.

Takeuchi, H, Nakamura, H, Iwasaki, T & Watano, S 2012, 'Numerical modeling of fluid and particle behaviors in impact pulverizer', *Powder technology,* vol. 217, no. 0, pp. 148-156.

Takeuchi, H, Nakamura, H & Watano, S 2013, 'Numerical simulation of particle breakage in dry impact pulverizer', *AIChE Journal,* vol. 59, no. 10, pp. 3601-3611.

Tavares, LM & King, RP 2002, 'Modeling of particle fracture by repeated impacts using continuum damage mechanics', *Powder technology,* vol. 123, no. 2-3, pp. 138-146.

Tavares, LM 2009, 'Analysis of particle fracture by repeated stressing as damage accumulation', *Powder technology,* vol. 190, no. 3, pp. 327-339.

Teng, S, Wang, P, Zhang, Q & Gogos, C 2011, 'Analysis of Fluid Energy Mill by gas-solid two-phase flow simulation', *Powder technology,* vol. 208, no. 3, pp. 684-693.

Tilman, D, Balzer, C, Hill, J & Befort, BL 2011, 'Global food demand and the sustainable intensification of agriculture', *Proceedings of the National Academy of Sciences,* vol. 108, no. 50, pp. 20260-20264.

Toneva, P & Peukert, W 2007, 'Chapter 20 Modelling of Mills and Milling Circuits', in Agba D. Salman, MG & Michael, JH (eds), *Handbook of Powder Technology*, vol. Volume 12, Elsevier Science B.V., pp. 873-911.

Toneva, P, Epple, P, Breuer, M, Peukert, W & Wirth, K-E 2011, 'Grinding in an air classifier mill -- Part I: Characterisation of the one-phase flow', *Powder technology*, vol. 211, no. 1, pp. 19-27.

Toneva, P, Wirth, K-E & Peukert, W 2011, 'Grinding in an air classifier mill -- Part II: Characterisation of the two-phase flow', *Powder technology*, vol. 211, no. 1, pp. 28-37.

Turner, W, Suggs, C & Dickens, J 1967, 'Impact damage to peanuts and its effects on germination, seedling development, and milling quality', *Transaction of the ASAE*, vol. 10, no. 2, pp. 248-251.

Uhl, J & Lamp, B 1966, 'Pneumatic separation of grain and straw mixtures', *Transactions of the ASAE*, vol. 9, no. 2, pp. 244-246.

Vervoorn, PMM & Austin, LG 1990, 'The analysis of repeated breakage events as an equivalent rate process', *Powder technology*, vol. 63, no. 2, pp. 141-147.

Vogel, L & Peukert, W 2003a, 'Breakage behaviour of different materials--construction of a mastercurve for the breakage probability', *Powder technology*, vol. 129, no. 1-3, pp. 101-110.

Vogel, L & Peukert, W 2003b, 'Modelling of grinding in an air classifier mill based on a fundamental material function', *Kona*, vol. 21, pp. 109-120.

Vogel, L & Peukert, W 2004, 'Determination of material properties relevant to grinding by practicable labscale milling tests', *International Journal of Mineral Processing*, vol. 74, Supplement, no. 0, pp. S329-S338.

Vogel, L & Peukert, W 2005, 'From single particle impact behaviour to modelling of impact mills', *Chemical Engineering Science*, vol. 60, no. 18, pp. 5164-5176.

Walsh, MJ & Newman, P 2007, 'Burning narrow windrows for weed seed destruction', *Field Crops Research*, vol. 104, no. 1-3, pp. 24-30.

Walsh, MJ & Powles, SB 2007, 'Management strategies for herbicide-resistant weed populations in Australian dryland crop production systems', *Weed technology*, vol. 21, no. 2, pp. 332-338.

Walsh, MJ & Harrington, RB 2011, 'Development of the Harrington Seed Destructor', paper presented at the Agribusiness Crop Updates, Perth, 23 and 24 Feb. 2011.

Walsh, MJ, Harrington, RB & Powles, SB 2012, 'Harrington Seed Destructor: A new nonchemical weed control tool for global grain crops', *Crop Science*, vol. 52, no. 3, pp. 1343-1347.

Walsh, MJ, Newman, P & Powles, SB 2013, 'Targeting Weed Seeds In-Crop: A New Weed Control Paradigm for Global Agriculture', *Weed technology*, vol. 27, no. 3, pp. 431-436.

Weerasekara, NS, Powell, MS, Cleary, PW, Tavares, LM, Evertsson, M, Morrison, RD, Quist, J & Carvalho, RM 2013, 'The contribution of DEM to the science of comminution', *Powder technology*, vol. 248, no. 1, pp. 3-24.

Weibull, W 1951, 'A statistical distribution function of wide applicability', *Journal of applied mechanics*, vol. 18, no. 3, pp. 293-297.

White, B 2010, 'New Holland CR 9090 loaded and headed down under', *Kondinin Group: Farming Ahead*, July, vol. 222

Wojtkowski, M, Pecen, J, Horabik, J & Molenda, M 2010, 'Rapeseed impact against a flat surface: Physical testing and DEM simulation with two contact models', *Powder technology*, vol. 198, no. 1, pp. 61-68.

Yu, Q, Cairns, A & Powles, S 2007, 'Glyphosate, paraquat and ACCase multiple herbicide resistance evolved in a *Lolium rigidum* biotype', *Planta*, vol. 225, no. 2, pp. 499-513.

Zamora, DL & Olivarez, JP 1994, 'The viability of seeds in feed pellets', *Weed technology*, vol. 8, no. 1, pp. 148-153.

Zani, P 2001, *Harvest residue destruction system*, Australian Patent 771302.

Zani, P 2012, *Development and testing of the Rotomill*, Interviewed by: Berry, N.K at Harvestaire PTY LTD, Perth, Australia, 29/09/2012.

Appendix A Impact testing emergence counts

The 14 and 28 day emergence counts of the control germination three sets of impact tests performed are shown in this Appendix. The mass of seed collected after testing is also shown. Reduced seedling emergence (RSE) was calculated based on the average maximum emergence of the control (448).

Table A.1 Control seedling emergence counts

Replication	Total seeds	Day 14	Day 28	Max	Max proportion emerged
1	574	430	450	450	78%
2	574	438	454	454	79%
3	574	433	430	433	75%
4	574	444	441	444	77%
5	574	434	444	444	77%
6	574	464	464	464	81%
	Mean	441	447	448	78%
	C.V (%)	2.83%	2.61%	2.35%	2.35%

Table A.2 - Impact test series 1: multiple impacts at constant speed

Impacts	Speed	Day 14	Day 28	RSE	Mass added (g)	Mass collected (g)
1	30	447	434	0.2%	1.250	1.246
1	40	439	453	-1.1%	1.250	1.244
1	50	345	336	23.0%	1.250	1.236
1	60	314	329	26.6%	1.250	1.244
1	70	232	216	48.2%	1.250	1.228
1	80	195	185	56.5%	1.250	1.229
1	90	135	127	69.9%	1.250	1.209
1	100	165	154	63.2%	1.250	1.201
1	110	165	157	63.2%	1.250	1.192
1	120	155	152	65.4%	1.250	1.206
2	30	418	431	3.8%	1.250	1.240
2	40	394	396	11.6%	1.250	1.220
2	50	302	275	32.6%	1.250	1.216
2	60	187	209	53.3%	1.250	1.234

2	70	85	81	81.0%	1.250	1.181
2	80	79	71	82.4%	1.250	1.192
2	90	53	47	88.2%	1.250	1.140
4	30	410	409	8.5%	1.250	1.214
4	40	343	347	22.5%	1.250	1.215
4	50	121	108	73.0%	1.250	1.183
4	50	157	131	65.0%	1.250	1.211
4	60	47	43	89.5%	1.250	1.185
4	70	21	14	95.3%	1.250	1.105
4	70	17	19	95.8%	1.250	1.161
8	20	412	409	8.0%	1.250	1.150
8	30	341	353	21.2%	1.250	1.201
8	40	171	165	61.8%	1.250	1.182
8	50	14	10	96.9%	1.250	1.084
16	30	222	237	47.1%	1.250	1.162

Table A.3 - Impact test series 2 results: 3 impacts in increasing and decreasing speed order

Impacts	speed 1	speed 2	speed 3	Day 14	Day 28	RSE	Mass added (g)	Mass collected (g)
3	30	40	50	159	292	34.8%	1.250	1.218
3	30	40	50	322	304	28.1%	1.250	1.218
3	50	40	30	327	295	27.0%	1.250	1.217
3	50	40	30	316	327	27.0%	1.250	1.216
3	40	50	60	184	172	58.9%	1.250	1.213
3	40	50	60	230	203	48.7%	1.250	1.205
3	60	50	40	202	182	54.9%	1.250	1.203
3	60	50	40	176	193	56.9%	1.250	1.189
3	50	60	70	89	80	80.1%	1.250	1.181
3	50	60	70	69	62	84.6%	1.250	1.200
3	70	60	50	104	82	76.8%	1.250	1.186
3	70	60	50	93	83	79.2%	1.250	1.179
3	60	70	80	71	56	84.2%	1.250	1.185
3	60	70	80	65	57	85.5%	1.250	1.166
3	80	70	60	50	52	88.4%	1.250	1.168
3	80	70	60	49	43	89.1%	1.250	1.182

Table A.4 - Impact test series 3 results: impact combinations at elevated moisture content

Moisture (%)	Impacts	Speed	Day 14	Day 28	RSE	Mass added (g)	Mass collected (g)
13.4%	1	50	392	400	10.7%	1.308	1.299
13.4%	1	70	235	252	43.8%	1.308	1.293
13.4%	4	50	260	239	42.0%	1.308	1.278
13.4%	4	70	57	40	87.3%	1.308	1.227
16.8%	1	50	358	397	11.4%	1.365	1.345
16.8%	1	70	358	321	20.1%	1.365	1.348
16.8%	4	50	299	303	32.4%	1.365	1.320
16.8%	4	70	119	88	73.4%	1.365	1.182
23.8%	1	50	398	425	5.1%	1.485	1.449
23.8%	1	70	365	351	18.5%	1.485	1.448
23.8%	4	50	107	236	47.3%	1.485	1.402
23.8%	4	70	94	135	69.9%	1.485	1.389

Appendix B Impact mill emergence counts

Four large soil bins were used in the seed devitalisation tests (Bin no). Each bin was split into four 700×1500 mm soil bins (positions) for each treatments. Replications and subsamples were spread over the four soil bins. The position within each soil bin was also varied between replications and subsamples to ensure that there was no bias due to bin number or position. The layout for each test is shown in this Appendix. The emergence counts are shown for 14, 21 and 28 days. The reduced seedling emergence (RSE) was calculated using the maximum emergence of the treatment and the average of the maximum emergence counts- of the two controls for each trial.

The test code for each treatment is given by:

[speed(rpm)].[throughput(g/s)].[replication number].[subsample number]

Harrington Seed Destructor (HSD) cage mill

Table B1: HSD cage mill 0.5 kg/s test layout, date of planting: 12/10/2011

Bin no / **Position**	**1**	**2**	**3**	**4**
1	900.500.1.1	1100.500.3.1	1440.500.1.1	control.1
2	1100.500.1.1	control.2	1300.500.3.1	900.500.2.1
3	1440.500.2.1	1300.500.1.1	900.500.4.1	1100.500.4.1
4	1300.500.2.1	900.500.3.1	1100.500.2.1	1440.500.3.1

Table B2:HSD cage mill emergence counts

	Day 14	Day 21	Day 28	RSE	sample weights (g)
control 1	434	447	447		434.1
control 2	474	480	483		430.7
900.500.1.1	57	56	70	84.9%	450.9
900.500.2.1	22	30	25	93.5%	467.2
900.500.3.1	22	35	38	91.8%	461.2
900.500.4.1	28	29	31	93.3%	452.5
1100.500.1.1	29	36	40	91.4%	420.3
1100.500.2.1	11	10	12	97.4%	424.3
1100.500.3.1	36	34	39	91.6%	467.6
1100.500.4.1	14	18	17	96.1%	452.1
1300.500.1.1	36	36	38	91.8%	405.2
1300.500.3.1	25	31	33	92.9%	437.1
1300.500.4.1	6	7	8	98.3%	437.8
1440.500.1.1	28	30	28	93.5%	416.0
1440.500.2.1	6	7	8	98.3%	399.0
1440.500.3.1	20	21	21	95.5%	419.8

Prototype 1

Table B3: Prototype 1 0.5 kg/s test layout, date of planting: 05/10/2012

Bin no / **Position**	**1**	**2**	**3**	**4**
1	2000.500.1.2	2500.500.1.2	3000.500.2.2	control 1.1
2	1500.500.1.1	2000.500.1.1	2500.500.2.1	3000.2.1
3	3000.500.1.2	control 1.1	2000.500.2.1	2500.2.2
4	2500.500.1.1	3000.500.1.1	1500.500.2.1	2000.2.2

Table B4: Prototype 1.5 kg/s test layout, date of planting: 13/11/2012

Bin no / Position	1	2	3	4
1	2500.1500.1.1	2000.1500.1.1	control 2.2	3000.1500.2.1
2	control 2.1	3000.1500.1.2	2000.1500.2.1	2500.1500.2.1
3	2000.1500.1.2	2500.1500.1.2	3000.1500.2.2	1500.500.2.2
4	3000.1500.1.1	1500.500.1.2	2500.1500.2.2	2000.1500.2.2

Table B5: Prototype 1 emergence counts

	Day 14	Day 21	Day 28	RSE	Subsample mass (g)
control.500.1.1	324	418	456		335.5
control.500.1.2	216	360	423		357.2
1500.500.1.1	219	285	312	29.0%	384.4
1500.500.1.2	339	351	323	20.1%	392.6
1500.500.2.1	229	306	311	29.2%	361.9
1500.500.2.2	342	339	300	22.2%	352.9
2000.500.1.1	139	154	142	65.0%	418.7
2000.500.1.2	63	97	114	74.1%	430.7
2000.500.2.1	104	139	134	68.4%	417
2000.500.2.2	114	134	133	69.5%	417.9
2500.500.1.1	26	37	31	91.6%	431.6
2500.500.1.2	26	30	28	93.2%	435.2
2500.500.2.1	45	43	48	89.1%	418.6
2500.500.2.2	47	54	46	87.7%	438.5
3000.500.1.1	4	7	4	98.4%	402.1
3000.500.1.2	5	9	7	98.0%	420.4
3000.500.2.1	15	18	14	95.9%	425.2
3000.500.2.2	7	8	5	98.2%	434.6
control.1500.1.1	630	658	656		309.6
control.1500.2.2	555	610	612		315.0
2000.1500.1.1	463	463	430	27.1%	399.7
2000.1500.1.2	371	381	348	40.0%	388.7
2000.1500.2.1	440	412	383	30.7%	400.8
2000.1500.2.2	402	412	359	35.1%	402.9
2500.1500.1.1	188	194	151	69.4%	415.5
2500.1500.1.2	233	221	194	63.3%	418.5
2500.1500.2.1	192	185	147	69.8%	412.7

2500.1500.2.2	176	160	153	72.3%	400.7
3000.1500.1.1	40	46	38	92.8%	415.2
3000.1500.1.2	90	77	63	85.8%	405.6
3000.1500.2.1	48	45	35	92.4%	428.4
3000.1500.2.2	81	71	62	87.2%	441.1

Prototype 2

Table B6: Prototype 1 0.5 kg/s test layout, date of planting: 08/06/2013

Bin no / Position	1	2	3	4
1	2000.500.1.2	1500.500.1.2	3000.500.2.2	control 2.2
2	1500.500.1.1	2000.500.1.1	2500.500.2.2	3000.500.2.1
3	3000.500.1.2	control 2.1	2000.500.2.1	1500.500.2.2
4	2500.500.2.1	3000.500.1.1	1500.500.2.1	2000.500.2.2

Table B7: Prototype 1 1.5 kg/s test layout, date of planting: 02/05/2013

Bin no / Position	1	2	3	4
1	2500.1500.1.1	2000.1500.1.1	control 1.2	3000.1500.2.1
2	control 1.1	3000.1500.1.2	2000.1500.2.1	2500.1500.2.1
3	2000.1500.1.2	2500.1500.1.2	3000.1500.2.2	2500.500.1.2
4	3000.1500.1.1	2500.500.1.1	2500.1500.2.2	2000.1500.2.2

Table B8: Prototype 2 emergence counts

	Day 14	Day 21	Day 28	RSE	Subsample mass (g)
control.500.1.1	501	546	549		322.3
control.500.1.2	344	483	529		321.7
1500.500.1.1	206	241	245	54.5%	417.6
1500.500.1.2	265	316	306	41.4%	432
1500.500.2.1	175	225	242	55.1%	404.3
1500.500.2.2	313	307	297	41.9%	428.3
2000.500.1.1	109	178	180	66.6%	439.7
2000.500.1.2	92	153	194	64.0%	451.3
2000.500.2.1	129	173	197	63.5%	417
2000.500.2.2	185	226	236	56.2%	417.9
2500.500.1.1	38	77	92	82.9%	437.9
2500.500.1.2	58	63	78	85.5%	453.4
2500.500.2.1	68	91	120	77.7%	444.3
2500.500.2.2	101	123	129	76.1%	453.2
3000.500.1.1	29	52	63	88.3%	456.1
3000.500.1.2	17	36	45	91.7%	474.4
3000.500.2.1	24	32	32	94.1%	466.5
3000.500.2.2	25	47	50	90.7%	453.1
control.1500.1.1	473	559	503		334.6
control.1500.2.2	439	518	521		339.3
2000.1500.1.1	107	149	187	65.4%	421.1
2000.1500.1.2	169	186	194	64.1%	406
2000.1500.2.1	188	242	238	55.2%	435.2
2000.1500.2.2	142	178	173	67.0%	406.6
2500.1500.1.1	82	105	127	76.5%	436.7
2500.1500.1.2	79	127	154	71.5%	447.6
2500.1500.2.1	66	81	106	80.4%	433.4
2500.1500.2.2	67	127	137	74.6%	448.5
3000.1500.1.1	48	72	77	85.7%	443.2
3000.1500.1.2	45	73	68	86.5%	457.3
3000.1500.2.1	18	35	45	91.7%	441.2
3000.1500.2.2	42	76	71	85.9%	454.4